Institut für Geodäsie und Geoinformation der Universität Bonn

Professur für Theoretische Geodäsie

Nonstationary Least-Squares Collocation

Dissertation

zur Erlangung des akademischen Grades

Doktor der Ingenieurwissenschaften (Dr.-Ing.)

der

Agrar-, Ernährungs- und Ingenieurwissenschaftlichen Fakultät

der

Rheinischen Friedrich-Wilhelms-Universität Bonn

vorgelegt von

Johannes Dietrich Friedrich Korte

aus Minden

Bonn 2025

igg

UNIVERSITÄT BONN

Referent	Prof. Dr. techn. Wolf-Dieter Schuh
Korreferent (1)	Prof. Dr. Mirko Reguzzoni
Korreferent (2)	Prof. Dr.-Ing Jan-Henrik Haunert

Tag der Mündlichen Prüfung 18.07.2025

Angefertigt mit Genehmigung der Agrar-, Ernährungs- und Ingenieurwissenschaftlichen Fakultät der Universität Bonn

Abstract

Many geodesists worldwide deal with the modelling of functions to approximate or interpolate measured data. For this purpose, a functional model is usually set up and adjusted by parameters so that it fits as precisely as possible to the data. One of the most important questions is how to select the functions of the model. One method, which has the advantage of being as independent as possible from the choice of functions is provided by least-squares collocation. Here, function values are estimated from the dependencies (covariances) between the observations themselves. Even though, when predicting values between the data, an analytic model, which describes the track of the covariances, still must be specified.

This is where this dissertation starts. After a general introduction and the discussion of the crucial terms (chapter 1) as well as the current state of the field (chapter 2), thus it is firstly shown how the estimate of autoregressive (AR) processes can be used to create a continuation of the sequence of variances, while the resulting function also must satisfy all requirements of a covariance function (chapter 3). The benefit of this method lies in the fact that the estimate of AR processes is data-driven. After finding the most suitable AR process of order p, uniquely given by the p coefficients α_1, α_2,..., α_p and the variance of the white noise σ^2_ε, a continuous continuation of the discrete covariances is to be found which is (1) clearly assigned to the AR process, (2) reproduces the discrete covariances and (3) is positive definite. Furthermore, I show - as the spectrum of these covariance functions differ from the spectrum of the discrete variances - how and why they can ultimately be transformed into one another by a multiplication with a dirac comb. It must be mentioned that this thesis is limited to one dimensional time series associated with time.

The results of chapter 3 shows that instead of depending on the coefficients directly, the constructed covariance function depends on the roots of the characteristic polynomial of the AR process. These roots are also used to compute the spectrum of the AR process. Since many important properties of the process can be derived from the shape of the spectrum, the characteristics of the AR process are also discussed in this context. This is the starting point of chapter 4, where time variable AR (TVAR) processes are estimated. As they offer the advantage of the coefficient being variable in time, the approach of using a TVAR process with known root motion guarantees that the roots of the characteristic polynomial of the process stay within the unit circle which implies that the variance of the resulting process stays finite. From this, we derive three methods to estimate TVAR processes, i.e. with linear, quadratic and piecewise linear root motion. Following the transformation from the coefficients of the AR process into the corresponding roots with linear or quadratic motions, only TVAR processes of order one, two and three are estimated directly. Since there is no analytic solution for computing the roots of a polynomial of order five or higher, the TVAR processes of higher order are estimated by a successive calculation using TVAR(1) and TVAR(2) processes.

As its title suggests, this study provides a method to compute the least-squares collocation under the assumption of nonstationary time series. As such, chapter 5 combines the findings of chapter 3 and chapter 4. This way, an approximation by least-squares collocation can be computed, using a TVAR process to create a covariance function and fill the needed covariance matrices. Therefore the discrete covariances of a TVAR process are derived. In contrast to the discrete covariances of the stationary AR process these discrete covariances not only depend on the lag, but also on the epoch of the first observation as well as on the fact whether the second epoch relative to the first is in the past or in the future. As a result, the continuous continuation of the discrete covariances embodies a function of two parameters; the epoch of the first observation and the difference between the second and the first epoch including the sign of the difference. This way for the first time an analytical representation for a time variable covariance function is presented.

In chapter 6, the different theories are tested on discrete measurements. First, sea level anomalies

are estimated either by the Gauss-Markov model and trigonometric base functions, or by the least-squares collocation with a covariance function from AR processes. Second, TVAR processes with predetermined root motions are estimated by GNSS elevation measurements and validated over the roots of stationary AR processes estimated for a moving window. In a final example, functions are estimated by temperature anomalies, wherein the covariances for the least-squares collocation come once from an AR(1) process estimate and another time from a TVAR(1) process estimate.

Zusammenfassung

Ein großer Teil der Geodäten weltweit beschäftigt sich mit der Modellierung von Funktionen um gemessene Daten zu approximieren oder diese zu interpolieren. Dafür wird in der Regel ein funktionales Modell aufgestellt, welches die gewählte Funktion möglichst genau die Daten anpasst. Die größte Aufgabe dabei besteht darin, die Funktionen des Modells zu wählen. Eine Methode möglichst unabhängig von der Funktionswahl zu sein ist die Kollokation, bei der Kovarianzen aus den Abhängigkeiten zwischen den Beobachtungen selbst bestimmt werden. Jedoch wird bei der Prädiktion mit dieser Methode immer noch eine Kovarianzfunktion benötigt, welche den Verlauf der Abhängigkeiten analytisch beschreibt.

Hier setzt die vorliegende Dissertation an. Nach einer kurzen Einführung zur Einbettung meiner Studie in den aktuellen Stand der Forschung (Kap. 1), und einer Darstellung wichtiger Definitionen und benötigtem Vorwissen (Kap. 2) zeige ich in Kap. 3, wie autoregressive (AR) Prozesse genutzt werden können, um den Verlauf der diskreten Kovarianzen kontinuierlich fortzusetzen und dabei allen Anforderungen an eine Kovarianzfunktion zu genügen. Der Vorteil dieses Verfahrens ist, dass die Schätzung von AR Prozessen bekannt und automatisiert ist. Der geschätzte AR Prozess der Ordnung p wird durch p Koeffizienten α_1, α_2,..., α_p und der Varianz des Rauschens σ^2_ε eindeutig beschrieben. Ziel ist es, eine Methodik zu entwickeln, die aus diesen Parametern eine eindeutige Funktion aufstellt, welche die Varianzen kontinuierlich erweitert. Dabei wird auch gezeigt, dass die Funktion den Anforderungen einer Kovarianzfunktion genügt und wie sich das Spektrum der diskreten Kovarianzen aus dem Spektrum der kontinuierlichen Kovarianzfunktion herleiten lässt. Es sollte noch erwähnt werden, dass diese Arbeit auf eindimensionale Zeitreihen beschränkt ist.

Die Betrachtungen in Kap. 3 zeigen jedoch auch, dass die Kovarianzfunktion nicht von den Koeffizienten direkt abhängig ist, sondern dass die Kovarianzfunktion die Nullstellen des charakteristischen Polynoms des AR Prozesses beinhaltet. Diese Nullstellen werden auch verwendet um das Spektrum des AR Prozesses zu berechnen, aus dem sich viele wichtige Eigenschaften des Prozesses ableiten lassen. Aus diesem Grund ist in diesem Zusammenhang auch von der Charakteristik des AR Prozesses die Rede. Kap. 4 widmet sich daher der Schätzung zeitvariabler autoregressiver (TVAR) Prozesse, bei denen die Variabilität nicht durch die zeitliche Änderung der Koeffizienten vordefiniert ist. Statdessen werden Prozesse erstellt, bei denen die Änderung der Nullstellen über die Zeit vordefiniert ist. Somit besteht eine direkte Verbindung zwischen der vorgegeben Bewegung der Nullstellen der TVAR Prozesse und der später daraus zu bestimmenden Kovarianzfunktion. Insbesondere werden in dieser Arbeit Schätzverfahren für TVAR Prozesse mit linearen, quadratisch und stückweise linearen Nullstellenbewegungen hergeleitet. Die Umrechnung der Koeffizienten in die Nullstellen leitet sich aus dem Nullstellenproblem vom Charakteristischen Polynom her. Da diese Nullstellensuche für Polynome höherer Ordnung (Ordnungen höher als 5) nicht analytisch gelöst werden kann, wird hier ein Weg aufgezeigt, wie Prozesse höherer Ordnung über sukzessive Schätzung von time variable autoregressive (TVAR)(1) und TVAR(2) Prozessen dargestellt werden können.

Das Ziel dieser Dissertation ist es, eine Methode zu erarbeiten, um eine Kollokation nach kleinsten Quadraten für zeitvariable (oder auch nicht stationäre) Prozesse, zu berechnen. In diesem Sinne verknüpft Kap. 5 die Ergebnisse von Kap. 3 und Kap. 4 um eine zeitvariable Kovarianzfunktion aus einem TVAR Prozess zu erstellen und damit die Kovarianzmatrizen für die Kollokation aufzustellen. Zunächst werden die diskreten Kovarianzen des TVAR Prozesses bestimmt. Diese sind nicht mehr, wie im stationären Fall, nur vom Lag abhängig, sondern auch vom Zeitpunkt der Beobachtung, und davon ob die zweite Beobachtung in der Zukunft oder in der Vergangenheit liegt. Dementsprechend ist auch die kontinuierliche Fortsetzung der Kovarianzen eine zweidimensionale Funktion. Obwohl sich diese Ausarbeitung auf TVAR Prozesse der Ordnung 1 mit linearer Änderung der Nullstelle beschränkt, zeigt sich eine starke Flexibilität der Kovarianzfunktion über die Zeit. Damit wird hier erstmals eine analytische Darstellung für eine zeitvariable Kovarianzfunktion

präsentiert.

In Kap. 6 werden letztlich die verschiedenen Theorien an diskreten Messungen getestet. So werden Anomalien des Meeresspiegels mit dem Gauß-Markov Model und trigonometrischen Basisfunktionen, beziehungsweise mit der Kollokation mit einer Kovarianzfunktion aus AR Prozessen, geschätzt und verglichen. Anschließend werden TVAR Prozesse mit vorgegebenen Nullstellenbewegungen durch GNSS Höhenmessungen geschätzt und über die Nullstellen von gefensterten stationären AR Prozessen validiert. In einem abschließenden Beispiel werden Funktionen durch Temperaturanomalien geschätzt, wobei die Kovarianzen für die Kollokation einmal aus einer AR(1) Prozessschätzung und ein andermal aus einer TVAR(1) Prozessschätzung kommen.

Acknowledgments

First of all, I would like to thank my supervisor Prof. Dr. techn. (i.R.) Schuh. I just do not know where to start: At the opportunity to become a tutor in Statistics, with the employment as a research assistant, or the chance to complete my PHD thesis. Every time we meet to talk about my research, I was curious to find out where I had miscalculated or thought too inaccurately. Although this sounds rather negative, I am more than happy to have found someone able to understand my sporadic notes and -on top of that- recalculate every step to discuss the results. Prof. Schuh was not only there for me, but he was available to the entire TG group at all times. He was also a member of several bodies such as the Study Commission or a representative for degree program geodesy in the examination board translate, where he advocated for the students. Most of all, I have to thank him for continuing to supervise this thesis despite his retirement, so that this work could be completed. I am certain that I speak on behalf of the whole TG group when I say: Thank you for the family atmosphere in the workplace.

I would like to thank my two additional advisors of this thesis, Prof. Dr. Mirko Reguzzoni of the Politecnico di Milano and Prof. Dr.-Ing. Jan-Henrik Haunert of the research group Geoinformation at the University of Bonn. I got to know both professors during my master studies. Professor Reguzzoni offered a lecture at the University of Bonn, which was called "Collocation and Applications." There, I first got in contact with the theories and applications of least-squares collocation which would later form the basis of my thesis. Professor Haunert became professor at the University of Bonn in 2016. That is why I had only one lecture with him: "Otimierungsalgorithmen für räumliche Anaysen" in the summer semester of 2017. He showed me how maps are visualized and generalized, and how the complexity of algorithms can be calculated and optimized. The latter has been used more than once in this work.

Parts of this study and the publication were founded from 2019 to 2023 by the DFG project Nonstationary Least Squares Collocation (https://gepris.dfg.de/gepris/projekt/435703911 – Nonstop LSC: project number: 435703911). The computation as well as the figures were realized by Matlab R2021a, provided to me by the University of Bonn. The data for the applications are all free downloadable data: The sea level anomalies are provided by "Global Ocean Gridded L 4 Sea Surface Heights. E.U. Copernicus Marine Service Information (CMEMS). Marine Data Store (MDS). DOI: 10.48670/moi-00145 (Accessed on 21-Sep-2023)," the GNSS heights are provided by La Rochelle Université and can be downloaded from the website: https://www.sonel.org/-GPS-.html, and the annual temperature anomalies can be downloaded from the website: https://esgf-data.dkrz.de/projects/esgf-dkrz/. The data itself was processed by different teams, how exactly this processing took place is described in the paper Eyring et al. 2016. A special thanks is given to Sebastian Buschow for preparing the annual temperature anomalies for this work.

I consider myself really lucky for having the best colleagues I could imagine. Thanks to Jan Martin who is always there to help me with computer problems, mathematical discussions or team building activities. The same goes for Lukas, who listened and discussed my twisted ideas, as well as Christian, who was my roommate before Lukas, and who put me up and supported me. I further like to thank Till who was PHD student in the same project like me. We discussed a lot and helped each other to understand the magic of time series analysis. My thanks also got to Christina, Bernd and Joël, who had been PHD students for longer than I had and supported me in pushing forward a proposal and teaching. A special thanks goes to Joël, because he renewed the exercises that I later took over and helped me to correct the elaborations even after wards. Even though he was no longer at the University of Bonn during my time as a research assistant, I want to thank Prof. Dr. Boris Kargoll (now professor at the Anhalt University of Applied Sciences) for bringing me closer to the fun of painstaking dissecting mathematical backgrounds with my bachelor's thesis. I am sure without him I would not have come so close to a doctoral thesis. Finally, I cannot thank Bernd Binnenbruck und Ines Barczewski enough. Without their support, neither teaching nor working at

the university would have been possible. I am happy to have met so many people I would like to thank. So I apologize to every who is not named here. I did not intentionally leave you out, but the space is not enough ;P.

I would like to thank my family and friends for supporting me for all this years, and for not asking when I will finish it too often. Here, I want to highlight three people in particular: Helena and Georg Derksen, for giving me the strength to work on even in problematic times; and Prof. Dr. Sabine Weber for the proofreading and more important for supporting me and my weirdness for such a long time. I love you and I'm really happy to be part in your life.

Contents

Chapter 1

Introduction

1.1 Motivation

A main task of geodesy is to approximate models from discrete observations in order to eliminate noise in the measurements or to interpolate the values between the observation points. For example Yuan et al. 2020 estimate the sea level from various satellite missions to interpolate pseudo-observations of the sea level on a regular grid, or in Brockmann et al. 2021 the earth gravity field is computed from GOCE (the Gravity Field and Steady-State Ocean Circulation Explorer) data. Since least-squares collocation (LSC) is the regular procedure to interpolate signals, this method is used in this and many more applications. The procedure of LSC is for example summarized in Schuh et al. 2019, where it is shown that in this method, predictions (or pseudo-observations) are estimated from the values of a weighted sum of the original observations. The weighting is determined by statistical similarities, the covariances between the predicted values and the observations. These weights are computed by a matrix-vector product that includes the covariances and the roots.
One problem of the LSC is given by the large dimension of the covariance matrices used. These are the covariance matrix of the observations and the common covariance matrix of the observations and the predictions. The problems of high dimensions concerns both covariance matrices. First the autocovariance matrix of the observations is required. Here the memory demand increases quadratically with the number of observations n. Second the covariance matrix of the observations and the predicted values is required. This is a matrix of the dimension $n \times w$, with w being the numbers of predicted values. Furthermore computational challenges arise, as the autocovariance matrix of the observations must be inverted. This operation corresponds to an effort of $\mathrm{O}(n^3)$, i.e. a cubic increase of the necessary operations of the number of observations.
This is where AR processes come into play. One important property of these processes is that the inverse covariance matrix of a time series generated by an AR process of order p is a band matrix with bandwidth p. The use of banded matrices results in the advantage that the inverse covariance matrix which is required in least-squares collocation, despite its size, requires limited amount of memory. Calculations can be optimized from the banded system, which plays an important role for large observation systems. For this reason, the idea is to create covariance functions from the estimated autoregressive processes, so that derived covariance matrices inherit this advantage.
A further disadvantage associated with the least-squares collocation lies in the fact that the stochastic process (or the time series of observations) needs to be stationary. This means that the moments of the process do not change over the entire observation period[1].
In order to relax this constrain concerning the stationarity, the idea is to use time variable auto regressive processes in least-squares collocation. In these processes, the influence of previous observations on the estimated observation changes over time. This has also already been applied by current research, compare for example Kargoll et al. 2018. But in these applications, the spectral

1. In particular, this means that for normally distributed processes, the expectation value, the variance and the covariance each only depend on the distances between the observations but not on the discrete times or locations (see Khintchine 1934, p. 606)

properties of the resulting process from the time variability were not taken into account. However, since the characteristic of the process is shown in the spectrum, the predefined functions do not describe the motion of time variable coefficients of the AR process, but the movements of the spectrum itself. This is achieved by approximating the movements of the characteristic polynomial's roots over time (e.g. by a linear function). This is possible because the AR coefficients, the roots of the characteristic polynomial and the spectrum of the AR process are equivalent and can be converted into one another (see Box et al. 1970, p. 55).
With the help of these time variable autoregressive processes, for which the temporal change of spectral properties is known, a time variable covariance function can be created, and a **nonstationary least-squares collocation** can be performed.

1.2 Level of Research

Three areas of the current level of research are relevant for this section: (1) least-squares collocation in general; (2) methods for representing covariance functions and (3) stochastic, especially autoregressive processes. The last section concerning autoregressive processes is further divided into the discussion of time constant (or static) and time variable processes. Finally, a summary is given, including the publications on which this thesis is based.

Least-squares collocation (LSC), which is also called kriging, Wiener filtering, or best linear unbiased prediction (BLUP), is a method of filtering observations in order to separate them from noise or to predict the values between observation points (e.g. Koch 1999). The basic idea of least-squares collocation goes back to Krarup 1969 and Moritz 1973, who independently derived the same calculation rule. The commonalities and differences of these three related methods (i.e. least-squares collocation, BLUP and Wiener filtering) are discussed for example in Dermanis 1984 and Schuh 2016. Additionally Reguzzoni et al. 2005 introduced a more general approach called "general kriging". However, since all methods require the same covariance functions, the findings shown in the following thesis can be applied in any of these individual methods. In the current research, least-squares collocation is particularly applied in satellite gradiometry such as in Albertella et al. 2004, as well as during the calculation of the mean sea surface from different satellites and measurement systems such as in Jin et al. 2016, Yuan et al. 2020 and Hamden et al. 2021. Another typical application is found in the field of regional or general geoid modelling, e.g. Reguzzoni et al. 2005, Gilardoni et al. 2012, Doganalp et al. 2015 and Ramouz et al. 2019. Also, the location of the Moho depths (the interface between the earth's crust and mantle) is estimated by inverting the GOCE second radial derivative using the least-squares collocation method (see Rossi et al. 2022). A rather atypical application shown in Reguzzoni et al. (2022) by calculating GNSS-based dam monitoring via LSC.
The methodology of least-squares collation has also been adapted for other applications. For example, Schuh et al. 2023 and Jendges 2022 showed different examples how this method can be extended for spatio-temporal data. Teunissen 2007 introduced modification of the BLUP for new classes of predictors to improve the mean squared error performance.

The most important step in least-squares collocation is the modelling of covariance functions. These functions are often manually chosen with respect to best fitting through the discrete variance and covariances of the observations. This requires a considerable repertoire of functions to cover the different characteristics of the time series. Schubert et al. 2020 develop conditions to determine covariance functions from autoregressive moving average processes, which is further developed in Schubert et al. 2021a. Compared to these papers, here in the following thesis the covariance function is calculated from the estimated processes and not adjusted to the discrete covariance via parameters. Based on this, Schubert et al. 2024 established a family of covariance functions which have a high flexibility to respond to individual effects in the covariances from observation time series.

Furthermore autoregressive processes are used to decorrelate time series. In Schuh et al. 2019,

Schubert et al. 2021b and Brockmann et al. 2021 autoregressive processes with time constant coefficients are estimated to create filters, which are used to remove highly correlated noise from GOCE (the Gravity Field and Steady-State Ocean Circulation Explorer) data. Over the years, Schuh 1996, Schuh 2003a, Schuh 2003b, Siemes et al. 2007, and Krasbutter et al. 2011 have continued to process the data with the help of adapted autoregressive processes. However, the general estimate of autoregressive processes is also further investigated: for example Moon et al. 2020 as well as Schubert et al. 2021c show how autoregressive processes from time series with high noise content can be robustly estimated.
The term time variable is often used differently. Following Priestley 1988, time variable processes can be subdivided into models with a deterministic trend (e.g. polynomial or seasonal) or with 'explosive' AR models where the roots of the characteristic polynomial are not only inside but also outside the unit circle (Schuh et al. 2023). Another type of nonstationary processes can be determined by processes where the coefficients of the autoregressive process are variable in time (see e.g. Dahlhaus 1997). The extension to time variable autoregressive processes with given functions for the coefficients already exists: e.g. Grenier 1983 describes the motion of the coefficients via trigonometric functions, while Hall et al. 1977 approximate the motion via Legendre polynomials. Slepian 1978 represents the motion by spherical sequences and Alkhatib et al. 2021 use a time variable autoregressive process with linear changing coefficients, and show that this method is more suitable than using time stable autoregressive processes.

The problem with the least-squares collocation is that the size of the covariance matrices increase quadratically with the number of observations. That is why Sansò et al. 1987 switched to using finite covariance functions to be able to use band matrices in least-squares collocation. Arabelos et al. 1998 used these finite covariance functions to estimate a global gravity field of the earth. The use of finite covariance functions in least-squares collocation is as well pursued by Korte et al. 2018. But in this presentation, there is discussed not only a banded covariance matrix based on finite covariance functions, but also another covariance matrix generated from an AR(1) process. The covariance matrix computed by the covariances of an AR process might not be a banded matrix, but its inverse is. And the inverse is also used in the least-squares collocation. Based on this idea, a method has been published in Korte et al. 2021, with which a continuous covariance function can be derived from AR processes of any order. In order to arrive at a time variable least-squares collocation in Korte et al. 2023b and Korte et al. 2023a the time variable AR processes of order one, two and three as well as a successive method for estimating higher time variable AR processes have been developed. The results of the last three papers will be presented in more detail and expanded on the next pages.

1.3 Objectives

The aim of this thesis is to find a general representation for stochastic processes that change their characteristic over the observation period, and to integrate them for covariance modelling in least-squares collocations. These time variable processes are often needed to adapt the covariances for real data series and are illustrated here in three steps:
In a first step, a method is required to calculate the continuous covariance function for time constant processes by estimating the best fit autoregressive processes. In the second step, time variable autoregressive processes are estimated using the Gauss-Markov model. The fact that the characteristics of this autoregressive process change over time is shown by the spectrum in which the peaks change in both amplitude and frequency. To model these spectra, the roots of the characteristic polynomial are used, as these roots have a direct influence on the spectra. In the third part, the continuous time variable covariance functions for a time variable autoregressive process with a linear root motion are derived.

1. *Construction of a continuous covariance function from an autoregressive process of order p*
   Through the Yule-Walker equations, any p successive covariances are connected to each other.

These equations can also be converted into difference equations, for which there is a representation which allows the direct calculation of the covariances. This representation can also be continuously expanded. Nevertheless, until now it has neither been investigated whether this function is positive definite or not, nor how continuation of a discrete sequence has influence on the spectrum. So in this work, first the continuous function is either proved or forced to be positive definite. And second, it is shown that a change of the spectrum is only caused by the transition from discrete values to a continuous function.

2. *Estimation of time variable autoregressive processes whose spectral density (characteristic) changes linearly or quadratically*
   In the estimation of time variable autoregressive processes, the change of the process over time must be modelled. Hall et al. 1977 and Grenier 1983 analysed speeches with time variable AR processes, where the coefficients were created by trigonometric functions or modified Legendre polynomials. Also, Slepian 1978 showed how time variable AR processes whose coefficients are defined via the discrete prolate spheroidal sequences are estimated. In all theses approaches, the time variable autoregressive processes were defined via the motion of the coefficients without paying attention to the effect on the temporal changes on the spectral representation. The disadvantage of these methods lies in the time variable changes of the spectrum, which can only be determined for discrete realizations of time variable coefficients of the autoregressive processes, while no function being deduced for describing the motion of the roots. To solve this problem, the roots of the characteristic polynomial of the autoregressive processes are described by functions, which then represent the change of the spectrum, but can also be converted into the change of the coefficients. In turn, this special time variable coefficients can be estimated. In particular, the coefficients for linear, piecewise linear and quadratic root movements as well as the additional necessary constraints are derived here.

3. *Covariance function of a time variable autoregressive process of first order*
   The synthesis of the first two chapters leads to a time variable covariance function useable for covariance modelling in least-squares collocation. Accordingly, a covariance function of a time variable autoregressive process is determined from arbitrary lags in order to set up the covariance matrices for the least-squares collocation. It should be noted here that this is limited to time variable autoregressive processes of the first order.

Chapter 2

Definitions and Prerequisite Knowledge

2.1 Method of Least-Squares Collocation

In this thesis, the observations $\mathcal{L}_t$ are represented by the definition used in least-squares collocation according to Krarup 1969 or Moritz 1972, i.e.

$$\mathcal{L}_t = \underbrace{\boldsymbol{A}_t\boldsymbol{\xi}}_{\text{trend}} + \mathcal{S}_t.$$

Here, $\mathcal{L}_t$ and $\mathcal{S}_t$ are random variables that represent the observation process and the signal at the time t, respectively. Hereby the white noise is included as apart of $\mathcal{S}_t$. $\boldsymbol{A}_t \in \mathbb{R}^{1\times m}$ represents the functional relationship between the observation $\mathcal{L}_t$ and the m (true) parameters $\boldsymbol{\xi} \in \mathbb{R}^m$, and the product of $\boldsymbol{A}_t\boldsymbol{\xi}$ is called the deterministic trend. Hereby $\boldsymbol{\xi}$ is unknow and it has to be estimated too. t gives the index for the individual states of the random variables by assigning a unique description of the situation to each random variable, (these situations can be defined, for example, by the time t as done here or by the location).
Schuh (2016, section 3.1) shows that the trend can be estimated by an adjustment and removing the trend from the observations in a further step, yields the stochastic part of the signal:

$$\mathcal{S}_t = \mathcal{L}_t - \boldsymbol{A}_t\xi = \tilde{\mathcal{S}}_t + \mathcal{N}_t.$$

The stochastic part is divided into the fully correlated part of the signal $\tilde{\mathcal{S}}$, which should be estimated by least-squares collocation and $\mathcal{N}_t$, which is a purely random interference signal for most occurrences (noise).

2.2 Least-Squares Collocation

In the least-squares collocation (LSC) a signal ($\widetilde{\boldsymbol{\mathcal{S}}} = [\tilde{\mathcal{S}}_1, \tilde{\mathcal{S}}_2, ..., \tilde{\mathcal{S}}_r]$) is estimated from an observed time series ($\boldsymbol{\mathcal{S}} = [\mathcal{S}_1, \mathcal{S}_2, ..., \mathcal{S}_n]$). Given that $M\{.\}$ be the mean value of a given vector, and given the assumption that both, the observations and the predicted values have the mean expected value of zero:

$$M\{E\{\tilde{\boldsymbol{\mathcal{S}}}\}\} = 0 \qquad\qquad M\{E\{\boldsymbol{\mathcal{S}}\}\} = 0,$$

then Moritz (1980, p. 102 eq. 14-27) shows that the estimate of $\widetilde{\boldsymbol{\mathcal{S}}}$ can be determined via the least-squares collocation

$$\widetilde{\boldsymbol{\mathcal{S}}} = \Sigma\{\widetilde{\boldsymbol{\mathcal{S}}}, \boldsymbol{\mathcal{S}}\}\left(\Sigma\{\boldsymbol{\mathcal{S}}\} + \Sigma\{\boldsymbol{\mathcal{N}}\}\right)^{-1}\boldsymbol{\mathcal{S}} \tag{2.2.1}$$

(see e.g. Schuh 2022, section 3.3.3). Here $\Sigma\{\boldsymbol{\mathcal{N}}\}$ represents the covariance matrix of a vector of normally distributed random variables. These random variables must also be independent of the

signal whose covariance matrix is described by $\Sigma\{\boldsymbol{\mathcal{S}}\}$. The last matrix needed for the estimation in (2.2.1) is the common covariance matrix $\Sigma\{\widetilde{\boldsymbol{\mathcal{S}}}, \boldsymbol{\mathcal{S}}\}$ with the entries

$$\Sigma\{\widetilde{\boldsymbol{\mathcal{S}}}, \boldsymbol{\mathcal{S}}\}(r, c) = \Sigma\{\widetilde{\mathcal{S}}_r, \mathcal{S}_c\}$$

in row r and column c, representing the influence of the c-th observation ($\mathcal{S}_c$) on the r-th estimation ($\widetilde{\mathcal{S}}_r$). The entries of the covariances are in general performed by the evaluations of covariance functions. These have to fulfil the conditions described in section 2.6 under the assumption of stationarity (see 2.5). In this thesis, in order to model the individual covariances, this method is extended to special time variable processes as described in section 2.16.

2.3 Covariance Propagation

Moritz (1980, p. 86ff) shows, that a linear functional $f(\widetilde{\boldsymbol{\mathcal{S}}})$ of a given signal $\boldsymbol{\mathcal{S}}$ can be estimated by LSC:

$$\begin{aligned} f(\widetilde{\boldsymbol{\mathcal{S}}}) &= \Sigma\{f(\widetilde{\boldsymbol{\mathcal{S}}}), \boldsymbol{\mathcal{S}}\} \left(\Sigma\{\boldsymbol{\mathcal{S}}\} + \Sigma\{\boldsymbol{\mathcal{N}}\}\right)^{-1} \boldsymbol{\mathcal{S}} \\ &= f\left(\Sigma\{\widetilde{\boldsymbol{\mathcal{S}}}, \boldsymbol{\mathcal{S}}\}\right) \left(\Sigma\{\boldsymbol{\mathcal{S}}\} + \Sigma\{\boldsymbol{\mathcal{N}}\}\right)^{-1} \boldsymbol{\mathcal{S}}. \end{aligned}$$

For example, with $f\left(\Sigma\{\widetilde{\boldsymbol{\mathcal{S}}}, \boldsymbol{\mathcal{S}}\}\right) = \frac{d}{dh}\left(\Sigma\{\widetilde{\boldsymbol{\mathcal{S}}}, \boldsymbol{\mathcal{S}}\}\right)$, the slope of the signal $\widetilde{\mathcal{S}}$ is predicted. The entries in the common covariance matrix $\Sigma\{\widetilde{\boldsymbol{\mathcal{S}}}, \boldsymbol{\mathcal{S}}\}$ are interpreted as functions of a covariance function (CF)

$$\Sigma\{\widetilde{\boldsymbol{\mathcal{S}}}, \boldsymbol{\mathcal{S}}\} = \begin{bmatrix} \gamma(t'_0 - t_0) & \gamma(t'_0 - t_1) & \gamma(t'_0 - t_2) & \dots & \gamma(t'_0 - t_n) \\ \gamma(t'_1 - t_0) & \gamma(t'_1 - t_1) & \gamma(t'_1 - t_2) & \dots & \gamma(t'_1 - t_n) \\ \dots & & & & \\ \gamma(t'_m - t_0) & \gamma(t'_m - t_1) & \gamma(t'_m - t_2) & \dots & \gamma(t'_m - t_n) \end{bmatrix}_{m \times n},$$

with t_i $i = 1, 2, ..., n$ are the epochs of the observations and t'_j $j = 1, 2, ..., m$ are the epochs of the predicted values. The difference quotient is then calculated via the derivative of the distribution functions:

$$\frac{d}{dh}\Sigma\{\widetilde{\boldsymbol{\mathcal{S}}}, \boldsymbol{\mathcal{S}}\} = \begin{bmatrix} \frac{d}{dh}\gamma(h)|_{h=t'_1-t_1} & \frac{d}{dh}\gamma(h)|_{h=t'_1-t_2} & \frac{d}{dh}\gamma(h)|_{h=t'_1-t_3} & \dots & \frac{d}{dh}\gamma(h)|_{h=t'_1-t_n} \\ \frac{d}{dh}\gamma(h)|_{h=t'_2-t_1} & \frac{d}{dh}\gamma(h)|_{h=t'_2-t_2} & \frac{d}{dh}\gamma(h)|_{h=t'_2-t_3} & \dots & \frac{d}{dh}\gamma(h)|_{h=t'_2-t_n} \\ \dots & & & & \\ \frac{d}{dh}\gamma(h)|_{h=t'_m-t_1} & \frac{d}{dh}\gamma(h)|_{h=t'_m-t_2} & \frac{d}{dh}\gamma(h)|_{h=t'_m-t_3} & \dots & \frac{d}{dh}\gamma(h)|_{h=t'_m-t_n} \end{bmatrix}_{m \times n}.$$

Here m is the number of predicted Signals $\widetilde{\boldsymbol{\mathcal{S}}}$ and n is the number of used Signals in $\boldsymbol{\mathcal{S}}$. Since the derivative can only be properly determined from a continuous function, it is necessary to switch to the continuous CF $\gamma(h)$ with $h \in \mathbb{R}$, even if the entries of the covariance matrices are only evaluated at discrete points $h_{t'_u - t_v}$ with $u \in \{1, 2, ..., m\}$ and $v \in \{1, 2, ..., n\}$.

2.4 Stochastic Process

Brockwell et al. (1991, p. 8 Def. 1.2.1) define: A stochastic process is a family of random variables $\{\mathcal{S}_{t_j}, t_j \in T\}$ defined by a probability space $(\Omega, \mathscr{A}, \Pi)$. Here T denotes the index set (e.g. $\mathbb{N}, \mathbb{Z}, \mathbb{R}$), Ω is the set of all sub events, $\mathscr{A}$ is the σ-algebra of Ω, and Π is a function that assigns a probability to each element in $\mathscr{A}$. Schuh (2016, chapter 2) additionally differentiates between a discrete stochastic process $\mathcal{S}_{t_j}$ with $j \in \mathbb{Z}$ in case of discrete sampling points t_j and otherwise the continuous stochastic process $\mathcal{S}(t)$ with $t \in \mathbb{R}$.
Alternatively Watts et al. (1968, p. 134 f.) describe a stochastic process by defining a collection of continuous observations $\mathcal{S}_t$ with a valid $t \in \mathbb{R}$ and a cumulative distribution function (CDF) ($F_{\cdot}(.)$). In most observations, the data is associated with time or a location. This thesis is limited to one dimensional time series associated with time.

2.5 Stationary Process

A subclass of the stochastic processes defined in 2.4 are stationary processes. KHINTCHINE (1934, p. 606) defines a process as stationary if for two sequences $(\mathcal{S}_{t_1}, \mathcal{S}_{t_2}, ..., \mathcal{S}_{t_n})$ and $(\mathcal{S}_{t_1+u}, \mathcal{S}_{t_2+u}, ..., \mathcal{S}_{t_n+u})$ the distributions are identical, regardless of the choice of the number $n \in \mathbb{Z}$, the times $j \in \mathbb{Z}$ and the distance $u \in \mathbb{R}$. In particular, this definition is equivalent to the definition of PRIESTLEY (1983, p. 105), which defines stationarity as:

$$F_{\mathcal{S}_{t_1},\mathcal{S}_{t_2},...,\mathcal{S}_{t_n}}(s_1, s_2, ..., s_n) \equiv F_{\mathcal{S}_{t_1+k},\mathcal{S}_{t_2+k},...,\mathcal{S}_{t_n+k}}(s_1, s_2, ..., s_n),$$

where $F_{.}(.)$ is the CDF of $\{\mathcal{S}_j\}_{j\in\mathbb{Z}}$. The term $\{.\}_{j\in\mathbb{Z}}$ is used for the entire time series, and s_j is the parameter of the CDF, which refers to the random variable $\mathcal{S}_t$.
Furthermore, BROCKWELL et al. (1991, def. 1.3.2) clarify the concept of strict stationary when the properties of a process, defined by the moments of the process, are constant. In particular, the expected value, variance and the covariances over the entire process are constant, i.e.

$$\begin{aligned}
\mu_j &:= E\{\mathcal{S}_{t_j}\} = \int_{-\infty}^{\infty} t_j f_{\mathcal{S}_{t_j}}(t_j) dt_j = \mu && \text{is constant for all } j \in \mathbb{Z},\\
\sigma_j^2 &:= E\{(\mathcal{S}_{t_j} - E\{\mathcal{S}_{t_j}\})^2\} = \int_{-\infty}^{\infty} (t_j - \mu_j)^2 f_{\mathcal{S}_{t_j}}(t_j) dt_j = \sigma^2 && \text{is constant for all } j \in \mathbb{Z}, \text{ and}\\
\sigma_{j,k} &:= E\{(\mathcal{S}_{t_j} - E\{\mathcal{S}_{t_j}\})(\mathcal{S}_{t_k} - E\{\mathcal{S}_{t_k}\})\}\\
&= \int_{-\infty}^{\infty} (t_j - \mu_j)(t_k - \mu_k) f_{\mathcal{S}_{t_j},\mathcal{S}_{t_k}}(t_j, t_k) dt_j dt_k\\
&= \sigma_{|j-k|}
\end{aligned}$$

only depend on the relative distance $|j-k|$ for all $j, k \in \mathbb{Z}$. Here $f_{.}(.)$ means the probability density function (PDF), $E\{.\}$ is the expected value of a random variable and σ_j^2 is the variance of the time series $\mathcal{S}_t$. HAMILTON (1994, p. 46) differentiates between weak stationarity, in which only the first two moments are independent of time or space, and strict stationarity, in which all moments are independent of time or space. Since Gaussian-distributed (or normally distributed) observations are assumed here, all moments with order greater than two are constants. Therefore, not only the moments are always independent of time and space, but also weak stationarity is followed by strict stationarity.

2.6 Covariance Functions

In BOX et al. (1970, p. 27) it is shown that the condition of stationarity of section 2.5 requires that the CDF is independent of the absolute time and depends only on the lag. Thus, the covariances are only dependent on the lag j:

$$\Sigma_j = E\{(\mathcal{S}_{t-j} - \mu)(\mathcal{S}_t - \mu)\}. \tag{2.6.1}$$

Here, a constant expectation value is used for the times $t-j$ and t: $\mu = E\{\mathcal{S}_t\} = E\{\mathcal{S}_{t-j}\}$. Furthermore, PRIESTLEY (1983, p. 109) has shown that a CF $\{\Sigma_j\}_{j\in\mathbb{Z}}$ must meet four conditions:

1. $\Sigma_0 > 0$, i.e. the variance is always greater than zero.
2. $|\Sigma_j| \leq \Sigma_0 \ \forall j \in \mathbb{Z}$, i.e. the absolute value of the variance does not exceed the variance.
3. $\Sigma_j = \Sigma_{-j}$, i.e. the function is symmetrical.
4. Σ_j is a positive semi-definite function.

In this thesis we differentiate between the discrete CF ($\{\Sigma_j\}_{j\in\mathbb{Z}}$) for discrete stochastic processes $\mathcal{S}_{t_k}$ with $k \in \mathbb{Z}$ and the continuous CF ($\gamma(h)$) for continuous stochastic processes $\mathcal{S}(t)$ with $t \in \mathbb{R}$, but the conditions apply to both.

2.7 Autoregressive Processes

According to Wold 1938, any stationary process $\mathcal{S}_t$ can be divided into two parts: a moving average (MA) part, in which the signal at any time is represented by a weighted sum of white noise, and an autoregressive (AR) part that describes the process at any time as a weighted sum of its predecessors. Thus, each stationary process can be easily described by an autoregressive moving average (ARMA) process. This consists of a recursion formula for the autoregressive (AR) part and a sum of weighted white noise $\mathcal{E}_t$ for the moving average (MA) part (see e.g. Buttkus 2000, p. 240):

$$\mathcal{S}_t = \sum_{k=1}^{p} \alpha_k \mathcal{S}_{t-k} + \sum_{l=1}^{q} \phi_l \mathcal{E}_l.$$

Here, p is the order of the AR part, and q is the order of the MA part. In addition, α_k are the coefficients of the AR part, respectively the weights for the sum of the AR part. ϕ_l are the weights for the MA part.
In time series analysis, the AR processes are preferred, as this type of processes can be used to decorrelate the observations or to determine the covariances between the discrete observations. So, an autoregressive process of order p (AR(p)) for observations $\mathcal{S}_t$ is defined by:

$$\mathcal{S}_t = \alpha_1 \mathcal{S}_{t-1} + \alpha_2 \mathcal{S}_{t-2} + ... + \alpha_p \mathcal{S}_{t-p} + \mathcal{E}_t, \tag{2.7.1}$$

where α_1, α_2, ..., α_p are the coefficients of the AR process and $\mathcal{E}_t$ is an independently and identically distributed (i.i.d) noise sequence with variance $\sigma^2_{\mathcal{E}}$. The parameters uniquely describing an AR(p) process are the p coefficients α_k, $k \in \{1, 2, ..., p\}$ and the variance of the noise $\sigma^2_{\mathcal{E}}$.

2.8 Yule-Walker Equations

The Yule-Walker (Y.-W.) equations provide a linear relation between the covariances and the coefficients of a stationary AR(p) process. Schlittgen et al. (1991, p. 102) derive the equations from the product of two arbitrary states of a time series $\{\mathcal{S}_j\}_{j\in\mathbb{Z}}$:

$$\mathcal{S}_t \mathcal{S}_{t-j} = \alpha_1 \mathcal{S}_{t-1}\mathcal{S}_{t-j} + \alpha_2 \mathcal{S}_{t-2}\mathcal{S}_{t-j} + ... + \alpha_p \mathcal{S}_{t-p}\mathcal{S}_{t-j} + \mathcal{S}_{t-j}\mathcal{E}_t. \tag{2.8.1}$$

Here $\mathcal{S}_t$ is replaced by (2.7.1). Bearing in mind that

$$E\{\mathcal{S}_t \mathcal{S}_{t-j}\} = \Sigma_j \qquad \text{and} \qquad E\{\mathcal{E}_t \mathcal{S}_{t-j}\} = \begin{cases} \sigma_{\mathcal{E}}{}^2 & \text{if } j = 0 \\ 0 & \text{else} \end{cases}$$

this allows the formation of the expected value on both sides of (2.8.1) to infer the Y.-W. equations i.e.

$$\Sigma_0 = \alpha_1 \Sigma_1 + \alpha_2 \Sigma_2 + ... + \alpha_p \Sigma_p + \sigma_{\mathcal{E}}{}^2 \tag{2.8.2}$$

$$\Sigma_j = \alpha_1 \Sigma_{|j-1|} + \alpha_2 \Sigma_{|j-2|} + ... + \alpha_p \Sigma_{|j-p|} \qquad \forall j \in \mathbb{Z} \setminus \{0\}. \tag{2.8.3}$$

2.9 Characteristic Polynomials

Some characteristics of the AR process can be seen by using the characteristic polynomial. For example for example it can be proven whether or not the process is stationary. Therefore Box et al. (1970, p. 55) defined the characteristic polynomial (CP) of an AR(p) process represented by (2.7.1) as

$$\begin{aligned} \bar{\chi}(x) &= 1 - \alpha_1 x - \alpha_2 x^2 - ... - \alpha_p x^p \\ &= \prod_{k=1}^{p} (1 - \xi_k x). \end{aligned}$$

With regard to the stationarity of AR processes (see section 2.5 and 2.7), the roots of this equation ξ_k must lie outside the unit circle. By redefining the CP as

$$\chi(x) = x^p - \alpha_1 x^{p-1} - \alpha_2 x^{p-2} - ... - \alpha_p \tag{2.9.1}$$

$$= \prod_{k=1}^{p} (x - P_k), \tag{2.9.2}$$

(like it is done in Priestley 1983, p. 133) the condition of stationarity changes to roots P_k within the unit circle, with $P_k = \frac{1}{\xi_k}$. These roots P_k occur only as real numbers or as pairs of complex conjugated numbers, as long as the coefficients are real-valued as in the case of the AR coefficients.

2.10 Auxiliary Equation/ Difference Equation

The characteristic polynomial from section 2.9 can be transformed into a difference equation, giving a formula to compute each signal directly. The homogeneous difference equation (DE) (or alternatively, 'auxiliary equation', see Goldberg 1986, p. 134, eq. {3.33 })) is defined by

$$Y_t - \phi_1 Y_{t-1} - \phi_2 Y_{t-2} - ... - \phi_p Y_{t-p} = 0, \tag{2.10.1}$$

where Y_t is a sequence of n variables for $t \in [1, n]$, and ϕ_k with $k \in \{1, 2, ..., p\}$ are the coefficients of the differential equation (see Box et al. (1970, p. 115, eq. {A4.1.1})). Y_T from (2.10.1) has the general solution (see e.g. Goldberg 1986, p. 163f.)

$$Y_t = \sum_{k=1}^{p} A_k P_k^t. \tag{2.10.2}$$

Here P_k are the roots of the CP defined in (2.9.2) and the A_k are constant weights independent of the time t. The calculation of the weights can be found in Appendix B.1. Hamilton (1994, p. 34, eq. 2.4.7) shows that the difference equation is invertible exactly when the roots P_k are unambiguous and lie within the unit circle, e.g. $|P_k| < 1$. Only in this case Y_t can be calculated directly using (2.10.2).

2.11 Visual Representation of the Coefficients of an AR(2) Process

For the AR(2) process Sansò (1985, p. 505, figure 3.5.2) has presented a visual method to show whether the associated process is stationary and -if so- whether the roots are complex or real. The limits for the triangle in Figure 2.1 are based on the consideration that for an AR(2) process the roots of the CP follow from

$$P_{1,2} = \frac{\alpha_1}{2} \pm \sqrt{\left(\frac{\alpha_1}{2}\right)^2 + \alpha_2} \tag{2.11.1}$$

and must be within the unit circle as a stationarity condition. This results in the two conditions

$$1 < \alpha_2 - \alpha_1 \qquad \text{and} \qquad \alpha_2 + \alpha_1 < 1.$$

These inequalities can be used for each other to determine the limits of the parameter $-1 \leq \alpha_2 \leq 1$. Also the condition of whether the roots are real or complex is missing. This depends only on the sign of the term under the root in (2.11.1). This thus provides us with the conditions

$$\left(\frac{\alpha_1}{2}\right)^2 < -\alpha_2 \qquad \text{if the roots are complex valued,}$$

$$\left(\frac{\alpha_1}{2}\right)^2 > -\alpha_2 \qquad \text{if the roots are real-valued and}$$

$$\left(\frac{\alpha_1}{2}\right)^2 = -\alpha_2 \qquad \text{if there is a double real root.}$$

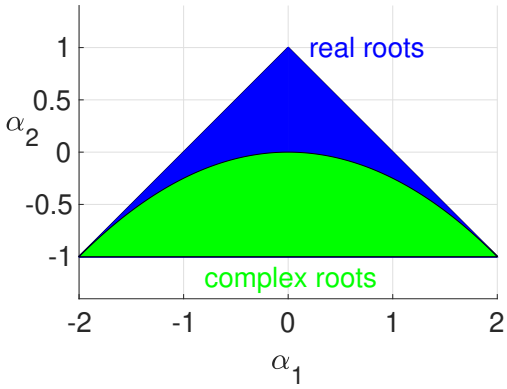

Figure 2.1: Visual representation of the possible coefficient pairings for stationary AR(2) processes shown as triangular in a plane.

Visually, these boundaries can be merged into the diagram in Figure 2.1. In this representation, the x-axis corresponds to the value of the first coefficient α_1 and the y-axis corresponds to the value of the second coefficient α_2. If the coordinates are in the green area, then the resulting roots are complex valued, if the coordinates are in the blue area, then the roots are real valued, and outside the triangle the coefficients give a nonstationary process. The line between the two ranges described by the equation $(\alpha_1/2)^2 - \alpha_2 = 0$ provide a special case. Here, the results pose a double root, meaning that both roots assume the same real value.

2.12 Fourier Transformations

The Fourier transformation (FT) for nonperiodic continuous processes $g(h)$ is given by the integral (see e.g. Buttkus 2000, p. 13, eq. 2.1)

$$G(\nu) := \mathcal{F}\{g(h)\}(\nu) = \int_{-\infty}^{\infty} g(h)e^{-i2\pi\nu h}dh.$$

The existence of this integral is guaranteed as long as the function $g(h)$ is square integrable:

$$\int_{-\infty}^{\infty} (g(h))^2 dh < \infty,$$

see Priestley (1983, p. 189). Furthermore, Buttkus (2000, p. 22, Table 2.1) shows some important properties of this transformation:

1. Scaling:

$$\mathcal{F}\{cg(h)\}(\nu) = cG(\nu) \text{ for any constant } c. \tag{2.12.1}$$

2. Addition:

$$\mathcal{F}\{g_1(h) + g_2(h)\}(\nu) = G_1(\nu) + G_2(\nu). \tag{2.12.2}$$

3. Multiplication::

$$\mathcal{F}\{g_1(h)g_2(h)\}(\nu) = G_1(\nu) \circledast G_2(\nu), \tag{2.12.3}$$

   here $\circledast$ means the convolution: $g_1 \circledast g_2 = \int_{-\infty}^{\infty} g_1(x)g_2(t-x)dx$.

4. Correlation:

$$\mathcal{F}\{g_1(h) \star g_2(h)\}(\nu) = G_1(\nu)G_2(\nu)^*, \tag{2.12.4}$$

   here $\star$ means the correlation: $g_1 \star g_2 = \int_{-\infty}^{\infty} g_1(x)g_2(x+t)dx$ and $.^*$ gives the complex conjugated value of the input. So $G_2(\nu)^*$ is the complex conjugated of $G_2(\nu)$.

Name	Description $g(x)$	Transform $G(\nu)$
Fourier transformation $\int_{-\infty}^{\infty} g(h)e^{-i2\pi\nu h}dh$	Continuous function (aperiodic)	Continuous function (aperiodic)
Periodic Fourier transformation $\frac{1}{T}\int_{-\frac{T}{2}}^{\frac{T}{2}} g(h)e^{-i2\pi\nu/Th}dh$	Continuous periodic function	Discrete sequence (Dirac delta function)

Table 2.1: Different types of Fourier transformations

5. Time shift:

$$\mathcal{F}\{g(h-c)\}(\nu) = G(\nu)e^{-i2\pi c\nu} \text{ for any constant } c.$$

In this thesis, no distinction is made between discrete and continuous FT. Sequences of observations are presented as the product of a continuous function with the Dirac delta comb, (for further information see section 2.15) which in turn is a continuous function that always takes a non-zero value only at equidistant intervals. Nevertheless, it should be noted that the result of the Fourier transformation is still continuous, but also becomes periodic. The period corresponds to the distance between two pulses of the Dirac delta comb (Δ_j). For symmetry reasons, this function is fully described by the value of half the period. This frequency at the discrete value of half the periodic

$$\nu_n = \frac{1}{2\Delta_j}$$

is called the Nyquist frequency (see for example Grenander 1959, p. 316). It should be mentioned that the researches distinguish between two FTs shown in Table 2.1 (see Watts et al. 1968, p. 26). The inverse of the FT is called inverse Fourier transform (IFT) and is calculated by

$$\mathcal{F}^{-1}\{G(\nu)\}(h) = \int_{-\infty}^{\infty} G(\nu)e^{i2\pi\nu h}d\nu.$$

For the IFT, the conditions 1-4 of section 2.6 apply just as for the FT. And for its frequency shift

$$\mathcal{F}^{-1}\{G(\nu-c)\}(h) = g(h)e^{i2\pi c\nu} \text{ for any constant } c \tag{2.12.5}$$

applies. Moreover, the relation between the multiplication and the convolution in the FT and in the IFT results in the so-called convolution theorem, which states that the convolution in the time domain results in a multiplication in the frequency domain and vice versa (see Buttkus 2000, p. 26, Table 2.2).

2.13 Power Spectral Density

The energy $\mathbb{E}(.)$ of a time series $\{\mathcal{S}_j\}_{j\in\mathbb{Z}}$ can be calculated using

$$\mathbb{E}(\mathcal{S}_t) = \int_{-\infty}^{\infty} \mathcal{S}_t^2 dt,$$

but can also be calculated by the Parseval's relation

$$\mathbb{E}(\{\mathcal{S}_j\}_{j\in\mathbb{Z}}) = \int_{-\infty}^{\infty} |\mathcal{F}\{\{\mathcal{S}_j\}_{j\in\mathbb{Z}}\}(\nu)|^2 d\nu$$

in the spectral domain (see Priestley 1983, p. 204). Since $|\mathcal{F}\{\{\mathcal{S}_j\}_{j\in\mathbb{Z}}\}(\nu)|^2$ is not a measure of energy but rather an energy density, it is also called the energy spectral density (ESD), or power spectral density (PSD) like in Watts et al. (1968, p. 217). Using the convolution theorem (see Priestley 1983, p. 211), the PSD can be interpreted as the FT of the discrete covariances $(\{\Sigma_j\}_{j\in\mathbb{Z}})$. This relation is shown in Appendix A.1:

$$\begin{aligned}\mathcal{F}^{-1}\{|\mathcal{F}\{\{\mathcal{S}_{j2}\}_{j2\in\mathbb{Z}}\}(\nu)|^2\}(t) &= \{\Sigma_j\}_{j\in\mathbb{Z}} \\ \Leftrightarrow |\mathcal{F}\{\{\mathcal{S}_{j2}\}_{j2\in\mathbb{Z}}\}(\nu)|^2 &= \mathcal{F}\{\{\Sigma_j\}_{j\in\mathbb{Z}}\}(\nu). \end{aligned} \tag{2.13.1}$$

Here $\mathcal{F}^{-1}\{.\}(t)$ denotes the IFT (see Buttkus 2000, p. 13)

$$\mathcal{F}^{-1}\{\mathcal{G}(\nu)\}(t) := \frac{1}{2\pi}\int_{-\infty}^{\infty}\mathcal{G}(\nu)e^{i2\pi\nu t}d\nu.$$

This is the Wiener-Khintchine theorem (see Priestley 1983, p. 219). The equation (2.13.1) means that the FT of the discrete variances is a quadratic function, and thus can only assume values greater than or equal to zero.
The FT of the discrete covariances, i.e. the PSD, of an AR(p) process is (see Box et al. 1970, p. 56)

$$\begin{aligned}\mathcal{H}^2(\nu) &:= \mathcal{F}\{\{\Sigma_j\}_{j\in\mathbb{Z}}\}(\nu) \\ &= \frac{{\sigma_\mathcal{E}}^2}{|1-\alpha_1 e^{-i2\pi\nu}-\alpha_2 e^{-i4\pi\nu}-...-\alpha_p e^{-i2p\pi\nu}|^2}. \end{aligned} \tag{2.13.2}$$

2.14 The Magic Square

In time series analysis, a distinction is made between two domains: the time domain in which time series are represented, and the frequency (or spectral) domain (or spectral domain) for the FT. This results in a transformation between these domains by the FT and the IFT. Krasbutter et al. 2015 introduced the Magic Square as a well-arranged representation of four quantities of a discrete finite moving average (MA) process in time and frequency domain. Loth et al. 2021 show an extension of the magic square for AR(p) processes by replacing them by infinite MA processes, i.e.

$$\begin{aligned}\mathcal{S}_t &= \alpha_1\mathcal{S}_{t-1}+\alpha_2\mathcal{S}_{t-2}+...+\alpha_p\mathcal{S}_{t-p}+\mathcal{E}_t \\ &= \sum_{j=1}^{\infty}\theta_j\mathcal{E}_{t-j}+\mathcal{E}_t.\end{aligned}$$

The illustration in Figure 2.2 of this magic square shows that there are always two paths from the upper states to the lower states: first, the direct path, and second, the 'detour' via a temporary domain change to execute the corresponding application. In particular, Figure 2.2 illustrates the relationship between the correlation and the Fourier transform found by a multiplication of two complex conjugate Fourier transformations. This relation is represented mathematically in (2.12.4).

It should be mentioned that this Figure is constructed from Schuh (2016, Figure 6), which shows the magic square for an AR process. Since in both representations, an integration of a random variable is needed, a Lebesque integral is used to compute the FT of the signal. This FT can then be used to compute the spectrum.

2.15 Dirac Delta Function and Dirac Comb

The Dirac delta function (DDF) ($\delta(h)$) is a mathematical construct defined only by mathematical formulas. Buttkus (2000, p. 41) defines the DDF with the help of a continuous function $x(h)$ by

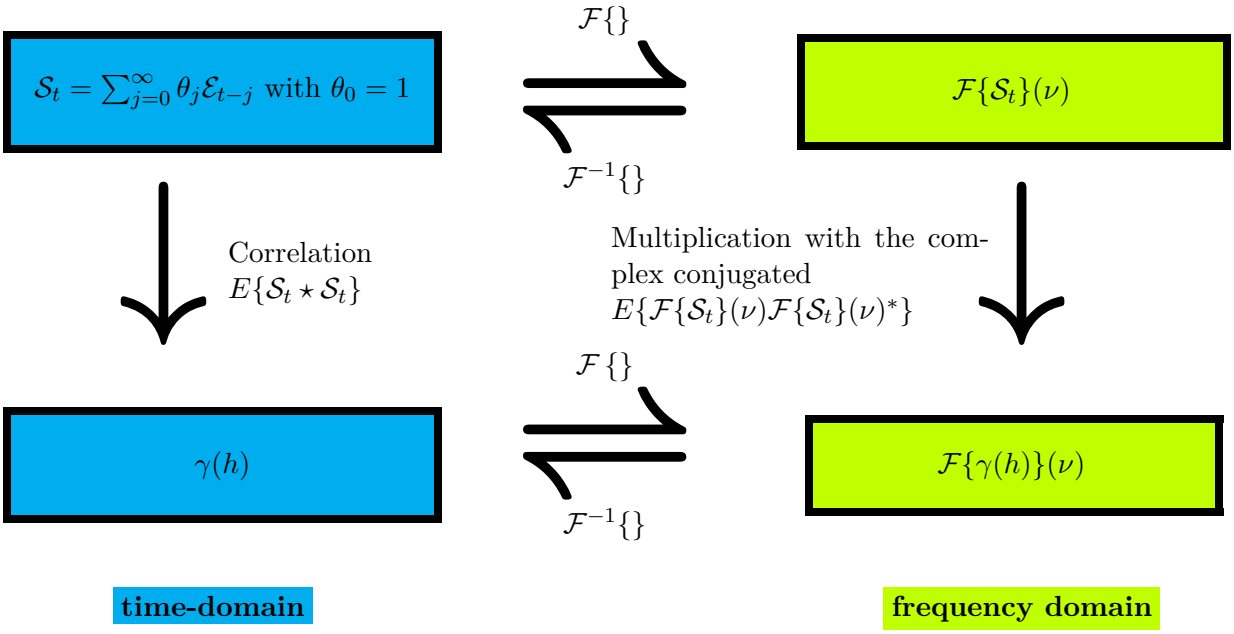

Figure 2.2: Visualization of the transition from correlation to multiplication with the complex conjugate counterpart by the FT.

the two equations

$$\begin{aligned} \delta(h - j_0) &= 0 && \text{if } h \neq j_0 \\ \int_{-\infty}^{\infty} \delta(h - j_0) x(h) dh &= x(j_0). && (2.15.1) \end{aligned}$$

A geometric interpretation of the DDF is deliberately omitted, since only the mathematical properties of the function are used here. A periodic series of DDF with a period of Δ_j is called a Dirac delta comb (DC) (see Buttkus 2000, p. 61). This corresponds to an infinite number of DDFs summed up, whose values j_0 follow each other equidistantly with distance Δ_j, e.g.

$$\sum_{l=-\infty}^{\infty} \delta(h - l\Delta_j).$$

For the DC, there are again two important properties. On the one hand, multiplying the DC with a continuous function $x(h)$ results in a discrete series $\{x_j\}_{j\in\mathbb{Z}}$:

$$\sum_{l=-\infty}^{\infty} \delta(h - l\Delta_j) x(h) = \{x_j\}_{j\in\mathbb{Z}}. \quad (2.15.2)$$

And on the other hand, Buttkus (2000), p. 46, eq. (3.28) shows that the FT of the DC is provided by:

$$\mathcal{F}\{\sum_{l=-\infty}^{\infty} \delta(h - l\Delta_j)\}(\nu) = \frac{1}{\Delta_j} \sum_{l=-\infty}^{\infty} \delta(\nu - \frac{l}{\Delta_j}).$$

In particular, for a DC with distance $\Delta_j = 1$, this means that the FT again is a DC with distance 1 (at least after the infinite sum has been rearranged):

$$\mathcal{F}\{\sum_{l=-\infty}^{\infty} \delta(h - l)\}(\nu) = \sum_{l=-\infty}^{\infty} \delta(\nu - l). \quad (2.15.3)$$

2.16 Time Variable AR Process

Dahlhaus 1997 defines the TVAR[1]. process as:

$$\mathcal{S}_t = \alpha_1(t)\mathcal{S}_{t-1} + \alpha_2(t)\mathcal{S}_{t-2} + ... + \alpha_p(t)\mathcal{S}_{t-p} + \mathcal{E}_t. \tag{2.16.1}$$

Analogous to time constant AR(p) processes, there are $p+1$ summands, and $\mathcal{E}_t$ is a constant i.i.d sequence with s variance $\sigma^2_{\mathcal{E}}$ over the entire time range. Here, the time series $\mathcal{S}_t$ no longer has to be a stationary process, and the coefficients ($\alpha_k(t)$, $k \in \{1, 2, ..., p\}$) are now functions in the time domain with parameter t. Therefore, the number of parameters of a time variable autoregressive process of order p (TVAR(p)) process is different from p.

2.17 Analytical Calculation of the Roots of a Polynomial

Given a polynomial of order p of the type

$$\mathcal{P}_p(x) = x^p + c_1 x^{p-1} + c_2 x^{p-2} + ... + c_p,$$

the fundamental theorem of algebra says that this polynomial has exactly p (maybe complex valued) zeros (see Bronstein et al. 2006, p. 44). Unfortunately, there exists purely analytical solutions for the problem if the order $p \in \{1, 2, 3, 4\}$, which furthermore dates back to the 19^{th} century (see Abel et al. 1889 or Galois 1846). In the following, the analytical solutions for polynomials up to order 3 are presented. Polynomials of order four are not used in this work.

1. First order polynomials

   $$\mathcal{P}_1(x) = x + c_1 \stackrel{!}{=} 0$$

   The roots of this polynomial can be found directly with

   $$P_1 = -c_1. \tag{2.17.1}$$

2. Second order polynomials

   $$\mathcal{P}_2(x) = x^2 + c_1 x + c_2 \stackrel{!}{=} 0$$

   The roots of this polynomial can be calculated using the so-called pq-formula (see Abramowitz et al. 1964, p. 17 eq. 3.8.1):

   $$P_{1,2} = -\frac{c_1}{2} \pm \sqrt{\left(\frac{c_1}{2}\right)^2 - c_2}. \tag{2.17.2}$$

3. Third order polynomials

   $$\mathcal{P}_3(x) = x^3 + c_1 x^2 + c_2 x + c_3 \stackrel{!}{=} 0$$

   The analytic calculation of the roots for this polynomial is found in Abramowitz et al. (1964, p. 17 eq. 3.8.1) and is much more complicated. Therefore, the calculation of the solution is divided into three steps:

   - Set auxiliary values q and r:

     $$q = \frac{c_2}{3} - \left(\frac{c_1}{3}\right)^2 \tag{2.17.3}$$

     $$r = \frac{1}{6}(c_1 c_2 - 3c_3) - \left(\frac{c_1}{3}\right)^3. \tag{2.17.4}$$

1. In literature TVAR also means time varying vector autoregressive processes. These are multivariate autoregressive processes with correlated time series (see e.g. Haslbeck et al. 2021, Li et al. 2024 or Cubadda et al. 2025). But these are not part of this thesis

- Set auxiliary values s_1 and s_2:

$$s_1 = \sqrt[3]{r + \sqrt{q^3 + r^2}} \tag{2.17.5}$$

$$s_2 = \sqrt[3]{r - \sqrt{q^3 + r^2}}. \tag{2.17.6}$$

- Calculation of the roots

$$P_1 = (s_1 + s_2) - \frac{c_1}{3} \tag{2.17.7}$$

$$P_2 = -\frac{s_1 + s_2}{2} - \frac{c_1}{3} + i\frac{\sqrt{3}}{2}(s_1 - s_2) \tag{2.17.8}$$

$$P_3 = -\frac{s_1 + s_2}{2} - \frac{c_1}{3} - i\frac{\sqrt{3}}{2}(s_1 - s_2). \tag{2.17.9}$$

2.18 Akaike Information Criterium

Akaike 1974 has developed the Akaike information criterion (AIC) to compare models of different complexity for estimation. He shows that the minimum of

$$AIC = 2m - \ln(L(\boldsymbol{y}, \boldsymbol{\phi}))$$

gives the best number of parameters m in the parameter vector ϕ. L is the likelihood function of the observations ($\boldsymbol{y}$) and the adjusted observations ($\tilde{\boldsymbol{y}}(\boldsymbol{\phi})$). If there are n observations and assuming that $L(\cdot)$ is the normal distribution, the residual sum of squares (RSS)

$$\breve{\sigma}^2_{\mathcal{E}} := \frac{(\boldsymbol{y} - \tilde{\boldsymbol{y}}(\boldsymbol{\phi}))^T(\boldsymbol{y} - \tilde{\boldsymbol{y}}(\boldsymbol{\phi}))}{n} \tag{2.18.1}$$

can be used instead. The AIC can then be represented in simplified terms by

$$AIC = \ln(\breve{\sigma}^2_{\mathcal{E}}) + \frac{2(m+1)}{n}. \tag{2.18.2}$$

2.19 How to Determine the best Order of an AR Process

The order of an AR process plays a fundamental role for the approximation of a stationary time series. According to Buttkus (2000, section 4.11), in case of the model order p, two things have to be balanced against each other: on the one hand, using a low number of parameters results in a model error. While on the other hand, using to many parameters leads to an error caused by over parametrization. Buttkus (2000, section 4.11) also shows that the order p of an AR process can be determined in three steps:

1. Set a lower (b_l) and upper boundary (b_u) for the order of the AR processes:

$$b_l \leq p \leq b_u.$$

2. Approximate the time series with AR process of all orders in the interval and determine the corresponding AIC:

$$AIC = \ln(\breve{\sigma}^2_{\mathcal{E}}) + \frac{2(p+1)}{n}.$$

   Here, p is the order of the AR Process, n is the number of observations and $\breve{\sigma}^2_{\mathcal{E}}$ is the variance of the white noise computed by the mean of the RSS:

$$\breve{\sigma}^2_{\mathcal{E}} = \frac{1}{n-p}\sum_{j=p}^{n}\left(\mathcal{S}_j - \sum_{k=1}^{p}\alpha_k\mathcal{S}_{j-k}\right)^2.$$

3. Find the first local minimum AIC in the interval $[b_u, b_o]$ and use the corresponding AR process. By choosing the first minimum, the modelling of the noise (over-fitting) should be prevented.

2.20 Gamma Function and the Pochhammer Symbol

The gamma function ($\mathbb{\Gamma}(t)$) is defined by the integral

$$\mathbb{\Gamma}(t) = \int_0^\infty x^{t-1} e^{-x} dx$$

(see Abramowitz et al. 1964, p. 255, eq. 6.1.1) and represents the continuation of the discrete faculty function:

$$\mathbb{\Gamma}(t+1) = t!$$

(see Abramowitz et al. 1964, p. 255, eq. 6.1.5). The function $\mathbb{\Gamma}(t)$ is sketched in Figure 2.3 which shows how the continuous function runs for the natural numbers $\hat{t} \in \mathbb{N}$ through the discrete values $(\hat{t}-1)!$. Another special function is the Pochhammer symbol ($\mathbb{P}(t,j)$), which describes the quotient

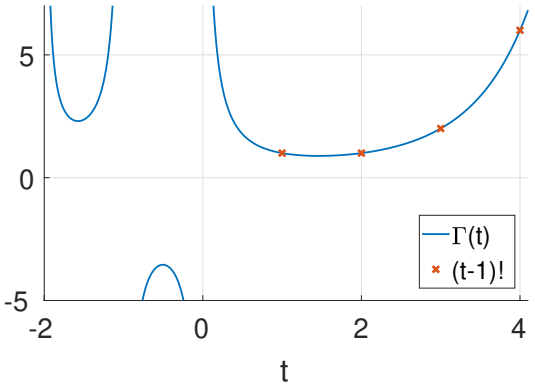

Figure 2.3: The track of the gamma function and how it proceeds through the solutions of $t!$ with $t = 0, 1, 2, 3, ...$

of two gamma functions, i.e.

$$\mathbb{P}(t,j) := \frac{\mathbb{\Gamma}(t+j)}{\mathbb{\Gamma}(t)} = \prod_{k=0}^{j-1} t+k$$

with $j \geq 0$ (see p. 256, eq. 6.1.22) if $t, j > 0$.

Chapter 3

Continuous Covariance Function for Time Constant AR Processes

Although this thesis focuses on time-variable AR processes, this chapter provides new important insights for the LSC of stationary processes. The results will be used as foundation for the nonstationary LSC.

When a signal has been measured, one is generally also interested in discrete values between the individual measurements. These can be determined by LSC as presented in section 2.2, but only if a valid CF is known that continues the discrete covariances of the process used to model the signal. In this chapter, a continuous CF is created which is precisely matched by the discrete covariances of a stationary AR process. The Y.-W. equations can be modified to the DE, which posses an unambiguous solution. Its development demands two steps: first, the roots of the CP are derived. In the second step, the weights can be determined from any p equations of the Y.-W. equations. In order to prove that this function is a suitable and valid CF, it must be shown that it is positive semi-definite. Furthermore the relation between the PSD of the discrete CF and the PSD of the continuous CF is examined. Chapter 3 comply with Korte et al. 2021, but goes into more detail and further provides an additional framework for AR processes with negative roots.

3.1 Construction of a Continuous Covariance Function

Section 2.8 has shown how to gain the Y.-W. equations for AR(p) processes. Combining both sides of the Y.-W. equations of order $j \neq 0$ (see (2.8.3)) gives a difference equation (DE) as described in section 2.10:

$$\Sigma_j - \sum_{k=1}^{p} \alpha_k \Sigma_{|j-k|} = 0 \qquad \forall j \neq 0. \tag{3.1.1}$$

It was shown in section 2.10 that for the DE any discrete covariance Σ_j can be calculated directly from the sum of the p-th powers of weighted bases

$$\Sigma_j = \sum_{k=1}^{p} A_k P_k^{|j|}, \tag{3.1.2}$$

where P_k are the roots of the CP, and A_k are weights that can be uniquely determined from any p discrete CF (for details see Appendix B.1).
It should be noted that Σ_0 includes the variance of the white noise ($\sigma_\mathcal{E}^2$) (see (2.8.2)). The DE deriving from the Y.-W. equation of order 0 then is

$$\Sigma_0 - \sigma_\mathcal{E}^2 - \sum_{k=1}^{p} \alpha_k \Sigma_k = 0.$$

Nevertheless, the direct calculation in (3.1.2) is also valid for the variance Σ_0. The reason for this is that the DE are only defined for covariances Σ_k with $k \geq p$, while the direct calculation is also valid for Σ_k with $j < p$ (since these are used in the DE of higher order). That means that the variance of the signal and the variance of the noise cannot be separated from each other just via the direct formula.
Nevertheless, (3.1.2) is only useful to determine the discrete covariances ($\{\Sigma_j\}_{j\in\mathbb{Z}}$), but not the **continuous** CF ($\gamma : \mathbb{R} \to \mathbb{R}$) we are looking for. This demands the replacement of the discrete parameter $j \in \mathbb{N}_0$ in (3.1.2) with a continuous parameter $h \in \mathbb{R}$ in order to create continuous function

$$\gamma(h) := \sum_{k=1}^{p} A_k P_k^{|h|}. \tag{3.1.3}$$

If P_l is a negative real-valued number for any $l \in \{1, 2, ..., p\}$, then, due to

$$P_l^{|h|} = |P_l|^{|h|} e^{i\pi|h|}$$

with $e^{i\pi|h|} \in \mathbb{C}\ \forall h \notin \mathbb{Z}$, the continuous function $\gamma(h)$ becomes complex. But this contradicts the definition in (2.6.1). The continuous CF must be limited to a section of real values, so the construction of a continuous CF is precisely represented by

$$\gamma(h) = \mathcal{R}\left(\sum_{k=1}^{p} A_k P_k^{|h|}\right), \tag{3.1.4}$$

with $\mathcal{R}(.)$ being the real part of the complex number. A more detailed explanation as well as a comparison with absolute values can be found in Appendix B.2.
In the sections 3.2 and 3.2, the PSD of the discrete CF ($\{\Sigma_j\}_{j\in\mathbb{Z}}$) is firstly compared to the PSD of the continuous CF $\gamma(h)$ (see section 3.2) and then secondly, in section 3.3, the positive semi-definiteness of the continuous CF is proven.

3.2 Comparison of the Spectra for the Discrete and the Continuous Covariance Function

In order to compare the PSDs of both CFs, they must first be derived. In the case of the discrete CF, the spectrum derives from (2.13.2). The PSD of continuous CF however must be derived via the FT. Then the continuous CF is derived.

3.2.1 Power Spectral Density of the Discrete Covariance Function

The PSD of the discrete CF is known and has already been presented in section 2.13:

$$\begin{aligned}\mathcal{H}^2(\nu) &:= \mathcal{F}\{\{\Sigma_j\}_{j\in\mathbb{Z}}\}(\nu) \\ &= \frac{{\sigma_\mathcal{E}}^2}{|1 - \alpha_1 e^{-i2\pi\nu} - \alpha_2 e^{-i4\pi\nu} - ... - \alpha_p e^{-i2p\pi\nu}|^2}.\end{aligned} \tag{3.2.1}$$

in order to simplify its comparison with the PSD of continuous CF, this thesis limits its examination to the AR(1) and AR(2) processes. This is acceptable since both the discrete CF and the continuous CF are written as weighted potency sum of the roots P_k. These roots occur only as real numbers or as complex conjugated pairs, whereby a real root corresponds to an AR(1) process, and a pair of complex conjugated roots corresponds to an AR(2) process. Furthermore, it is appropriate to perform a parameter change and to replace the coefficients α_k with the help of the CP by the means of the roots P_k. For the AR(1) process, the CP (from (2.9.1)) is

$$\chi(x) = x - \alpha_1,$$

immediately providing the roots

$$\chi(P_1) = 0 \qquad \Rightarrow \qquad P_1 = \alpha_1. \tag{3.2.2}$$

However, for the CP of the AR(2) process

$$\chi(x) = x^2 - \alpha_1 x - \alpha_2,$$

it is known that the roots could be calculated using the pq-formula (2.17.2) with $c_1 = -\alpha_1$ and $c_2 = -\alpha_2$:

$$P_{1,2} = \frac{\alpha_1}{2} \pm \sqrt{\left(\frac{\alpha_1}{2}\right)^2 + \alpha_2}.$$

From this, it is easy to obtain that

$$\alpha_1 = P_1 + P_2 \tag{3.2.3}$$
$$\alpha_2 = -P_1 P_2. \tag{3.2.4}$$

With the help of the general solution of the PSD and the conversion between coefficients (α_k) and roots (P_k), the PSD for the AR(1) and AR(2) process can be calculated directly. A detailed derivation can be found in Appendix B.3. Using (3.2.2), the PSD for the AR(1) process is given by

$$\mathcal{H}^2(\nu) = \frac{{\sigma_\mathcal{E}}^2}{1 - 2P_1\cos(2\pi\nu) + {P_1}^2},$$

and for the AR(2) process the PSD derives from the use of (3.2.3) and (3.2.4)

$$\mathcal{H}^2(\nu) = \frac{{\sigma_\mathcal{E}}^2}{1 - 2(P_1+P_2)\cos(2\pi\nu) + {P_1}^2 + {P_2}^2 + P_1P_2(2 + 2\cos(4\pi\nu) - 2(P_1+P_2)\cos(2\pi\nu) + P_1P_2)}.$$

3.2.2 Power Spectral Density of the Continuous Covariance Function

To determine the PSD of the continuous CF, the Fourier transformation of $\gamma(h)$ is needed. This transformation is done in Appendix B.4 and results in

$$\begin{aligned}\Gamma_p(\nu) :&= \mathcal{F}\{\gamma(h)\}(\nu) \\ &= \sum_{k=1}^{p} A_k \frac{-2\ln(P_k)}{\ln(P_k)^2 + (2\pi\nu)^2}.\end{aligned}$$

Especially for the AR(1) and AR(2) process the weights for the CF have been derived (see Appendix B.1), which results in the PSD for the AR(1) process

$$\Gamma_1(\nu) = \frac{{\sigma_\mathcal{E}}^2}{1 - {P_1}^2} \frac{-2\ln(P_1)}{\ln(P_1)^2 + (2\pi\nu)^2} \tag{3.2.5}$$

and for the AR(2) process

$$\begin{aligned}\Gamma_2(\nu) = &\frac{{\sigma_\mathcal{E}}^2 P_1}{(P_2 - P_1)(1 - {P_1}^2)(P_1P_2 - 1)} \frac{-2\ln(P_1)}{\ln(P_1)^2 + (2\pi\nu)^2} \cdots \\ &+ \frac{{\sigma_\mathcal{E}}^2 P_2}{(P_1 - P_2)(1 - {P_2}^2)(P_1P_2 - 1)} \frac{-2\ln(P_2)}{\ln(P_2)^2 + (2\pi\nu)^2}.\end{aligned} \tag{3.2.6}$$

3.2.3 Relationship between the Covariance Functions

A direct comparison between the PSD of the continuous CF and the discrete CF is not necessary, since $\mathcal{H}^2(\nu) \neq \Gamma(\nu)$ applies without limitation to the general case. To establish a connection between the CFs, $\gamma(h)$ is converted to $\{\Sigma_j\}_{j\in\mathbb{Z}}$ using the DC whose mathematical property is described in (2.15.2). Figure 3.2 is a variation of the magic square from Krasbutter et al. 2015 (see section 2.14) and represents exactly this transformation, i.e. shows the time-domain in relation to the frequency domain with its Fourier transformed counterparts. The discretization of a continuous function corresponds to the multiplication with a DC with period $\Delta l = 1$ (see (2.15.2)). According to the convolution theorem, the FT of the continuous CF can be transferred to the PSD of the AR(p) process by convoluting it with a DC whose period is again $1/\Delta l = 1$ (see (2.15.3)).
This is shown in Figure 3.1, where the dependencies of the discrete and continuous CF and its FT are illustrated by the arrows. The arrow reaching from the right top to the right bottom deserves special attention, as this correlation has not yet been proven and is derived via a 'detour'. Starting in the upper right, the FT of the continuous CF ($\Gamma_p(\nu)$), the function is transformed by the IFT into the function $\gamma(h)$ in the time domain. Here, the discrete covariances $\{\Sigma_j\}_{j\in\mathbb{Z}}$ are extracted by multiplying $\gamma(h)$ with the DC. Finally, by computing the FT of the sequence of discrete covariances ($\{\Sigma_j\}_{j\in\mathbb{Z}}$), the PSD of the AR process is calculated. Applying the convolution theorem (see Buttkus 2000, p. 22, Table 2.1), it follows that the function $\Gamma_p(\nu)$ is transformed into PSD $\mathcal{H}^2(\nu)$ by convoluting $\Gamma_p(\nu)$ with the DC. For clarification, the magic square is demonstrated with an AR(3) process in Figure 3.2. In this case, the variance of the noise ($\sigma_\mathcal{E}^2$) is equal to one and the roots $P_1 = 0.40 + 0.68i$, $P_2 = 0.40 - 0.68i$ and $P_3 = 0.64$ all have a positive real part.

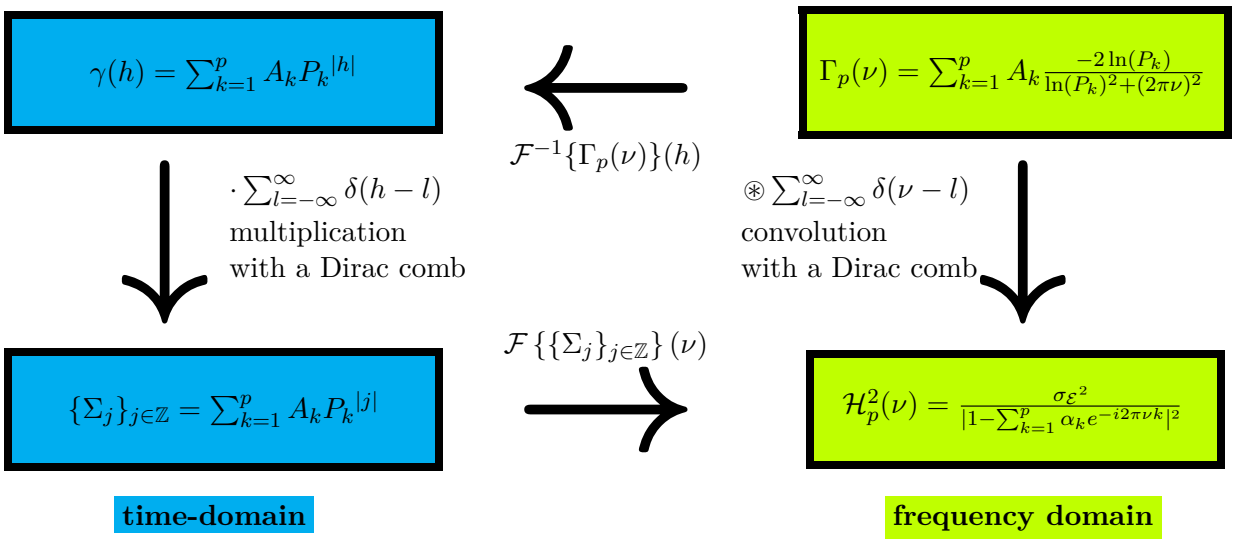

Figure 3.1: Conversion of the PSD formula in the magic square, once by the means of the 'detour' in the time-domain, and once directly in the frequency domain.

The transformation described in Figure 3.2 can also be represented pictorially by performing the following two steps.

1. First the $\Gamma_p(\nu)$ is copied and plotted with its maximum at each integer $(\ldots -2, -1, 0, 1, 2, \ldots)$,

2. then the values of all these functions are summed up for each frequency.

The general proof that, without limiting the general applicability, the convolution $\Gamma_p(h) \circledast \sum_{l=-\infty}^{\infty} \delta(\nu - l)$ on the right side is equal to $\mathcal{H}_p^2(\nu)$, is given in the Appendix B.5.

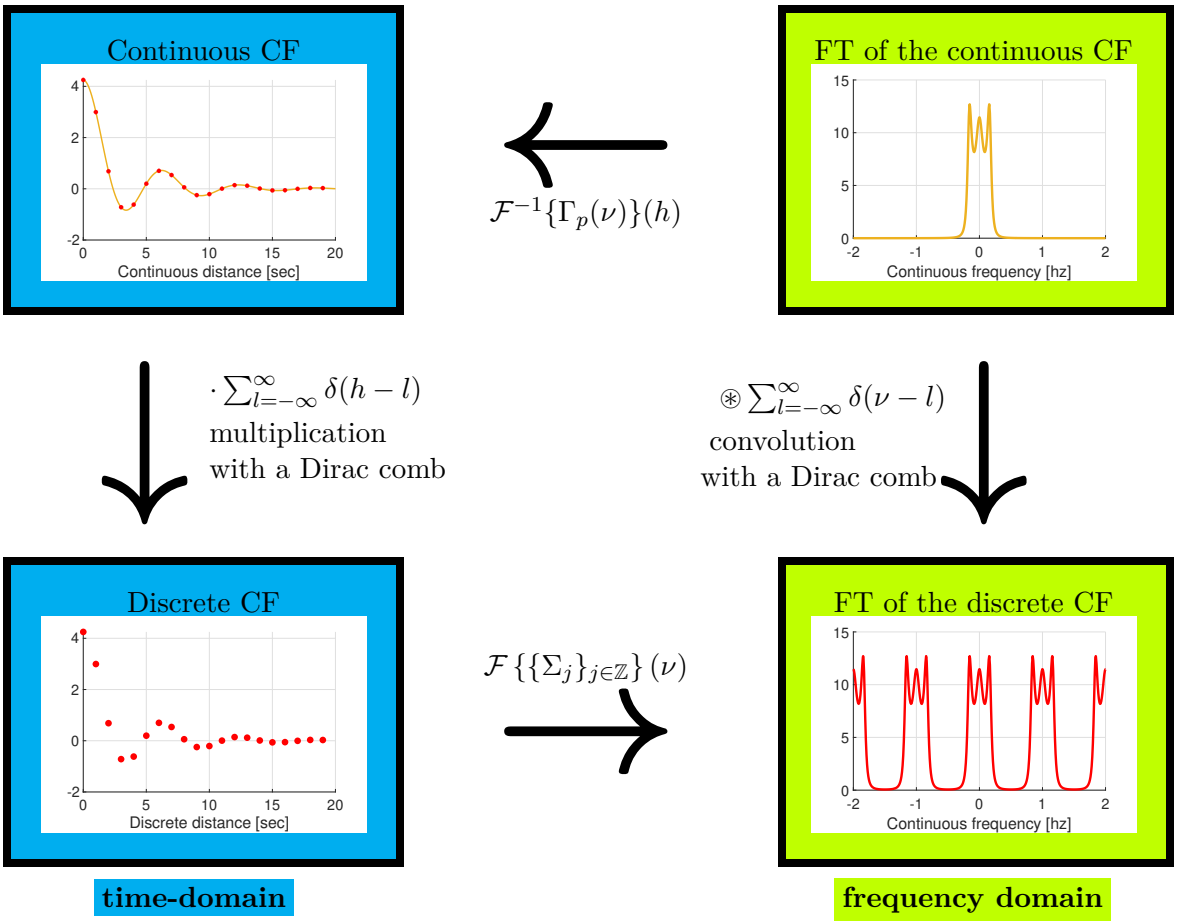

Figure 3.2: Example of a magic square for the PSD of an AR(3) process with the roots: $P_1 = 0.40 + 0.68i$, $P_2 = 0.40 - 0.68i$, $P_3 = 0.64$ and variance $\sigma_{\mathcal{E}}^2 = 1$.

3.3 Suitability as a Covariance Function

Since the PSD of the discrete CF and the continuous CF do not coincide ($\mathcal{H}_p^2(\nu) \neq \Gamma_p(\nu)$), that the continuous function ($\gamma(h)$) is a valid CF has yet to be demonstrated. So, it has to be proven that $\gamma(h)$ meets the conditions of a CF given in section 2.6:

1. $\gamma(0) > 0$.
   The discrete CF meets the first condition due to the fact that it is a CF. From $\gamma(0) = \Sigma_0 > 0$ follows that the first condition is also met for $\gamma(h)$.

   To prove the following conditions, it is sufficient to look at the individual summands of $\gamma(h)$ in (3.1.4) provided by $A_k P_k^{|h|}$: if they meet the conditions, the sum does as well.

2. $|\gamma(h)| \leq \gamma(0)\ \forall h \in \mathbb{R}$.
   Since every single root P_k lies within the unit circle ($|P_k| < 1$), each addend becomes smaller with increasing distance $|h|$. In particular, $\gamma(h)$ is largest at distance $h = 0$.

3. $\gamma(h) = \gamma(-h)$.
   Since the continuous distance h occurs only in a absolute value, this condition is fulfilled.

4. $\gamma(h)$ is a positive semi-definite function.

In order to prove the last condition, it is not quite sufficient to only rely on the individual summand. Rather, it demands a further differentiation depending on whether the roots are real valued, or whether the roots occur as conjugate pairs. In the first case, a single summand, and in the latter

case, both summands of a complex conjugated pair can be considered.
Beginning with the AR(1) process, (3.1.4) is used:

$$\gamma(h) = \mathcal{R}\left(A_1 P_1^{|h|}\right).$$

Since the coefficients A_k only appear as complex conjugated pairs or as real-valued numbers, A_1 is always a real number for the AR(1) process. Therefore:

$$\gamma(h) = A_1 \mathcal{R}\left(P_1^{|h|}\right).$$

If P_1 is negative, it can be rewritten as

$$P_1^{|h|} = (e^{i\pi}|P_1|)^{|h|} = (\cos(\pi|h|) + i\sin(\pi|h|))|P_1|^{|h|}.$$

After taking the real part of the complex values, there is only

$$\cos(\pi|h|)|P_1|^{|h|} = \cos(\pi h)|P_1|^{|h|}$$

left, where due to the symmetry of the cosine relative to the y-axis the absolute value of h can be exchanged with the distance itself: $\cos(|h|) = \cos(h) = \cos(-h)$. in the case of a negative root $P_1 < 0$, this means the function $\gamma(h)$ is derived by the means of multiplication of

$$\gamma(h) = \cos(\pi h) A_1 |P_1|^{|h|} \qquad \text{if } P_1 < 0.$$

As has been shown in Appendix B.8, the FT of a product of a positive definite function ($A_1|P_1|^{|h|}$) with a cosine remains positive definite. However, the case of a positive root remains to be checked. To do this, one needs to simply apply the general FT of $\gamma(h)$ from Appendix B.4 to the AR(1) process and replace A_1 with $\sigma_\mathcal{E}^2/(1-P_1^2)$ by using (B.1.3):

$$\Gamma(\nu) = \frac{\sigma_\mathcal{E}^2}{1-P_1^2} \frac{-2\ln(P_1)}{(\ln(P_1))^2 + (2\pi\nu)^2} \overset{!}{\geq} 0.$$

The individual numerators and denominators are checked separately, while also showing that they are all positive. The square terms ($\sigma_\mathcal{E}^2$, $(\ln(P_1))^2$ and $(2\pi\nu)^2$) are all larger than zero. Furthermore, P_1 lies in the unit circle, which is equivalent to $|P_1| < 1$. This results in the fulfilment of the two conditions required to prove the positive definiteness of the CF of AR(1) processes: it holds $P_1^2 < 1$ and also $1 - P_1^2 > 0$, while the property $\ln(P_1) < 0$ is valid. From this follows the last condition: $-2\ln(P_1) > 0$. Thus, all factors or the quotients are greater than zero, remaining the positive definiteness is proven.
It remains the case of the AR(2) process with two complex conjugated roots (P_1=P_2^*). Here, the covariance function is

$$\gamma(h) = A_1 P_1^{|h|} + A_2 P_2^{|h|},$$

i.e. the sum of two roots that are potentiated by h and multiplied by the weights A_1 and A_2. Since both $A_1 = A_2^*$, and $P_1^{|h|} = \left(P_2^{|h|}\right)^*$ apply, $\gamma(h)$ is the sum of a complex number and its complex conjugated counterpart. Since this is a real value, the real part operator in (3.1.4) is not necessary. But it also applies for the FT $\Gamma(\nu) = \mathcal{F}\{\gamma(h)\}(\nu)$ it applies that $\Gamma(\nu)$ is the sum of two complex conjugated values. This follows from section 2.12, especially from the linearity of FT in (2.12.1) and (2.12.2). Thus, it follows for the FT:

$$\Gamma(\nu) = \mathcal{F}\{\gamma(h)\}(\nu) = A_1\mathcal{F}\{P_1^{|h|}\}(\nu) + A_2\mathcal{F}\{P_2{}^{|h|}\}(\nu).$$

Rewriting P_1 and P_2 as $P_1 = re^{i\phi}$ and $P_2 = re^{-i\phi}$, it can be seen that

$$\begin{aligned}\Gamma(\nu) &= A_1\mathcal{F}\{(re^{i\phi})^{|h|}\}(\nu) + A_2\mathcal{F}\{(re^{-i\phi})^{|h|}\}(\nu) \\ &= A_1\mathcal{F}\{r^{|h|}(\cos(\phi|h|) + i\sin(\phi|h|))\}(\nu) + A_2\mathcal{F}\{r^{|h|}(\cos(\phi|h|) - i\sin(\phi|h|))^{|h|}\}(\nu).\end{aligned}$$

Also taking into account the linearity of the FT,

$$\begin{aligned}\Gamma(\nu) = A_1\mathcal{F}\{r^{|h|}\cos(\phi|h|)\}(\nu) + iA_1\mathcal{F}\{r^{|h|}\sin(\phi|h|)\}(\nu)...\\ +A_2\mathcal{F}\{r^{|h|}\cos(\phi|h|)\}(\nu) - iA_2\mathcal{F}\{r^{|h|}\sin(\phi|h|)\}(\nu)\end{aligned}$$

means that $\Gamma(\nu)$ is a sum of two complex conjugated values. This sum is equal to twice its real part:

$$\Gamma(\nu) = 2\mathcal{R}\left(A_1\mathcal{F}\{P_1^{|h|}\}(\nu)\right).$$

Further (B.1.5) and (B.4.3) show that

$$A_1 = \frac{-\sigma_\mathcal{E}^2 P_1}{(P_2-P_1)(1-P_1^2)(1-P_1P_2)} \qquad \text{and} \qquad \mathcal{F}\{P_1^{|h|}\}(\nu) = \frac{-2\ln(P_1)}{(\ln(P_1))^2+(2\pi\nu)^2},$$

are valid, remaining in

$$\begin{aligned}\Gamma(\nu) &= 2\mathcal{R}\left(\frac{-\sigma_\mathcal{E}^2 P_1}{(P_2-P_1)(1-P_1^2)(1-P_1P_2)}\frac{-2\ln(P_1)}{(\ln(P_1))^2+(2\pi\nu)^2}\right)\\ &= 2\frac{2\sigma_\mathcal{E}^2}{(1-P_1P_2)}\mathcal{R}\left(\frac{P_1}{(P_2-P_1)(1-P_1^2)}\frac{\ln(P_1)}{(\ln(P_1))^2+(2\pi\nu)^2}\right).\end{aligned} \tag{3.3.1}$$

In this last step, 2, $\sigma_\mathcal{E}^2$ and $(1-P_1P_2)^{-1}$ were isolated from the function $\mathcal{R}(.)$ because they meet two properties. First, the fraction has no imaginary part. This is easy to see if P_1P_2 is replaced by r^2. This is possible if

$$P_1 = r(\cos(\phi) + i\sin(\phi)) \text{ and} \tag{3.3.2}$$
$$P_2 = r(\cos(\phi) - i\sin(\phi)), \tag{3.3.3}$$
$$\text{with } r \in (0,1), \text{ and } \phi \in (0,\pi)$$

is used. Second, the fraction and the 2, which was previously outside the $\mathcal{R}(.)$ function, is greater than zero. So it suffices to show that

$$\mathcal{R}\left(\frac{P_1}{(P_2-P_1)}\frac{1}{(1-P_1^2)}\frac{\ln(P_1)}{(\ln(P_1))^2+(2\pi\nu)^2}\right) \overset{!}{\geq} 0, \tag{3.3.4}$$

to prove the positive definiteness of $\gamma(h)$.
This proof is separated into three steps: First, for each of the three fractions

$$\frac{P_1}{(P_2-P_1)}, \quad \frac{1}{(1-P_1^2)} \text{ and } \frac{\ln(P_1)}{(\ln(P_1))^2+(2\pi\nu)^2},$$

the denominator is expanded so that these become real and positive. As a result, the individual denominators no longer play a role in the positive definiteness and can be neglected. Secondly it is necessary to multiply the numerators with each other and eliminate the imaginary part. These two steps can be found in Appendix B.9. Finally, the terms greater than zero are eliminated from (B.9.7):

$$\begin{aligned}&\left[-\ln(r)\sin(\phi)(1+r^2) + \phi\cos(\phi)(1-r^2)\right][\ln(r)^2+\phi^2]...\\ &+\left[-\ln(r)\sin(\phi)(1+r^2) - \phi\cos(\phi)(1-r^2)\right](2\pi\nu)^2,\end{aligned} \tag{3.3.5}$$

and a condition for positive definiteness is derived. First we show that the lower row is always positive. Using the scopes for the parameters

$$r \in (0,1), \ \phi \in (0,\pi) \text{ and } \nu \in \mathbb{R},$$

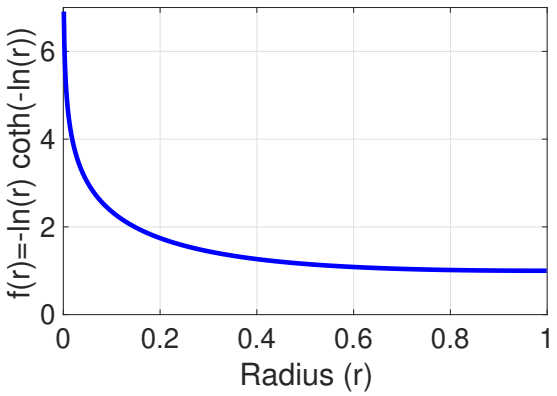

Figure 3.3: Decreasing function $f(r) = -\ln(r)\coth(-\ln(r))$ with $r \in (0,1)$.

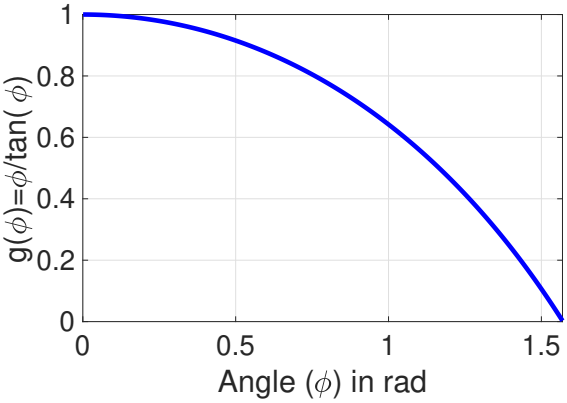

Figure 3.4: Function $g(\phi) = \phi/\tan(\phi)$ with $\phi \in (0, \pi/2]$.

it is obvious that $(2\pi\nu)^2 \geq 0$ is always true. The same applies to $-\ln(r)$, $\sin(\phi)$, $(1+r^2)$, ϕ and $(1-r^2)$. Because of the negative sign of $-\phi\cos(\phi)(1-r^2)$, the lower row in 3.3.5 is positive if $\cos(\phi) \leq 0$. This is the case if $\phi \in (\pi/2, \pi)$. For $\phi \in (0, \pi/2]$, it remains to show

$$\begin{aligned} -\ln(r)\sin(\phi)(1+r^2) - \phi\cos(\phi)(1-r^2) &\overset{!}{\geq} 0 \\ -\ln(r)\frac{1+r^2}{1-r^2} &\overset{!}{\geq} \phi\frac{\cos(\phi)}{\sin(\phi)} \\ \underbrace{-\ln(r)\coth(-\ln(r))}_{f(r)} &\overset{!}{\geq} \underbrace{\frac{\phi}{\tan(\phi)}}_{g(\phi)}. \end{aligned}$$

Since r and ϕ are independent, $f(r)$ and $g(\phi)$ can also be analysed separately (see Figure 3.3 and Figure 3.4). The figures show that Infimum$\{f(r)\}$ = Supremum$\{g(\phi)\}$, remaining $f(r) \geq g(\phi)$ $\forall$ $r \in [0,1]$ and $\phi \in [0, \pi/2]$. This means that the lower term of (3.3.5) is always greater or equal to zero. To uniquely determine the positive definiteness, the lower row in (3.3.5) is set to zero, which corresponds to the evaluation at the position $\nu = 0$. This way setting the lower row to zero is always feasible regardless of r and ϕ.
Only the first line of (3.3.5) remains, where again the quadratic terms ($[\ln(r)^2 + \phi^2]$) have no influence on the positive definiteness. Furthermore, the contents of the brackets are similar ti their counterparts in the second row, except for the minus, which has been replaced by a plus. So, positive definiteness also applies if $\cos(\phi) \geq 0$, which is equivalent to $\phi \in (0, \pi/2]$. In the end, it only remains to show that

$$-\ln(r)\sin(\phi)(1+r^2) + \phi\cos(\phi)(1-r^2) \overset{!}{\geq} 0 \qquad \forall r \in (0,1) \text{ and } \phi \in (\pi/2, \pi).$$

Analogously, the same transformations can be made here which then leads to

$$\underbrace{-\ln(r)\coth(-\ln(r))}_{f(r)} \overset{!}{\geq} \underbrace{-\frac{\phi}{\tan(\phi)}}_{-g(\phi)}.$$

However, since this problem cannot be solved analytically, the determination of the areas possessing positive definiteness demands an empirical approach as provided in Figure 3.5. Although the border to separate whether or not the AR(2) process is positive definite cannot be analytically represented by a function, this range is nevertheless approximate via the angle $\phi < 2.029$[rad] (or 116.24°), which is symbolized by the yellow line.
To find a suitable CF generated by AR(2) processes with complex roots P_1 and P_2 including negative real parts, we use the same idea as in the case of the TVAR(1) process with negative roots

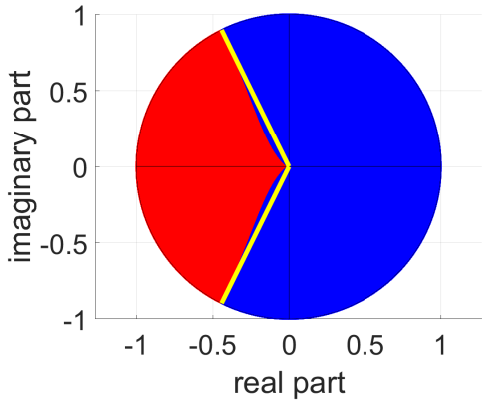

Figure 3.5: Areas for roots that lead to positive definiteness in the AR(2) process. Depending on whether the roots are in the blue or the red area the CF is positive definite or not. The yellow line approximates the border at $\phi = 2.028$ [rad] between these areas.

(see Appendix B.2). So, P_1 and P_2 are exchanged for the roots $\bar{P}_1$ and $\bar{P}_2$ with positive real parts multiplied with $(-1) = e^{i\pi}$. The transformations of P_1 and P_2 to $\bar{P}_1$ and $\bar{P}_2$ are shown in Appendix B.7.1:

$$P_1 = e^{i\pi}\bar{P}_2, \text{ and } P_2 = e^{i\pi}\bar{P}_1.$$

With this change of the used roots, the CF of an AR(2) process with a complex conjugated pair of roots whose real parts are negative (P_1 and P_2), can be traced back to the AR(2) process based on roots with positive real parts ($\bar{P}_1$, $\bar{P}_2$). Additionally, according to Appendix B.7.2, the indices of the coefficients of the CF rotate, meaning that the new weights for a permissible CF $\bar{A}_k$ for $k \in \{1, 2\}$ derive from their permissible roots and the equations of $A_1 = \bar{A}_2$ and $A_2 = \bar{A}_1$. This leads to the conclusion that if the roots P_1, P_2 have a negative real part, $\gamma(h)$ is given as:

$$\gamma(h) = e^{i\pi|h|}(\bar{A}_1\bar{P}_1^{|h|} + \bar{A}_2\bar{P}_2^{|h|}).$$

This equation as a whole is not positive definite but the sum in the brackets describes a positive definite function. And furthermore, if (as in the AR(1) process,) $e^{i\pi|h|} = \cos(\pi h) + i\sin(\pi|h|)$ is exchanged for its real part ($\cos(\pi h)$), the continuous covariance function is composed on the one hand of the discrete covariances and on the other hand of the product of two positive definite functions. In summary,

$$\gamma(h) = \begin{cases} A_1P_1^{|h|} + A_2P_2^{|h|} & \text{if } \mathcal{R}(P_1) \geq 0 \\ \cos(\pi h)(\bar{A}_1\bar{P}_1^{|h|} + \bar{A}_2\bar{P}_2^{|h|}) & \text{else} \end{cases} \tag{3.3.6}$$

results always in a positive definite covariance function for AR(2) processes.

3.4 Example of a Covariance Function Deriving from an AR(2) Process

This section provides a simulation of an AR process and the determination of the resulting CF. The applied parameters consists of the white noise and the two roots of the CP:

$$\sigma_{\mathcal{E}}^2 = 1 \qquad \text{and} \qquad P_{1,2} = -0.6 \pm 0.3i. \tag{3.4.1}$$

The aim is to illustrate the problem of a CF of non-positive definiteness, if the real part of the roots is negative. The simulated time series consists of fifty observations (see Figure 3.6). A subsequent

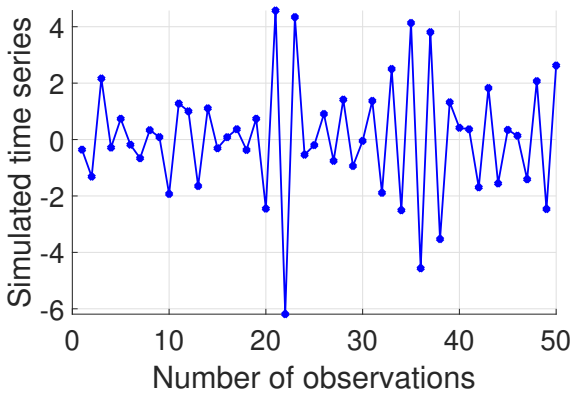

Figure 3.6: Simulated time series of an AR porcess of order 2 with the parameters in (3.4.1).

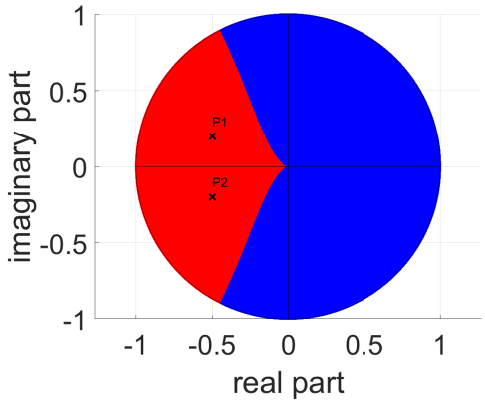

Figure 3.7: The roots $P_{1,2} = -0.6 \pm 0.3i$ plotted in the unit circle. These roots lie within the part of a not usable CF.

estimation of the Y.-W. equations reveals the values $\tilde{\alpha}_1 \approx 1.2$ and $\tilde{\alpha}_2 \approx 0.45$ for the coefficients of the AR(2) process. In addition, the variance of noise has been estimated with $\tilde{\sigma}^2_{\mathcal{E}} \approx 1$ by the means of the Y.-W. equation of order zero. If the roots of the CP are calculated from the estimated coefficients, the parameters

$$\tilde{\sigma}^2_{\mathcal{E}} \approx 1 \qquad \text{and} \qquad \tilde{P}_{1,2} \approx -0.6 \pm 0.3i \tag{3.4.2}$$

are obtained. Comparing the parameters in (3.4.1), which were used to simulate the signal in Figure 3.6 with the estimated parameters in (3.4.2), reveals that the estimation leads to the parameters used for the initialization. In addition the corresponding roots P_1 and P_2 are shown in Figure 3.7. They are clearly located in the red area, where the simple representation of the covariance function

$$\gamma_1(h) := A_1 P_1^{|h|} + A_2 P_2^{|h|}$$

is not positive definite. The covariance function itself is shown in Figure 3.8, while

$$\gamma_2(h) := \left(\bar{A}_1 \bar{P}_1^{|h|} + \bar{A}_2 \bar{P}_2^{|h|}\right) \cos(\pi h)$$

is shown in Figure 3.9. The additional cosine is highlighted in grey in Figure 3.9 and shows that its maxima and minima are always at the observation epochs. In contrast, the extrema of $\gamma_2(h)$ are no longer exactly at the observation epochs. This is a result of the superposition of the oscillating cosine and the function

$$\gamma_3(h) := \bar{A}_1 \bar{P}_1^{|h|} + \bar{A}_2 \bar{P}_2^{|h|},$$

shown in Figure 3.10 (also see chapter 2). The resulting spectra $\Gamma_1(\nu) = \mathcal{F}\{\gamma_1(h)\}(\nu)$, computed by (3.3.1) and $\Gamma_2(\nu) = \mathcal{F}\{\gamma_2(h)\}(\nu)$ are shown together in Figure 3.11. Appendix B.8 shows that the construction of the spectrum of $\gamma_2(h)$ demands three steps:

1. Divide the CF of $\mathcal{F}\{\gamma_3(h)\}(\nu)$ into two functions with half amplitude height,
2. then shift one of these two functions by $a = \frac{1}{2}$ and the other by $-a = -\frac{1}{2}$.
3. Finally, at each frequency sum these shifted functions up.

It is of special interest here that, inside the Nyquist frequency $[-\nu_n, \nu_n]$), the two spectra are very similar, only that $\Gamma_2(\nu) > 0 \ \forall \nu$. So, $\Gamma_2(\nu)$ not only remains positive, but also maintains the characteristic of the PSD of the discrete CF shown in Figure 3.12. In comparison to the PSD of the discrete CF in Figure 3.12 and the PSD of the continuous CF Γ_2 in Figure 3.11, the amplitude is twice as high. At first glance, this seems to be a contradiction, but it is consistent with the findings

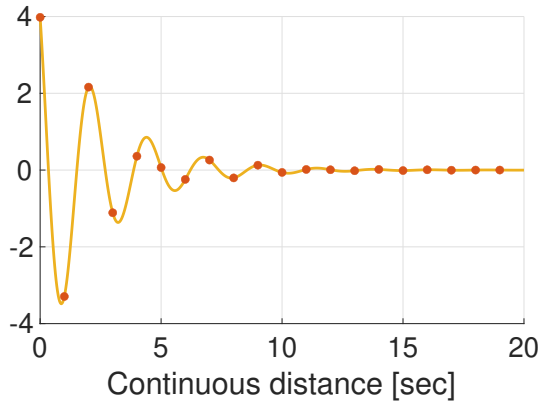

Figure 3.8: Function $\gamma_1(h) = A_1 P_1^{|h|} + A_2 P_2^{|h|}$ with $P_{1,2} = -0.6 \pm 0.3i$.

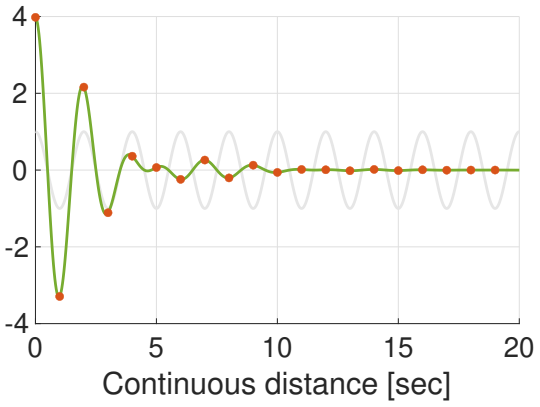

Figure 3.9: Function $\gamma_2(h) = (\bar{A}_1 \bar{P}_1^{|h|} + \bar{A}_2 \bar{P}_2^{|h|}) \cos(\pi h)$ with $P_{1,2} = -0.6 \pm 0.3i$.

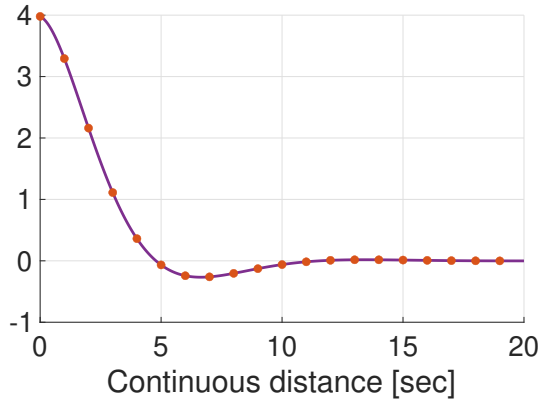

Figure 3.10: Function $\gamma_3(h) = \bar{A}_1 \bar{P}_1^{|h|} + \bar{A}_2 \bar{P}_2^{|h|}$ with $\bar{P}_{1,2} = 0.6 \pm 0.3i$.

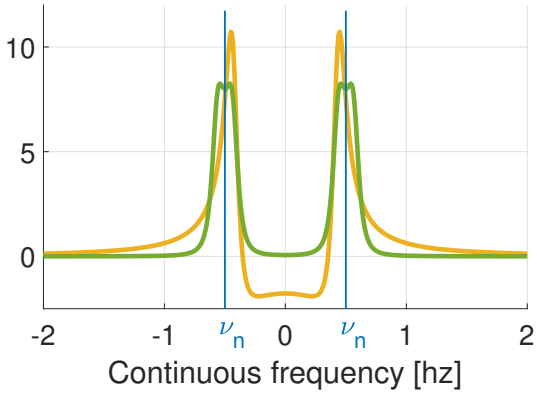

Figure 3.11: The PSD of the functions $\Gamma_1(\nu)$ **in orange** and $\Gamma_2(\nu)$ **in green**.

of section 3.2.3 (the discretization always causes a sum of shifted PSDs). Here it was described how in order to build the PSD of the discrete function, the transition from the continuous CF to the discrete CF leads to a sum of infinitely many shifted PSDs of the continuous function (see Appendix B.5). Two of these shifted functions are depicted in Figure 3.13. This figure also shows that the maxima overlap exactly, meaning that they are doubled by the summation. This explains why the amplitudes of the PSD of the continuous CF are only half as large as those of the discrete CF.

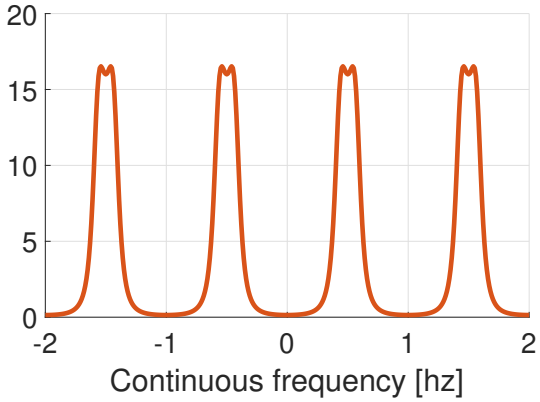

Figure 3.12: PSD of the discrete CF of an AR(2) process with the parameters of (3.4.2).

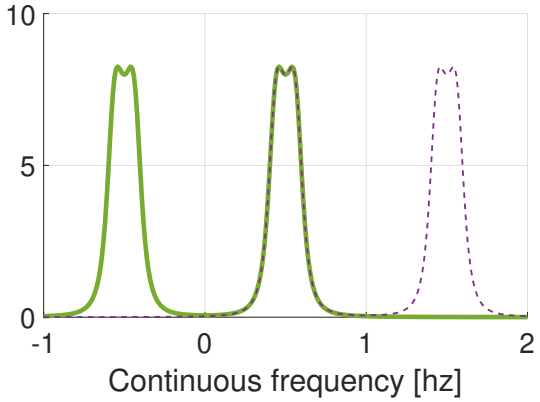

Figure 3.13: The PSD of the functions $\Gamma_2(\nu)$ **in green** and shifted $\Gamma_2(\nu)$ **in dashed purple**.

Chapter 4

Time Variable AR Processes

One of the main limitations of AR estimation is its requirement of stationarity, which imposes a strong condition on the analysed data characteristics. In order to soften this condition, the concept of nonstationary processes is introduced here, specifically the concept of nonstationary AR processes. This study deals exclusively with nonstationary AR representations, in which the coefficients are allowed to change over time, while the roots remain inside the unit circle for any given time. Otherwise the covariance function might diverge. In comparison, a time constant process with roots of the CP from (2.9.2) outside the unit circle is also classified as nonstationary, but are excluded here. Accordingly, this chapter provides the discussion of the analytic relationships between the time variable roots and the time variable parameters of TVAR processes. The roots are developed according to these relation methods to estimate the TVAR coefficients from a given motion model. In order to fully explain the process behind this result, the following chapter is divided into seven sections: Section 4.1 provides a description of the estimation of the parameters of a TVAR process using undefined basis functions. It shows that the estimation by using the Y.-W. equations is not appropriate in this case, and that the unknown parameters of the coefficients need to be determined by using the observation equations. This further means that the variance of the noises must also be gained from the observation equation. In section 4.2, polynomials are used for these basis functions. Following two examples, the roots of the TVAR processes at discrete times are determined. These discrete values shows an unknown motions which are not controllable. This is of special consequence when looking at their positioning inside or outside the unitary circle. To solve this problem, the roots are defined as linear functions and the corresponding coefficients in the TVAR process are derived in section 4.3. These coefficients have to meet additional constraints to obtain the linear root motions for the TVAR process of orders 1 and 2. Processes of higher order are estimated by successively estimating TVAR(1) and TVAR(2) processes. Then, the estimate of TVAR processes with linear root motion will been modified in section 4.4. Here TVAR processes with piecewise linear roots are estimated. Two more extensions are set up in section 4.5 to estimate TVAR processes with quadratic root movements and to determine the TVAR(3) process without recursion. Section 4.6 provides the synthesis of the derived estimation methods and gives an evaluation of their individual advantages and disadvantages. These methods are then tested and compared in section 4.7.

4.1 Representation of TVAR Processes by the means of Basis Functions

This section deals with the estimation of time variable AR coefficients and their discrete covariances. For this purpose, a purely mathematical construct is needed, which describes the calculation and properties of the covariance of TVAR processes. Starting from the formula of TVAR processes given in (2.16.1)

$$\mathcal{S}_t = \alpha_1(t)\mathcal{S}_{t-1} + \alpha_2(t)\mathcal{S}_{t-2} + ... + \alpha_p(t)\mathcal{S}_{t-p} + \mathcal{E}_t, \tag{4.1.1}$$

the coefficients are functions in the time domain. In order to derive the parameters by the means of a linear Gauss-Markov model, the functions $\alpha_k(t)$ can be represented as linear combinations of the unknown parameters $\beta_l^{(k)}$ and the known basis functions $b_l(t)$:

$$\alpha_k(t) = \sum_{l=0}^{q_k} \beta_l^{(k)} b_l(t). \tag{4.1.2}$$

The basis functions $b_l(t)$ can be specified, i.e. for example as polynomial bases $(1, t, t^2, ...)$, spline functions or similar bases. The number of basis functions per coefficient $(\alpha_k(t))$ may vary for each k and is denoted by q_k. The total number of parameters defining the TVAR(p) process increases from p to $\sum_{k=1}^{p} q_k$, which in turn means that when estimating TVAR processes with high orders the number of parameters increases significantly and thus the redundancy within the estimation decreases.
In the following examinations the coefficients are calculated only for a limited time interval $T = [t_1, t_n]$. For numerical stability, to transformation of the interval T to the unit interval $\bar{T} = [0, 1]$ is appropriate. It is required that for any time $\tau \in T$, the TVAR process is stationary. This means that the roots $P_k(\tau)$ of the time constant AR process at $t = \tau$

$$\breve{\mathcal{S}}_t = \alpha_1(\tau)\breve{\mathcal{S}}_{t-1} + \alpha_2(\tau)\breve{\mathcal{S}}_{t-2} + ... + \alpha_p(\tau)\breve{\mathcal{S}}_{t-p} + \breve{\mathcal{E}}_t \tag{4.1.3}$$

are inside the unit circle. In this process, t and τ are independent of each other and the functions of $\alpha_k(\tau)$ are constant.

4.1.1 Yule-Walker Equations for TVAR Processes at a Specific Time

For the time constant AR process in (4.1.3), section 2.8 shows how the Y.-W. equations are constructed. For the case of (4.1.3), this results in

$$\begin{aligned} \breve{\Sigma}_0 &= \alpha_1(\tau)\breve{\Sigma}_1 + \alpha_2(\tau)\breve{\Sigma}_2 + ... + \alpha_p(\tau)\breve{\Sigma}_p + \breve{\sigma}_{\mathcal{E}}{}^2 && \text{and} \\ \breve{\Sigma}_j &= \alpha_1(\tau)\breve{\Sigma}_{|j-1|} + \alpha_2(\tau)\breve{\Sigma}_{|j-2|} + ... + \alpha_p(\tau)\breve{\Sigma}_{|j-p|} && \forall j \in \mathbb{Z} \setminus \{0\}, \end{aligned}$$

where $\breve{\Sigma}_j$ is the discrete covariance of the two observations $\breve{\mathcal{S}}_t$ and $\breve{\mathcal{S}}_{t+j}$. In the following sections, the Y.-W. equations for TVAR processes are derived and their properties are analysed in the context of parameter estimation and determination of covariances.

4.1.2 Yule-Walker Equations of Time Variable AR Processes

This section shows how the Y.-W. equations for TVAR processes are derived. It argues that these equations are not suitable to determine the desired coefficients $\beta_l^{(k)}$ from example (4.1.2). But they are used to adapt many properties of the time constant AR processes to the TVAR process. First, the Y.-W. equations for the general TVAR processes are derived (see Appendix C.1), which results in

$$\Sigma_{-j}(t) = \begin{cases} \alpha_1(t)\Sigma_{-j+1}(t-1) + \alpha_2(t)\Sigma_{-j+2}(t-2) + ... + \alpha_p(t)\Sigma_{-j+p}(t-p) + \sigma_{\mathcal{E}}^2 & \text{if } j = 0 \\ \alpha_1(t)\Sigma_{-j+1}(t-1) + \alpha_2(t)\Sigma_{-j+2}(t-2) + ... + \alpha_p(t)\Sigma_{-j+p}(t-p) & \text{else} \end{cases} \tag{4.1.4}$$

to compute the covariance of $\mathcal{S}_t$ and a past signal $\mathcal{S}_{t-j}$. The following transformations are only demonstrated with the Y.-W. equation for $j \neq 0$, as the special case of $j = 0$ can be dealt with analogously. In the case that the time variable coefficients $\alpha_k(t)$ of (4.1.4) are replaced by the linear basis functions combinations in (4.1.2), then the known basis functions can be combined with the time variable covariances into

$$\hat{\Sigma}_{-j+k}^{(b(l,t))}(t-k) := b_l(t)\Sigma_{-j+k}(t-k)$$

to obtain a linear equation for the unknown coefficients $\beta_l^{(k)}$:

$$\begin{aligned}
&\Sigma_{-j}(t)\\
&= \sum_{l=0}^{q_1} \beta_l^{(1)} \underbrace{b_l(t)\Sigma_{-j+1}(t-1)} \quad + \sum_{l=0}^{q_2} \beta_l^{(2)} \underbrace{b_l(t)\Sigma_{-j+2}(t-2)} \quad + \ldots + \sum_{l=0}^{q_p} \beta_l^{(p)} \underbrace{b_l(t)\Sigma_{-j+p}(t-p)}\\
&= \sum_{l=0}^{q_1} \beta_l^{(1)} \quad \hat{\Sigma}_{-j+1}^{b(l,t)}(t-1) \quad + \sum_{l=0}^{q_2} \beta_l^{(2)} \quad \hat{\Sigma}_{-j+2}^{(b(l,t))}(t-2) \quad + \ldots + \sum_{l=0}^{q_p} \beta_l^{(p)} \quad \hat{\Sigma}_{-j+p,l}^{b(l,t)}(t-p).
\end{aligned}$$

The new parameters $\beta_l^{(k)}$ can be determined by the means of the linear equations. Since the covariances now depend on both the distance j between the observations, and the observation time of the subsequent observation (t), there is exactly one realization for each covariance ($\hat{\Sigma}$). Accordingly, because the redundancy is missing, the derived covariances are too inaccurate to pose an advantage to the estimations gained by the Y.-W. equations for TVAR processes.
The same applies for the case of Y.-W. equations for $\mathcal{S}_t$ and a Signal oriented towards future values $\mathcal{S}_{t+j}$. This can be seen when replacing the coefficients $\alpha_k(t)$ in (C.1.3) with the linear combination with basis functions from (4.1.2). The result is

$$\begin{aligned}
&\Sigma_j(t)\\
&= \alpha_1(t+j)\Sigma_{j-1}(t) \qquad\qquad + \alpha_2(t+j)\Sigma_{j-2}(t) + \ldots + \alpha_p(t+j)\Sigma_{j-p}(t)\\
&= \sum_{l=0}^{q_1} \beta_l^{(1)} \underbrace{b_l(t+j)\Sigma_{j-1}(t)} \quad + \sum_{l=0}^{q_2} \beta_l^{(2)} \underbrace{b_l(t+j)\Sigma_{j-2}(t)} + \ldots + \sum_{l=0}^{q_p} \beta_l^{(p)} \underbrace{b_l(t+j)\Sigma_{j-p}(t)}\\
&= \sum_{l=0}^{q_1} \beta_l^{(1)} \quad \hat{\Sigma}_{j-1}^{(b(l,t+j))}(t) \quad + \sum_{l=0}^{q_2} \beta_l^{(2)} \quad \hat{\Sigma}_{j-2}^{(b(l,t+j))}(t) + \ldots + \sum_{l=0}^{q_p} \beta_l^{(p)} \quad \hat{\Sigma}_{j-p}^{(b(l,t+j))}(t).
\end{aligned}$$

Since $\hat{\Sigma}$ again depends on both the time (t) and the distance to the other observation (j), there is exactly one realization for each state.

4.1.3 Estimation of Time Variable AR Processes

Since the covariances cannot be constructed without the coefficients of the TVAR process, an estimation method based directly the observations has to be developed here. This is done in two steps. First, the coefficients $\beta_l^{(k)}$'s estimations are gained directly from the observations. Subsequently, the residuals are used to determine the variance of the noise ($\sigma_{\mathcal{E}}^2$).

4.1.3.1 Parameters Estimation

This section shows how the time variable TVAR process coefficients can be estimated by a Gauss-Markov model. For this, it is firstly assumed that all TVAR coefficients $\alpha_k(t)$ in (4.1.2) have the same order $q = \max\{q_1, q_2, ..., q_p\}$:

$$\alpha_k(t) = \sum_{l=0}^{q} \beta_l^{(k)} b_l(t).$$

The general case with different q_k can be created from this assumption, by eliminating the corresponding parameters $\beta_l^{(k)}$ with $l > q_k$ and the corresponding columns from the design matrix. This is shown in Appendix C.3. Since all TVAR coefficients now consist of the same number of unknown parameters, the conversion of the coefficients $\alpha_k(t)$ to the parameters $\beta_l^{(k)}$ by a simple

formula results in the matrix vector product:

$$\begin{bmatrix}\alpha_1(t)\\ \alpha_2(t)\\ \vdots\\ \alpha_p(t)\end{bmatrix} = \begin{bmatrix} b_0(t) & b_1(t) & \dots & b_q(t) & & & & & & & & \\ & & & & b_0(t) & b_1(t) & \dots & b_q(t) & & & & \\ & & & & & & & & \ddots & & & \\ & & & & & & & & & b_0(t) & b_1(t) & \dots & b_q(t)\end{bmatrix} \begin{bmatrix}\beta_0^{(1)}\\ \beta_1^{(1)}\\ \vdots\\ \beta_q^{(1)}\\ \beta_0^{(2)}\\ \beta_1^{(2)}\\ \vdots\\ \beta_q^{(2)}\\ \beta_0^{(p)}\\ \beta_1^{(p)}\\ \vdots\\ \beta_q^{(p)}\end{bmatrix}. \tag{4.1.5}$$

Here the increase of the number of parameters becomes clear. $\beta_l^{(k)}$ are ordered according to k of $\alpha_k(j)$, but by a re-ordering according to the variable l of the sum in (4.1.2), a new parameter vector is created:

$$\boldsymbol{\beta} := \begin{bmatrix}\beta_0^{(1)} & \beta_0^{(2)} & \dots \beta_0^{(p)} & \beta_1^{(1)} & \beta_1^{(2)} & \dots \beta_1^{(p)} & \dots \beta_q^{(1)} & \beta_q^{(2)} & \dots \beta_q^{(p)}\end{bmatrix}^T. \tag{4.1.6}$$

This also causes a reorganization of the basis functions in (4.1.5):

$$\begin{bmatrix}\alpha_1(t)\\ \alpha_2(t)\\ \vdots\\ \alpha_p(t)\end{bmatrix} = \begin{bmatrix} b_0(t) & & & b_1(t) & & & \dots & b_q(t) & \\ & b_0(t) & & & b_1(t) & & \dots & & b_q(t) \\ & & \ddots & & & \ddots & & & & \ddots \\ & & & b_0(t) & & & b_1(t) & \dots & & & b_q(t)\end{bmatrix} \boldsymbol{\beta}.$$

This re-ordering results in a design matrix composed of diagonal matrices. Furthermore, each of these diagonal matrices is a scaled identity matrix. Here, the unit matrix is denoted by $\mathbb{1}$. This simplifies the representation of (4.1.5):

$$\begin{bmatrix}\alpha_1(t)\\ \alpha_2(t)\\ \vdots\\ \alpha_p(t)\end{bmatrix} = \begin{bmatrix}\mathbb{1}b_0(t) & | & \mathbb{1}b_1(t) & | & \dots & | & \mathbb{1}b_q(t)\end{bmatrix}_{[p\times pq]} \boldsymbol{\beta}. \tag{4.1.7}$$

Converting (4.1.1) into a vector product yields

$$\mathcal{S}_t = \begin{bmatrix}\mathcal{S}_{t-1} & \mathcal{S}_{t-2} & \dots & \mathcal{S}_{t-p}\end{bmatrix} \begin{bmatrix}\alpha_1(t)\\ \alpha_2(t)\\ \vdots\\ \alpha_p(t)\end{bmatrix} + \mathcal{E}_t$$

and inserting it into (4.1.7) results in

$$\mathcal{S}_t = \begin{bmatrix}\mathcal{S}_{t-1} & \mathcal{S}_{t-2} & \dots & \mathcal{S}_{t-p}\end{bmatrix}_{[1\times p]} \begin{bmatrix}\mathbb{1}b_0(t) & | & \mathbb{1}b_1(t) & | & \dots & | & \mathbb{1}b_q(t)\end{bmatrix}_{[p\times pq]} \boldsymbol{\beta} + \mathcal{E}_t.$$

In this problem, neither the parameter's vector $\boldsymbol{\beta}$ nor the residual's vector $\mathcal{E}_t$ is known. To determine these vectors, the residual's vector $\mathcal{E}_t$ is subtracted on both sides of the equation, and then $\boldsymbol{\beta}$ is used as a parameter's vector from the Gauss-Markov model (Koch 1999, chapter 3):

$$\underbrace{\mathcal{S}_t} + \underbrace{(-\mathcal{E}_t)} = \underbrace{\begin{bmatrix}\mathcal{S}_{t-1} & \mathcal{S}_{t-2} & \dots & \mathcal{S}_{t-p}\end{bmatrix}_{[1\times p]} \begin{bmatrix}\mathbb{1}b_0(t) & | & \mathbb{1}b_1(t) & | & \dots & | & \mathbb{1}b_q(t)\end{bmatrix}_{[p\times pq]}}_{\boldsymbol{X}_i} \boldsymbol{\beta}$$

$$y_i + e_i = \boldsymbol{X}_i \boldsymbol{\beta}. \tag{4.1.8}$$

As mentioned at the beginning of this section, the adjustment model can be applied to any parametrization of $\alpha_k(t)$ with basis functions by subsequently removing columns from the design matrix $\boldsymbol{X}$ as well as the corresponding parameters from $\boldsymbol{\beta}$ (see Appendix C.3).

4.1.3.2 Estimation of Noise Variance

In section 2.16, the TVAR process was defined by its time variable coefficients $\alpha_k(t)$, but also by the white noise process $\mathcal{E}_t$ whose only parameter is its standard deviation $\sigma_{\mathcal{E}}^2$. These have yet to be determined. In (4.1.8), the unknown residuals e_i represented realizations of the process $\mathcal{E}_t$, but with the opposite sign. Since the residuals in the Gauss-Markov model and the white noise in the TVAR process both follow the same distribution (i.e. the i.i.d normal distribution with a mean value of zero), they also share the same standard derivation. So, the variance of the white noise process $\sigma_{\mathcal{E}}^2$ can be approximated via an estimation of the variance of the observations provided by the Gauss-Markov model. Therefore, each error can be resolved as

$$e_i = \boldsymbol{X}_i\tilde{\boldsymbol{\beta}} - y_i$$

$\forall i \in \{1, 2, ..., n\}$ or directly via the vector of errors

$$\boldsymbol{e} = \boldsymbol{X}\tilde{\boldsymbol{\beta}} - \boldsymbol{y}.$$

An estimator for the white noise's variance is then given by the a posteriori variance

$$\sigma_{\mathcal{E}}^2 \approx \tilde{s}^2 = \frac{\boldsymbol{e}^T\boldsymbol{e}}{r}.$$

Here, r refers to the redundancy calculated by the formula

$$r = (n - p) - m,$$

with m being the number of parameters in $\boldsymbol{\beta}$. Actually, the redundancy is simply calculated by the means of the difference between the number of observations (n) and the number of parameters (m). Mathematically n and m are given by the length of the observation vector $\boldsymbol{y}$ and the parameter vector $\boldsymbol{\beta}$. Since the first p observations are not included in $\boldsymbol{y}$ (see Appendix C.2), the redundancy must be additionally reduced by p.

4.2 Relevance

Until now, all sections of chapter 4 have been exclusively concerned with the modelling and estimation of time variable TVAR process coefficients. The intention of this thesis, however, is the creation of a TVAR process with known motion of the time variable roots of the CP. The goal, then, is to select the basis functions of the coefficients in such a way that the type of movement of the roots is predefined. However, this is not as simple, as the following two examples will demonstrate.

As described in section 4.1, the coefficients and the roots of a TVAR process are linked via the CP. The CP is, as the name suggests, a special case of a polynomial. However, there is a difference in sign and a difference in index change between the coefficients of a general polynomial $\mathcal{P}_p(x)$ (with coefficients $c_1(t), c_2(t), ..., c_p(t)$) and a CP $\chi(x)$ (with coefficients $\alpha_1(t), \alpha_2(t), ..., \alpha_p(t)$):

$$\mathcal{P}_p(x) = x^p + c_1(t)x^{p-1} + c_2(t)x^{p-2} + ... + c_p(t) \tag{4.2.1}$$

$$\chi(x) = x^p - \alpha_1(t)x^{p-1} - \alpha_2(t)x^{p-2} - ... - \alpha_p(t). \tag{4.2.2}$$

These two equations show that finding the roots of a difference equation or the CP of a TVAR process in (4.2.1) is related to finding the zeros of a polynomial with time variable coefficients in (4.2.2). This allows the application of experiences gained from general time variable polynomials to the construction of TVAR processes with known root motion.

4.2.1 Example 1: Contemporary Research

An example for time variable polynomials can be found in Kamen (1988, example 1). Here, the roots of the time variable polynomial

$$\mathcal{P}_2(x) = x^2 + c_1(t)x + c_2(t) \qquad \text{with } c_1(t) = -1 + 2.5t \text{ and } c_2(t) = 0.5$$

are determined. In this case t can assume all values between 0 and 1, whereby $c_1(t)$ is a linear function with $c_1(0) = -1$ and $c_1(1) = 1.5$ and $c_2(t)$ remains constant at $c_2(t) = 0.5 \quad \forall t \in [0, 1]$. The motion of the roots for this polynomial can be determined by the pq-formula in (2.17.2), while they are also functions in time:

$$P_{1,2}(t) = -\frac{c_1(t)}{2} \pm \sqrt{\left(\frac{c_1(t)}{2}\right)^2 - c_2(t)}. \tag{4.2.3}$$

These are illustrated lying within the unit circle in Figure 4.2. The CP, which has the same root motions as the exemplary polynomial, corresponds to the AR process coefficients:

$$\alpha_1(t) = -c_1(t) = 1 - 2.5t \qquad \text{and} \qquad \alpha_2(t) = -c_2(t) = -0.5.$$

This follows from the comparison of (4.2.1) and (4.2.2) and results in

$$P_{1,2}(t) = \frac{\alpha_1(t)}{2} \pm \sqrt{\left(\frac{\alpha_1(t)}{2}\right)^2 + \alpha_2(t)}. \tag{4.2.4}$$

The transition from the polynomial to the CP allows to use the representation of the TVAR(2) process from section 2.9 to visualize the motion of the coefficients. To do this, the time variable coefficients $\alpha_1(\tau)$ and $\alpha_2(\tau)$ are evaluated at discrete points $t = \tau$. The normalized time $t \in [0, 1]$ is indicated as a colour gradient on the right edge of the graphic. For each discrete time $t = \tau$ a three dimensional point is created. The dimensions are given by the x-value $\alpha_1(\tau)$, the y-value $\alpha_2(\tau)$ and the colour of the point. The colour references to the colour of $t = \tau$. The movement of the coefficients is depicted in Figure 4.1 and takes the shape of a straight line. Then, at each

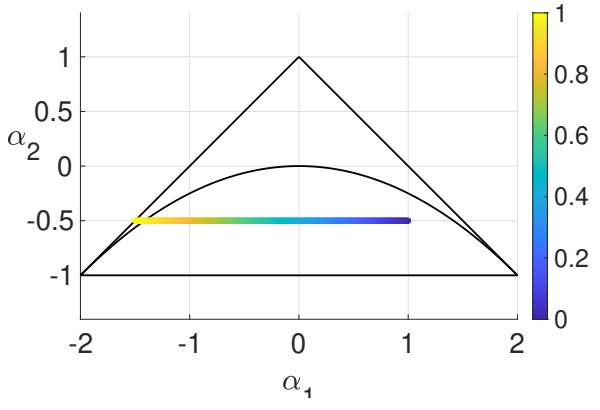

Figure 4.1: Coefficient motion of a TVAR process with the coefficients $\alpha_1(t) = 1 - 2.5t$ and $\alpha_2(t) = -0.5$ for $t \in [0, 1]$, or for t from blue to yellow.

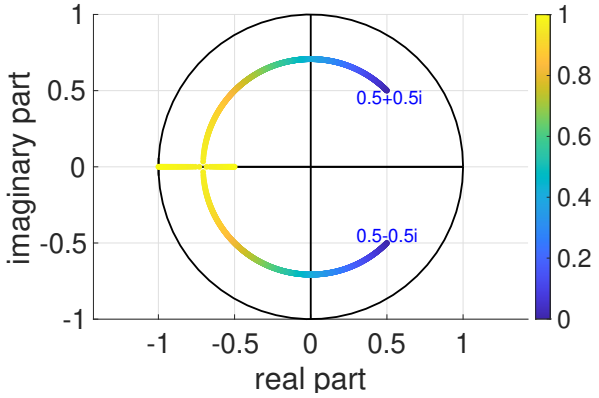

Figure 4.2: Root motion of a TVAR process with the coefficients $\alpha_1(t) = 1 - 2.5t$ and $\alpha_2(t) = -0.5$ for $t \in [0, 1]$, or for t from blue to yellow.

point in time $t = \tau$, a pair of coefficients $\alpha_1(\tau)$ and $\alpha_2(\tau)$ is given. The possibly complex-valued roots $P_1(\tau)$ and $P_2(\tau)$ of the CP can be calculated via (4.2.4) for each pair of coefficients $\alpha_1(\tau)$ and $\alpha_2(\tau)$. These roots are visualized in Figure 4.2. In this case, each three dimensional point corresponds to a root $P_i(t)$ with $i \in \{1, 2\}$. The x-value corresponds to the real part of $P_i(t)$, whose

y-value corresponds to the imaginary part of $P_i(t)$, and whose colour is again associated with the time on the right.
However, while the motion of the coefficients in Figure 4.1 has a constant velocity, both the roots in Figure 4.2 initially have the same constant angular velocity but only as long as the roots are complex valued, and then, as soon as they become real valued, assume different speeds in different directions. Thus, this example shows that the complex representation of the roots as a coefficient's function (4.2.3) performs a motion that is difficult to predict. The challenge now is to specify a simpler motion of the roots, from which the corresponding functions of the coefficients $\alpha_k(t)$ can be constructed. Finally, it should be mentioned that both figures show that the roots are inside the unit circle at any given time of the open interval $[0, 1)$. This means that any time constant process of a fixed time $\tau \in [0, 1)$

$$\mathcal{S}_t = (1 - 2.5\tau)\mathcal{S}_{t-1} - 0.5\mathcal{S}_{t-2} + \mathcal{E}_t$$

is stationary.

4.2.2 Example 2: Higher Order Polynomials

To predict the motion of roots by the means of time variable coefficients with higher order polynomials states a more complicated case. Section 2.17 has shown that, if the order is higher or equal to five, a functional relationship between the polynomials and roots can no longer be established. In these cases, in order to determine the roots of the time constant AR process, the coefficients of the CP are evaluated for a specific $\tau \in [0, 1]$. For this purpose, the coefficients

$$\alpha_1 = 1 - 2.5t, \quad \alpha_2 = -0.5, \quad \alpha_3 = 0.3, \quad \alpha_4 = 0.1, \quad \text{and} \quad \alpha_5 = -0.09$$

of a TVAR(5) process are chosen and evaluated at the equidistant times $\tau_j = 0.05j$ with $j \in \{0, 1, 2, 3, ..., 40\}$ to construct a total of 41 AR processes. For each of them, the roots of the corresponding CP are determined (see Figure 4.3). These discrete roots approximate five root

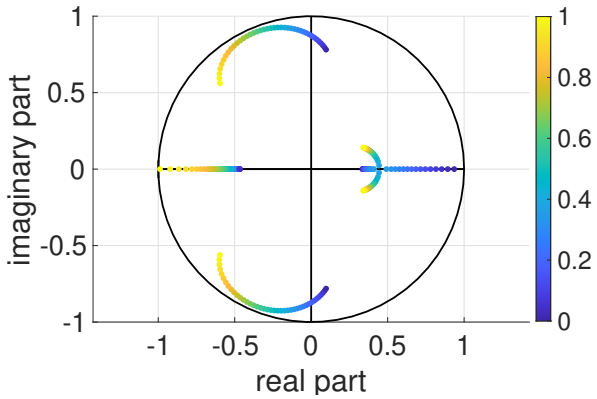

Figure 4.3: Root motions of a stationary AR(5) process inside the unit circle.

motions. Of these five root motions, four differ: the roots on the right side change over time from real-valued roots to a pair of complex conjugated roots. The roots in the upper left area, which follow a quadratic track, as well as the real-valued root on the left, are non-linear. While the complex roots seem to move in a quadratic motion, the non-linear motion of the real-valued root is caused by the different distances between the discrete points. In this case, the roots are also always within the unit circle and thus always provide a stationary process for any $\tau \in [0, 1]$:

$$\mathcal{S}_t = (1 - 2.5\tau)\mathcal{S}_{t-1} - 0.5\mathcal{S}_{t-2} + 0.3\mathcal{S}_{t-3} + 0.1\mathcal{S}_{t-4} - 0.09\mathcal{S}_{t-5} + \mathcal{E}_t.$$

4.2.3 Problematization

These two examples have shown that there are three fundamental challenges for TVAR estimation:

1. We are looking for a parametrization of the functions $\alpha_k(t)$, which allows that the function of the roots $P_k(t)$ can be represented as continuous functions,
2. while the function of the roots remain simple enough to check the stationarity of the TVAR process for each point in time, and
3. an analytical way to determine the roots of TVAR(p) processes with $p > 5$.

The aim of the following sections is therefore to determine basis functions that allows the estimation of the coefficients in (4.1.2) in such a way that both the coefficients and the roots can be represented as functions in time (and which also remain as simple as possible).

4.3 Linear Root Motion

This section examines the root motion caused by the time variable approach. This estimation method is influenced by many variables, such as the order of the TVAR process p, the number of parameters in the coefficients q_k and, of course, the choice of the basis functions. The main challenge, however, lies in the ability to represent the root motions and the coefficients as functions. The basic ideas of section 4.3 have been described in Korte et al. 2023b and are discussed here in more detail.

4.3.1 The Conversion of Roots into Coefficients (Necessary Condition)

This section provides the construction of the AR process coefficients by the means of the roots of the CP. In this context, Vieta's formulas show that the coefficients $-\alpha_k$ can be calculated by sums and products of the roots (P_k) (see Bronstein et al. 2006, p. 44). This provides us with:

$$\begin{aligned}\alpha_k =&(-1)^{k+1}\left(\sum_{m_1=1}^{p-k+1} P_{m_1}\right)\cdot\left(\sum_{m_2=m_1+1}^{p-k+2} P_{m_2}\right)\cdot\left(\sum_{m_3=m_2+1}^{p-k+3} P_{m_3}\right)\ldots\\ &\left(\sum_{m_{k-1}=m_{k-2}+1}^{p-1} P_{m_{k-1}}\right)\cdot\left(\sum_{m_k=m_{k-1}+1}^{p} P_{m_k}\right).\end{aligned} \tag{4.3.1}$$

To gain a transition to the time variable roots $P_k(t)$, the formula is applied with linear combinations of the basis functions $\bar{b}_l(t)$:

$$P_k(t) = \sum_{l=0}^{q} \zeta_l^{(k)} \bar{b}_l(t)$$

just as it has been done for the $\alpha_k(t)$ in (4.1.2). This time, to distinguish them from the basis functions $b_l(t)$ of the parameters, the basis functions are $\bar{b}_l(t)$. They all have the same number of parameters q. First, when considering any sum $\sum_{m_c=m_{c-1}+1}^{p-k+c} P_{m_c}(t)$ of (4.3.1), it is noticeable that

$$\begin{aligned}\sum_{m_c=m_{c-1}+1}^{p-k+c} P_{m_c}(t) &= \sum_{m_c=m_{c-1}+1}^{p-k+c}\sum_{l=0}^{q} \zeta_l^{(m_c)} \bar{b}_l(t)\\ &= \sum_{l=0}^{q} \underbrace{\left(\sum_{m_c=m_{c-1}+1}^{p-k+c} \zeta_l^{(m_c)}\right)}_{\bar{\zeta}_l^{(m_c)}} \bar{b}_l(t)\\ &= \sum_{l=0}^{q} \bar{\zeta}_l^{(m_c)} \bar{b}_l(t)\end{aligned}$$

is valid, and thus each bracket in (4.3.1) again consists of a linear combination of the basis functions $\bar{b}_l(t)$. The number of used basis functions does not change. Second, if two roots are multiplied, the

basis functions $\bar{b}_l(t)$ are also multiplied. These products build the form of the basis functions of the coefficients $b_l(t)$. Here, I provided an example with two roots:

$$\begin{aligned}
P_{m_c}(t)P_{m_d}(t) = \left(\sum_{l_1=0}^{q} \bar{\zeta}_{l_1}^{(m_c)}\bar{b}_{l_1}(t)\right)\left(\sum_{l_2=0}^{q} \bar{\zeta}_{l_2}^{(m_d)}\bar{b}_{l_2}(t)\right) &= \sum_{l_2=0}^{q}\left(\sum_{l_1=0}^{q} \bar{\zeta}_{l_1}^{(m_c)}\bar{b}_{l_1}(t)\right)\bar{\zeta}_{l_2}^{(m_d)}\bar{b}_{l_2}(t) \\
&= \sum_{l_2=0}^{q}\left(\sum_{l_1=0}^{q} \bar{\zeta}_{l_1}^{(m_c)}\bar{b}_{l_1}(t)\bar{\zeta}_{l_2}^{(m_d)}\right)\bar{b}_{l_2}(t) \\
&= \sum_{l_2=0}^{q}\left(\sum_{l_1=0}^{q} \bar{\zeta}_{l_1}^{(m_c)}\bar{\zeta}_{l_2}^{(m_d)}\bar{b}_{l_1}(t)\right)\bar{b}_{l_2}(t) \\
&= \sum_{l_2=0}^{q}\left(\sum_{l_1=0}^{q} \underbrace{\bar{\zeta}_{l_1}^{(m_c)}\bar{\zeta}_{l_2}^{(m_d)}}\,\underbrace{\bar{b}_{l_1}(t)\bar{b}_{l_2}(t)}\right) \\
&= \sum_{l_2=0}^{q}\sum_{l_1=0}^{q} \qquad \hat{\zeta}_{l_1,l_2}^{m_{c,d}} \qquad \hat{b}_{l_1 l_2}(t). \quad (4.3.2)
\end{aligned}$$

The number of basis functions has been squared from $\bar{b}_{l_1}(t)$, with $l_1 \in \{0, 1, ..., q\}$ to $\hat{b}_{l_1 l_2}(t)$ with $l_1 l_2 \in \{0, 1, ..., q^2\}$. And with each further multiplication, the exponent of q^k increases by one. That means for example, that the product of three sums gives a total of q^3 basis functions $\hat{b}_{l_1 l_2 l_3}$. (4.3.1) shows that the coefficient $\alpha_2(t)$ is calculated from the sum of all possible combinations of $P_{m_c}(t)P_{m_d}(t)$ with $m_c < m_d$. This results in $\alpha_2(t)$ as a polynomial of degree q^2. Similarly, $\alpha_k(t)$ is a polynomial of order q^k. Therefore, it is efficient to keep the number of basis elements q as small as possible.
In summary, two design choices suggested themself: (1) the basis functions $\bar{b}_l(t)$ of the roots should be as simple as possible and (2) the number of basis functions q per root should be as small as possible. This keeps the number of basis functions low when estimating the coefficients $\alpha_k(t)$. The function that combines these properties the most is a polynomial of degree one:

$$P_k(t) = \zeta_0^{(k)} + \zeta_1^{(k)} t \;\forall\; k = 1, 2, ..., p.$$

With applying this basis function to (4.3.1) and (4.3.2), the k-th coefficient $\alpha_k(t)$ becomes a polynomial of order k, and

$$\alpha_k(t) = \sum_{l=0}^{k} \beta_l^{(k)} t^l \tag{4.3.3}$$

can be used for the parameter estimation as described in section 4.1. Switching from $\alpha_k(t)$ to $\beta_l^{(k)}$ increases the number of parameters from p to $\frac{p^2+3p}{2}$ (see Appendix (C.7.3).

4.3.2 The Conversion of Coefficients to Roots (Sufficient Condition)

The most important statements in the last two sections seem to contradict each other, as the parameters in the example in section 4.2

$$\alpha_1(t) = 1 - 2.5t \qquad \text{and} \qquad \alpha_2(t) = -0.5 \qquad \text{for } t \in [0, 1]$$

fulfil the conditions of section 4.3.1 without possessing linear root movements. This shows that parametrization of coefficients by ascending order polynomials in (4.3.3) poses only a necessary but not sufficient condition for linear root motions. For further conditions, a transformation of the coefficients α_k from (2.9.1) to the roots P_k from (2.9.2) is required. Fortunately, the CP

poses a special case of general polynomials (as described in section 2.17), which only demands the specification of the coefficients c_k as:

$$c_k = -\alpha_k. \tag{4.3.4}$$

This also means that the computation of the roots of the CP demands the same function as the function for the zeros of a time variable polynomial -even if the coefficients and the roots are functions of time.
In case of a first order polynomial, using

$$P_1(t) = \alpha_1(t), \tag{4.3.5}$$

(a combination of (2.17.1) and (4.3.4)), the root can be computed directly. It remains to determine the restrictions of the parameters $\beta_l^{(k)}$ with $l \in \{0, 1\}$ and $k = 1$ in such a way that that the root motion of the TVAR(1) process is linear. Fortunately, $\alpha_1(t)$ is a linear function (see the construction in (4.3.3)). This also means that the coefficient of the TVAR(1) process is calculated with

$$\alpha_1(t) = \beta_0^{(1)} + \beta_1^{(1)} t, \tag{4.3.6}$$

and because of (4.3.5), the same applies to the time variable root $P_1(t)$ in the TVAR(1) process. It is therefore always linear.
The next step poses the TVAR(2) process. According to (2.17.2), the conversion of the coefficients to the roots is given via the quadratic formula for polynomials of order two:

$$\begin{aligned} P_{1,2}(t) &= -\frac{c_1(t)}{2} \pm \sqrt{\left(\frac{c_1(t)}{2}\right)^2 - c_2(t)} \\ &= \frac{\alpha_1(t)}{2} \pm \sqrt{\left(\frac{\alpha_1(t)}{2}\right)^2 + \alpha_2(t)}. \end{aligned}$$

Since the addition and the subtraction of linear functions yields a gain a linear function, it is sufficient to show that $\alpha_1(t)/2$ is always linear, and then to establish a restriction that ensures that the solution of the root ($\sqrt{(\alpha_1(t)/2)^2 + \alpha_2(t)}$) is always a linear function. Since the calculation of $\alpha_1(t)$ from $\beta_0^{(1)}$ and $\beta_1^{(1)}$ does not change with increasing order, (4.3.6) still applies. This then also means that

$$\frac{\alpha_1(t)}{2} = \frac{\beta_0^{(1)} + \beta_1^{(1)} t}{2}$$

is a linear function. So, it remains to identify the circumstances under which the restriction of the roots $P_1(t)$ and $P_2(t)$ are linear

$$\sqrt{\left(\frac{\alpha_1(t)}{2}\right)^2 + \alpha_2(t)} \stackrel{!}{=} f_1 + f_2 t \tag{4.3.7}$$

is fulfilled. Here, f_1 and f_2 are two unknown constants. To find the restriction, both sides of (4.3.7) are squared:

$$\left(\frac{a_1(t)}{2}\right)^2 + a_2(t) = f_1^2 + 2 f_1 f_2 t + f_2^2 t^2. \tag{4.3.8}$$

If $\alpha_1(t)$ shown in (4.3.6) and $\alpha_2(t) = \beta_0^{(2)} + \beta_1^{(2)} t + \beta_2^{(2)} t^2$ following (4.3.3) are inserted into the left side of the equation (4.3.8), then

$$\begin{aligned} \left(\frac{a_1(t)}{2}\right)^2 + a_2(t) &= \left(\frac{\beta_0^{(1)} + \beta_1^{(1)} t}{2}\right)^2 + \beta_0^{(2)} + \beta_1^{(2)} t + \beta_2^{(2)} t^2 \\ &= \frac{(\beta_0^{(1)})^2 + 2\beta_0^{(1)}\beta_1^{(1)} t + (\beta_1^{(1)})^2 t^2}{4} + \beta_0^{(2)} + \beta_1^{(2)} t + \beta_2^{(2)} t^2 \\ &= \frac{(\beta_0^{(1)})^2}{4} + \beta_0^{(2)} + \left(\frac{\beta_0^{(1)}\beta_1^{(1)}}{2} + \beta_1^{(2)}\right) t + \left(\frac{(\beta_1^{(1)})^2}{4} + \beta_2^{(2)}\right) t^2 \end{aligned}$$

shows that there are polynomials of degree two on both sides of equations (4.3.8). To show that these are equal, it must be shown that the coefficients on the left side are equal to the coefficients on the right side. So, each coefficient provides us with one condition:

$$\begin{aligned}
&\frac{(\beta_0^{(1)})^2}{4} + \beta_0^{(2)} \stackrel{!}{=} f_1^2 && \Rightarrow f_1 = \sqrt{\frac{(\beta_0^{(1)})^2}{4} + \beta_0^{(2)}} \\
&\frac{\beta_0^{(1)}\beta_1^{(1)}}{2} + \beta_1^{(2)} \stackrel{!}{=} 2 f_1 f_2 && \\
&\frac{(\beta_1^{(1)})^2}{4} + \beta_2^{(2)} \stackrel{!}{=} f_2^2 && \Rightarrow f_2 = \sqrt{\frac{(\beta_1^{(1)})^2}{4} + \beta_2^{(2)}}.
\end{aligned}$$

From the first restriction, f_1 can be determined, and the same applies to the last restriction to determine f_2. Finally, these results can be used in the second restriction to find the parameter's restriction:

$$\frac{\beta_0^{(1)}\beta_1^{(1)}}{2} + \beta_1^{(2)} = 2\sqrt{\left(\frac{(\beta_0^{(1)})^2}{4} + \beta_0^{(2)}\right)\left(\frac{(\beta_1^{(1)})^2}{4} + \beta_2^{(2)}\right)}.$$

To remove the root, both sides are squared:

$$\left(\frac{\beta_0^{(1)}\beta_1^{(1)}}{2} + \beta_1^{(2)}\right)^2 = 4\left(\frac{(\beta_0^{(1)})^2}{4} + \beta_0^{(2)}\right)\left(\frac{(\beta_1^{(1)})^2}{4} + \beta_2^{(2)}\right)$$

$$\frac{(\beta_0^{(1)})^2(\beta_1^{(1)})^2}{4} + \beta_0^{(1)}\beta_1^{(1)}\beta_1^{(2)} + (\beta_1^{(2)})^2 = \frac{(\beta_0^{(1)})^2(\beta_1^{(1)})^2}{4} + (\beta_0^{(1)})^2\beta_2^{(2)} + \beta_0^{(2)}(\beta_1^{(1)})^2 + 4\beta_0^{(2)}\beta_2^{(2)}$$

$$\beta_0^{(1)}\beta_1^{(1)}\beta_1^{(2)} + (\beta_1^{(2)})^2 = (\beta_0^{(1)})^2\beta_2^{(2)} + \beta_0^{(2)}(\beta_1^{(1)})^2 + 4\beta_0^{(2)}\beta_2^{(2)}.$$

Summarizing all terms on one side results in the non-linear restriction:

$$\mathcal{C}^{\text{lin}}(\boldsymbol{\beta}) = (\beta_0^{(1)})^2\beta_2^{(2)} + \beta_0^{(2)}(\beta_1^{(1)})^2 - \beta_0^{(1)}\beta_1^{(1)}\beta_1^{(2)} + 4\beta_0^{(2)}\beta_2^{(2)} - (\beta_1^{(2)})^2 \stackrel{!}{=} 0. \tag{4.3.9}$$

This states the sufficient restriction to calculate the TVAR(2) processes with linear root movements. The resulting procedure for the adjustment problem is described in Appendix C.4. Finally, while this section is limited to first and second order polynomials, section 4.3.3 provides a method for approximating TVAR processes of higher orders by the means of successive estimation with TVAR(1) and TVAR(2) processes. The TVAR(3) process is discussed separately in section 4.5.1.

4.3.3 TVAR Processes with Linear Root Movements of Higher Orders

This section explains how to derive the estimation of a TVAR process of any degree from TVAR(1) and TVAR(2) processes and how to determine the most suitable order by the AIC. This allows a TVAR(p) process with linear root motions to be estimated without having to impose additional restrictions. To start, the TVAR(1) or TVAR(2) process is estimated for the time series $\mathcal{S}_t$. The residuals

$$\hat{\mathcal{S}}_t := \mathcal{E}_t = \mathcal{S}_t - \sum_{k=1}^{p} \alpha_k(t)\mathcal{S}_{t-k}$$

are then regarded as a new time series to again estimate a TVAR(1) or TVAR(2) process. This procedure is repeatedly applied until the desired order of the TVAR process is reached. In Appendix C.5, it is shown how a TVAR(p+1) or TVAR(p+2) process is generated by the TVAR estimation for the residuals of a TVAR(p) process. A distinction between the extension with a TVAR(1) and a TVAR(2) process is necessary, since the TVAR(1) process is unable to reveal complex-valued root motions. This becomes a since the construction of TVAR processes of higher orders are ambiguous. A TVAR(3) process can for example result from three different combinations:

1. Triple estimation of a TVAR(1) process.
2. Estimation of a TVAR(1) process followed by a TVAR(2) estimation.
3. The estimate a TVAR(2) process followed by the estimate of a TVAR(1) process.

In Appendix C.6, it is shown that each combination demads different solutions, all of which have to be tested with the AIC. For the AIC, Appendix C.7 shows that it is irrelevant of how many TVAR processes of order one and two the estimate consists. Instead, only the total number of roots or -in other words- the order of the process matters. Section 2.19 has shown how to estimate the order of a time constant AR process is estimated. This procedure is adapted here for the TVAR estimation:

1. Set a lower and upper boundary (b_l, b_u) for the order p of the TVAR process:

   $$b_l \leq p \leq b_u$$

   and, in order to represent all processes, determine all possible permutations of sums including one and two for each order, as it was done in the case of the TVAR(3) process.

2. Calculate the TVAR process and the AIC for all representations, whereby the AIC for this estimate is given as

   $$AIC = \ln\left(\frac{\boldsymbol{e}^T\boldsymbol{e}}{n-p}\right) + \frac{2(2p+1)}{n-p},$$

   where n is the length of the time series, p is the order of the TVAR process and

   $$e_t = \begin{cases} \bar{\mathcal{S}}_t - (\beta_0^{(1)} + \beta_1^{(1)}t)\bar{\mathcal{S}}_{t-1} & \text{for TVAR(1) process} \\ \bar{\mathcal{S}}_t - (\beta_0^{(1)} + \beta_1^{(1)}t)\bar{\mathcal{S}}_{t-1} - (\beta_0^{(2)} + \beta_1^{(2)}t + \beta_2^{(2)}t^2)\bar{\mathcal{S}}_{t-2} & \text{for TVAR(2) process} \end{cases}$$

   are the residuals from the last TVAR process estimation (see Appendix C.7.2).

3. Find the minimum AIC in the interval $[b_u, b_o]$ and use the corresponding TVAR process.

4.4 Piecewise TVAR Estimation

To create more complex root movements, the time series can be subdivided into several intervals which in turn serve to estimate TVAR processes with linear root motions. As with the global estimation of TVAR processes, processes with order higher than two can be approximated by the means of a successive estimation, which is why again only processes with orders $p \leq 2$ are considered.

4.4.1 Division into Intervals

We begin with the discussions of this method's main problem: The division of the observation into smaller groups. These should be chosen in a way that a non-linear root movement is subdivided into segments, so that each interval can be approximated by a TVAR process with linear root movements. In order to detect these intervals, or respectively their borders, a moving window should be used to estimate time stable AR processes for the individual windows. The roots of the CPs can be calculated for each window and plotted into the unit circle. This way, the boundaries between the intervals can be derived from visual inspection of the time tracks of the specific roots. As such, the entire vector of the observations $(\boldsymbol{y})$ is divided into observation groups. In order to distinguish these groups, a new notation is introduced: Each observation group is indicated by a superscripted roman number corresponding to the interval:

$$\boldsymbol{y} = \begin{bmatrix} \boldsymbol{y}^{(I)} \\ \boldsymbol{y}^{(II)} \\ \boldsymbol{y}^{(III)} \\ \vdots \end{bmatrix} \quad \text{with} \quad \begin{aligned} \boldsymbol{y}^{(I)} &= \begin{bmatrix} \mathcal{S}_{p+1} & \mathcal{S}_{p+2} & \dots & \mathcal{S}_{n_1} \end{bmatrix}^T \\ \boldsymbol{y}^{(II)} &= \begin{bmatrix} \mathcal{S}_{n_1+1} & \mathcal{S}_{n_1+2} & \dots & \mathcal{S}_{n_1+n_2} \end{bmatrix}^T \\ \boldsymbol{y}^{(III)} &= \begin{bmatrix} \mathcal{S}_{n_1+n_2+1} & \mathcal{S}_{n_1+n_2+2} & \dots & \mathcal{S}_{n_1+n_2+n_3} \end{bmatrix}^T \\ &\vdots \end{aligned} .$$

Here, n_j denotes the number of observations in the j-th group. Note that, similar to the vector of observations in the estimation of global time series, $\boldsymbol{y}^{(I)}$ does not include the first p observations. When dividing the observations into intervals, it must be noted that the observations on the boundary points always belongs to the preceding interval (e.g. the second interval is set to $(\mathcal{S}_{n1}, \mathcal{S}_{n1+n2}]$).
To achieve a continuous function in both the roots and the coefficients of the TVAR process, the root at the end of the k-th interval must match the beginning of the $(k+1)$-th interval, -regardless of the order of the polynomial root motion. The vector $\boldsymbol{t}$ containing the time steps for all observations and the parameter vector $\boldsymbol{\beta}$ are adapted, to fulfil this condition. First, $\boldsymbol{t}$ is divided in the same manner as $\boldsymbol{y}$

$$\hat{\boldsymbol{t}} = \begin{bmatrix} \hat{\boldsymbol{t}}^{(I)} \\ \hat{\boldsymbol{t}}^{(II)} \\ \hat{\boldsymbol{t}}^{(III)} \\ \vdots \end{bmatrix} \quad \text{with} \quad \begin{aligned} \hat{\boldsymbol{t}}^{(I)} &= \begin{bmatrix} t_{p+1} & t_{p+2} & ... & t_{n_1} \end{bmatrix}^T \\ \hat{\boldsymbol{t}}^{(II)} &= \begin{bmatrix} t_{n_1+1} & t_{n_1+2} & ... & t_{n_1+n_2} \end{bmatrix}^T \\ \hat{\boldsymbol{t}}^{(III)} &= \begin{bmatrix} t_{n_1+n_2+1} & t_{n_1+n_2+2} & ... & t_{n_1+n_2+n_3} \end{bmatrix}^T \\ &\vdots \end{aligned} .$$

This partitioning allows the normalization of the time intervals of each individual group. The first interval is the only one normalized to the interval $[0, 1]$. This is also the reason why the step width in this interval must be reduced by 1 in addition to the p missing observations. Any following interval with index $j > 1$ is normalised to $[1/n_j, 1]$, resulting in equidistant steps of $1/n_j$ between the time points in a single interval:

$$\boldsymbol{t} = \begin{bmatrix} \boldsymbol{t}^{(I)} \\ \boldsymbol{t}^{(II)} \\ \boldsymbol{t}^{(III)} \\ \vdots \end{bmatrix} \quad \text{with} \quad \begin{aligned} \boldsymbol{t}^{(I)} &= \begin{bmatrix} 0 & \frac{1}{n_1-p-1} & ... & 1 \end{bmatrix}^T \\ \boldsymbol{t}^{(II)} &= \begin{bmatrix} \frac{1}{n_2} & \frac{2}{n_2} & ... & 1 \end{bmatrix}^T \\ \boldsymbol{t}^{(III)} &= \begin{bmatrix} \frac{1}{n_3} & \frac{2}{n_3} & ... & 1 \end{bmatrix}^T \\ &\vdots \end{aligned} .$$

This division allows the piecewise TVAR estimates to be directly merged into a continuous function. This is so because for the second interval, $t^{(II)} = 0$ is the time of the first interval boundary $(\hat{t}_{n_1})$, and thus results in:

$$\mathcal{S}_{n_1} = \sum_{k=1}^{p} \sum_{l=0}^{q_k} \beta_l^{(k,II)} 0^l = \sum_{k=1}^{p} \beta_0^{(k,II)},$$

with $\beta_l^{(k,II)}$ being the coefficient $\beta_l^{(k)}$ of the second interval. Of course, for the first interval,

$$\mathcal{S}_{n_1} = \sum_{k=1}^{p} \sum_{l=0}^{q_k} \beta_l^{(k,I)} 1^l = \sum_{k=1}^{p} \sum_{l=0}^{q_k} \beta_l^{(k,I)}$$

is also true. It follows that

$$\sum_{k=1}^{p} \beta_0^{(k,II)} = \sum_{k=1}^{p} \sum_{l=0}^{q_k} \beta_l^{(k,I)}.$$

Since the roots of the CP for the first and second intervals must be similar at the point $\hat{t}_{n_1}$, this must also be the case for each coefficient $\alpha_k(t)$ of the TVAR process at time $\hat{t}_{n_1}$:

$$\begin{aligned} \alpha_k^{(I)}(1) &= \alpha_k^{(II)}(0) && \forall k = 1, 2, ..., p \text{ and} \\ \sum_{l=0}^{q_k} \beta_l^{(k,I)} &= \beta_0^{(k,II)} && \forall k = 1, 2, ..., p. \end{aligned} \tag{4.4.1}$$

This means that $\beta_0^{(k,II)}$ is determined for $k = 2, ..., p$ by the previous interval and no longer appears in the adjustment. So, for the second interval, the parameter vector from (4.1.6) is shortened to

$$\boldsymbol{\beta}^{(II)} = \Big[\underbrace{\beta_1^{(1,II)} \quad \beta_1^{(2,II)} \quad \dots \quad \beta_1^{(p,II)}}_{p \text{ elements}} \Big| \underbrace{\beta_2^{(2,II)} \quad \dots \quad \beta_2^{(p,II)}}_{p-1 \text{ elements}} \Big| \dots \Big| \underbrace{\beta_{p-1}^{(p-1,II)} \quad \beta_{p-1}^{(p,II)}}_{2 \text{ elements}} \Big| \underbrace{\beta_p^{(p,II)}}_{1 \text{ element}} \Big]^T .$$

This also accounts for all subsequent intervals $III, IV, V, \dots$. With $\boldsymbol{\beta}^{(I)}$ being the same as in the global case shown in (C.4.2), the vector includes a total number of $(Np^2 + (2+N)p)/2$ parameters for N intervals. Since the estimate for piecewise TVAR processes with orders greater than two is reached by successive estimation again, it is sufficient to analyse the estimates for the piecewise TVAR(1) and the piecewise TVAR(2) processes.

4.4.2 Piecewise TVAR(1) Processes over Two Intervals

The first step for calculating piecewise TVAR(1) processes with linear root motions lies in finding the parameter vector. In the case of two intervals, the parameters per interval are given as:

$$\boldsymbol{\beta}^{(I)} = \begin{bmatrix} \beta_0^{(1,I)} & \beta_1^{(1,I)} \end{bmatrix}^T \qquad \text{for the first interval, and}$$

$$\boldsymbol{\beta}^{(II)} = \begin{bmatrix} \beta_1^{(1,II)} \end{bmatrix} \qquad \text{for the second interval.}$$

For the adjustment, the joint parameter vector is then:

$$\boldsymbol{\beta} = \begin{bmatrix} \boldsymbol{\beta}^{(I)} \\ \boldsymbol{\beta}^{(II)} \end{bmatrix} = \left[\begin{array}{cc|c} \beta_0^{(1,I)} & \beta_1^{(1,I)} & \beta_1^{(1,II)} \end{array} \right]^T .$$

In the same way, the vector representing the observations is partitioned into

$$\boldsymbol{y}^{(I)} = \begin{bmatrix} \mathcal{S}_2 & \mathcal{S}_3 & \dots & \mathcal{S}_{n_1} \end{bmatrix}^T \quad \text{and} \quad \boldsymbol{y}^{(II)} = \begin{bmatrix} \mathcal{S}_{n_1+1} & \mathcal{S}_{n_1+2} & \dots & \mathcal{S}_{n_1+n_2} \end{bmatrix}^T .$$

For the least-squares estimate, the design matrices are created as in Appendix C.3, i.e. by first calculating the columns of the Toeplitz matrices

$$\boldsymbol{T}^{(I)} = \begin{bmatrix} \mathcal{S}_1 & \mathcal{S}_2 & \dots & \mathcal{S}_{n_1-1} \end{bmatrix}^T \quad \text{and} \quad \boldsymbol{T}^{(II)} = \begin{bmatrix} \mathcal{S}_{n_1} & \mathcal{S}_{n_1+1} & \dots & \mathcal{S}_{n_1+n_2-1} \end{bmatrix}^T ,$$

for the two intervals. The design matrix for the first interval ($\boldsymbol{X}^{(I)}$) is set up analogously to the approximation with global functions, but then expanded with a zero column, as $\beta_1^{(1,II)}$ is not estimated in the first interval:

$$\boldsymbol{X}^{(I)} = \left[\begin{array}{c|c|c} \boldsymbol{T}^{(I)} & \boldsymbol{T}^{(I)} \odot \boldsymbol{t}^{(I)} & \boldsymbol{0}_{n_1 \times 1} \end{array} \right] .$$

The case is different for the design matrix of the second interval. Here, $\boldsymbol{T}^{(I)}$ is not only replaced by $\boldsymbol{T}^{(II)}$, but the $\boldsymbol{X}^{(I)}$'s zero line is replaced by the element wise matrix vector product $\boldsymbol{T}^{(II)} \odot \boldsymbol{t}^{(II)}$ shown in (C.2.4). In all other columns, $\boldsymbol{T}^{(II)}$ are used:

$$\boldsymbol{X}^{(II)} = \left[\begin{array}{c|c|c} \boldsymbol{T}^{(II)} & \boldsymbol{T}^{(II)} & \boldsymbol{T}^{(II)} \odot \boldsymbol{t}^{(II)} \end{array} \right] .$$

The entries for the first two columns of $\boldsymbol{X}^{(II)}$ are the result of (4.4.1), because $\beta_0^{(k,II)}$ is replaced by the sum of all previous $\beta_l^{(k,I)}$:

$$\beta_k^{(0,II)} = \beta_k^{(0,I)} + \beta_k^{(1,I)}.$$

Similar to the case of the global estimation, no further restrictions are needed in the TVAR(1) process to obtain linear root movements. So, in order to determine the desired parameters and their covariance matrix by the linear Gauss-Markov model, the matrices

$$\boldsymbol{X} = \begin{bmatrix} \boldsymbol{X}^{(I)} \\ \boldsymbol{X}^{(II)} \end{bmatrix} \qquad \text{and} \qquad \boldsymbol{y} = \begin{bmatrix} \boldsymbol{y}^{(I)} \\ \boldsymbol{y}^{(II)} \end{bmatrix}$$

can be used in the global TVAR estimate in (C.2.6) and (C.2.7).

4.4.3 General Estimate of Piecewise TVAR(1) Processes

Now, both the observation vector $\boldsymbol{y}$ and the design matrix $\boldsymbol{X}$ can be divided into distinguished parts for each interval, and then set up individually. If $\eta \leq N$ is the placeholder for the Roman numbering of an arbitrary interval, and further let n_η be the number of observations in that interval, then

$$\boldsymbol{y}^{(\eta)} = \begin{cases} \begin{bmatrix} \mathcal{S}_2 & \mathcal{S}_3 & \dots & \mathcal{S}_{n_1} \end{bmatrix}^T & \text{if } \eta = I \\ \begin{bmatrix} \mathcal{S}_{(\sum_{n_j<n_\eta} n_j)+1} & \mathcal{S}_{(\sum_{n_j<n_\eta} n_j)+2} & \dots & \mathcal{S}_{(\sum_{n_j<n_\eta} n_j)+n_\eta} \end{bmatrix}^T & \text{else} \end{cases} \tag{4.4.2}$$

are the observations in that interval and

$$\boldsymbol{t}^{(\eta)} = \begin{cases} [0,1] \text{ with a uniform distance of } \frac{1}{n_1-2} & \text{if } \eta = I \\ \left[\frac{1}{n_\eta}, 1\right] \text{ with a uniform distance of } \frac{1}{n_\eta} & \text{else} \end{cases} \tag{4.4.3}$$

is the vector with the time steps.

$$\boldsymbol{T}^{(\eta)} = \begin{cases} \begin{bmatrix} \mathcal{S}_1 & \mathcal{S}_2 & \dots & \mathcal{S}_{n_1-1} \end{bmatrix}^T & \text{if } \eta = I \\ \begin{bmatrix} \mathcal{S}_{(\sum_{n_j<n_\eta} n_j)} & \mathcal{S}_{(\sum_{n_j<n_\eta} n_j)+1} & \dots & \mathcal{S}_{(\sum_{n_j<n_\eta} n_j)+n_\eta-1} \end{bmatrix}^T & \text{else} \end{cases} \tag{4.4.4}$$

is the corresponding Toeplitz matrix (C.3.1). Then, the $N+1$ parameters are given by

$$\boldsymbol{\beta} = \begin{cases} \begin{bmatrix} \beta_0^{(1,I)} & \beta_1^{(1,I)} \end{bmatrix}^T & \text{if } N = 1 \\ \left[\begin{array}{cc|c|c|c|c|c} \beta_0^{(1,I)} & \beta_1^{(1,I)} & \beta_1^{(1,II)} & \beta_1^{(1,III)} & \dots & \beta_1^{(1,N)} \end{array}\right]^T & \text{else} \end{cases}$$

and the rows of the design matrix corresponding to the interval η can be expressed as

$$\boldsymbol{X}^{(\eta)} = \Big[\underbrace{\boldsymbol{T}^{(\eta)} \,\Big|\, \boldsymbol{T}^{(\eta)} \,\Big|\, \dots \,\Big|\, \boldsymbol{T}^{(\eta)}}_{\eta \text{ elements}} \,\Big|\, \boldsymbol{T}^{(\eta)} \odot \boldsymbol{t}^{(\eta)} \,\Big|\, \boldsymbol{0}_{n_\eta \times (N-\eta)} \Big]. \tag{4.4.5}$$

Here, $\boldsymbol{0}_{n_\eta \times (N-\eta)}$ is a zero matrix of dimension $n_\eta \times (N-\eta)$. After this has been done for all intervals, the adjustment of the joint observations and the joint design matrices

$$\boldsymbol{y} = \begin{bmatrix} \boldsymbol{y}^{(1)} \\ \boldsymbol{y}^{(2)} \\ \vdots \\ \boldsymbol{y}^{(\eta)} \\ \vdots \\ \boldsymbol{y}^{(N)} \end{bmatrix} \qquad \text{and} \qquad \boldsymbol{X} = \begin{bmatrix} \boldsymbol{X}^{(1)} \\ \boldsymbol{X}^{(2)} \\ \vdots \\ \boldsymbol{X}^{(\eta)} \\ \vdots \\ \boldsymbol{X}^{(N)} \end{bmatrix} \tag{4.4.6}$$

can be performed using (C.2.6) and (C.2.7).

4.4.4 Piecewise TVAR(2) Processes over Two Intervals

In order to be able to create a successive TVAR construction, the estimation of piecewise TVAR(2) processes is still missing. Its first step is analogous to that of the piecewise TVAR(1) process. In this case, there is not only the TVAR coefficient $\alpha_1(t)^{(I)}$, but also the coefficient $\alpha_2(t)^{(I)}$, causing the parameters in the first interval to expand to

$$\boldsymbol{\beta}^{(I)} = \left[\begin{array}{cc|cc|c} \beta_0^{(1,I)} & \beta_0^{(2,I)} & \beta_1^{(1,I)} & \beta_1^{(2,I)} & \beta_2^{(2,I)} \end{array}\right]^T. \tag{4.4.7}$$

For the second interval,

$$\boldsymbol{\beta}^{(II)} = \left[\begin{array}{cc|c} \beta_1^{(1,II)} & \beta_1^{(2,II)} & \beta_2^{(2,II)} \end{array}\right]^T$$

is added. These are in turn merged with the vector

$$\boldsymbol{\beta} = \begin{bmatrix}\boldsymbol{\beta}^{(I)} \\ \boldsymbol{\beta}^{(II)}\end{bmatrix} = \left[\begin{array}{cc|cc|cc|cc|c} \beta_0^{(1,I)} & \beta_0^{(2,I)} & \beta_1^{(1,I)} & \beta_1^{(2,I)} & \beta_2^{(2,I)} & \beta_1^{(1,II)} & \beta_1^{(2,II)} & \beta_2^{(2,II)} \end{array}\right]^T.$$

For the observation vector, only the contribution of the first interval -which starts from the third observation- changes. The vector for the second interval remains the same. For this reason,

$$\boldsymbol{y}^{(I)} = \begin{bmatrix}\mathcal{S}_3 & \mathcal{S}_4 & ... & \mathcal{S}_{n_1}\end{bmatrix}^T \quad \text{and} \quad \boldsymbol{y}^{(II)} = \begin{bmatrix}\mathcal{S}_{n_1+1} & \mathcal{S}_{n_1+2} & ... & \mathcal{S}_{n_1+n_2}\end{bmatrix}^T$$

apply, but the Toeplitz matrix ($\boldsymbol{T}$), which is derived by Y.-W. equations, changes fundamentally. The reason for this is that according to (C.2.3)

$$\boldsymbol{T}^{(I)} = \begin{bmatrix}\mathcal{S}_2 & \mathcal{S}_3 & ... & \mathcal{S}_{n_1-1} \\ \mathcal{S}_1 & \mathcal{S}_2 & ... & \mathcal{S}_{n_1-2}\end{bmatrix}^T \quad \text{and} \quad \boldsymbol{T}^{(II)} = \begin{bmatrix}\mathcal{S}_{n_1} & \mathcal{S}_{n_1+1} & ... & \mathcal{S}_{n_1+n_2-1} \\ \mathcal{S}_{n_1-1} & \mathcal{S}_{n_1} & ... & \mathcal{S}_{n_1+n_2-2}\end{bmatrix}^T$$

are now matrices instead of vectors. As in the TVAR(2) process estimate for only one interval, the process of the estimation is again divided into two steps: In the first step the coefficients are estimated by the means of a Gauss-Markov model. But for a TVAR(2) process, an additional restriction is needed (see section 4.3.2). The same restrictions must be fulfilled for each interval. However, the restrictions of an interval includes all parameters of the previous intervals.
For the first interval, the design matrices $\boldsymbol{X}^{(I)}$ is computed as in (C.4.4), only that a zero matrix has again been added:

$$\boldsymbol{X}^{(I)} = \left[\begin{array}{c|c|c|c} \boldsymbol{T}^{(I)} & \boldsymbol{T}^{(I)} \odot \boldsymbol{t}^{(I)} & \boldsymbol{T}_2^{(I)} \odot \left(\boldsymbol{t}^{(I)}\right)^{\odot 2} & \boldsymbol{0}_{n_1,3} \end{array}\right],$$

with $\boldsymbol{T}_2^{(I)} = \boldsymbol{T}^{(I)}(:, 2 : \text{end})$ (as shown in (C.4.3)). $\left(\boldsymbol{t}^{(I)}\right)^{\odot 2}$ means that the exponent is applied element-wise for every entry in $\boldsymbol{t}^{(I)}$, like it is used in (C.4.4). For the second interval, $\beta_0^{(1,II)}$ and $\beta_0^{(2,II)}$ must be replaced by all previous coefficients $\beta_l^{(k,I)}$:

$$\beta_0^{(1,II)} = \beta_0^{(1,I)} + \beta_1^{(1,I)} \quad \text{and} \tag{4.4.8}$$
$$\beta_0^{(2,II)} = \beta_0^{(2,I)} + \beta_1^{(2,I)} + \beta_2^{(2,I)}. \tag{4.4.9}$$

This again leads to the fact that all first interval's coefficients are multiplied by $T^{(II)}$ or $T_1^{(II)}$, resulting in the design matrix

$$\boldsymbol{X}^{(II)} = \left[\begin{array}{c|c|c|c|c} \boldsymbol{T}^{(II)} & \boldsymbol{T}^{(II)} & \boldsymbol{T}_2^{(II)} & \boldsymbol{T}^{(II)} \odot \boldsymbol{t}^{(II)} & \boldsymbol{T}_2^{(II)} \odot \left(\boldsymbol{t}^{(II)}\right)^{\odot 2} \end{array}\right].$$

With this, the first step can now be calculated by computing an adjustment with

$$\boldsymbol{X} = \begin{bmatrix}\boldsymbol{X}^{(I)} \\ \boldsymbol{X}^{(II)}\end{bmatrix} \quad \text{and} \quad \boldsymbol{y} = \begin{bmatrix}\boldsymbol{y}^{(I)} \\ \boldsymbol{y}^{(II)}\end{bmatrix}.$$

Finally, the restrictions of the parameters have to be satisfied, which means that the restriction for the first interval again equals the one for the global approach:

$$\mathcal{C}_1^{\text{PW}}(\boldsymbol{\beta}) = (\beta_0^{(1,I)})^2\beta_2^{(2,I)} + \beta_0^{(2,I)}(\beta_1^{(1,I)})^2 - \beta_0^{(1,I)}\beta_1^{(1,I)}\beta_1^{(2,I)} + 4\beta_0^{(2,I)}\beta_2^{(2,I)} - (\beta_1^{(2,I)})^2. \tag{4.4.10}$$

In the second interval, since this interval can satisfy the restriction for linear root movements independently of the first interval, the underlying restriction remains the same. Only the end of

the first interval and the beginning of the second one still need to match, so that $\beta_0^{(1,II)}$ and $\beta_0^{(2,II)}$ must be replaced by the right sides of (4.4.8) and (4.4.9):

$$\begin{aligned}\mathcal{C}_2^{\mathrm{PW}}(\boldsymbol{\beta}) = &\left(\beta_0^{(1,I)} + \beta_1^{(1,I)}\right)^2 \beta_2^{(2,II)} + \left(\beta_0^{(2,I)} + \beta_1^{(2,I)} + \beta_2^{(2,I)}\right)(\beta_1^{(1,II)})^2 ... \\ &- \left(\beta_0^{(1,I)} + \beta_0^{(1,I)} + \beta_1^{(1,I)}\right)\beta_1^{(1,II)}\beta_1^{(2,II)} + 4\left(\beta_0^{(2,I)} + \beta_1^{(2,I)} + \beta_2^{(2,I)}\right)\beta_2^{(2,II)} - (\beta_1^{(2,II)})^2.\end{aligned} \tag{4.4.11}$$

Since these restrictions are again nonlinear, for the determination of the parameter vector $\boldsymbol{\beta}$ via the Gauss-Markov method, an adjustment in two steps as in Appendix C.4 is recommended.

4.4.5 General Estimate of Piecewise TVAR(2) Processes

There is also a general method for TVAR(2) processes to estimate linear root movements through any number of intervals. To find this method, the observations $\boldsymbol{y}$ and the times $\boldsymbol{t}$ are divided into individual intervals. The observations for each interval are defined by (4.4.2) and the times are normalized for each interval as it is shown (4.4.3). Here, $\eta \in \{I, II, III, ...\}$ is the number interval currently being considered. So far, everything is analogous to the structure of the TVAR(1) process with piecewise linear root motions. However, both the vector with the parameters ($\boldsymbol{\beta}$) and the Toeplitz matrix ($\boldsymbol{T}$) change to the pattern of the TVAR(2) process over two intervals discussed in the previous chapter. $\boldsymbol{\beta}$ is composed of the five parameters of (4.4.7) from the first interval and the parameters

$$\boldsymbol{\beta_\eta} = \left[\begin{array}{cc|c} \beta_1^{(1,\eta)} & \beta_1^{(2,\eta)} & \beta_2^{(2,\eta)} \end{array}\right]^T$$

for each further interval, resulting in a total of $3N + 2$ parameters. This means that first, the Toeplitz matrix for the interval η has the dimension $[(n_1 - 1) \times 2]$, just like the TVAR(2) process for two intervals, and second, uses the same cases as the TVAR(1) process in (4.4.4):

$$\boldsymbol{T}^{(\eta)} = \begin{cases} \begin{bmatrix} \mathcal{S}_2 & \mathcal{S}_3 & ... & \mathcal{S}_{n_1-1} \\ \mathcal{S}_1 & \mathcal{S}_2 & ... & \mathcal{S}_{n_1-2} \end{bmatrix}^T & \text{if } \eta = 1 \\ \begin{bmatrix} \mathcal{S}_{(\sum_{n_j<n_\eta} n_j)} & \mathcal{S}_{(\sum_{n_j<n_\eta} n_j)+1} & ... & \mathcal{S}_{(\sum_{n_j<n_\eta} n_j)+n_\eta-1} \\ \mathcal{S}_{(\sum_{n_j<n_\eta} n_j)-1} & \mathcal{S}_{(\sum_{n_j<n_\eta} n_j)} & ... & \mathcal{S}_{(\sum_{n_j<n_\eta} n_j)+n_\eta-2} \end{bmatrix}^T & \text{else.} \end{cases}$$

The design matrix $\boldsymbol{X}^{(\eta)}$ for the observations $\boldsymbol{y}^{(\eta)}$ can be established with $\boldsymbol{T}^{(\eta)}$, and using the same logical continuation as in (4.4.5):

$$\boldsymbol{X}^{(\eta)} = \left[\underbrace{\boldsymbol{T}^{(\eta)} \,\middle|\, \boldsymbol{T}^{(\eta)} \,\middle|\, \boldsymbol{T}_1^{(\eta)}}_{\text{interval I}} \underbrace{\boldsymbol{T}^{(\eta)} \,\middle|\, \boldsymbol{T}_1^{(\eta)}}_{\text{interval II}} ... \underbrace{\boldsymbol{T}^{(\eta)} \,\middle|\, \boldsymbol{T}_1^{(\eta)}}_{\text{interval } (\eta-1)} \underbrace{\boldsymbol{T}^{(\eta)} \odot \boldsymbol{t}^{(\eta)} \,\middle|\, \boldsymbol{T}_1^{(\eta)} \odot \left(\boldsymbol{t}^{(\eta)}\right).^2}_{\text{interval } \eta} \,\middle|\, \boldsymbol{0}_{n_\eta \times 3(N-\eta)}\right].$$

From this, $\boldsymbol{X}$ and $\boldsymbol{y}$ can then be constructed by the means of (4.4.6) to calculate the parameters of the first step (see (4.4.6)). The second step, now demands the restriction for TVAR(2) processes with linear root movements. This is done for each interval individually, resulting in exactly N additional restrictions. The restrictions of the first two intervals are provided in (4.4.10) and (4.4.11). For all subsequent intervals, they follow from the restrictions of the first interval by replacing

$$\beta_0^{(1,\eta)} = \beta_0^{(1,I)} + \sum_{\mu=1}^{\eta-1} \beta_1^{(1,\mu)} \qquad \text{and}$$

$$\beta_0^{(2,\eta)} = \beta_0^{(2,I)} + \sum_{\mu=1}^{\eta-1} (\beta_1^{(2,\mu)} + \beta_2^{(2,\mu)}).$$

The restriction for the interval η can be expressed by the means of

$$\mathcal{C}_\eta^{\mathrm{PW}}(\boldsymbol{\beta}) = \left(\beta_0^{(1,I)} + \sum_{\mu=1}^{\eta-1}\beta_1^{(1,\mu)}\right)^2 \beta_2^{(2,\eta)} + \left(\beta_0^{(2,I)} + \sum_{\mu=1}^{\eta-1}(\beta_1^{(2,\mu)} + \beta_2^{(2,\mu)})\right)(\beta_1^{(1,\eta)})^2 \ldots$$
$$- \left(\beta_0^{(1,I)} + \sum_{\mu=1}^{\eta-1}\beta_1^{(1,\mu)}\right)\beta_1^{(1,\eta)}\beta_1^{(2,\eta)} + 4\left(\beta_0^{(2,I)} + \sum_{\mu=1}^{\eta-1}(\beta_1^{(2,\mu)} + \beta_2^{(2,\mu)})\right)\beta_2^{(2,\eta)} - (\beta_1^{(2,\eta)})^2.$$

As in the global case, this condition is approximated by a Taylor linearization expansion until the conditions are sufficiently fulfilled. For this purpose, the derivatives of the conditions according to the parameters are required for each individual interval. For any interval η the derivative of the conditions can be found in Appendix C.11.1. These can be used to establish the conditional matrix $\boldsymbol{H}^T$, which is then used in the second stage to compute the parameters $\hat{\boldsymbol{\beta}}$ by (C.4.10) and the parameters Q-factor matrix $Q\{\hat{\boldsymbol{\beta}}\}$ by (C.4.11).

4.5 Further TVAR Estimate Extensions with Given Root Motions

To increase the possible root movements, modifications for the estimation of TVAR processes are included in this section. The extensions refer either to the movement of the roots by increasing the degree of the polynomial, or to method of increasing the process order to TVAR(3) processes.

4.5.1 Root Motions from Quadratic Polynomials

The first method deals with estimating the root motion by the means of a polynomial of higher orders. In particular, quadratic movements of the roots of TVAR processes are derived here:

$$P_k(t) = \zeta_0^{(k)} + \zeta_1^{(k)}t + \zeta_2^{(k)}t^2 \quad \forall\ k = 1, 2, ..., p.$$

According to section 4.3.1, quadratic root motions result in TVAR coefficients of polynomials whose order is twice as large as the index k of the coefficients $\alpha_k(t)$:

$$\alpha_k(t) = \sum_{l=0}^{2k}\beta_l^{(k)}t^l. \tag{4.5.1}$$

As for the linear root movements, this parametrization is not sufficient to guarantee a quadratic movement. Therefore, it is again necessary to derive restrictions from the parameters which ensure that the TVAR(1) and TVAR(2) process estimates resulting in quadratic root motions. For this reason, again, a successive method of TVAR(1) and TVAR(2) process estimates is used. Even in the case of quadratic motions, the root for the TVAR(1) process

$$\mathcal{S}_t = \alpha_1(t)\mathcal{S}_t + \mathcal{E}_t$$

derives from

$$P_1(t) = \alpha_1(t) = \beta_0^{(1)} + \beta_1^{(1)}t + \beta_2^{(1)}t^2$$

and thus always follows a parabolic motion without the need for further restrictions.
The need of the quadratic root movement of the TVAR(2) process demands the establishment of restrictions paralleling the linear root case of section 4.3.2 while adapting them to the current situation. This means that the same approach as in (4.3.7) can be used, but the coefficient $\alpha_1(t)$ needs to be changed into a polynomial of degree two, and $\alpha_2(t)$ into one of degree four. Furthermore, the right side needs to be a quadratic polynomial instead of a linear one, i.e.

$$\sqrt{\left(\frac{\alpha_1(t)}{2}\right)^2 + \alpha_2(t)} \stackrel{!}{=} f_1 + f_2t + f_3t^2.$$

The squaring of both sides results in two polynomials of degree four. These are equal if -and only if- all five coefficients are equal, equalling five restrictions. Out of these restrictions, three can be eliminated by the free parameters f_1, f_2 and f_3. The remaining two constraints are derived in Appendix (C.8.8) and (C.8.9) and result in the non-linear restrictions

$$\mathcal{C}_1^{\text{quad}}(\boldsymbol{\beta}) = \left(\beta_0^{(1)}\beta_1^{(1)} + 2\beta_1^{(2)}\right)^2 \left((\beta_2^{(1)})^2 + 4\beta_4^{(2)}\right) - \left(\beta_1^{(1)}\beta_2^{(1)} + 2\beta_3^{(2)}\right)^2 \left((\beta_0^{(1)})^2 + 4\beta_0^{(2)}\right) \stackrel{!}{=} 0 \tag{4.5.2}$$

and

$$\begin{aligned}&\mathcal{C}_2^{\text{quad}}(\boldsymbol{\beta})\\ &= 4\left(\frac{(\beta_0^{(1)})^2}{4} + \beta_0^{(2)}\right)\left(\frac{(\beta_2^{(1)})^2}{4} + \beta_4^{(2)}\right) - \left(\frac{\beta_0^{(1)}\beta_2^{(1)}}{2} + \frac{(\beta_1^{(1)})^2}{4} + \beta_2^{(2)} - \frac{(\beta_0^{(1)}\beta_1^{(1)} + 2\beta_1^{(2)})^2}{4((\beta_0^{(1)})^2 + 4\beta_0^{(2)})}\right)^2 \stackrel{!}{=} 0.\end{aligned} \tag{4.5.3}$$

Forcing the parameters to solve the conditions $\mathcal{C}_1^{\text{quad}}(\boldsymbol{\beta})$ and $\mathcal{C}_2^{\text{quad}}(\boldsymbol{\beta})$ with the procedure of the TVAR estimate from Appendix C.2, it is now possible to estimate TVAR processes of any order with quadratic root motions. After the parameters have been determined from the necessary condition (like it is demonstrated in Appendix C.3), the conditions are applied in a second step. The partial derivatives, as well as the resulting design matrix, are derived and documented in Appendix C.11.2.

4.5.2 Gaining Linear Roots from TVAR(3) Processes

It is also possible to determine the roots of the CP of higher order processes analytically -at least up to and including TVAR processes of order four (see section 2.17). For this reason, the restrictions of the TVAR(3) process with linear root movements have been determined in Korte et al. 2023a and are further elaborated here.
To start with a TVAR(3) process with the coefficients

$$\alpha_1(t) = \beta_0^{(1)} + \beta_1^{(1)}t, \tag{4.5.4}$$
$$\alpha_2(t) = \beta_0^{(2)} + \beta_1^{(2)}t + \beta_2^{(2)}t^2 \quad \text{and} \tag{4.5.5}$$
$$\alpha_3(t) = \beta_0^{(3)} + \beta_1^{(3)}t + \beta_2^{(3)}t^2 + \beta_3^{(3)}t^3, \tag{4.5.6}$$

it has been shown in (2.17.7), (2.17.8) and (2.17.9) that the roots are provided by the functions

$$\begin{aligned}P_1(t) &= (s_1(t) + s_2(t)) - \frac{-\alpha_1(t)}{3}\\ &= s_1(t) + s_2(t) + \frac{1}{3}\alpha_1(t),\\ P_2(t) &= -\frac{s_1(t) + s_2(t)}{2} - \frac{-\alpha_1(t)}{3} + i\frac{\sqrt{3}}{2}(s_1(t) - s_2(t))\\ &= \left(-\frac{1}{2} + i\frac{\sqrt{3}}{2}\right)s_1(t) + \left(-\frac{1}{2} - i\frac{\sqrt{3}}{2}\right)s_2(t) + \frac{1}{3}\alpha_1(t) \quad \text{and}\\ P_3(t) &= -\frac{s_1(t) + s_2(t)}{2} - \frac{-\alpha_1(t)}{3} - i\frac{\sqrt{3}}{2}(s_1(t) - s_2(t))\\ &= \left(-\frac{1}{2} - i\frac{\sqrt{3}}{2}\right)s_1(t) + \left(-\frac{1}{2} + i\frac{\sqrt{3}}{2}\right)s_2(t) + \frac{1}{3}\alpha_1(t).\end{aligned}$$

By rewriting the functions of the time variable roots like this, it becomes clear that each is a linear combination of $s_1(t)$, $s_2(t)$ and $\alpha_1(t)$. It follows if $s_1(t)$, $s_2(t)$ and $\alpha_1(t)$ are linear functions, so are $P_1(t)$, $P_2(t)$ and $P_3(t)$. There may exist corner cases where the sum $s_1(t) + s_2(t)$ is linear, while $s_1(t)$ and $s_2(t)$ contain non-linear functions with opposing signs. This would result in their

canceling in the sum. Those cases are excluded in the following elaborations.
Consequently, the problem simplifies to the equations

$$s_1(t) \stackrel{!}{=} f_1 + f_2 t, \tag{4.5.7}$$

$$s_2(t) \stackrel{!}{=} g_1 + g_2 t \qquad \text{and} \tag{4.5.8}$$

$$\alpha_1(t) \stackrel{!}{=} h_1 + h_2 t. \tag{4.5.9}$$

Fortunately, because of (4.5.4), $\alpha_1(t)$ is again a linear function, which means that the third restriction of (4.5.9) is always fulfilled. However, $s_1(t)$ and $s_2(t)$ must also satisfy the condition

$$2r(t) = s_1^3 + s_2^3 \text{ and } -q(t) = s_1 s_2. \tag{4.5.10}$$

Appendix C.9 shows, that $r(t)$ and $q(t)$ are expressed by the coefficients $\beta_l^{(k)}$, which must equal the polynomials of (4.5.10). Since $r(t)$ is a polynomial of degree three and $-q(t)$ is a polynomial of order two, their coefficient comparison results in seven restrictions, one for each coefficient. Four of these restrictions can be solved by the free parameters f_1, f_2, g_1 and g_2 of (4.5.7) and (4.5.8). The three remaining non-linear restrictions are derived in Appendix C.9:

$$\begin{aligned}&\mathcal{C}_1^{\mathrm{TVAR}(3)}(\boldsymbol{\beta}) \\ &= \frac{2(\beta_0^{(1)})^2\beta_1^{(1)}}{3^2} + \frac{\beta_0^{(1)}\beta_1^{(2)} + \beta_1^{(1)}\beta_0^{(2)}}{3} + \beta_1^{(3)} - 3\left[\left(\sqrt[3]{f_1^3}\right)^2\sqrt[3]{f_2^3} + \left(\sqrt[3]{g_1^3}\right)^2\sqrt[3]{g_2^3}\right] \stackrel{!}{=} 0\end{aligned} \tag{4.5.11}$$

$$\begin{aligned}&\mathcal{C}_2^{\mathrm{TVAR}(3)}(\boldsymbol{\beta}) \\ &= \frac{2\beta_0^{(1)}(\beta_1^{(1)})^2}{3^2} + \frac{\beta_0^{(1)}\beta_2^{(2)} + \beta_1^{(1)}\beta_1^{(2)}}{3} + \beta_2^{(3)} - 3\left[\sqrt[3]{f_1^3}\left(\sqrt[3]{f_2^3}\right)^2 + \sqrt[3]{g_1^3}\left(\sqrt[3]{g_2^3}\right)^2\right] \stackrel{!}{=} 0\end{aligned} \tag{4.5.12}$$

$$\begin{aligned}&\mathcal{C}_3^{\mathrm{TVAR}(3)}(\boldsymbol{\beta}) \\ &= \frac{2\beta_0^{(1)}\beta_0^{(2)}}{3^2} + \frac{\beta_1^{(2)}}{3} - \sqrt[3]{f_1^3}\sqrt[3]{g_2^3} + \sqrt[3]{f_2^3}\sqrt[3]{g_1^3} \stackrel{!}{=} 0.\end{aligned} \tag{4.5.13}$$

Also, the immediate calculation of the TVAR(3) process demands two steps. First, the necessary condition leads to the approximation of the needed parameters, which then secondly allow the calculation of the Taylor linearization for the constraints. In order to construct the conditional matrix $\boldsymbol{H}^T$, Appendix C.11.3 shows the partial derivatives of the three conditions in accordance to the parameters.

4.6 Evaluation

This section consists of a comparison and evaluation of the methods discussed above. These are:

1. The direct estimation of TVAR(1) and TVAR(2) processes with linear root movements (see Appendix C.4, TVAR(1) and TVAR(2) process);
2. the estimation of higher order TVAR processes with linear roots ($p > 2$) by successive estimation of TVAR(1) and TVAR(2) processes with linear root motions (see section 4.3.3, successive TVAR process);
3. the piecewise estimation of TVAR processes by the means of several observation intervals, (also in combination with successive estimation) (see section 4.4, piecewise TVAR process);
4. the estimation of TVAR(1) and TVAR(2) processes with quadratic movements (see section 4.5.1 (TVAR process with quadratic root motion);
5. as well as the direct estimation of TVAR(3) processes with linear root movements (see section 4.5.2: TVAR(3) process).

In order to obtain the most accurate result in TVAR estimation, the determination of the method best suited for the given time series is crucial. The key factor in this is the correct identification of the part of the root motion that poses the noise: if the roots are too rigid, the spectrum characteristic caused by them and their motion cannot be accurately mapped. However, if the roots are too flexible, one is prone to the risk of overparameterization, which results in the modelling of the noise and thus a distortion of the signal. In addition, the order of the TVAR process must be determined by estimating the TVAR process for several orders, while then further comparing the solutions against each other by the means of the adapted AIC for TVAR processes from Appendix C.7. In order to link the estimation methods to the different conditions, Figure 4.4 provides a decision tree to find the best method for a given case.

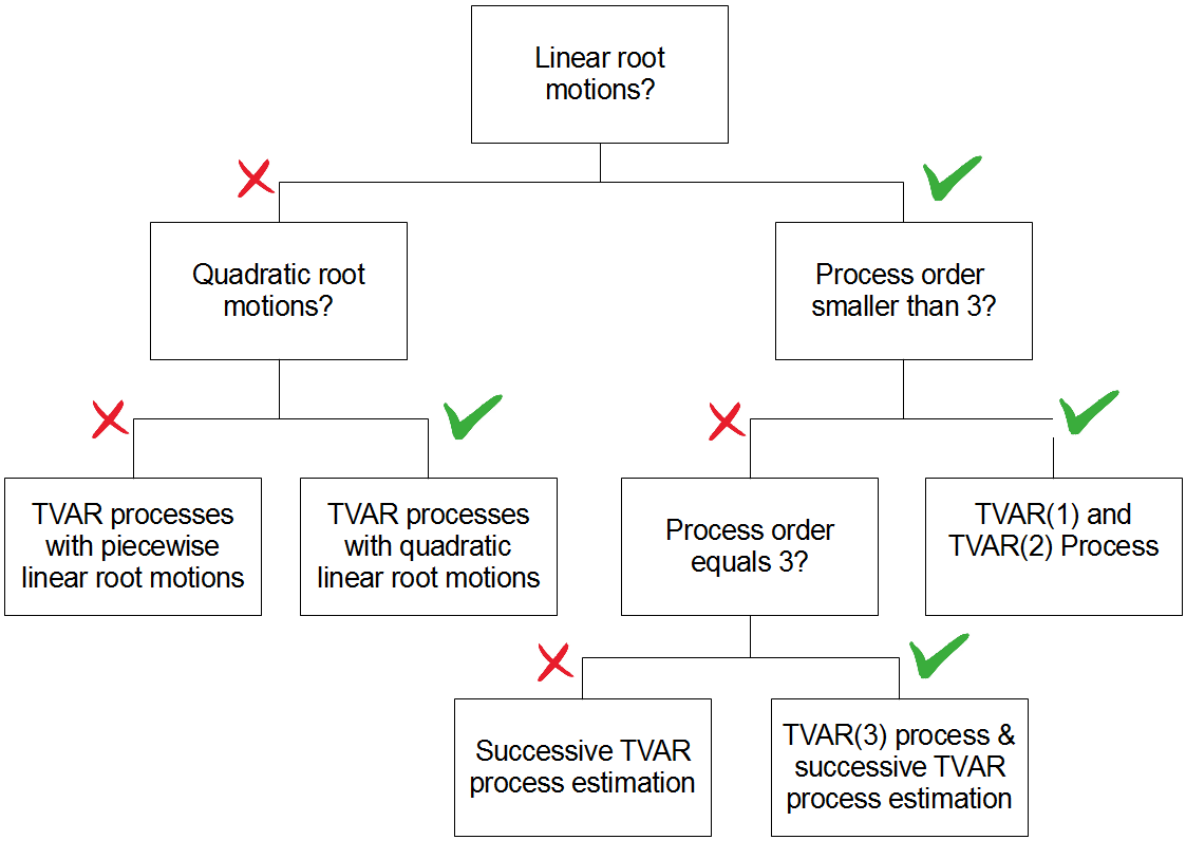

Figure 4.4: Decision tree to select the optimal TVAR processes for the respective problem.

4.7 Comparison of TVAR Estimates Based on Simulations

Two simulations are shown, to test the individual methods. The first one represents the advantages and disadvantages of estimating a TVAR process with quadratic root motion or piecewise linear root motions, and the second one shows the advantages and disadvantages of TVAR(3) with linear root movements, which have either been successively estimated from a TVAR(1) and a TVAR(2) process, or have been estimated directly by the means of the TVAR(3) process.

4.7.1 Piecewise Linear vs. Quadratic Root Motions

In order to compare the TVAR estimation with piecewise linear roots against the TVAR estimation with quadratic root movements, the root movement from the first example in Kamen 1988 (from

section 4.2.1) is used together with

$$P_{1,2}(t) = \frac{1-2.5t}{2} \pm \sqrt{\left(\frac{-1+2.5t}{2}\right)^2 - 0.5} \qquad t \in [0,1).$$

Using the time variable coefficients $\alpha_1(t) = 1 - 2.5t$ and $\alpha_2(t) = -0.5$ in combination with the variance of the noise $\sigma_\mathcal{E}^2 = 10^{-4}$, a time series of 512 observations is simulated via the recursion provided in (2.7.1).
This simulation is computed in three steps: first a vector $\boldsymbol{e}$ of 512 i.i.d normal distributed random variables with variance $\sigma_\mathcal{E}^2$ is generated. Second, the coefficients $\alpha_1(t)$ and $\alpha_2(t)$ are evaluated for $t \in [-0.0179, 0)$ for 512 equidistant values. This way, the first 12 signals can be removed, and the remaining observations lie within $t \in [0,1)$. These values are stored in the vectors a_1 and a_2. Thirdly the $\boldsymbol{e}$, a_1 and a_2 are used to compute the time series $\boldsymbol{\mathcal{S}}$ by the recursive formula

$$\mathcal{S}_{j-12} = a_1(j)\mathcal{S}_{j-13} + a_2(j)\mathcal{S}_{j-14} + e(j), \tag{4.7.1}$$

with $j = 3, 4, ..., 512$. Here, the initialization values are given by $[\mathcal{S}_{-11}; \mathcal{S}_{-10}] = [e_1; e_2]$. Furthermore the Signal is reduced by the first 12 observations. From all 512 observations the first 12 observations cannot be used, since two of them are needed for initializing the recursive formula in (4.7.1), and the other ten are needed for warming up the process. So, a vector consisting of exactly 500 observations remains. This generated time series is depicted in Figure 4.5, and for this time series a TVAR(2) process with quadratic root motion and a TVAR(2) process with piecewise linear root motion is approximated.

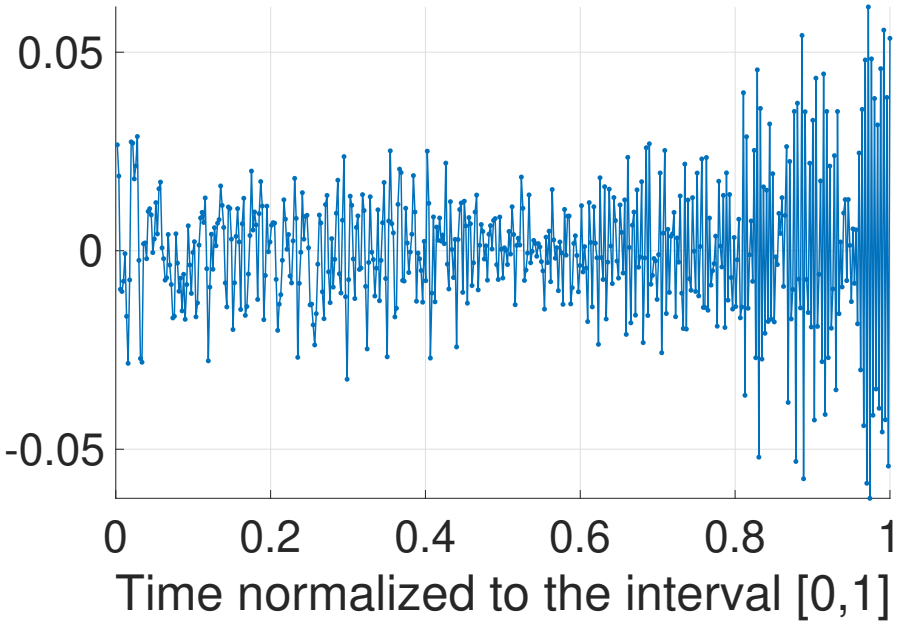

Figure 4.5: A realization of a TVAR process with variance $\sigma_\mathcal{E}^2 = 10^{-4}$ and the coefficients $\alpha_1(t) = 1 - 2.5t$ and $\alpha_2(t) = -0.5$ for $t \in [0,1]$.

In order to compare these findings, the resulting root movements of both estimations are calculated for discrete times and visualized in the unit circle. The approximation with quadratic root motion is a better approximation of the circular motion, as can be seen in Figure 4.6. The figure however also visualises that the quadratic movements show, in contrast, strong deviations from the predetermined root movement towards the end ($t \to 1$) and even leave the unit circle, so that the TVAR(2) process with quadratic root motion no longer meets the requirements of stationarity at any given time step. The piecewise estimate in Figure 4.7 maintains a similar deviation, but do

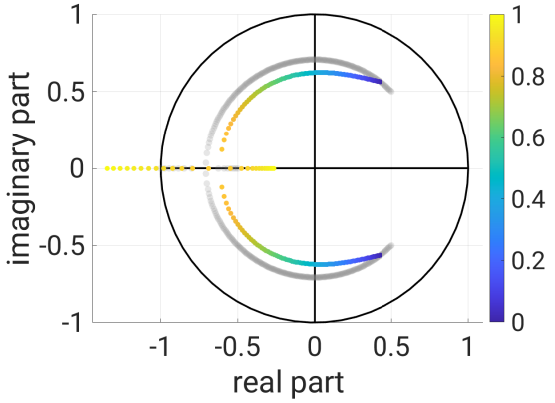

Figure 4.6: TVAR estimate for the time series with quadratic root movements, and the root movement used for the simulation of the time series (grey).

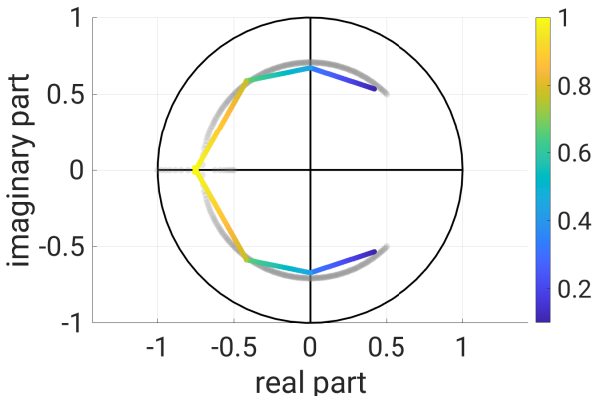

Figure 4.7: TVAR estimate for the time series with piecewise linear root movements, and the root movement used for the simulation of the time series (grey).

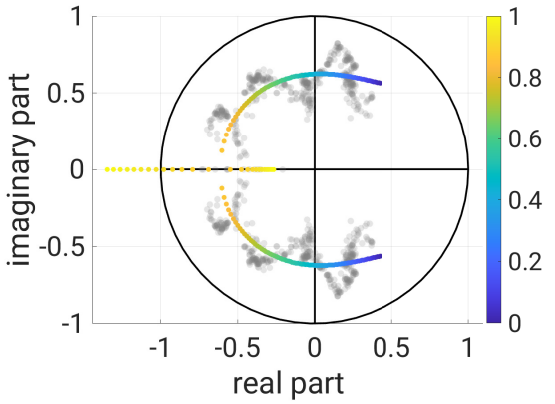

Figure 4.8: TVAR estimate for the time series with quadratic movements, and the discrete roots of a moving window of 60 observations moving across the time series (grey).

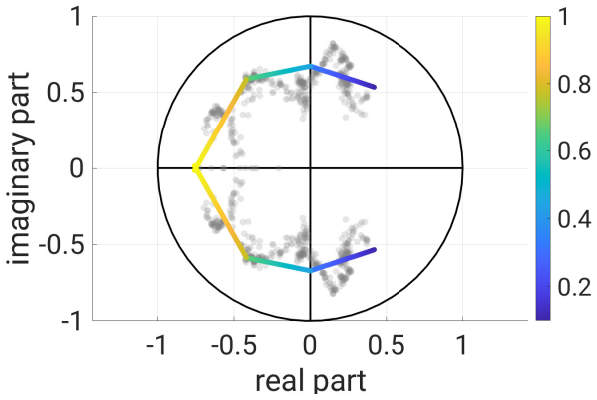

Figure 4.9: TVAR estimate for the time with piecewise linear root movements, and the discrete roots of a moving window of 60 observations moving across the time series (grey).

not leave the unit circle. Therefore fulfils the requirements of stationarity at any time and thus gives a more suitable approximation.
Both estimates have in common that they are continuously below the predetermined root movement. The explanation of this phenomenon demands a further estimate. A window of 60 observations is shifted in steps of one observation across the time series, and for each window, a time stable AR process is estimated. The resulting time constant roots are displayed in the unit circle (see Figures 4.8 and 4.9).
These discrete roots are plotted together with one of the estimated root movements into the unit circle. Figure 4.9 shows that the linear roots of the piecewise estimated TVAR process with linear root motions are well in the track of the window function, while Figure 4.8 illustrates the same for the TVAR estimation with quadratic root motions. For this specific example, the differences between the discrete roots of the moving window and the estimated root motions result from the fact that the simulated noise influences the TVAR coefficients during the simulation and therefore draws the roots closer to the origin for this specific realization.

In a second example, a time series of 500 observations is simulated, but this time the root movement

is reduced to 60% in comparison the root motion discussed in the previous example. This is done by multiplying all the coefficients of the roots not by t^l but by $(0.6t)^l$, which means that in this particular case, $\alpha_1(t)$ is replaced by

$$\bar{\alpha}_1(t) = 1 - 1.5t$$

while $\alpha_2(t)$ remains the same. With the new set of parameters, the new time series as shown in Figure 4.10 is simulated like in the previous simulation. However this time Figure 4.11 shows that the discrete roots for the moving window fit the root movement used for initialization very well. So, there is no reason to differentiate between these two root movements, meaning that it is sufficient to use the given root motion as a validation for the different TVAR estimates. For this time series,

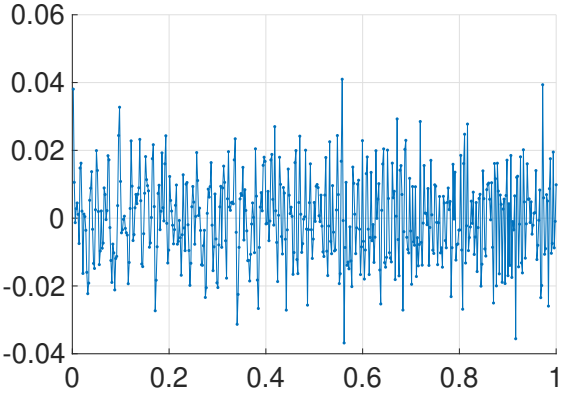

Figure 4.10: A realization of the TVAR process with the coefficients $\alpha_1(t) = 1 - 1.5t$ and $\alpha_2(t) = -0.5$ for $t \in [0, 1]$.

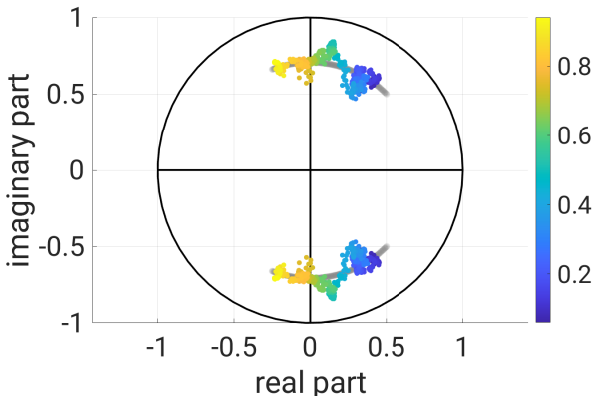

Figure 4.11: Roots of a moving window for the time series, and the root movement used in the simulation (grey).

a TVAR(2) process with piecewise linear root motions as well as a TVAR(2) process with quadratic root motions was estimated, and the resulting root motions then depicted in Figure 4.12 (TVAR estimation with restrictions of quadratic root motions) and in Figure 4.13 (piecewise estimation).

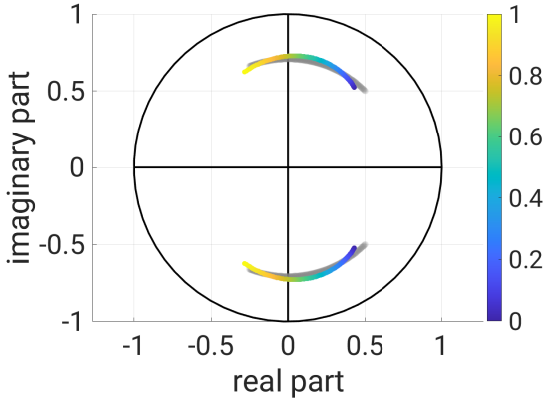

Figure 4.12: TVAR estimate for the time series with quadratic root movements, and the root movement used for the simulation of the time series (grey).

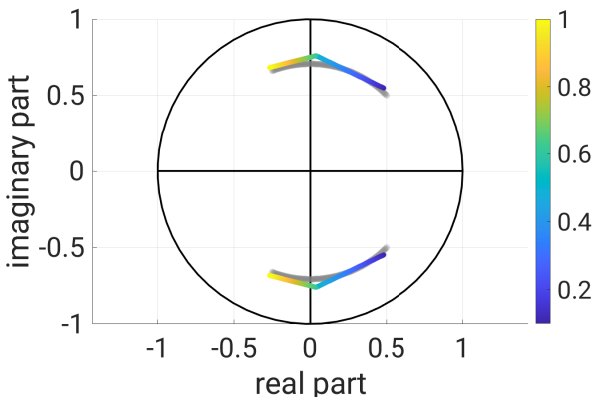

Figure 4.13: TVAR estimate for the time series with piecewise linear root movements, and the root movement used for the simulation of the time series (grey).

When comparing the two root movements, it is first to mention that both approximate well, but that using quadratic root motions has one advantage: no further limit has to be specified. The piecewise estimation, however, demands knowledges of the time at which the piece estimate is separated for this has a big influence on the shape of the root movements.

4.7.2 Direct vs. Successive Estimation of a TVAR(3) Process

In this section, a time series of 1000 observations (Figure 4.14) was simulated by a TVAR(3) process. The process' parameters are provided by the variance $\sigma_\varepsilon^2 = 10^{-6}$ and the time variable linear roots

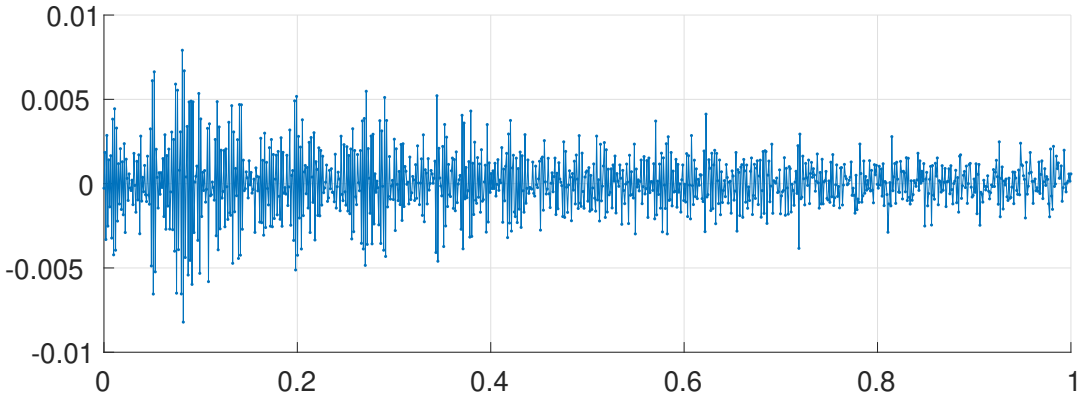

Figure 4.14: A time series process simulated by a TVAR(3) process with variance $\sigma_\varepsilon^2 = 10^{-6}$, and the roots $P_1(t) = -0.5 - 1t$ and $P_{2,3}(t) = -0.6 \pm 0.3i + (0.3 \pm 0.2i)t$ for $t \in [0, 1]$.

of the CP:

$$P_1 = -0.5 + 1t \qquad P_2 = -0.6 + 0.3i + (0.3 + 0.2i)t \qquad P_3 = -0.6 - 0.3i + (0.3 - 0.2i)t$$

with $t \in [0, 1]$. These roots and their movement over time are shown in Figure 4.15. The discrete roots from a moving window of 200 observations over the simulated time series are in comparison shown in Figure 4.16. It is noticeable that the complex-valued roots in the representations differ, which means that the example's root motions do not reproduce the given roots. Therefore, the validation is done by the roots of a moving window. To compare the estimations of a TVAR(3)

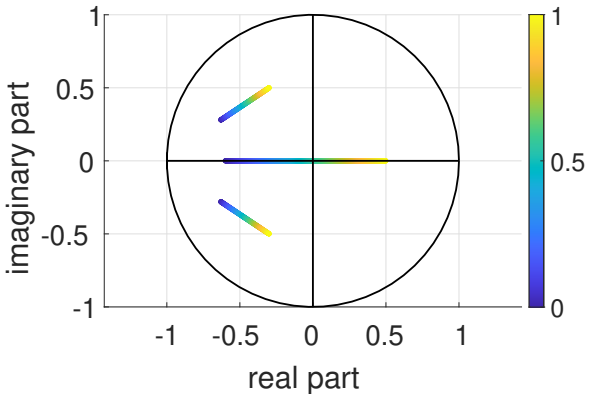

Figure 4.15: Given roots of the TVAR(3) process which were used to simulate the time series in Figure 4.14.

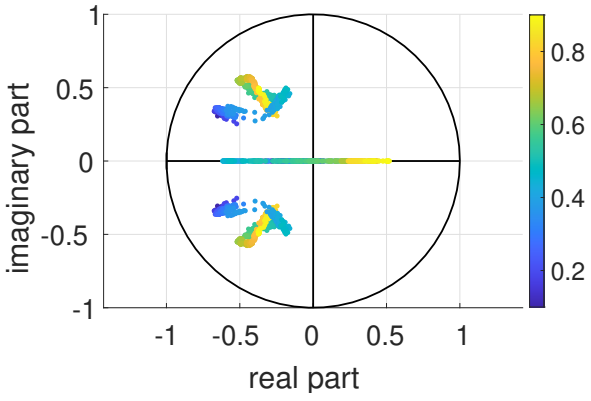

Figure 4.16: Roots of AR(3) processes for a moving window of 200 observations sliding over the time series in Figure 4.14.

process given in 4.3.3 with the direct estimation of section 4.5.2, this time series is estimated by applying both methods. The roots and their motions for the successive estimate are depicted in Figure 4.17, which shows that all roots are real valued. This problem might occur when the complex roots get too close to the x-axis that. In conjunction with the real root, they start to influence the TVAR(1) estimate in the first iteration up to the degree that this solution compensates too much influence of the complex roots in the characteristic of the time series. Nevertheless, the given result of the successive TVAR estimation is also the one with the minimum AIC for successively

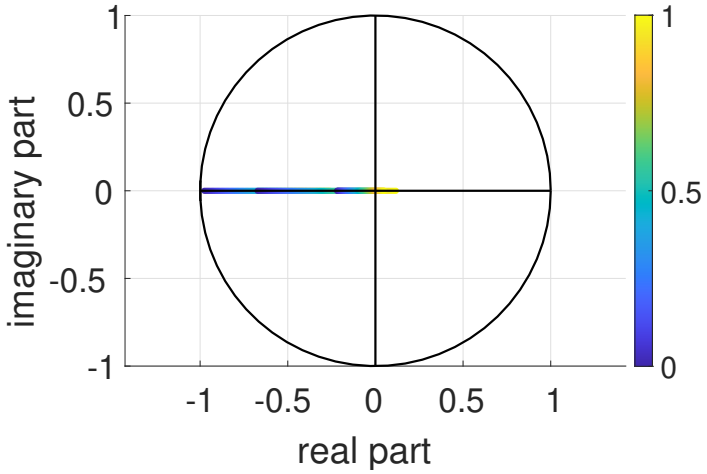

Figure 4.17: Root motion of the successive estimate of a TVAR(3) process. The process is simulated with the help of the roots of Figure 4.15.

estimated TVAR processes up to order six.
In the direct TVAR(3) computation, the estimation is carried out as in (4.5.4)–(4.5.6) without using the additional constraints of (4.5.11)–(4.5.13). The resulting root movement is visualized in Figure 4.18 and shows a strong similarity to the discrete roots of the moving window in Figure 4.16. In order to obtain a TVAR(3) process with linear roots, an additional adjustment according to the conditions in (4.5.11)–(4.5.13) is calculated (compare Appendix C.11.3). The linear root motions of the directly estimated TVAR(3) can be seen in Figure 4.19. They are very similar to the root motions used for the simulation of Figure 4.15. Based on this simulation, it is possible to show how

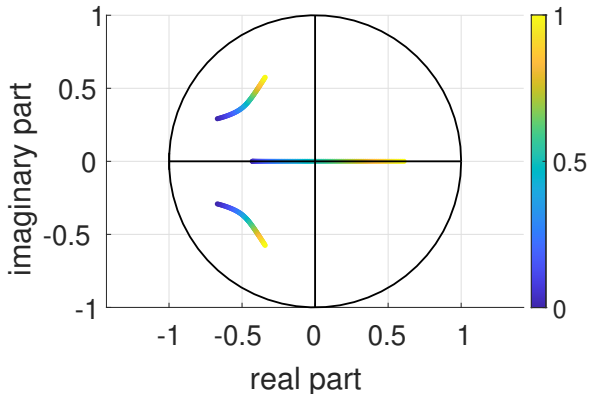

Figure 4.18: Root motion of the direct estimate of a TVAR(3) process with polynomial coefficients simulated with the help of the roots from Figure 4.15.

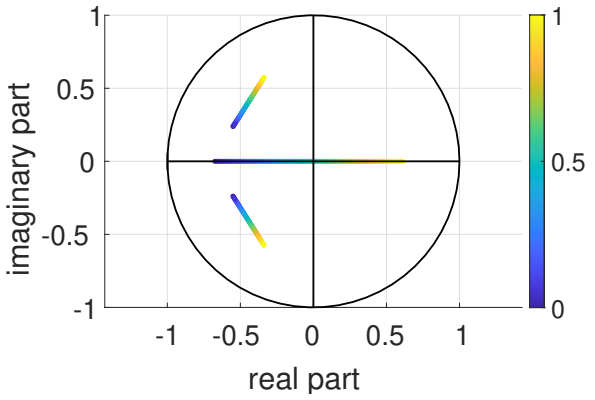

Figure 4.19: Root motion of the direct estimate of a TVAR(3) process with linear root motion simulated with the help of the roots from Figure 4.15.

the direct determination of TVAR(3) processes extends the successive TVAR estimation in order to detect hard-to-separate roots (like the one shown in Figure 4.15), and to distinguish them from superimposed roots (as in Figure 4.17).
Admittedly, the successive estimate is very rarely as vague as shown here. In most cases, the roots of the successive and the direct TVAR(3) process' estimates matches -at least if the restrictions linearization of the direct TVAR(3) process' estimates converge.

Chapter 5

Covariance Functions for Time Variable AR(1) Processes with Linear Root Motions

In this chapter, the nonstationary processes are prepared to be used as covariance models for LSC (see section 2.2). In order to model the covariances of the signal, the necessary covariance matrix is derived from the estimate of a TVAR(1) process with linear root motion (see chapter 4). With this matrix, the adjusted observations are calculated by applying LSC for smoothing (or as a filter). In order ot predict the values between the observations, a continuous covariance function is required. This is derived from the discrete covariances by finding a continuous representation, as shown in chapter 3.
Because of complexity, this chapter limits its examination to the TVAR process of order $p = 1$:

$$\mathcal{S}_t = \alpha_1(t)\mathcal{S}_{t-1} + \mathcal{E}_t \tag{5.0.1}$$

with linear root motion. Since it was shown in (4.3.5) that for the TVAR(1) process, the time variable coefficient is equal to the root of the corresponding CP, i.e.

$$\alpha_1(t) = P_1(t),$$

(as shown in (4.3.5),) the resulting covariances and covariance functions are directly related to the coefficient $\alpha_1(t)$.

5.1 Discrete Covariance Matrices of the TVAR(1) Process with Linear Root Motions

In order to determine the covariance matrix of TVAR(1) processes, the variances as well as the covariances must be calculated. To do so the subsection 5.1.1 provides the representation of the time variable covariances of a TVAR(1) process as a function of the time variable variances. Since section 4.1.2 and Appendix C.1, both illustrate that the direction in which the TVAR process' development is decisive for the resulting covariances, this subsection is limited to the covariance ($\Sigma_j(t)$) between an observation $\mathcal{S}_t$ at time t and an observation $\mathcal{S}_{t+j}$, which is j time steps further in the future. The second subsection 5.1.2 derives the time variable variances of TVAR(1) -mentioned in section 5.1.1- as a function of the time variable parameters $\alpha_1(t)$ and the variance of the noise $\sigma^2_{\mathcal{E}}$. The third subsection 5.1.3 combines the results of sections 5.1.1 and 5.1.2, to compute the values of the covariance matrix derived from TVAR(1) processes.

5.1.1 Representation of the covariances of a TVAR(1) process by the variances

Take a covariance of a TVAR(1) process with linear root motion from a signal $\mathcal{S}_t$ at a discrete time t to a signal $\mathcal{S}_{t+j}$ with j steps in the future and applies the time variable Y.-W. equation from

(C.1.3). This simplifies the computation of the variance to

$$\Sigma_j(t) = E\{\mathcal{S}_{t+j}\mathcal{S}_t\} = \alpha_1(t+j)\Sigma_{j-1}(t) \qquad \text{for } j \geq 0.\text{for } j > 0. \tag{5.1.1}$$

Just as in the case of the time stable Y.-W. equations, the covariance between two observations with a distance j is reduced to the covariance between two observations with a distance of $j-1$, whereby the applies random variables are provided by $\mathcal{S}_t$ and $\mathcal{S}_{t+j}$. This makes the same method applicable to the covariance $\Sigma_{j-1}(t)$, means that the equation

$$\Sigma_{j-1}(t) = E\{\mathcal{S}_{t+j-1}\mathcal{S}_t\} = \alpha_1(t+j-1)\Sigma_{j-2}(t) \tag{5.1.2}$$

also applies. This way, $\Sigma_j(t)$ can be represented by $\Sigma_{j-2}(t)$. To do so $\Sigma_{j-1}(t)$ in (5.1.1) is exchanged by the right side of equation (5.1.2):

$$\Sigma_j(t) = \alpha_1(t+j)\alpha_1(t+j-1)\Sigma_{j-2}(t).$$

Since the covariance $\Sigma_j(t)$ at time t remains unaffected, and since the calculation is only applied for for covariances covering future signals (i.e. $j > 0$), the recursion can be repeated j times until the covariance reaches the variance $\Sigma_0(t)$. This results in

$$\begin{aligned}\Sigma_j(t) &= \alpha_1(t+j)\alpha_1(t+j-1)\dots\ \alpha_1(t+1)\Sigma_0(t) \\ &= \Sigma_0(t)\prod_{\ell=1}^{j}\alpha_1(t+\ell).\end{aligned} \tag{5.1.3}$$

The coefficients $\alpha_1(t+\ell)$ are known from the TVAR(1) estimate given in chapter 4, but note that usage of the discrete times $t, (t+\ell) \in [1, 2, ..., n]$, first demands a normalization to the interval $\bar{t}$ and $\overline{t+\ell} \in [0, 1/(n-1), 2/(n-1), ..., 1]$. The resulting conversion of the parameters can be seen in Appendix D.1.

5.1.2 Discrete Variance of the TVAR(1) process

Equation (5.1.3) shows that the covariance $\Sigma_j(t)$ between the signal $\mathcal{S}_t$ and $\mathcal{S}_{t+j}$ with $j > 0$ can be traced back to the variance $\Sigma_0(t)$ at time t. Schuh et al. 2023 have proven that the variances of a TVAR(1) process ($\Sigma_0(t)$) can be determined for each time t: their proposed method demands a recursive calculation. For this purpose, the variance $\Sigma_0(t)$ at a time t is rewritten as

$$\begin{aligned}\Sigma_0(t) &= E\{\mathcal{S}_t\mathcal{S}_t\} \\ &\overset{(1)}{=} E\{(\alpha_1(t)\mathcal{S}_{t-1} + \mathcal{E}_t)(\alpha_1(t)\mathcal{S}_{t-1}\mathcal{E}_t)\} \\ &= E\{\alpha_1(t)^2\mathcal{S}_{t-1}\mathcal{S}_{t-1} + 2\alpha_1(t)\mathcal{S}_{t-1}\mathcal{E}_t + \mathcal{E}_t\mathcal{E}_t\} \\ &= \alpha_1(t)^2\underbrace{E\{\mathcal{S}_{t-1}\mathcal{S}_{t-1}\}}+2\alpha_1(t)\underbrace{E\{\mathcal{S}_{t-1}\mathcal{E}_t\}}+\underbrace{E\{\mathcal{E}_t\mathcal{E}_t\}} \\ &\overset{(2)}{=} \alpha_1(t)^2\ \ \Sigma_0(t-1)\ \ + 2\alpha_1(t)\qquad 0\qquad +\quad \sigma^2_{\mathcal{E}} \\ &= \alpha_1(t)^2\Sigma_0(t-1) + \sigma^2_{\mathcal{E}}\end{aligned} \tag{5.1.4}$$

This way the variance at any time can be recursively represented by the variance at time $t-1$. In (1), the recursion formula for TVAR(1) processes of (5.0.1) is used. (2) uses the definitions of the TVAR(1) process variance

$$\Sigma_0(t-1) = E\{\mathcal{S}_{t-1}\mathcal{S}_{t-1}\},$$

and the variance of noise

$$\Sigma(\mathcal{E}_t) = E\{\mathcal{E}_t\mathcal{E}_t\} = \sigma^2_{\mathcal{E}}.$$

Furthermore, in our case,

$$E\{\mathcal{S}_{t-1}\mathcal{E}_t\} = E\{\mathcal{S}_{t-1}\}E\{\mathcal{E}_t\} = 0$$

remains applicable, as the white noise process at time t and the signal at time $t-1$ are independent from each other, and $E\{\mathcal{E}_t\} = 0$. As such, the recursion from t to $t-1$ can be successively applied, until the time $t = t_0$ is reached. This defines the start of the process

$$\begin{aligned}
\Sigma_0(t) &= \alpha_1(t)^2[\alpha_1(t)^2\Sigma_0(t-2) + \sigma_{\mathcal{E}}^2] + \sigma_{\mathcal{E}}^2 \\
&= ... \\
&= \underbrace{\alpha_1(t)^2[\alpha_1(t-1)^2(\alpha_1(t-2)^2...(\alpha_1(t_0+1)^2}_{(t-t_0)\times\alpha^2}\Sigma_0(t_0) + \underbrace{\sigma_{\mathcal{E}}^2) + ... + \sigma_{\mathcal{E}}^2)\sigma_{\mathcal{E}}^2] + \sigma_{\mathcal{E}}^2}_{(t-t_0)\times\sigma_{\mathcal{E}}^2} \\
&= \prod_{k=t_0+1}^{t}\alpha_1^2(k)\Sigma_0(t_0) + \sum_{l=t_0+1}^{t-1}\prod_{k=l+1}^{t}\alpha_1^2(k)\sigma_{\mathcal{E}}^2 + \sigma_{\mathcal{E}}^2. \qquad (5.1.5)
\end{aligned}$$

Thus, the initial value problem of the variance at any time is reduced to the initial value problem for the variance at time t_0. To solve this problem, it is assumed that the TVAR(1) process starts its motion at the time t_0, while previously being a time constant stationary AR(1) process whose coefficient is $\breve{\alpha}_1 = \alpha_1(t_0)$. Under this assumption, the variance of the TVAR(1) process at time t_0 is known, for it is the same as for the time constant AR(1) process provided by

$$\breve{\mathcal{S}}_t = \breve{\alpha}_1\breve{\mathcal{S}}_{t-1} + \mathcal{E}_t = \alpha_1(t_0)\breve{\mathcal{S}}_{t-1} + \mathcal{E}_t. \qquad (5.1.6)$$

Furthermore Buttkus 2000, p. 243, eq. (11.15) argues that, if the AR process is stationary, the variance of the AR(1) process provided in (5.1.6) derives from

$$\Sigma_0(t_0) = \frac{\sigma_{\mathcal{E}}^2}{1-\alpha_1^2(t_0)}. \qquad (5.1.7)$$

The requirement of stationarity of the TVAR process to be stationary for all t (compare chapter 4), ensures that the variance is valid at all times due to the derivation of a stationary AR processes. Thus, the time variable variance in (5.1.5) can be calculated from any discrete time t by the means of a function depending only on the time variable coefficients $\alpha_1(t)$ and the variance of the white noise $\sigma_{\mathcal{E}}^2$:

$$\begin{aligned}
\Sigma_0(t) &= \prod_{k=t_0+1}^{t}\alpha_1^2(k)\frac{\sigma_{\mathcal{E}}^2}{1-\alpha_1^2(t_0)} + \sum_{l=t_0+1}^{t-1}\prod_{k=l+1}^{t}\alpha_1^2(k)\sigma_{\mathcal{E}}^2 + \sigma_{\mathcal{E}}^2 \\
&= \sigma_{\mathcal{E}}^2\left(1 + \prod_{k=t_0+1}^{t}\frac{\alpha_1^2(k)}{1-\alpha_1^2(t_0)} + \sum_{l=t_0+1}^{t-1}\prod_{k=l+1}^{t}\alpha_1^2(k)\right) \qquad \text{for } t > t_0. \qquad (5.1.8)
\end{aligned}$$

5.1.3 Discrete Covariance matrix of TVAR(1) process

Joining the variances of (5.1.3) with the covariances in (5.1.8) allows the construction of the covariance matrix of the process observations $\Sigma\{\mathcal{S}\}$. Thus, exchanging the variance $\Sigma_0(t)$ in (5.1.3) for (5.1.8) yields

$$\Sigma_j(t) = \sigma_{\mathcal{E}}^2\left(1 + \prod_{k=t_0+1}^{t}\frac{\alpha_1^2(k)}{1-\alpha_1^2(t_0)} + \sum_{l=t_0+1}^{t-1}\prod_{k=l+1}^{t}\alpha_1^2(k)\right)\prod_{\ell=1}^{j}\alpha_1(t+\ell), \qquad (5.1.9)$$

which can be used to fill the upper triangle of the covariance matrix

$$\Sigma\{\mathcal{S}\} = \begin{bmatrix}
\Sigma_0(1) & \Sigma_1(1) & \Sigma_2(1) & ... & \Sigma_{n-1}(1) \\
\Sigma_{-1}(2) & \Sigma_0(2) & \Sigma_1(2) & ... & \Sigma_{n-2}(2) \\
\Sigma_{-2}(3) & \Sigma_{-1}(3) & \Sigma_0(3) & ... & \Sigma_{n-3}(3) \\
\cdots & & & & \\
\Sigma_{-n+1}(n) & \Sigma_{-n+2}(n) & \Sigma_{-n+3}(n) & ... & \Sigma_0(n)
\end{bmatrix} \qquad (5.1.10)$$

of the observed signals. To complete the covariance matrix, it is necessary to also consider the observations covariances in the past $\Sigma_{-j}(t)$. But due to

$$\Sigma_{-j}(t) = E\{\mathcal{S}_t \mathcal{S}_{t-j}\} = E\{\mathcal{S}_{t-j} \mathcal{S}_t\} = \Sigma_j(t-j), \tag{5.1.11}$$

the covariance between the observation $\mathcal{S}_t$ and an observation $\mathcal{S}_{t-j}$ do not have to be calculated by (C.1.2), but can simply be traced back to the case of positive lag j.
In addition, the covariance transformations of (5.1.11) shows that the covariance matrix $\Sigma_{\mathcal{S}}$ is symmetrical. As can be seen in (5.1.10), where the entry of $\Sigma_{\mathcal{S}}$ in row r and column c is provided by

$$\Sigma_{\mathcal{S}}(r,c) = \Sigma_{c-r}(r).$$

In conjunction with the conversion (5.1.11) (which transforms a covariance of the past to a covariance in the future),

$$\Sigma_{\mathcal{S}}(r,c) = \Sigma_{c-r}(r) = \Sigma_{r-c}(c) = \Sigma_{\mathcal{S}}(c,r)$$

shows that the matrix $\Sigma_{\mathcal{S}}(r,c)$ is symmetrical and that (5.1.3) is sufficient to compute every entry of the covariance matrix:

$$\Sigma_{\mathcal{S}} = \begin{bmatrix} \Sigma_0(1) & \alpha_1(2)\Sigma_0(1) & \alpha_1(3)\alpha_1(2)\Sigma_0(1) & \dots & \left(\prod_{\ell=1}^{n-1} \alpha_1(1+\ell)\right)\Sigma_0(1) \\ & \Sigma_0(2) & \alpha_1(3)\Sigma_0(2) & \dots & \left(\prod_{\ell=1}^{n-2} \alpha_1(2+\ell)\right)\Sigma_0(2) \\ \textbf{Symmetrical} & & \Sigma_0(3) & \dots & \left(\prod_{\ell=1}^{n-3} \alpha_1(3+\ell)\right)\Sigma_0(3) \\ & & & \ddots & \vdots \\ & & & & \Sigma_0(n) \end{bmatrix}.$$

With $\Sigma_{\mathcal{S}}$, the theoretical covariance matrix of the TVAR(1) process is found. In the next section, a continuous representation of the time variable CF of a TVAR(1) will be derived.

5.2 Normalization of the Time Interval after TVAR Estimation

As mentioned before, this part's contributions are limited to the TVAR(1) process whose coefficient (and thus also the single root ($P_1(t)$) of the CP) is linear

$$\alpha_1(t) = P_1(t) = \beta_0^{(1)} + \beta_1^{(1)} t. \tag{5.2.1}$$

To generalize the procedure for any given epoch, the time vector t is transformed into

$$\bar{\boldsymbol{t}} = \left[0, \frac{1}{n-1}, \frac{2}{n-1}, ..., \frac{n-2}{n-1}, 1\right].$$

As a result, the following equations can be applied for any interval -regardless of how long it is or where it starts. The transformation of the discrete times to the interval $[0,1]$, and the resulting transformed lags $\bar{j}$, are derived in Appendix D.1. They are provided by

$$\bar{t} = \frac{t-1}{n-1} \qquad \text{and} \qquad \bar{j} = \frac{j}{n-1}. \tag{5.2.2}$$

To ensure conformity of the equations, the coefficients $\alpha_1(t)$ also have to be transformed according to the shift in t:

$$\alpha_1(t) = \beta_0^{(1)} + \beta_1^{(1)} t = \overline{\beta_0^{(1)}} + \overline{\beta_1^{(1)}}\bar{t} = \bar{\alpha}_1(\bar{t}).$$

Since $\alpha_1(t)$ is still a function of t, $\bar{t}$ has to be transformed according to (5.2.2):

$$\alpha_1(t) = \overline{\beta_0^{(1)}} + \overline{\beta_1^{(1)}} \frac{t-1}{n-1}. \tag{5.2.3}$$

The corresponding covariance representation in (5.1.9) is adjusted accordingly:

$$\begin{aligned}\Sigma_j(t) =&\sigma_\mathcal{E}^2 \left(1 + \prod_{k=t_0+1}^{t} \frac{\alpha_1^2(k)}{1-\alpha_1^2(t_0)} + \sum_{l=t_0+1}^{t-1} \prod_{k=l+1}^{t} \alpha_1^2(k) \right) \prod_{\ell=1}^{j} \alpha_1(t+\ell) \\ =&\sigma_\mathcal{E}^2 \left(1 + \prod_{k=t_0+1}^{t} \frac{\left(\overline{\beta_0^{(1)}} + \overline{\beta_1^{(1)}} \frac{k-1}{n-1} \right)^2}{1 - \left(\overline{\beta_0^{(1)}} + \overline{\beta_1^{(1)}} \frac{t_0-1}{n-1} \right)^2} + \sum_{l=t_0+1}^{t-1} \prod_{k=l+1}^{t} \left(\overline{\beta_0^{(1)}} + \overline{\beta_1^{(1)}} \frac{k-1}{n-1} \right)^2 \right) \cdots \\ &\cdot \prod_{\ell=1}^{j} \overline{\beta_0^{(1)}} + \overline{\beta_1^{(1)}} \frac{t+\ell-1}{n-1}. \end{aligned} \tag{5.2.4}$$

Linking $\overline{\beta_0^{(1)}}$ and $\overline{\beta_1^{(1)}}$ to j in (5.2.4) results in two advantages. On the one hand, $\overline{\beta_0^{(1)}}$ and $\overline{\beta_1^{(1)}}$ are independent of the time interval, so that the continuous continuation always has the same frame given by $[0,1]$; and on the other hand, the use of the discrete time points $t \in [1,2,...,n]$ ensures that the upper boundary of the product provided by the lag j remains a discrete number, which is the prerequisite for exchanging the product of discrete values by the continuos function. The discrete CF's continuation is discussed in the next section.

5.3 Continuous Covariance Function for Time Variable AR(1) Processes with Linear Root Motions

In this section, the discrete covariance section of (5.2.4) shall be broadened to a continuous function. This is done in the following two subsections: In subsection 5.3.1 a continuous function $\gamma(0,t_c)$ with $t_c \in [1,n]$ is set up to replace the time variable but discrete variances $\Sigma_0(t)$ of $t \in \{1,2,...,n\}$. In the subsection 5.3.2, another continuous function $\gamma(h,t_c)$ is derived. This function allows the computation of the time variable covariances of the process, while also possessing the characteristic of being continuous in both time t_c and lag h.

5.3.1 Continuous Representation of the Variances

The continuous covariance function requires the variances $\Sigma_0(t_c)$ of the TVAR(1) process to be known for any given time $t_c \in [0,1]$. Until now, the variances have been calculated only for the discrete observation points $t = \{1,2,...,n\}$ (see (5.1.8)). However, so far, the time variable TVAR(1) coefficient has not been estimated as discrete values, but as a continuous function:

$$\alpha_1(t_c) = \overline{\beta_0^{(1)}} + \overline{\beta_1^{(1)}} t_c \quad \forall t_c \in [0,1].$$

These time variable coefficients provides the basis for the creation of the continuous variance function $\gamma(0,t_c)$. $\gamma(0,t_c)$ is supposed to satisfy the condition (5.1.4), while also to reproduce the discrete variances $\Sigma_0(t_c)$ at the point of the observation epochs. Figure 5.1 shows discrete realisations of variances over time of a TVAR(1) process for a different number of samples. The obtained variances show a strong dependence on the sampling rate. This seems to contradict the idea of a continuous function representing all variances. However, Figure 5.1 also shows that the variance functions converge towards a limit value – the higher the sampling, the closer to the limit. Since it can be evaluated at any time and satisfies the conditions of (5.1.4) for all time points, the very function of this limit is thus used to obtain the continuous function of general variance over time. It is defined by

$$\gamma(0,t_c) = \frac{\sigma_\mathcal{E}^2}{1-\alpha_1^2(t_c)} \tag{5.3.1}$$

and is proved in Appendix D.2. The function of (5.3.1) depends only on the current state of the coefficient and therefore it is independent of its predecessors.

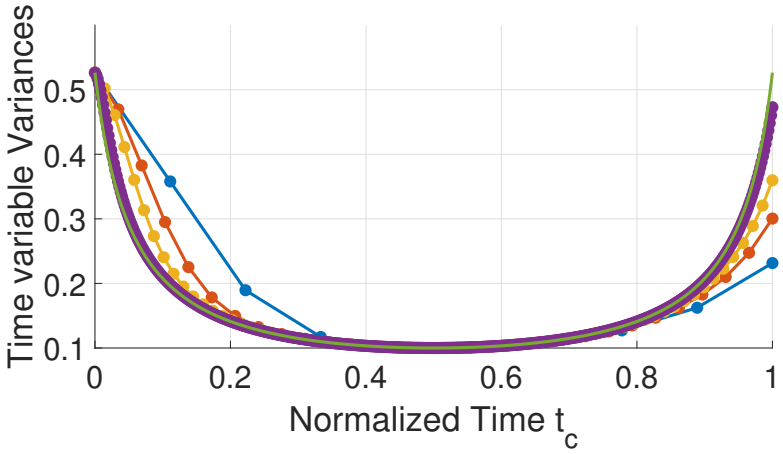

Figure 5.1: Variances of the TVAR(1) process with coefficient $\alpha_1(t_c) = 0.9 - 1.8t_c$ with $t_c \in [0,1]$ and $\sigma_{\mathcal{E}}^2 = 0.1$ being the variance of the white noise process. The variances are computed by the recursive formula (5.1.4) with the initialization value of (5.1.7). Different sampling rates were used: 10 samples (**blue**), 30 samples (**red**), 70 samples (**myOrange**), 500 samples (**violet**), continuous function (**mygreen**).

5.3.2 Continuous Representation of the Covariances

The CF for the TVAR(1) process with linear root motion is calculated similarly to the covariance function of (3.3.6), where the continuous CF for AR processes distinguishes between positive and negative real parts. In the case of the TVAR(1) processes (see (5.0.1)) with linear root motion (5.2.3), there are six cases (see Figure 5.2). The individual cases are distinguished by three characteristics of the coefficient $\alpha_1(t_c)$: (1) is $\alpha_1(0) > 0$ or $\alpha_1(0) < 0$, (2) does $\alpha_1(t_c)$ increasing decreasing, and (3) is $\alpha_1(t_c) = 0$ for any $t_c \in [0,1]$ or not. These case distinctions can also be described by the means of the parameters' signs, resulting in:

case 1: $\overline{\beta_0^{(1)}}, \overline{\beta_1^{(1)}} > 0$

case 2: $\overline{\beta_0^{(1)}}, \overline{\beta_1^{(1)}} < 0$

case 3: $\overline{\beta_0^{(1)}} < 0$, $\overline{\beta_1^{(1)}} > 0$ and $\overline{\beta_0^{(1)}} + \overline{\beta_1^{(1)}} > 0$

case 4: $\overline{\beta_0^{(1)}} > 0$, $\overline{\beta_1^{(1)}} < 0$ and $\overline{\beta_0^{(1)}} + \overline{\beta_1^{(1)}} > 0$

case 5: $\overline{\beta_0^{(1)}} < 0$, $\overline{\beta_1^{(1)}} > 0$ and $\overline{\beta_0^{(1)}} + \overline{\beta_1^{(1)}} < 0$

case 6: $\overline{\beta_0^{(1)}} > 0$, $\overline{\beta_1^{(1)}} < 0$ and $\overline{\beta_0^{(1)}} + \overline{\beta_1^{(1)}} < 0$.

For each of these six cases, the discrete covariances of (5.2.4) must be replaced by an individual continuous function. This is done again by the means of a case distinction with the parameters $\beta_0^{(1)}$ and $\beta_1^{(1)}$. Although there are six case distinctions, only three distinct groups represent the discretely covariances $\Sigma_j(t)$ in (5.2.4). These are called $\Sigma_j^{(1)}(t)$, $\Sigma_j^{(2)}(t)$ and $\Sigma_j^{(3)}(t)$. Each of these groups leads to their own continuous representation, which is respectively designated as $\gamma^{(1)}(h, t_c)$, $\gamma^{(2)}(h, t_c)$ and $\gamma^{(3)}(h, t_c)$.

Case 1: $\overline{\beta_0^{(1)}}, \overline{\beta_1^{(1)}} > 0$

For the first case, it is assumed that both $\overline{\beta_0^{(1)}}$ and $\overline{\beta_0^{(1)}}$ are greater than zero, since the product of (5.1.3) has only positive entries and is constantly growing. For this product, section 2.20 has

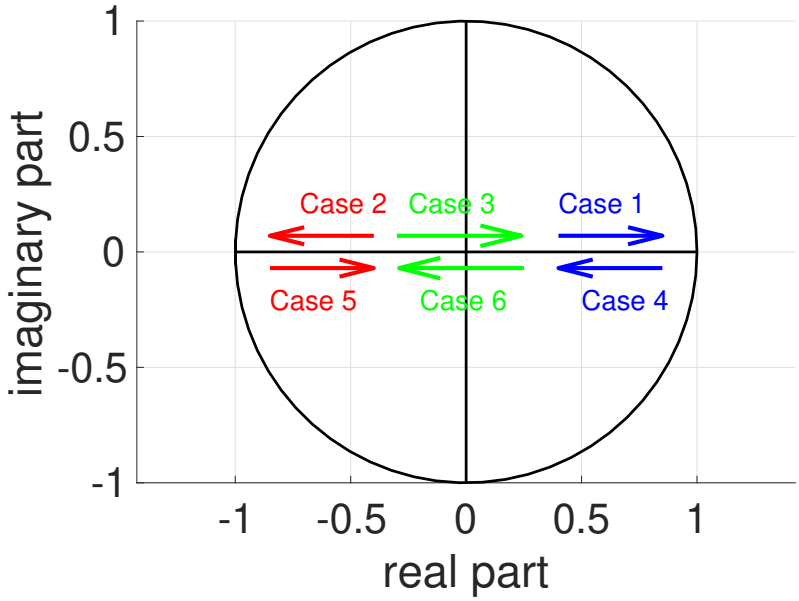

Figure 5.2: The different cases of linear root motions of a TVAR(1) processes.

shown that it can also be described with the Pochhammer symbol:

$$\mathbb{P}(t,j) := \frac{\Gamma(t+j)}{\Gamma(t)} = \prod_{k=0}^{j-1} t+k. \tag{5.3.2}$$

This function has the advantage of being a continuous function, means that it can be computed for the non-integer inputs $\bar{t}$ and $\bar{j}$ of (5.2.2). The extension of the product of (5.1.3) to the Pochhammer symbol demands that two consecutive factors must always be spaced by one. This is achieved by the transformation

$$\begin{aligned}\prod_{\ell=1}^{j} \overline{\beta_0^{(1)}} + \overline{\beta_1^{(1)}} \frac{t+\ell-1}{n-1} &= \prod_{\ell=1}^{j} \frac{\overline{\beta_1^{(1)}}}{n-1} \left(\frac{\overline{\beta_0^{(1)}}(n-1)}{\overline{\beta_1^{(1)}}} + t + \ell - 1 \right) \\ &= \left(\frac{\overline{\beta_1^{(1)}}}{n-1} \right)^j \prod_{\ell=1}^{j} \frac{\overline{\beta_0^{(1)}}(n-1)}{\overline{\beta_1^{(1)}}} + t + \ell - 1. \end{aligned} \tag{5.3.3}$$

When comparing this function with Pochhammer's symbol of (5.3.2), the demand for a shift by one of the running variable ($o = \ell - 1$), so that both products start at zero, becomes obvious:

$$\begin{aligned}\left(\frac{\overline{\beta_1^{(1)}}}{n-1} \right)^j \prod_{\ell=1}^{j} \frac{\overline{\beta_0^{(1)}}(n-1)}{\overline{\beta_1^{(1)}}} + t + \ell - 1 &= \left(\frac{\overline{\beta_1^{(1)}}}{n-1} \right)^j \prod_{o=0}^{j-1} \frac{\overline{\beta_0^{(1)}}(n-1)}{\overline{\beta_1^{(1)}}} + t + o \\ &= \left(\frac{\overline{\beta_1^{(1)}}}{n-1} \right)^j \mathbb{P}\left(\frac{\overline{\beta_0^{(1)}}(n-1)}{\overline{\beta_1^{(1)}}} + t, j \right). \end{aligned} \tag{5.3.4}$$

Until now t and j were needed in order to transform the product into Pochhammer's symbol. Now, to transform these parameters to the interval $[0,1]$, these can be modified by

$$t = \bar{t}(n-1) + 1 \text{ and } j = \bar{j}(n-1) \tag{5.3.5}$$

from (D.1). Inserting the normalized parameters into (5.3.4) results in

$$\left(\frac{\overline{\beta_1^{(1)}}}{n-1} \right)^{\bar{j}(n-1)} \mathbb{P}\left(\frac{\overline{\beta_0^{(1)}}(n-1)}{\overline{\beta_1^{(1)}}} + \bar{t}(n-1) + 1, \bar{j}(n-1) \right).$$

Applying this together with the transformation of the parameters to the unit interval, (5.1.3) changes to

$$\Sigma_j^{(1)}(t) = \Sigma_0(\bar{t}(n-1)+1)\left(\frac{\overline{\beta_1^{(1)}}}{n-1}\right)^{\bar{j}(n-1)} \mathbb{P}\left(\frac{\overline{\beta_0^{(1)}}(n-1)}{\overline{\beta_1^{(1)}}} + \bar{t}(n-1)+1, \bar{j}(n-1)\right) \tag{5.3.6}$$

for the calculation of the covariances between a discrete signal $\mathcal{S}_t$ and another signal $\mathcal{S}_{t+j}$ (if both parameters $\beta_0^{(1)}$ and $\beta_1^{(1)}$ are greater than zero). Replacing the discrete values $\bar{t}$ and $\bar{j}$ with the continuous parameters t_c and h results in the continuous CF

$$\gamma^{(1)}(h,t_c) = \gamma(0,t_c)\left(\frac{\overline{\beta_1^{(1)}}}{n-1}\right)^{h(n-1)} \mathbb{P}\left(\frac{\overline{\beta_0^{(1)}}(n-1)}{\overline{\beta_1^{(1)}}} + t_c(n-1)+1, h(n-1)\right) \tag{5.3.7}$$

with $h \in [0,1]$.[1] (5.3.7) represents the continuous function continuing the discrete function in (5.3.6), where the variances still have to be adjusted. Since $t \in \{0,1,...,n\}$ has been transformed into $\bar{t} \in [0,1]$, the discrete variance $\Sigma_0(t)$ can be replaced by the continuous function $\gamma(0,t_c)$ (as shown in section 5.3.1).

Case 2: $\overline{\beta_0^{(1)}}, \overline{\beta_1^{(1)}} < 0$

In this case, the time variable root $P_1(t) = \alpha_1(t)$ of (5.2.1) is negative for all $t \in [1,2,..,n]$. The continuous CF is found by transitioning from (5.1.3) with negative coefficients to **Case 1** by exchanging $\overline{\beta_0^{(1)}}$ for $-|\overline{\beta_0^{(1)}}|$ and $\overline{\beta_1^{(1)}}$ for $-|\overline{\beta_1^{(1)}}|$:

$$\begin{aligned}\Sigma_j^{(2)}(t) &= \Sigma_0(t)\prod_{\ell=1}^{j}\overline{\beta_0^{(1)}} + \overline{\beta_1^{(1)}}\frac{t+\ell-1}{n-1} \\ &= \Sigma_0(t)\prod_{\ell=1}^{j} -|\overline{\beta_0^{(1)}}| - |\overline{\beta_1^{(1)}}|\frac{t+\ell-1}{n-1}.\end{aligned}$$

Since the parameters in (5.3.1) are squared, this does not impact the computation of the time variable variances $\Sigma_0(t)$:

$$\begin{aligned}\Sigma_0(t) &= \frac{\sigma_\mathcal{E}^2}{1-\alpha_1^2(t)} \\ &= \frac{\sigma_\mathcal{E}^2}{1-(\overline{\beta_0^{(1)}} + \overline{\beta_1^{(1)}}\frac{t-1}{n-1})^2} \\ &= \frac{\sigma_\mathcal{E}^2}{1-(-|\overline{\beta_0^{(1)}}| - |\overline{\beta_1^{(1)}}|\frac{t-1}{n-1})^2} \\ &= \frac{\sigma_\mathcal{E}^2}{1-(-1)^2(|\overline{\beta_0^{(1)}}| + |\overline{\beta_1^{(1)}}|\frac{t-1}{n-1})^2} \\ &= \frac{\sigma_\mathcal{E}^2}{1-(|\overline{\beta_0^{(1)}}| + |\overline{\beta_1^{(1)}}|\frac{t-1}{n-1})^2}.\end{aligned}$$

1. When the covariance between the signals $\mathcal{S}_{\tau_1}$ and $\mathcal{S}_{\tau_2}$ is calculated, in most cases only the times τ_1 and τ_2 are known (instead of the lag h and the normalized time t_c). The method of how to represent the covariance function $\gamma_{\tau_2-\tau_1}(\tau_1)$ by τ_1 and τ_2 is shown in Appendix D.3.

For the product, proceed as in (5.3.3) to obtain:

$$\prod_{\ell=1}^{j} -|\overline{\beta_0^{(1)}}| - |\overline{\beta_1^{(1)}}|\frac{t+\ell-1}{n-1} = \left(\frac{-|\overline{\beta_1^{(1)}}|}{(n-1)}\right)^j \prod_{\ell=1}^{j} \frac{-|\overline{\beta_0^{(1)}}|(n-1)}{-|\overline{\beta_1^{(1)}}|} + t + \ell - 1$$
$$= \left(\frac{-|\overline{\beta_1^{(1)}}|}{(n-1)}\right)^j \prod_{\ell=1}^{j} \frac{|\overline{\beta_0^{(1)}}|(n-1)}{|\overline{\beta_1^{(1)}}|} + t + \ell - 1.$$

Inserting this product into the formula of the covariance in (5.2.4) provides

$$\Sigma_j^{(2)}(t) = \Sigma_0(t)\left(\frac{-|\overline{\beta_1^{(1)}}|}{(n-1)}\right)^j \prod_{\ell=1}^{j} \frac{|\overline{\beta_0^{(1)}}|(n-1)}{|\overline{\beta_1^{(1)}}|} + t + \ell - 1$$
$$= (-1)^j \underbrace{\Sigma_0(t)\left(\frac{|\overline{\beta_1^{(1)}}|}{(n-1)}\right)^j \prod_{\ell=1}^{j} \frac{|\overline{\beta_0^{(1)}}|(n-1)}{|\overline{\beta_1^{(1)}}|} + t + \ell - 1}_{\Sigma_j^{(1)}(t)}$$
$$= (-1)^j \Sigma_j^{(1)}(t).$$

Here, $\Sigma_j^{(1)}(t)$ is the continuous CF from (5.3.7) of **Case 1**. The multiplication with $(-1)^j$ corresponds to the negative real root in the time constant case from Appendix B.2. Again, $(-1)^j$ is replaced by $\cos(j\pi)$ in case of discrete values or by $\cos(h(n-1)\pi)$ in case of continuous values:

$$\Sigma_j^{(2)}(t) = \cos(j\pi)\Sigma_j^{(1)}(t).$$
$$\gamma^{(2)}(h, t_c) = \cos(h(n-1)\pi)\gamma^{(1)}(h, t_c).$$

Of course, as in **Case 1**, it still applies that h and $t_c \in [0, 1]$.

Case 3: $\overline{\beta_0^{(1)}} < 0$**,** $\overline{\beta_1^{(1)}} > 0$ **and** $\overline{\beta_0^{(1)}} + \overline{\beta_1^{(1)}} > 0$

The sign of the parameters makes this a special case:

$$\overline{\beta_0^{(1)}} = -|\overline{\beta_0^{(1)}}| \text{ and } \overline{\beta_1^{(1)}} = |\overline{\beta_1^{(1)}}|. \tag{5.3.8}$$

The roots of this case start with a negative sign and then become positive (as it is shown in Figure 5.2). Nevertheless, the process of the derivation of the continuous CF is similar to **Case 1** and **Case 2**. First, replace the parameters of (5.2.4) with their absolute values of (5.3.8):

$$\Sigma_j^{(3)}(t) = \Sigma_0(t)\prod_{\ell=1}^{j} \overline{\beta_0^{(1)}} + \overline{\beta_1^{(1)}}\frac{t+\ell-1}{n-1}$$
$$= \Sigma_0(t)\prod_{\ell=1}^{j} -|\overline{\beta_0^{(1)}}| + |\overline{\beta_1^{(1)}}|\frac{j+\ell-1}{n-1}. \tag{5.3.9}$$

This case cannot be traced back to one of the earlier cases, meaning that the creation of a new function is necessary. This is, however, again done by Pochhammer's symbol.
The variance $\Sigma_0(t)$ in (5.3.9) is still unaffected by the sign of the coefficients. Comparable to (5.3.3) the factor $\left(\frac{|\overline{\beta_1^{(1)}}|}{(n-1)}\right)$ is isolated from the product. This way, the factors always differ by a value of one:

$$\prod_{\ell=1}^{j} -|\overline{\beta_0^{(1)}}| + |\overline{\beta_1^{(1)}}|\frac{t+\ell-1}{n-1} = \left(\frac{|\overline{\beta_1^{(1)}}|}{(n-1)}\right)^j \prod_{\ell=1}^{j} \frac{-|\overline{\beta_0^{(1)}}|(n-1)}{|\overline{\beta_1^{(1)}}|} + t + \ell - 1$$
$$= \left(\frac{|\overline{\beta_1^{(1)}}|}{(n-1)}\right)^j (-1)^j \prod_{\ell=1}^{j} \frac{|\overline{\beta_0^{(1)}}|(n-1)}{|\overline{\beta_1^{(1)}}|} - t - \ell + 1. \tag{5.3.10}$$

Isolating -1 from the product results in a negative sign of the variable ℓ. Therefore, in each step, the factors of the product become smaller by one instead of increasing by one. Since the faculty function and thus also Pochhammer's symbol is only defined for a product of ascending values, that product must be rewritten according to the way described in (D.4.1) in order to obtain

$$\prod_{\ell=1}^{j} \frac{|\overline{\beta_0^{(1)}}|(n-1)}{|\overline{\beta_1^{(1)}}|} - t - \ell + 1 = \prod_{\ell=1}^{j} \frac{|\overline{\beta_0^{(1)}}|(n-1)}{|\overline{\beta_1^{(1)}}|} - t - j + \ell. \tag{5.3.11}$$

Although the factors values increase by one at a time, it remains impossible to simply switch to Pochammer's symbol. The reason for this lies in the fact that individual factors can turn negative and Pochhammer's symbol only equals the product in cases of increasing positive factors (see section 2.20). To solve this problem, first, a function

$$f(\overline{\beta_0^{(1)}}, \overline{\beta_1^{(1)}}, t, j) = \frac{|\overline{\beta_0^{(1)}}|(n-1)}{|\overline{\beta_1^{(1)}}|} - t - j \tag{5.3.12}$$

is defined. And second a case distinction is made, whether $f(\overline{\beta_0^{(1)}}, \overline{\beta_1^{(1)}}, t_c, h) > 0$ or $f(\overline{\beta_0^{(1)}}, \overline{\beta_1^{(1)}}, t_c, h) < 0$:

Case 3.a: $f(\overline{\beta_0^{(1)}}, \overline{\beta_1^{(1)}}, t, j) > 0$
Since (5.3.12) is greater than zero, all factors are positive while also increasing by one. So, the product can be replaced by Pochhammer's symbol like it was done in (5.3.4):

$$\begin{aligned}\prod_{\ell=1}^{j} \frac{|\overline{\beta_0^{(1)}}|(n-1)}{|\overline{\beta_1^{(1)}}|} - t - j + \ell &= \prod_{o=0}^{j-1} \frac{|\overline{\beta_0^{(1)}}|(n-1)}{|\overline{\beta_1^{(1)}}|} - t - j + 1 + o \\ &= \mathbb{P}\left(\frac{|\overline{\beta_0^{(1)}}|(n-1)}{|\overline{\beta_1^{(1)}}|} - t - j + 1, j\right).\end{aligned} \tag{5.3.13}$$

If finally $(-1)^j$ is modified by $(-1)^j = \cos(j\pi)$ as it was done in **Case 2**, and the product of (5.3.10) is transformed into Pochhammer's symbol as in (5.3.13), the discrete covariances of (5.2.4) can be calculated via

$$\Sigma_j^{(3)}(t) = \Sigma_0(t)\left(\frac{|\overline{\beta_1^{(1)}}|}{(n-1)}\right)^j \cos(j\pi)\mathbb{P}\left(\frac{|\overline{\beta_0^{(1)}}|(n-1)}{|\overline{\beta_1^{(1)}}|} - t - j + 1, j\right).$$

In this representation, the parameters can be transformed by (5.3.5) into the discrete parameters $\bar{t}$ and $\bar{j}$:

$$\begin{aligned}\Sigma_j^{(3)}(t) =& \Sigma_0(t)\left(\frac{|\overline{\beta_1^{(1)}}|}{(n-1)}\right)^j \cos(j\pi)\mathbb{P}\left(\frac{|\overline{\beta_0^{(1)}}|(n-1)}{|\overline{\beta_1^{(1)}}|} - (t+1) - j + 1, j\right) \\ =& \Sigma_0(\bar{t}(n-1)+1)\left(\frac{|\overline{\beta_1^{(1)}}|}{(n-1)}\right)^{\bar{j}(n-1)} \cos(\bar{j}(n-1)\pi)... \\ & \mathbb{P}\left(\frac{|\overline{\beta_0^{(1)}}|(n-1)}{|\overline{\beta_1^{(1)}}|} - \bar{t}(n-1) - \bar{j}(n-1) - 1, \bar{j}(n-1)\right).\end{aligned}$$

This can be converted into a continuous function

$$\gamma^{(3)}(h,t_c) = \Sigma_0(t_c(n-1)+1)\left(\frac{|\overline{\beta_1^{(1)}}|}{(n-1)}\right)^{h(n-1)} \cos(h(n-1)\pi)... \\ \mathbb{P}\left(\frac{|\overline{\beta_0^{(1)}}|(n-1)}{|\overline{\beta_1^{(1)}}|} - t_c(n-1) - h(n-1) - 1, h(n-1)\right), \tag{5.3.14}$$

which equals the continuous CF of ***Case 3.a***. It must be noted that, although h and t_c are continuous, they are still limited to the closed interval $[0,1]$.

Case 3.b: $f(\overline{\beta_0^{(1)}}, \overline{\beta_1^{(1)}}, t, j) < 0$

Now the sign of $f(\overline{\beta_0^{(1)}}, \overline{\beta_1^{(1)}}, t, j)$ in (5.3.12) is negative, but it was reversed by multiplying with $(-1)^j$ in (5.3.10). To change the sign of $f(\overline{\beta_0^{(1)}}, \overline{\beta_1^{(1)}}, t, j)$, a further multiplication with (-1) is required:

$$\begin{aligned}\prod_{k=0}^{j-1} -|f(\overline{\beta_0^{(1)}}, \overline{\beta_1^{(1)}}, t, j)| + k &= (-1)^j \prod_{k=0}^{j-1} |f(\overline{\beta_0^{(1)}}, \overline{\beta_1^{(1)}}, t, j)| - k \\ &= (-1)^j \prod_{k=0}^{j-1} |f(\overline{\beta_0^{(1)}}, \overline{\beta_1^{(1)}}, t, j)| - j + 1 + k \\ &= (-1)^j \mathbb{P}\left(|f(\overline{\beta_0^{(1)}}, \overline{\beta_1^{(1)}}, t, j)| - j + 1, j\right). \end{aligned} \tag{5.3.15}$$

Since both of the excluded (-1) of (5.3.10) and (5.3.15) posses the same power, and due to

$$(-1)^{h(n-1)}(-1)^{h(n-1)} = ((-1)^2)^{h(n-1)} = 1,$$

the (-1) disappears when Pochhammer's symbol in (5.3.14) is replaced by (5.3.15):

$$\gamma^{(3)}(h,t_c) = \gamma(0,t_c)\left(\frac{|\overline{\beta_1^{(1)}}|}{(n-1)}\right)^{h(n-1)} \cdot \mathbb{P}\left(\left|f(\overline{\beta_0^{(1)}}, \overline{\beta_1^{(1)}}, t_c, h)\right| - h(n-1) + 1, h(n-1)\right). \tag{5.3.16}$$

It must be noted again, that h and t_c are limited to the closed interval $[0,1]$ in the ***case 3.b*** as well.

Thus, the CF for **Case 3** is defined by the case distinction

$$\gamma^{(3)}(h,t_c) = \gamma(0,t_c)\left(\frac{|\overline{\beta_1^{(1)}}|}{(n-1)}\right)^{h(n-1)} ... \\ \begin{cases} \mathbb{P}\left(f(\overline{\beta_0^{(1)}}, \overline{\beta_1^{(1)}}, t_c, h), h(n-1)\right)\cos(h(n-1)\pi) & \text{if } f(\overline{\beta_0^{(1)}}, \overline{\beta_1^{(1)}}, t_c, h) > 0 \\ \mathbb{P}\left(\left|f(\overline{\beta_0^{(1)}}, \overline{\beta_1^{(1)}}, t_c, h)\right| - h(n-1), h(n-1)\right) & \text{if } f(\overline{\beta_0^{(1)}}, \overline{\beta_1^{(1)}}, t_c, h) < 0. \end{cases} \tag{5.3.17}$$

Case 4 to 6:

Cases 4 to **6** are not derived individually but solved by referring to **Cases 1** to **3**. In order to do so, the given time series must be reversed in order to be transformed into the Signal $\breve{\mathcal{S}}$:

$$\breve{\mathcal{S}}_t = \mathcal{S}_{n+1-t}.$$

In **Cases 4** and **5**, the inversion only reverses the sign of $\overline{\beta_1^{(1)}}$, while in **Case 6**, both the sign of $\overline{\beta_1^{(1)}}$ and $\overline{\beta_0^{(1)}}$ are reversed (see Figure 5.2).

- **Case 4**: $\overline{\beta_0^{(1)}} > 0$, $\overline{\beta_1^{(1)}} < 0$ and $\overline{\beta_0^{(1)}} + \overline{\beta_1^{(1)}} > 0$
  $\rightarrow$ Figure 5.2 shows that the reversed time series $\breve{\boldsymbol{\mathcal{S}}}$ equals **Case 1**: $\overline{\beta_0^{(1)}}$, $\overline{\beta_1^{(1)}} > 0$.
- **Case 5**: $\overline{\beta_0^{(1)}} < 0$, $\overline{\beta_1^{(1)}} > 0$ and $\overline{\beta_0^{(1)}} + \overline{\beta_1^{(1)}} < 0$
  $\rightarrow$ Figure 5.2 shows that the reversed time series $\breve{\boldsymbol{\mathcal{S}}}$ equals **Case 2**: $\overline{\beta_0^{(1)}}, \overline{\beta_1^{(1)}} < 0$.
- **Case 6**: $\overline{\beta_0^{(1)}} > 0$, $\overline{\beta_1^{(1)}} < 0$ and $\overline{\beta_0^{(1)}} + \overline{\beta_1^{(1)}} < 0$
  $\rightarrow$ Figure 5.2 shows that the reversed time series $\breve{\boldsymbol{\mathcal{S}}}$ equals **Case 3**: $\overline{\beta_0^{(1)}} < 0$, $\overline{\beta_1^{(1)}} > 0$ and $\overline{\beta_0^{(1)}} + \overline{\beta_1^{(1)}} > 0$.

5.4 Simulation

This section is divided into two parts. The first part provides the derivation of a covariance function for a TVAR(1) process, while the second part comprises the set up of the covariance functions for a TVAR(1) process with purely positive, purely negative and changing signs.

5.4.1 Simulation of a TVAR(1) Process with Negative and Positive Coefficients

In order to demonstrate how the CF of TVAR(1) processes with linear root motions is constructed, we define the root motion and the white noise's variance to compute the corresponding CF without further information. The root motion is given by

$$P_1(t) = \alpha_1(t) = -\left(0.5 + \frac{1}{n-1}\right) + \frac{1}{n-1}t, \tag{5.4.1}$$

and it is evaluated for $n = 20$ discrete equidistant observations at epochs $t \in \{1, 2, 3, ..., 20\}$. This motion is shown in Figure 5.3. In order to simplify (5.4.1), (D.1.1) is used to transform the time vector t to $\bar{t} = \frac{t-1}{n-1}$:

$$\begin{aligned} \alpha_1(t) &= -\left(0.5 + \frac{1}{n-1}\right) + \frac{\bar{t}(n-1)+1}{n-1} \\ &= -0.5 + 1\bar{t}. \end{aligned} \tag{5.4.2}$$

If the variance of the white noise is defined as $\sigma_{\mathcal{E}}^2 = 5$, it can be calculated at any time using (5.3.1) by evaluating the function

$$\gamma(0, t_c) = \frac{\sigma_{\mathcal{E}}^2}{1 - \alpha_1(t_c)} = \frac{5}{1 - (-0.5 + t_c)^2} \tag{5.4.3}$$

(which is shown in Figure 5.4). In order to visualize the flexibility of the CF of TVAR(1) processes, the continuous CF $\gamma(h, t_c)$ is computed by (5.3.17) for the discrete times $t_c \in \{0, 0.19737, 0.39474, 0.59211, 0.78947\}$. These times corresponds to the times $t \in \{1, 4.75, 8.5, 12.25, 16\}$, for which the variances are visualized by the dots in Figure 5.4. Since the root changes the sign from negative to positive (as can be seen in Figure 5.3), it stares an example for the CF of the third case from section 5.3.2. So $\gamma^{(3)}(h, t_c)$ is computed by the case distinction in (5.3.17).
The four resulting CFs are shown in Figure 5.5, wherein the CF for the first three epochs ($t \in \{1, 4.75, 8.5\}$) are computed by the means of the second case of (5.3.17). This leads to an oscillating CF, while the CF for the times $t \in \{12.25, 16\}$ are decaying functions with no further oscillations. These are computed by the first case of (5.3.17).
This simulation, shows that the CF of the TVAR(1) process covers a wide range of different functions, while TVAR process of the order of one being states the lowest possible. This is most impressively illustrated by the shape of the different CFs in Figure 5.5, which includes both oscillating CFs with positive and negative covariances as well as CFs with positive covariances only.

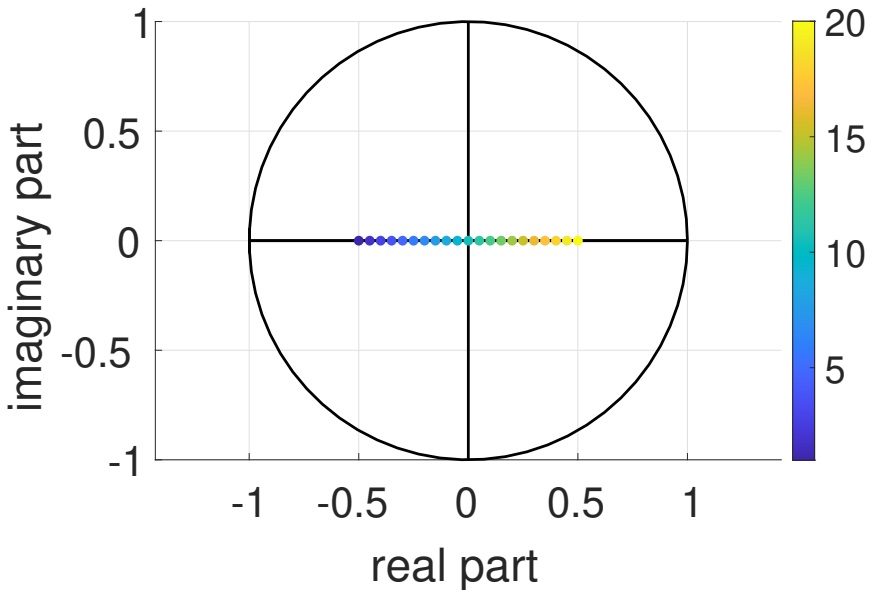

Figure 5.3: Given root movement of a TVAR(1) process with coefficient $\alpha_1(t) = -\left(0.5 + \frac{1}{19}\right) + \frac{1}{19}t$ and $t \in \{1, 2, ..., 20\}$.

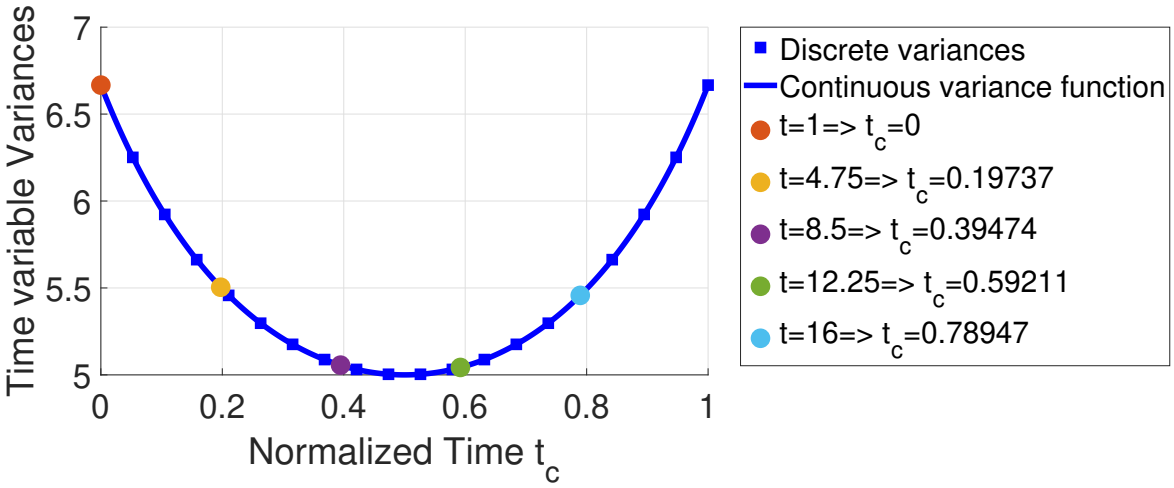

Figure 5.4: Variances of the TVAR(1) process of (5.4.3)

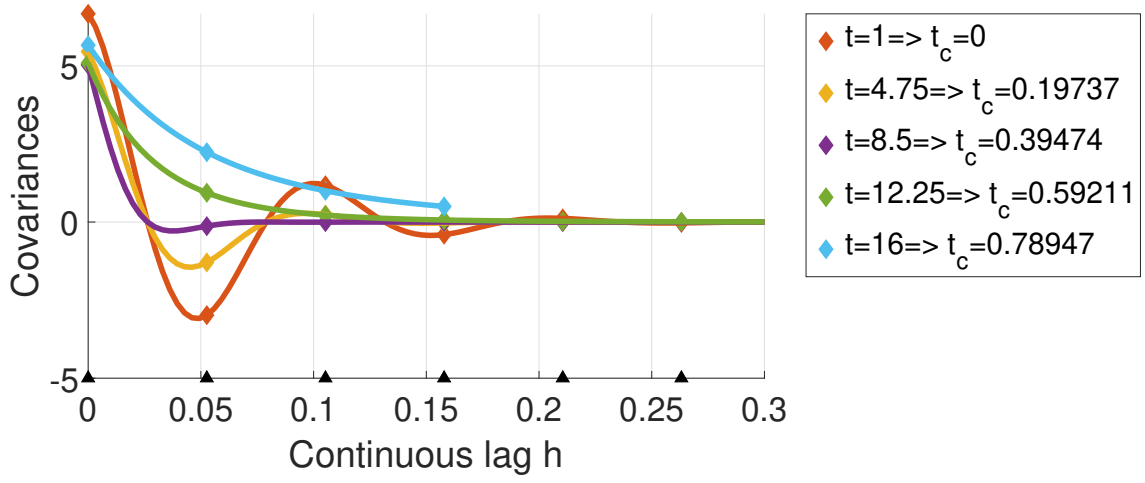

Figure 5.5: Continuous CF $\gamma^{(3)}(h, t_c)$ for lag $h \in [0, 0.3]$ and discrete times $t_c \in \{0, 0.19737, 0.39474, 0.59211, 0.78947\}$.

5.4.2 Comparison of the three Cases

For the sake of completeness, all three cases of TVAR(1) processes are discussed. For the first one, the coefficient

$$\alpha_1^{pos} = 0.2 + 0.9\bar{t}$$

is always positive, for the second one, the linear coefficient

$$\alpha_1^{neg} = -0.9 + 0.5\bar{t}$$

is always negative, and the third coefficient provided by

$$\alpha_1^{ind} = -0.5 + 1\bar{t}$$

is the time variable root negative and positive. The last case was discussed in detail in the example above. For each TVAR(1) process, the variance of the white noise is set to $\sigma_{\mathcal{E}}^2 = 5$. The motion of the root inside the unit circle, the variance and the CF resulting from TVAR(1) processes for all three cases are juxtaposed in Figure 5.6.
The comparison of the three processes in Figure 5.6 reveals that the CFs $\gamma(h, t_c)$ vary greatly according to the sign of the coefficient $\alpha_1(t_c)$ used to compute the variance $\Sigma_0(t_c)$. Even though the variance is not influenced by the sign of the coefficient, it has great influence on the shape of the CF, depending on whether $\alpha_1(t_c) > 0$ or not. If the variance is computed by a coefficient $\alpha_1(t_c) > 0$, (as it was done in the first case, or respectively, in the first half of the third case of Figure 5.6,) the continuous CF also only assumes positive values. However, if the variance is computed by a negative coefficient ($\alpha_1(t_c) < 0$), the continuous CF oscillates, whereby the frequency of this oscillation is equal to the inverse of the sampling rate Δj ($\nu = 1/(\Delta j)$). This is shown in example two and states the second part of the third case of Figure 5.6.

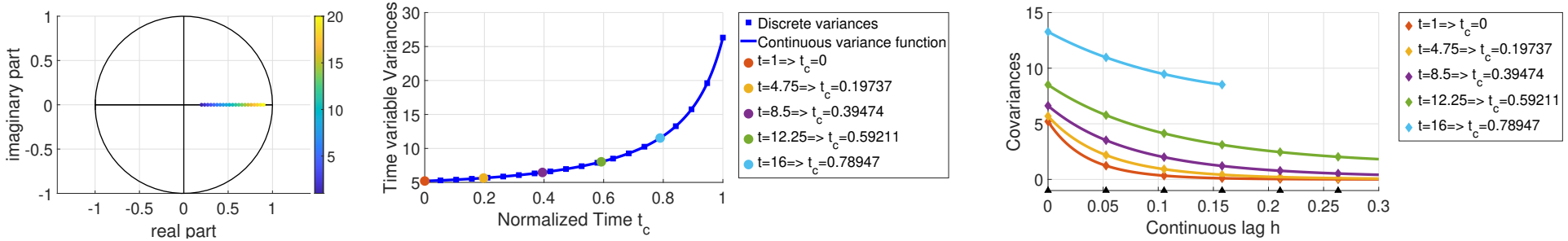

(a) Root motion, variances over time and some covariance functions for a TVAR(1) process with only positive coefficients.

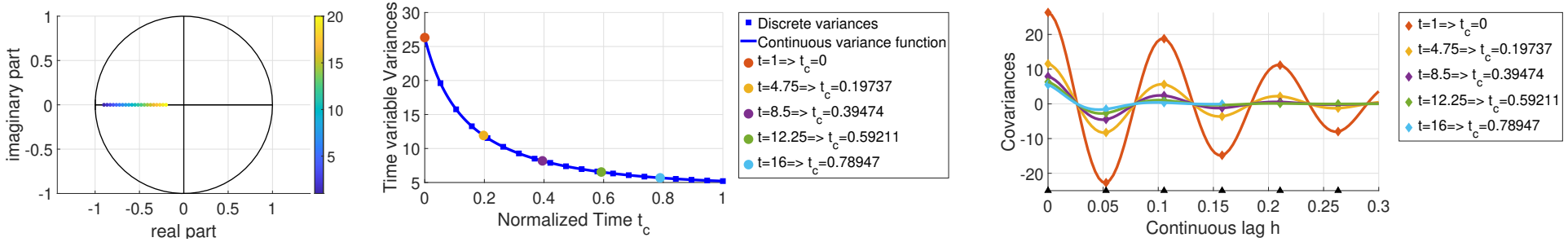

(b) Root motion, variances over time and some covariance functions for a TVAR(1) process with only negative coefficients.

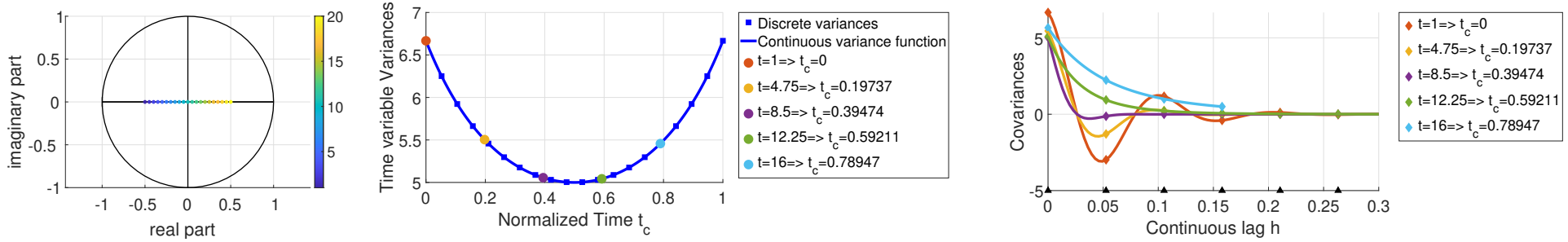

(c) Root motion, variances over time and some covariance functions for a TVAR(1) process with positive and negative coefficients.

Figure 5.6: Ranges of linear TVAR(1) process covariance functions.

Chapter 6

Application

In order to substantiate the findings of this thesis (a continuous CF from time stable AR processes, TVAR process estimation with defined root motions and a continuation of the discrete covariances of a TVAR(1) process), some applications will show how these CFs are computed. Furthermore their strengths and weaknesses are shown as well. In comparison to the second application, the first and the third application both use LSC (c.f. section 2.2). The first one generates CFs from AR processes and the other one computes the CF by a TVAR(1) process. In the second application, TVAR processes are estimated for time series derived from observations of Global Navigation Satellite Systems (GNSS) altitudes to visualize their characteristic variability.

6.1 Covariance Functions Derived from Time Stable AR Estimates

This section shows how the automated calculation of CFs from AR processes can be either used to filter a time series of observed sea level anomalies (SLA), or even to directly determine the derivative of the estimated function. These derivatives are often used to compute geostrophic currents. For reasons of numeracy and simplification, only one data set per 31 days will be used here to predict a time series of daily SLA data. The observed SLA, however, will be available for each day.

Approximation of Sea Level Anomalies using AR Processes

In the purpose of factual verification of the theoretical methods of CFs from AR processes derived from chapter 3, pseudo-observations between a time series of monthly SLA data will be predicted, in a way that a time series of daily data results.

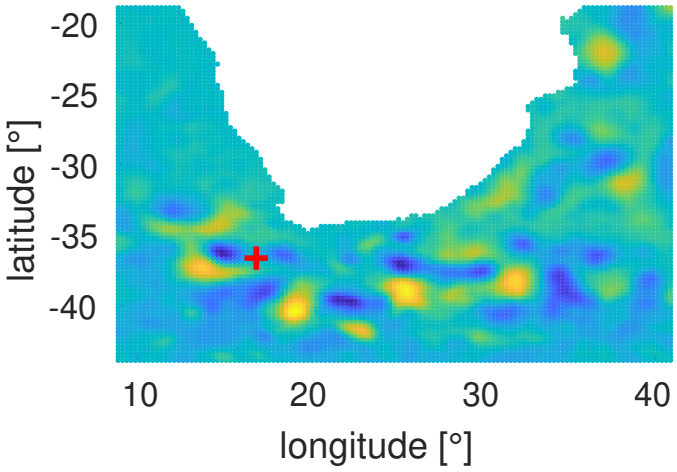

Figure 6.1: Map of sea level anomalies around the Agulhas current (south Africa) localizing the position of the used SLA time series of 01.01.1993. The "+" marks the coordinates (16.875°, -36.625°).

6.1.1 Data

The given SLA data[1] have a local resolution of 0.25° for longitude and latitude. Our test area is longitudinally bordered between $[8.875°, 40.875°]$ and latitudinally between $[-18.875°, -43.875°]$. The study region is South Africa as can be seen in Figure 6.1.
For each individual grid cell of Figure 6.1, a time series of daily SLA data from 01.01.1993 to 31.12.2021 is provided. Furthermore, the time series is diluted by only taking every 31st observation, remaining that the daily observations are reduced to monthly ones. In order to apply LSC, the mean value of the observations must be zero. To achieve this, the observations $\mathcal{L}$ are reduced by the linear trend (like it is shown in Appendix E.1.1) to obtain the signal $\boldsymbol{\mathcal{S}} = [\mathcal{S}_1, \mathcal{S}_2, ..., \mathcal{S}_n]$ with a mean value $M\{E\{\boldsymbol{\mathcal{S}}\}\} = -1.69 \cdot 10^{-17} \approx 0$. The remaining time series of $n = 342$ observations is shown in Figure 6.2.

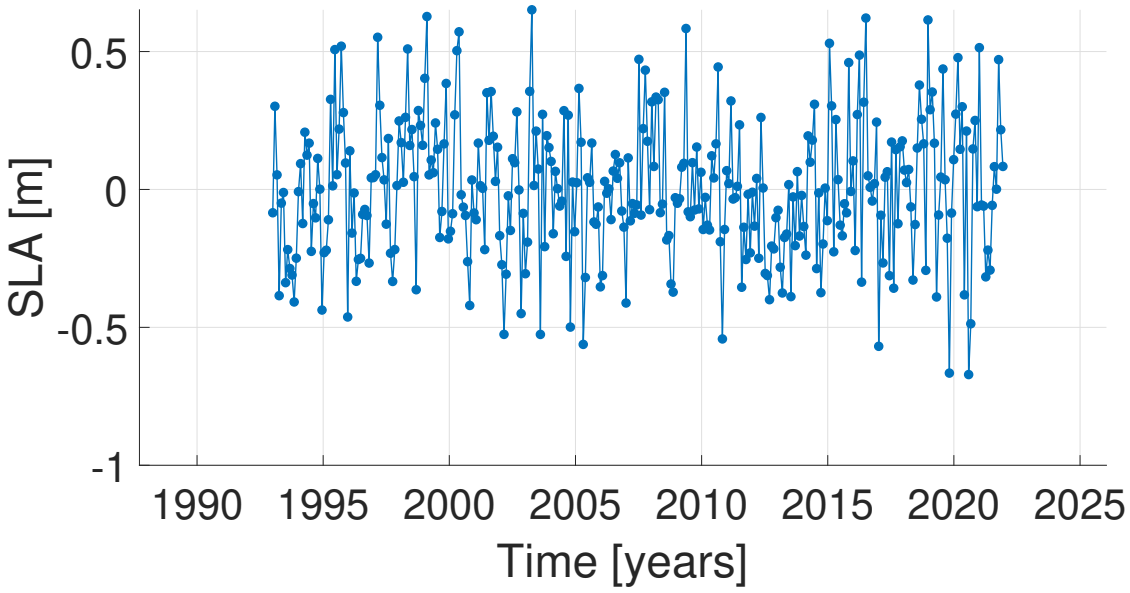

Figure 6.2: Time series of monthly SLA data at position $(16.875°, -36.625°)$ near the Agulas current. The dots are observations with a frequency of 31 days and last from 01.01.1993 to 31.12.2021.

6.1.2 Approximation of SLA Data by Trigonometric Functions

The approximation of this time series by the means of deterministic functions (like splines or trigonometric functions) requires a large number of parameters. In this approach, a signal $\mathcal{S}_t$ of the time series depicted in Figure 6.2 is approximated by 20 cosine and sine functions:

$$\mathcal{S}_t + v_t = \sum_{m=1}^{10} \xi(2m-1)\cos\left(\frac{2\pi}{365.25m}t\right) + \xi(2m)\sin\left(\frac{2\pi}{365.25m}t\right) + ... \\ \sum_{l=2}^{10} \xi(200+2l-1)\cos\left(\frac{2\pi}{365.25}lt\right) + \xi(200+2l)\sin\left(\frac{2\pi}{365.25}lt\right).$$

As the formula shows, a basic period of 365.25 days is assumed, which corresponds to a seasonal signal. The other periods are multiples of the annual oscillation: in case of the first sum, the periods are semi-annual, a time frame which is then successively reduced to quarterly up to 1/10 year. The lower sum adds the oscillations with periods of two to one hundred years. The estimation of the

1. Global Ocean Gridded L 4 Sea Surface Heights, E.U. Copernicus Marine Service Information (CMEMS), Marine Data Store (MDS). comp.:DOI: 10.48670/moi-00145 (accessed on 21-Sep-2023).

parameters

$$\boldsymbol{\xi} = \begin{bmatrix} \xi(1) \\ \xi(2) \\ \vdots \\ \xi(20) \\ \xi(21) \\ \xi(22) \\ \vdots \\ \xi(40) \end{bmatrix}$$

is again done using the Gauss-Markov method described in Appendix E.1.2. In this case o=10 which leads to a total number of $4o = 40$ parameters. But even with this large number of parameters, the reproduction of the function does not work well: Figure 6.3 shows the poor approximation of the monthly data. Increasing the number of parameters, i.e. a higher number of trigonometric

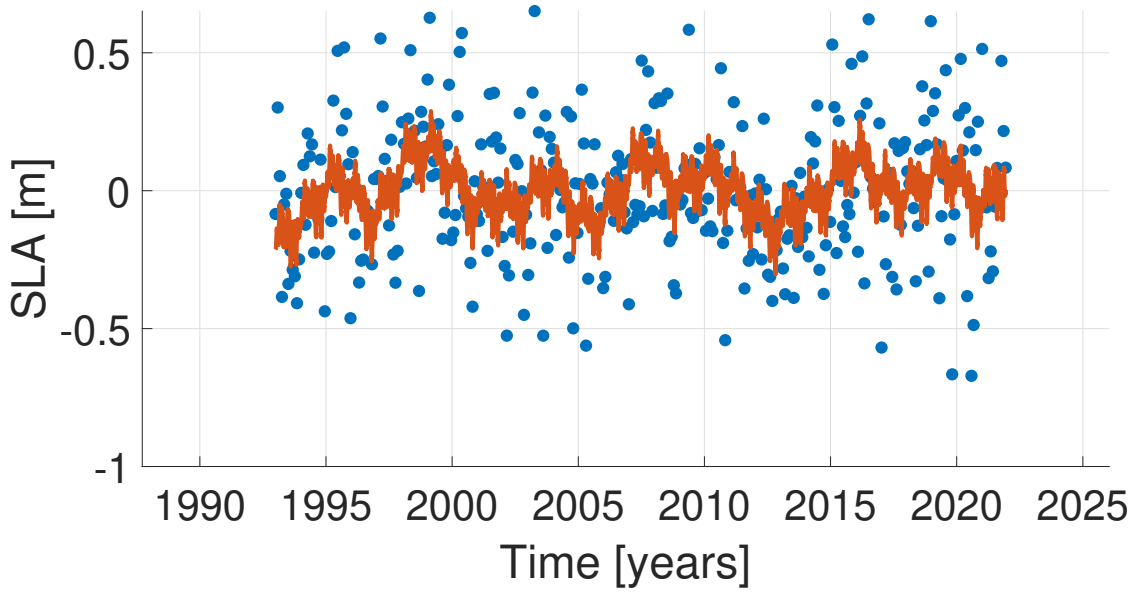

Figure 6.3: Monthly SLA data for the coordinate (16.875°, −36.625°) in Figure 6.1 (blue) and the estimated approximation using trigonometric functions with 40 parameters in a least-squares adjustment (red).

functions for approximation, also does not yield a good result here. As Figure 6.4 shows the result of approximation with trigonometric functions in (E.1.5) with $o = 12$. It is noticeable that the approximation exceeds the area of the observations which are in between ±0.5.

6.1.3 Approximation of SLA by Least-Squares Collocation using AR Processes for the Covariance Modelling

As a stochastic approach, LSC poses an alternative for the deterministic approximations. In this method, the predicted signal is computed by using two covariance matrices and the observations. As such, LSC as introduced in section 2.3, can be applied to approximate the daily observations $\widetilde{\boldsymbol{\mathcal{S}}}$ from monthly SLA data ($\boldsymbol{\mathcal{S}} = [\mathcal{S}_1, \mathcal{S}_2, ..., \mathcal{S}_n]$). Its application

$$\widetilde{\boldsymbol{\mathcal{S}}} = \Sigma\{\widetilde{\boldsymbol{\mathcal{S}}}, \boldsymbol{\mathcal{S}}\} \left(\Sigma\{\boldsymbol{\mathcal{S}}\} + \Sigma\{\boldsymbol{\mathcal{N}}\}\right)^{-1} \boldsymbol{\mathcal{S}} \tag{6.1.1}$$

demands the generation of the covariance matrix of the signal $\Sigma\{\boldsymbol{\mathcal{S}}\}$ as well as the joint covariance matrix of the predicted and the estimated Signal $\Sigma\{\widetilde{\boldsymbol{\mathcal{S}}}, \boldsymbol{\mathcal{S}}\}$ from an estimated AR process describing the signal $\boldsymbol{\mathcal{S}}$.

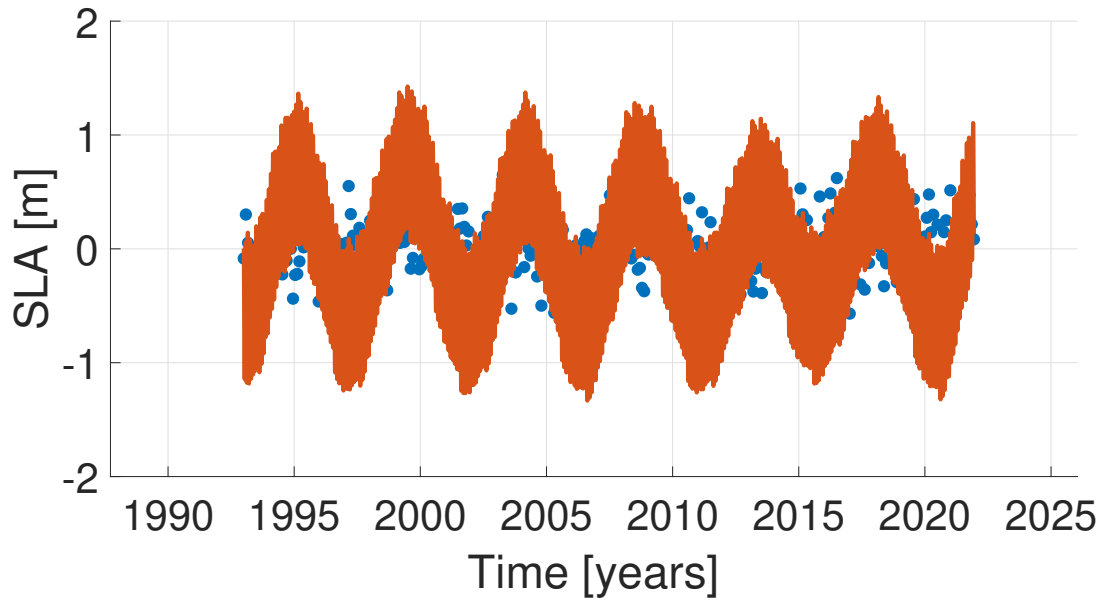

Figure 6.4: Monthly SLA data for the coordinate (16.875°, −36.625°) in Figure 6.1 (blue) and the estimated approximation using trigonometric functions with 48 parameters in a least-squares adjustment (red).

6.1.3.1 AR Process Estimation

The first step consists of the determination of the appropriate AR process. For this purpose AR processes of orders one ($b_l = 0$) to ten ($b_u = 10$) are estimated for the signal (compare section 2.19). In the second step, it follows the determination of the AR coefficients, the variance of the noise and the AIC for each process. Therefore, the empirical covariances are estimated for the lags $j = [0, 1, 2, ..., n/2]$ by approximating (2.6.1) by the means of

$$\Sigma_j = E\{(\mathcal{S}_{t-j} - \mu)(\mathcal{S}_t - \mu)\} \approx \frac{1}{n-j} \sum_{t=j}^{n} \mathcal{S}_{t-j}\mathcal{S}_{t-j}. \tag{6.1.2}$$

The AR parameters are estimated by constructing the Y.-W. equations from section 2.8 for the orders 0 to $n/2$. The adjustment according to the Gauss-Markov model from Koch (1999, chapter 3) is used to estimate the coefficients $[\tilde{\alpha}_1, \tilde{\alpha}_2, ..., \tilde{\alpha}_p]$ and $\tilde{\sigma}^2_{\mathcal{E}}$. For each of these AR processes, the AIC from section 2.18 is computed and the order generating the minimum AIC is determined. Figure 6.5 shows that the AR(3) process has the lowest AIC. This process is completely determined by the coefficients

$$\alpha_1 = 0.3796 \qquad \alpha_2 = 0.1184 \qquad \alpha_3 = -0.1367 \qquad \text{and} \qquad \sigma^2_{\mathcal{E}} = 0.0555[\text{m}^2].$$

The coefficients α_1, α_2 and α_3 are converted via the CP from section 2.9 into the roots

$$P_1 = -0.4751 \qquad P_2 = 0.4274 + 0.3242i \qquad P_3 = 0.4274 - 0.3242i, \tag{6.1.3}$$

which are shown in the unit circle in Figure 6.6. Since the roots are all inside the unit circle, it is proven that the estimated AR(3) process is stationary.

6.1.3.2 Separation of the additional Noise

As a next step, the estimated variance $\tilde{\sigma}^2_{\mathcal{E}}$ has to be divided into the variance of the AR process $\sigma^2_{\mathcal{S}}$ and into the variance of the noise $\sigma^2_{\mathcal{N}}$; i.e.:

$$\sigma^2_{\mathcal{E}} = \sigma^2_{\mathcal{S}} + \sigma^2_{\mathcal{N}}.$$

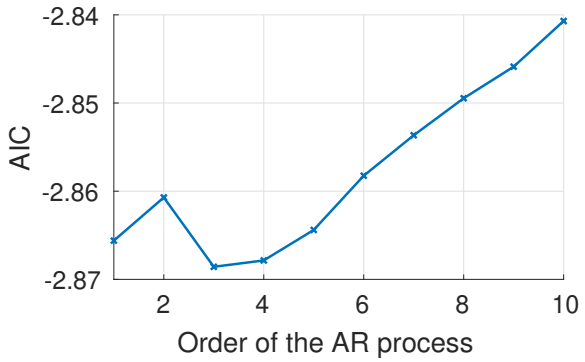

Figure 6.5: The AIC for the AR estimate of SLA data at the position $(16.875°, -36.625°)$ for order one to order ten with a minimum for order three.

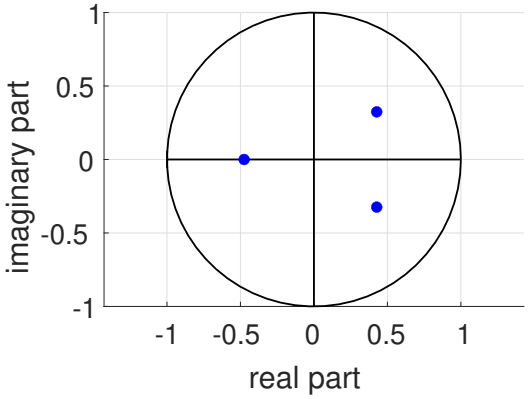

Figure 6.6: Roots of the AR(3) process estimated by the SLA data at position $(16.875°, -36.625°)$.

This separation by variance component is based on the application of Förstner 1985. The ratio between the variance of the AR process or the variance of the noise is determined through several iterations, converging to the variances

$$\sigma_{\mathcal{S}}^2 = 0.0296[\mathrm{m}^2] \qquad \sigma_{\mathcal{N}}^2 = 0.0258[\mathrm{m}^2]. \tag{6.1.4}$$

6.1.3.3 Determination of the Covariance Function

Now, a continuous covariance function has to be determined. This function also satisfies the conditions of section 2.6 and approximates the covariances from (6.1.2). But now, the CF should be determined by the parameters of the AR process found in the sections 6.1.3.1 and 6.1.3.2. With the roots of the AR process of (6.1.3) and the variance of the AR process of (6.1.4), the reorganized Y.-W. equations from B.1.1 can be used to calculate the discrete covariances Σ_j for the discrete distances $j = 0, 1, 2$:

$$\Sigma_0 = 0.0361[m^2], \qquad \Sigma_1 = 0.0143[m^2] \quad \text{and} \quad \Sigma_2 = 0.0077[m^2].$$

These result in the system of equations (B.1.2) which has a unique solution for the coefficients

$$\begin{bmatrix} A_1 \\ A_2 \\ A_3 \end{bmatrix} = \begin{bmatrix} 1 & 1 & 1 \\ P_1 & P_2 & P_3 \\ P_1^2 & P_2^2 & P_3^2 \end{bmatrix}^{-1} \begin{bmatrix} \Sigma_0 \\ \Sigma_1 \\ \Sigma_2 \end{bmatrix} = \begin{bmatrix} 0.0064 \\ 0.0148 - 0.0072i \\ 0.0148 + 0.0072i \end{bmatrix}.$$

The negativity of the real-valued root of (6.1.3) negates the usage of the CF γ provided in (3.1.3). Instead, it must be expanded by the means of (3.1.4):

$$\begin{aligned} \gamma(h) :&= \mathcal{R}\left(\sum_{k=1}^{3} A_k P_k^{|h|}\right) \\ &= A_1 |P_1|^h \cos(\pi h) + A_2 P_2^h + A_2 P_3^h \\ &= 0.0064 \cdot 0.4751^h \cos(\pi h) + (0.0148 - 0.0072i) \cdot (0.4274 + 0.3242i)^h ... \\ &\qquad + (0.0148 + 0.0072i) \cdot (0.4274 - 0.3242i)^h. \end{aligned} \tag{6.1.5}$$

In this form, the CF can be used to compute the covariances for any lag $h \in \mathbb{R}$. Figure 6.7 depicts the empirical covariances of (6.1.2) and the covariances of the CF of (6.1.5) for comparative purposes. This shows that, on the one hand, the CF of the AR process fits the empirical covariances very well. On the other hand, the separation of the variance into a signal and a noise variance leads to an offset between the empirical covariances and the variances of the AR process at lag $h = 0$. This is called the 'nugget effect' and describe the separation of the AR process' CF and the white noise's variance.

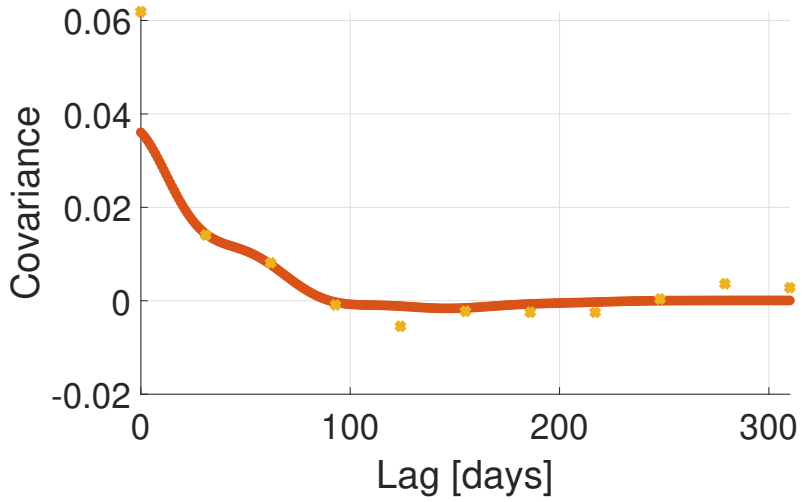

Figure 6.7: Covariance for monthly SLA measurements. With the CF from the AR approach computed by (6.1.5) (red), and the discrete covariances estimated by (6.1.2) (orange). Here the lag can either be in month ($j = 0, 31, 62, ...$)) for the discrete covariances, or daily ($h = 1, 2, ...,$) for the CF from the AR process.

6.1.3.4 Least-Squares Collocation

The performance of the estimation of (6.1.1) demands the determination of the covariance matrices

$$\Sigma\{\widetilde{\boldsymbol{\mathcal{S}}}, \boldsymbol{\mathcal{S}}\}, \qquad \Sigma\{\boldsymbol{\mathcal{S}}\} \qquad \text{and} \qquad \Sigma\{\boldsymbol{\mathcal{N}}\}. \tag{6.1.6}$$

The entries of $\Sigma\{\boldsymbol{\mathcal{S}}\}$ are calculated by the means of the CF from (6.1.5) for integer $h = 31j$ with $j \in \{0, 1, 2, ..., n-1\}$, where j is always the distance from the main diagonal:

$$\Sigma\{\boldsymbol{\mathcal{S}}\} = \begin{bmatrix} \gamma(0) & \gamma(31) & \gamma(62) & ... & \gamma(31(n-1)) \\ \gamma(31) & \gamma(0) & \gamma(31) & ... & \gamma(31(n-2)) \\ \gamma(62) & \gamma(31) & \gamma(0) & ... & \gamma(31(n-3)) \\ ... & & & & \\ \gamma(31(n-1)) & \gamma(31(n-2)) & \gamma(31(n-3)) & ... & \gamma(0) \end{bmatrix}_{n \times n}. \tag{6.1.7}$$

The common covariance matrix $\Sigma\{\widetilde{\boldsymbol{\mathcal{S}}}, \boldsymbol{\mathcal{S}}\}$ of the observed signal $\boldsymbol{\mathcal{S}}$ and the predicted signal $\widetilde{\boldsymbol{\mathcal{S}}}$ has a column for each observation and a row for each predicted value. This matrix comprises of entries calculated from the CF of (6.1.5) by using the lags $h \in \{0, 1, 2, 3, ..., 31(n-1)\}$:

$$\Sigma\{\widetilde{\boldsymbol{\mathcal{S}}}, \boldsymbol{\mathcal{S}}\} = \begin{bmatrix} \gamma(0) & \gamma(31) & \gamma(62) & ... & \gamma(31(n-1)) \\ \gamma(1) & \gamma(30) & \gamma(61) & ... & \gamma(31(n-1)-1) \\ \gamma(2) & \gamma(29) & \gamma(60) & ... & \gamma(31(n-1)-2) \\ ... & & & & \\ \gamma(31(n-1)) & \gamma(31(n-2)) & \gamma(31(n-3)) & ... & \gamma(0) \end{bmatrix}_{(32n-31) \times n}.$$

The covariance matrix of the white noise $\mathcal{N}$ is given by the variances of the extra noise of (6.1.4):

$$\Sigma\{\boldsymbol{\mathcal{N}}\} = \sigma_{\mathcal{N}}^2 \mathbb{1}_{n \times n}. \tag{6.1.8}$$

With these three matrices, everything is given to compute (6.1.1) and thus to predict the daily SLA ($\widetilde{\boldsymbol{\mathcal{S}}}$) from the monthly observations of $\boldsymbol{\mathcal{S}}$. The result is shown in Figure 6.8:

6.1.4 Evaluation

Comparing the results of the estimation from the trigonometric functions of Figure 6.3 with the results of the least-squares collocation of Figure 6.8, it becomes apparent that the latter is visually

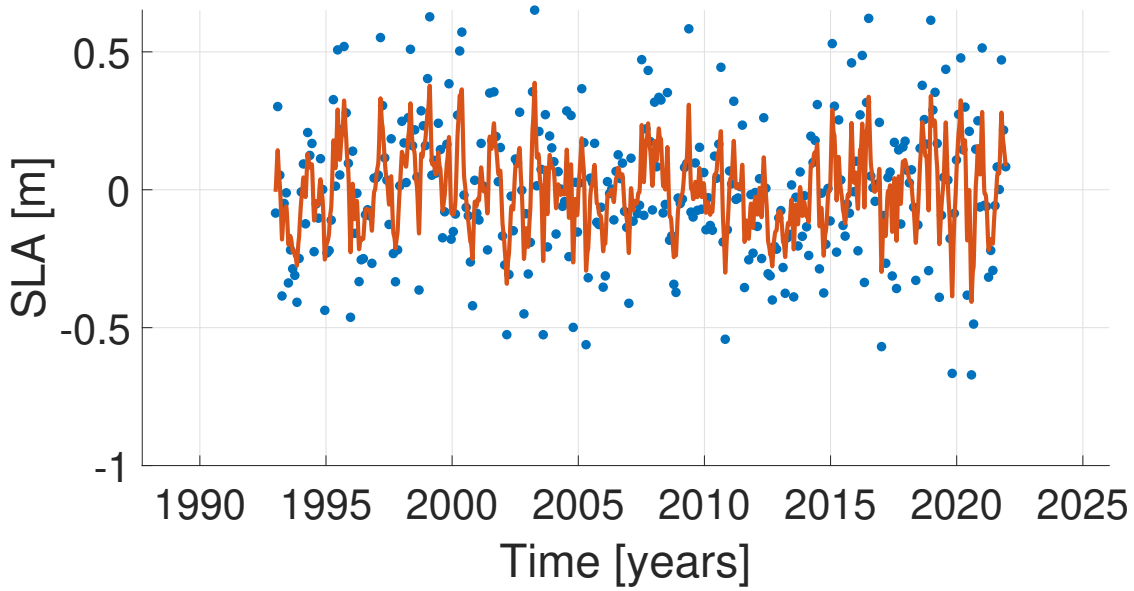

Figure 6.8: Monthly SLA data for the coordinates $(16.875°, -36.625°)$ of Figure 6.1 (blue) and the estimated function using least-squares collocation and a covariance matrix derived from an AR process (red).

more suitable to approximate a function through the observations. The mathematical validation of this comparison demands the calculation of the root mean square error (RMSE) for both estimation methods:

$$\begin{aligned} \text{RMSE} &:= \sqrt{\frac{\sum_{j=1}^{n}(\mathcal{S}_j - \tilde{\mathcal{S}}_j)^2}{n}} \\ \text{RMSE}_{\text{AR}} &= 0.1100\ [m] \\ \text{RMSE}_{\text{Trigo}} &= 0.2304\ [m]. \end{aligned} \tag{6.1.9}$$

This solution verifies the correctness gained from the visual impression, i.e. that the method of least-squares collocation using a CF from AR processes proves more accurate than an approximation based on some given basis functions. The detailed representation of LSC may give the impression that it is more effort to compute the LSC than do an approximation with basis functions, but this is in fact not the case. The steps of the AR processes estimation as well as computing the covariance function are generalized methods. The adjustment with basis functions, however, requires knowledge of possible basis functions. In this case, it was assumed that basis functions are trigonometric functions with the frequency of a year or parts of it. This is a general function used to describe SLA data, which in the end did not prove useful.

Approximation of the Derivative of SLA using AR Processes

When comparing the Gauß-Markow solution using a deterministic approximation with a LSC, the Gauß-Markov estimation has the advantage that it can be used to compute the estimated function derivative (the changes of the SLA data from application 1 in section 6.1, for example). The following section now demonstrated, that this can also be done by LSC with a CF derived from AR processes. Like it is shown in section 2.3, LSC in combination with covariance propagation can build a suitable procedure to estimate the derivatives of the observed time series at any point:

$$\frac{d}{dh}\widetilde{\boldsymbol{\mathcal{S}}} = \Sigma\left\{\frac{d}{dh}\widetilde{\boldsymbol{\mathcal{S}}}, \boldsymbol{\mathcal{S}}\right\}\left(\Sigma\{\boldsymbol{\mathcal{S}}\} + \Sigma\{\boldsymbol{\mathcal{N}}\}\right)^{-1}\boldsymbol{\mathcal{S}}. \tag{6.1.10}$$

Here h is the lag between the discrete observations.

6.1.5 Data

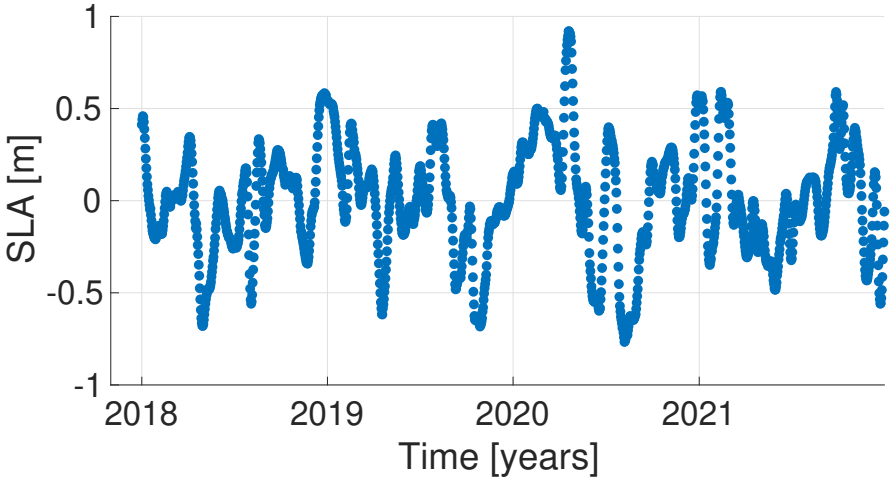

Figure 6.9: Time series of monthly SLA data at position $(16.875°, -36.625°)$ near the Agulas current. The dots are daily observations and cover a time frame of 01.01.2018 to 31.12.2021.

To test the shown theory, we first compute the derivative of the daily SLA data. Secondly we determine the extreme values of the approximate function, and thirdly prove the estimated derivative by showing that whenever there is an extreme value in the estimated function, the derivative is zero. For this, the time series at the coordinates $(16.875°, -36.625°)$ from application 6.1 is again used. This time, the observed interval is reduced to daily observations of the period from 01.01.2018 to 31.12.2021. Just like in the previous example, the trend is estimated by a linear function (see Appendix E.1) and subtracted from the observations $\mathcal{L}$ to obtain the signal $\boldsymbol{\mathcal{S}} = [\mathcal{S}_1, \mathcal{S}_2, ..., \mathcal{S}_n]$. The mean value of the remaining signal used as observations in LSC is $M\{E\{\boldsymbol{\mathcal{S}}\}\} = -5.6 \cdot 10^{-17} \approx 0$, and the resulting time series is depicted Figure 6.9.

6.1.6 AR Process Estimation

The use of daily data of a smaller time interval fundamentally changes the signal characteristic and therefore has a strong impact on the choice of the best-fit AR process. Notwithstanding, the procedure remains the same as in section 6.1.3: first, with the help of (6.1.2), the discrete covariances Σ_j are determined, in order to estimate the coefficients α_k and the variance of the noise $\sigma^2_{\mathcal{E}}$ for each AR process of order one to ten. Let n be the number of all observations, then, this time, instead of the AR estimation of the covariances up to lag $j = n/2$, we use the unambiguous solution of the Y.-W. equations (see section 2.8).[2] The discrete CF in Figure 6.12 explains the reason for the decision to use the Y.-W. equations here for the estimation. It shows an unmodelled deformation in the discrete covariance with lag between 20 and 40 days. When estimating the roots with the method used in the application in 6.1, this leads to AR processes with roots outside the unit circle. The choice of the most appropriate AR process and its order is determined by the AIC (see section 2.18). For the time series in Figure 6.9, the minimum AIC is found by order $p = 7$ (see Figure 6.10). The resulting parameters of the AR(7) process are given by the variance of the noise $\sigma^2_{\mathcal{E}} = 3.0293\ 10^{-4}[m^2]$ and the coefficients

$$\alpha_1 = 1.6681 \qquad \alpha_2 = -0.3711 \qquad \alpha_3 = -0.2714$$
$$\alpha_4 = -0.1135 \qquad \alpha_5 = -0.0129 \qquad \alpha_6 = 0.0482$$
$$\alpha_7 = 0.0437.$$

2. This is necessary because of the lower number of observations, which results in a lower accuracy of the empirical covariances of high lags.

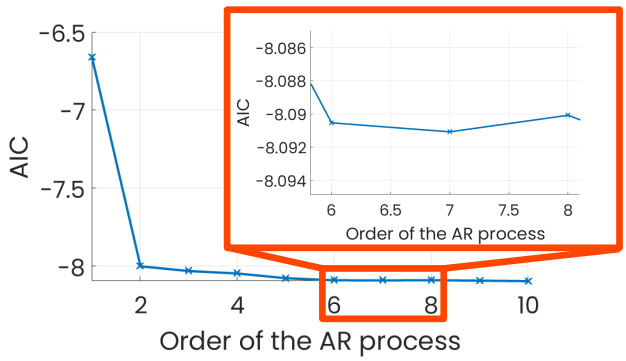

Figure 6.10: The AIC values for the AR estimate of SLA data at the position $(16.875°, -36.625°)$ and from 01.01.2018 to 31.12.2021 for order one to order ten with a minimum at seven.

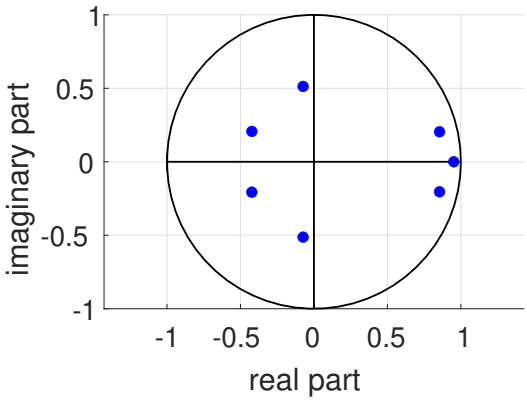

Figure 6.11: Roots of the AR(7) process estimated by the SLA data at position $(16.875°, -36.625°)$.

These coefficients can be converted via the CP of section 2.9 into the roots:

$$\begin{aligned} P_1 &= 0.9518 & P_{2,3} &= 0.8547 \pm 0.2041i \\ P_{4,5} &= -0.0739 \pm 0.5128i & P_{6,7} &= -0.0739 \pm 0.5128i \end{aligned} \tag{6.1.11}$$

which are depicted in Figure 6.11. The fact that all seven root lie within the unit circle proves that the estimated AR(7) process satisfies the condition of stationarity.

6.1.7 Construction of the Covariance Function

After determining the AR process, it is necessary to divide the estimated variance $\sigma_{\mathcal{E}}^2$ into the variance of the AR process ($\sigma_{\mathcal{S}}^2$) and the variance of noise ($\sigma_{\mathcal{N}}^2$). As in the previous application, this is done like in section 6.1 with the method presented in Förstner 1985, resulting in

$$\sigma_{\mathcal{S}}^2 = 2.9704\ 10^{-4}[m^2] \qquad \text{and} \qquad \sigma_{\mathcal{N}}^2 = 0.0588\ 10^{-4}[m^2].$$

The low variance of the noise in relation to the variance of the AR process shows that in this time series an AR process has been estimated which describes the process precisely and that the process contains hardly any further noise. With $\sigma_{\mathcal{S}}^2$, the CF can be established aa in section 6.1.3.3. Again, using the reorganized Y.-W. equations of (B.1.1) allows the determination of the first $p = 7$ covariances Σ_i with $i = 1, 2, ..., 7$. These covariances are then used in (B.1.2) to determine the weights

$$\begin{aligned} A_1 &= 0.0898 & A_{2,3} &= 0.0018 \mp 0.0104i \\ A_{4,5} &= 7.6095\ 10^{-6} \mp 3.1713\ 10^{-6}i & A_{6,7} &= 4.908\ 10^{-6} \mp 3.9009\ 10^{-7}i \end{aligned}$$

of the CF. From these and the roots of (6.1.11), the unambiguous CF of the AR(7) process is computed. It is shown in Figure 6.12 allowing a comparison with the discrete covariances. The two CFs differ greatly in the range between the lags of 20 and 40 days. In contrast to the method of least-squares collocation, the modelling of this difference by the means of AR process demands the estimation of an AR process of high order. For this reason, we again refer to the estimation based on the Y.-W. equations, which, compared to the estimation method of the first example, only uses the first p covariances and thus remains unaffected by this oscillation in the CF, while the roots all remain inside the unit circle.

6.1.8 Filling the Covariance Matrices

The matrices $\Sigma\{\boldsymbol{\mathcal{S}}\}$ and $\Sigma\{\boldsymbol{\mathcal{N}}\}$ of (6.1.6) correspond to the matrices of (6.1.1) and are accordingly described either by the CF of the AR process, or the CF of noise as described in (6.1.7)

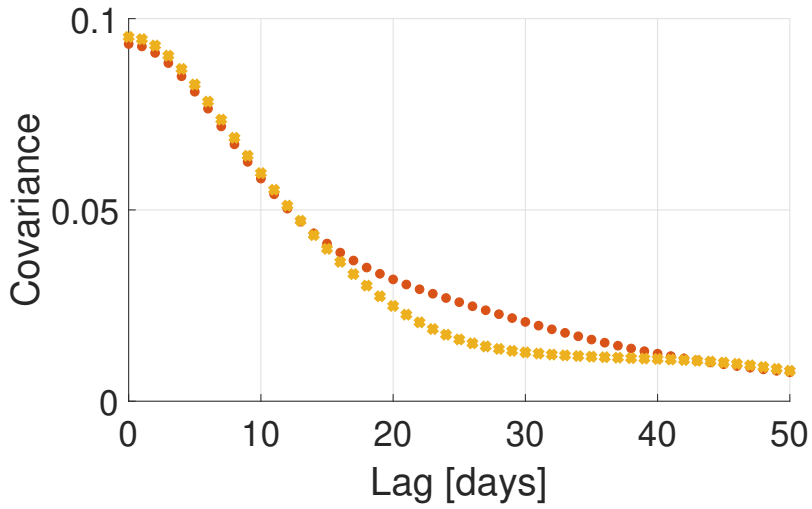

Figure 6.12: Covariances for the SLA measurement of Figure 6.9: the CF of an AR(7) process (red), and the discrete covariances of (6.1.2) in (orange).

and (6.1.8). Thus, only $\Sigma\left\{\frac{d}{dh}\widetilde{\boldsymbol{\mathcal{S}}}, \boldsymbol{\mathcal{S}}\right\}$, the common covariance function between the signal $\boldsymbol{\mathcal{S}}$ and the derivatives at the predicted locations $\frac{d}{dh}\widetilde{\boldsymbol{\mathcal{S}}}$, is missing. To fill the entries of this matrix, the covariance propagation of section 2.3 is used, after which the entries of this matrix are computed from the derivative of the CF. Appendix E.2 provides the methods to compute the derivative of CFs from AR processes. With (E.2.3) and (E.2.4) the derivative of the CF can be evaluated for the corresponding lags $h \in \{0, 1, ..., n\}$ and the joint covariance matrix accordingly filled:

$$\Sigma\{\frac{d}{dh}\widetilde{\boldsymbol{\mathcal{S}}}, \boldsymbol{\mathcal{S}}\} = \begin{bmatrix} \frac{d}{dh}\gamma(h)|_{h=0} & \frac{d}{dh}\gamma(h)|_{h=1} & \frac{d}{dh}(h)|_{h=2} & \dots & \frac{d}{dh}\gamma(h)|_{h=n-1} \\ \frac{d}{dh}\gamma(h)|_{h=1} & \frac{d}{dh}\gamma(h)|_{h=0} & \frac{d}{dh}\gamma(h)|_{h=1} & \dots & \frac{d}{dh}\gamma(h)|_{h=n-2} \\ \frac{d}{dh}\gamma(h)|_{h=2} & \frac{d}{dh}\gamma(h)|_{h=1} & \frac{d}{dh}\gamma(h)|_{h=0} & \dots & \frac{d}{dh}\gamma(h)|_{h=n-3} \\ & \dots & & & \\ \frac{d}{dh}\gamma(h)_{h=n-1} & \frac{d}{dh}\gamma(h)_{h=n-2} & \frac{d}{dh}\gamma(h)_{h=n-3} & \dots & \frac{d}{dh}\gamma(h)_{h=0} \end{bmatrix}_{n\times n}.$$

These three covariance matrices allow the prediction of the derivative of the SLA data via LSC in (6.1.10). The resulting derivative of the estimated function is shown in Figure 6.13.

6.1.9 Proof of Concept (Extreme Values Prediction)

To verify the LSC predicted derivative, we search for the times for which the derivative is equal to zero. If the approximation is calculated by LSC for the observations of Figure 6.9, then the extreme values of the function must be located at the same times when the derivative of this function shown in Figure 6.13 is equal to zero. So Figure 6.14 visualizes the predicted function and highlights the times with an 'x', where the derivatives are zero. Since these highlights match the function's extreme values, this crossover in Figure 6.14 verifies the derivative's correctness.

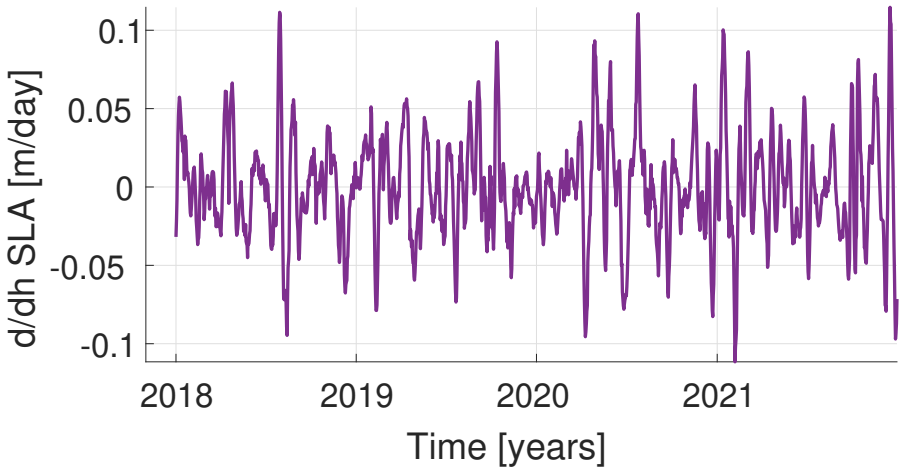

Figure 6.13: Derivative of the continuous function estimated by least-squares collocation for the SLA at position $(16.875°, -36.625°)$, covering a time frame of 01.01.2018 to 31.12.2021.

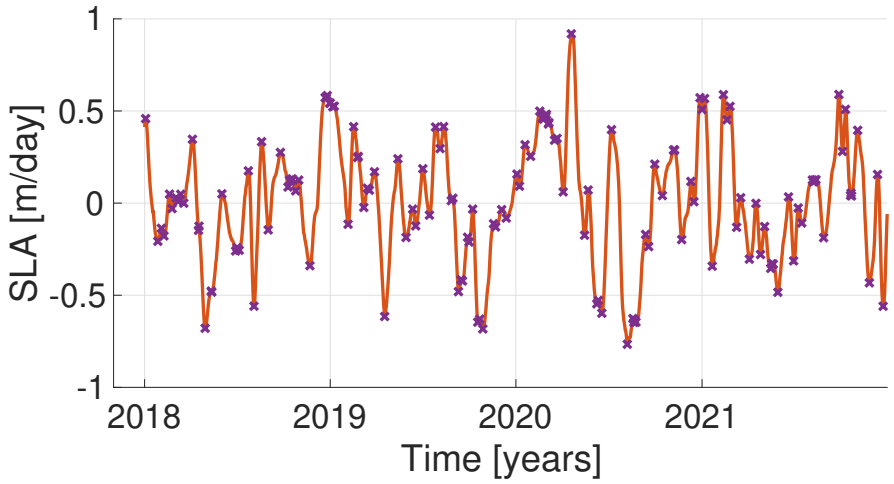

Figure 6.14: Estimated time series of SLA data at position $(16.875°, -36.625°)$ with minima and maxima. The red function is the estimated function covering a time frame of 01.01.2018 to 31.12.2021, and the purple crosses mark the minima and maxima found by the interpolated zeros of the estimated derivative function.

6.2 GNSS Data Analysis Using Time Variable AR Processes

In this section, time variable AR processes are estimated to model the height component of GNSS deviced coordinate time series.[3] Here, the temporal changes of the roots are modelled by polynomial functions (in particular linear, quadratic and piecewise linear functions) and validated by a sequence of discrete roots derived from time stable AR processes estimated from data of a moving window. This demands to detrend the time series. The trend is estimated by a Gauß-Markov model

$$\mathcal{L}_k - \mathcal{S}_k = \xi(1) + \xi(2)t_k + \sum_{j=1}^{2} \xi(2j+1)\cos(j \cdot t_k 2\pi) + \xi(2j+2)\sin(j \cdot t_k 2\pi),$$

which is shown in Appendix E.1.3. This trend itself is depicted in both Figure 6.15 and Figure 6.37 (for each individual GNSS time series as a red line in the plots of the left columns).
The individual estimated parameters of the vector $\boldsymbol{\xi}$ are used to reduce the trend for each time series. Afterwards, pseudo observations are predicted for equidistant times between the observations. This is done with the help of a cubic spline interpolation derived from the signal giving equidistant observations at these points, where the lag is equal to the original observations' the median lag. The resulting time series are shown in the right columns of Figure 6.15 and Figure 6.37. These results can now be used for TVAR estimations.
In order to validate the TVAR estimates, the movement of the roots is approximated by the roots of time stable AR processes estimated for every step of a moving window. Whereby, the estimation in every window is done by the assumption of a stationary time series. This results in roots of AR processes for each window. If the estimate of the TVAR processes succeeds, the root motion should fit the point cloud of roots found by the AR processes estimated for each step of the moving window. Since the spectrum and roots of the AR or TVAR processes can be clearly transformed into each other, this corresponds to the modelling of the process characteristics.

6.2.1 TVAR Processes Estimate with Linear Root Motions

Figure 6.15 depicts the time series, which are used to estimates TVAR processes with linear root motion. For all these time series successive TVAR process (derived in subsection 4.3.3), as well as AR processes are estimated. While it is sufficient to estimate the TVAR processes from order one to order five, the AR processes are estimated for the orders one to ten. The corresponding AIC values are depicted in Figure 6.16 [4].
When estimating TVAR processes with linear root movements, this study makes a distinction between two approaches: first, the approach via direct estimates for TVAR processes of orders one to three, and second there is the successive approach, which allows the estimation of higher order TVAR processes estimated by the means of cascades of TVAR processes with orders one or two. The AIC values of the TVAR estimate in Figure 6.16a depicts, that the time series shown in Figure 6.15a is best fit by a TVAR(1) process. Figure 6.15b depicts a processes, which, according to Figure 6.15b minimized the AIC by using a TVAR(2) process; and the AIC values in Figure 6.16c visualized a minimum of order three for the TVAR estimate of the time series in Figure 6.15c. And even though, Figure 6.16d shows a minimum for the successive TVAR(3) process, it will be shown, that a direct computation of the TVAR(3) process will be more suitable for the time series in Figure 6.15d. The following subsections provides the analysis of these estimates.

3. The data is provided by La Rochelle Université: https://www.sonel.org/-GPS-.html (last accessed: 11.03.2025).

4. The reason for the repetition of the orders is, that in the successive estimation there are several possibilities to produce a TVAR process (see section 4.3.3). The first TVAR estimate always only consists of TVAR(1) processes. Then, successively the first two TVAR(1) processes are exchanged for a TVAR(2) process, which is then shifted step by step. For example the possibilities for the TVAR(5) process. Let 1 denote a TVAR(1) estimate and 2 denotes a TVAR(2) process, then the possibilities and sequence of the TVAR(5) processes are given by $[1,1,1,1,1]$ $[2,1,1,1]$ $[1,2,1,1]$ $[1,1,2,1]$ $[1,1,1,2]$ $[2,2,1]$ $[2,1,2]$ $[1,2,2]$. Furthermore the empty spaces on the right side of Figure 6.16c are estimations where it is not possible to find suitable coefficients fulfilling the condition for the TVAR(2) (see Appendix (C.4.7)).

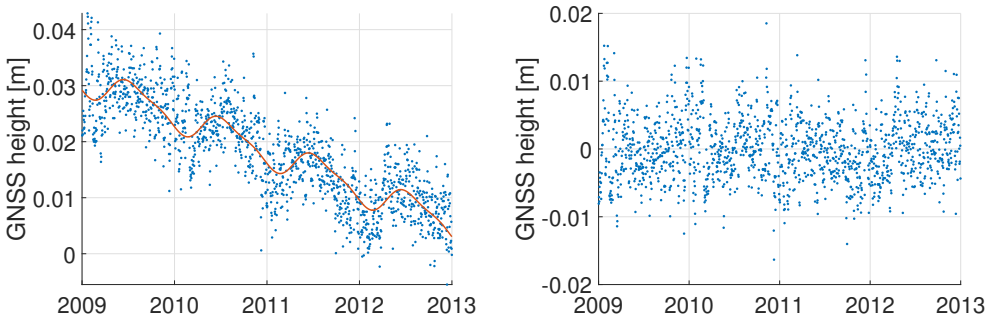

(a) DZYL in Delfzijl (Netherlands) from 2009 to 2013.
Analysis center: Nevada Geodetic Laboratory (NGL14).

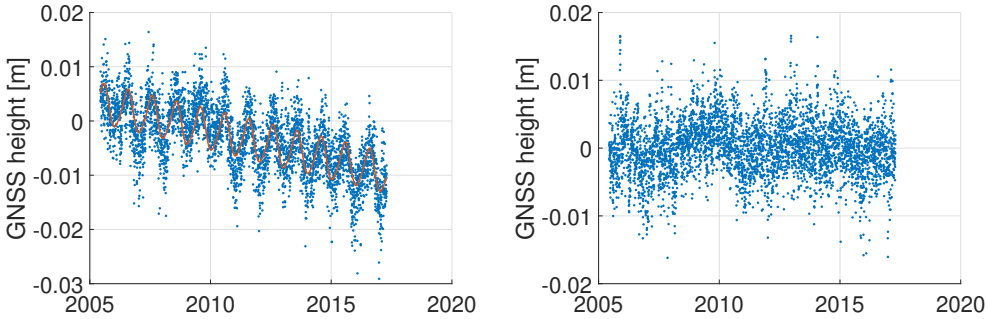

(b) BORJ in Brokum (Germany) from the middle of 2014 to 2020.
Analysis center: University of La Rochelle (URL7).

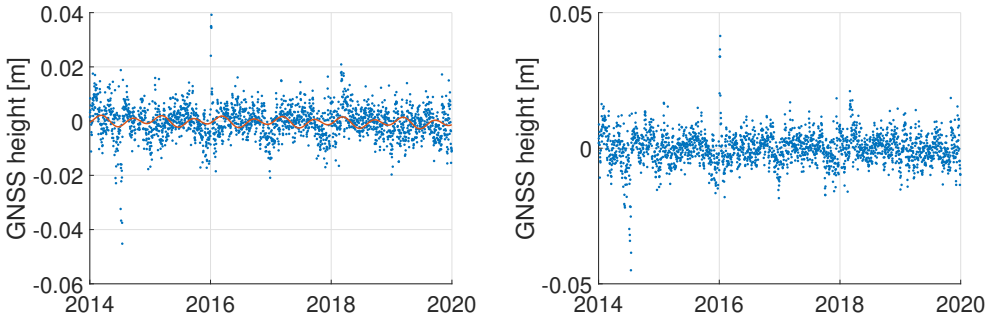

(c) TGBF in Brokum (Germany) from the middle of 2009 to 2017.
Analysis center: Nevada Geodetic Laboratory (NGL14).

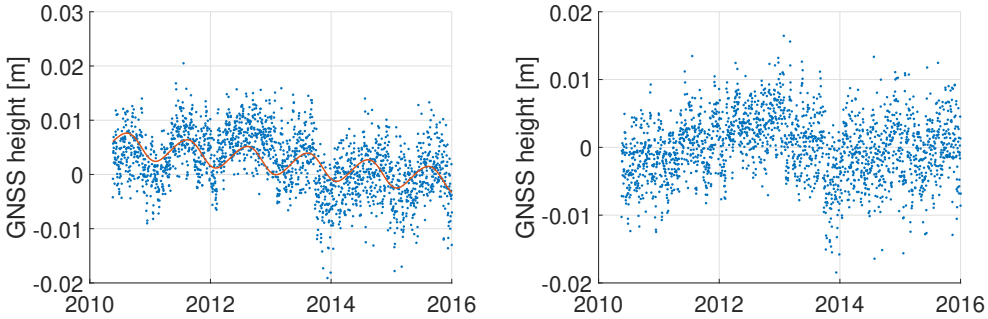

(d) HOL2 in Kiel (Germany) from the middle of 2010 to the beginning of 2016.
Analysis center: Geoforschungszentrum Potsdamm (GT2).

Figure 6.15: GNSS heights used for TVAR estimates with linear root motions, showing the observed GNSS heights (blue) and the estimated trends (red) on the left side, and the reduced and interpolated time series on the right side.

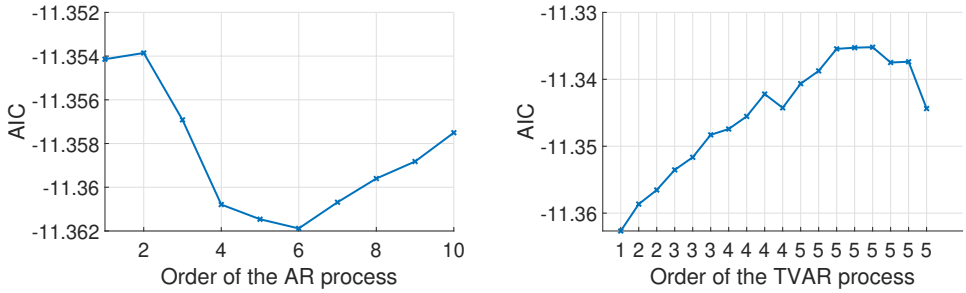

(a) AIC values of the time stable AR approximation of the reduced time series in Figure 6.15a (left) and the AIC values for the TVAR approximation of the same time series (right).

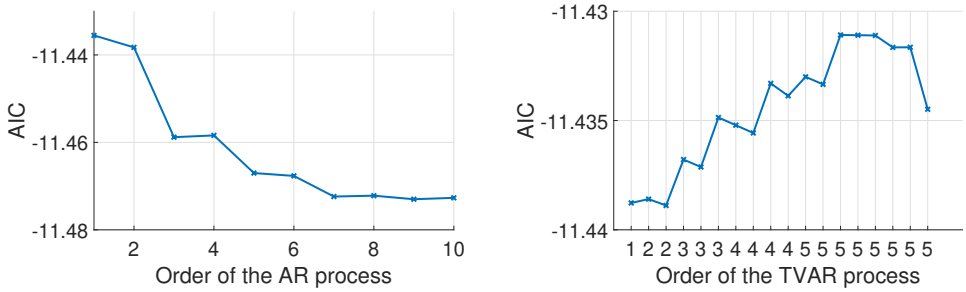

(b) AIC values of the time stable AR approximation of the reduced time series in Figure 6.15b (left) and the AIC values for the TVAR approximation of the same time series (right).

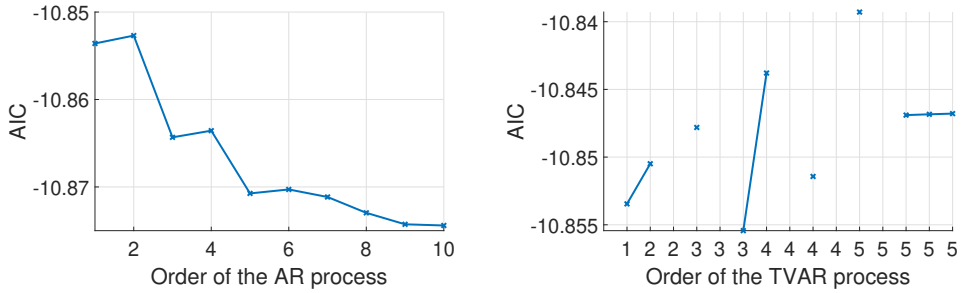

(c) AIC values of the time stable AR approximation of the reduced time series in Figure 6.15c (left) and the AIC values for the TVAR approximation of the same time series (right).

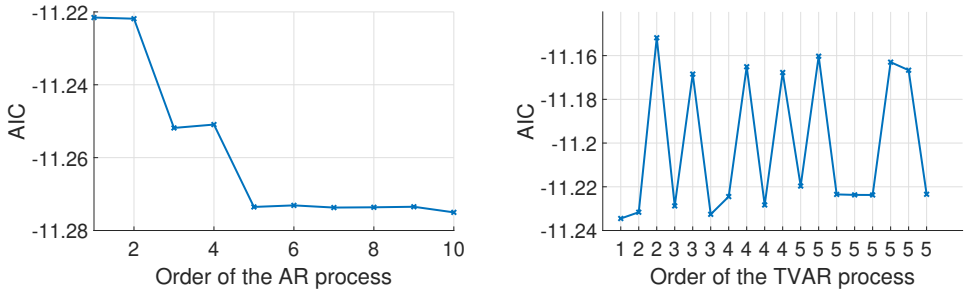

(d) AIC values of the time stable AR approximation of the reduced time series in Figure 6.15d (left) and the AIC values for the TVAR approximation of the same time series (right).

Figure 6.16: AIC values of the AR and TVAR estimate of the reduced GNSS heights shown in Figure 6.15. On the left side, the AIC values of the time stable AR estimates are shown, and on the right side, there are the AIC values from the TVAR estimations.

6.2.1.1 TVAR(1) Process Estimate

Since section 4.3.2 shows that the estimation of TVAR(1) processes is done without additional restrictions, section 4.3.2 demands the solution of the parameter by a Gauß-Markov model with the design matrix of (C.4.5). According to Figure 6.16a the TVAR(1) process with parameters

$$\beta_0^{(1)} = 0.7669 \quad \text{and} \quad \beta_1^{(1)} = -0.1965. \tag{6.2.1}$$

minimizes the AIC value for the estimate of the time series in Figure 6.15a. Respectively, the resulting time variable root is given as

$$P_1 = 0.7669 - 0.1965t \quad \text{with } t \in [0, 1]. \tag{6.2.2}$$

To validate the estimation of the TVAR(1) process given in (6.2.1), I shift a moving window with a width of 200 observations along the time series and a further estimated an AR(1) process for each one of them. This assumes stationarity in each window. In Figure 6.17 the roots resulting from the AR(1) estimates (violet) are depicted as well as the estimated linear root movement (orange). Comparing these two reveals that the estimation is adequately. Further examples of the TVAR(1) process estimates are provided in section 6.3 where annual temperature anomalies are interpolated by least-squares collocation using TVAR(1) processes.

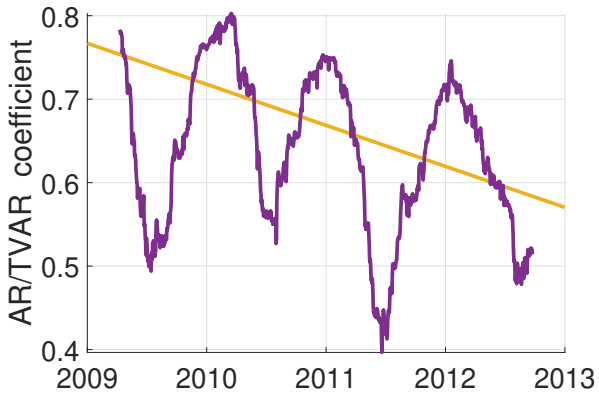

Figure 6.17: The linear root of an estimated TVAR(1) process (orange) compared to the roots of a AR estimation of a moving window with width of 200 observations (violet).

For the purpose of comparison, it is assumed, that the process is stationary. This way, an AR(1) process and the AR process minimizing the AIC, both are computed. The left side of Figure 6.16a shows that the minimum AIC is found for the AR(6) process. Figure 6.18 depicts the root of the AR(1) process. The root of the AR(1) process ($P_1 = 0.6756$), lies within the root motion of the TVAR(1) process given by (6.2.2). (Especially the roots are the same if $t = 0.4646$).
The AR(6) roots are illustrated in Figure 6.19. Since there is no real-valued root in this figure, it seems like the characteristic of this estimate does not fit the AR(1) and TVAR(1) estimate. But computing the RMSE values by (6.1.9), evaluated for these two stationary processes as well as for the TVAR(1) process provides

$$\begin{aligned} \text{RMSE}_{\text{TVAR(1)}} &= 3.4[mm] \\ \text{RMSE}_{\text{AR(1)}} &= 5.4[mm] \text{ and} \\ \text{RMSE}_{\text{AR(6)}} &= 3.4[mm]. \end{aligned}$$

This reveals that, not only the TVAR(1) process has a lower RMSE than the AR(1) process, but also the TVAR's RMSE is equal to the best AR estimations RMSE, but with less roots as well as less parameters.

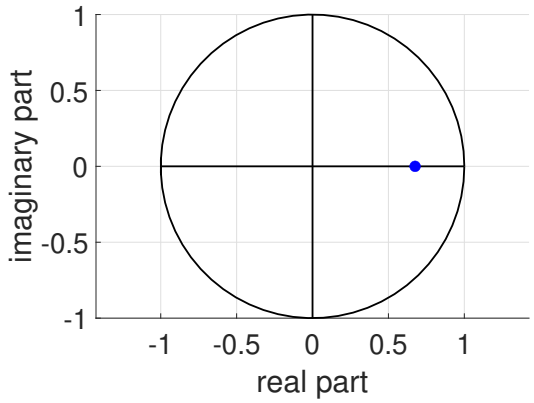

Figure 6.18: Roots of the AR(1) process of the GNSS heights of Figure 6.15a.

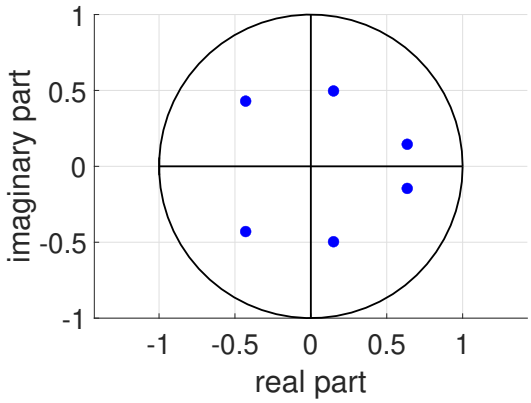

Figure 6.19: Roots of the AR(6) process of the GNSS heights of Figure 6.15a.

6.2.1.2 TVAR(2) Process Estimate

The right side of Figure 6.16b shows that the AIC for the TVAR estimation for the time series in Figure 6.15b minimized for the direct TVAR(2) process estimation without further successive estimation. This is surprising, since it shows that although the direct estimation of a TVAR(2) process with linear root motions provides two real-valued roots, the solution still differs from the successive estimation of two TVAR(1) processes with linear root motions. The method for estimating the TVAR(2) process is shown in Appendix C.4, where the formula (C.4.6) provides the design matrix for the TVAR(2) estimate. In this case, there is a further required restriction to include. This restriction is shown in (C.4.7) and must be fulfilled to guaranty two linear root motions. For this purpose, the design matrix of (C.4.8), as well as the covariance matrix of the estimated parameters from the Gauß-Markov model without further restrictions by the formula (C.4.9) is established. Then, according to the system in (C.4.10), the adjusted parameters are determined iteratively. The TVAR(2) estimation with linear root motion results in the roots

$$P_1 = 0.7345 - 0.3192t \quad \text{and} \quad P_2 = -0.1358 + 0.2061t \text{ with } t \in [0, 1]. \tag{6.2.3}$$

This is again verified by the means of a moving window. In this case, the width of the window is given as 1000 observations. However, for each window an AR(2) process is again estimated, while stationarity is assumed. Figure 6.20 provides the comparison of the individual roots of the AR(2) estimates from the moving window with the linear roots of the TVAR(2) process. This validates the TVAR(2) roots motion, as both show a similar variation over time.

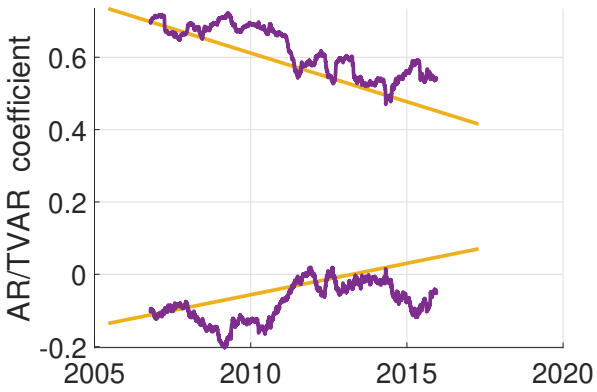

Figure 6.20: The linear root of an estimated TVAR(2) process (orange) compared to the roots of an AR estimation of a moving window with a width of 1000 observations (violet).

Furthermore, for this time series -and under the assumption of stationarity- time constant AR processes are estimated and compared to the TVAR process estimation results. Again, the AR processes of order one to ten are estimated revealing the best fit by minimizing the AIC. These AIC values are depicted on the left side of Figure 6.16b, and show, on the one hand, that the first minimum is found by using AR processes of order three, and, more importantly, on the other hand side, that the AIC is nearly constant when approximating the time series by AR process of order seven or higher. The roots of the AR(3) process are shown in Figure 6.23, where it can be seen

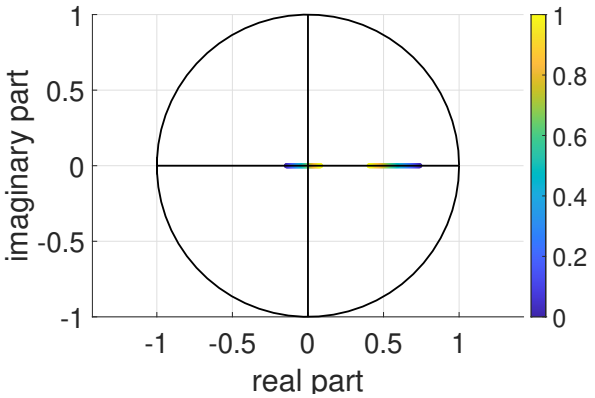

Figure 6.21: Roots of the TVAR(2) process of the GNSS heights of Figure 6.15b.

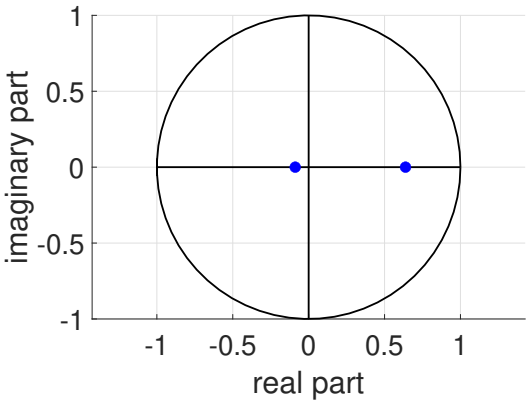

Figure 6.22: Roots of the AR(2) process of the GNSS heights of Figure 6.15b.

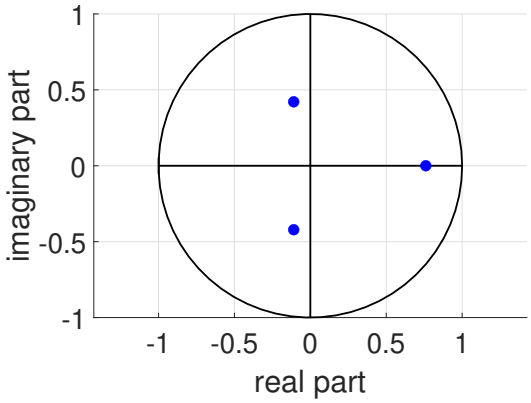

Figure 6.23: Roots of the AR(3) process of the GNSS heights in Figure 6.15b.

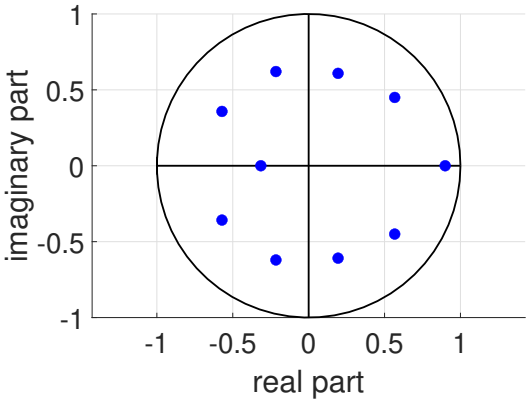

Figure 6.24: Roots of the AR(10) process of the GNSS heights in Figure 6.15b.

that, compared TVAR(2) process, the roots locations, and therefore the characteristic of the AR process changes. The roots of the estimated AR(2) process shown in Figure 6.22 are provided by

$$P_1 = 0.6381 \quad \text{and} \quad P_2 = -0.0884.$$

On the one hand, comparing the root motion of Figure 6.21 with the roots of Figure 6.22 shows, that the roots of the AR(2) lie in the centre of the linear root motion of (6.2.3). But on the other hand, comparing the AIC for the AR estimate on the left side of Figure 6.16b with the AIC for the TVAR estimate on the right side of Figure 6.16b, it follows, that the AIC for the AR estimate decreased until it reaches order seven, and the other one increases after order two. This means, that the AR processes of order higher than two do not have a linear trend. Furthermore, the RMSE of the TVAR(2) estimation and the AR processes estimation of order two, three and ten given by

(6.1.9) are all close to another:

$$\begin{aligned} \mathrm{RMSE}_{\mathrm{TVAR(2)}} &= 3.3\ [mm], \\ \mathrm{RMSE}_{\mathrm{AR(2)}} &= 3.3\ [mm], \\ \mathrm{RMSE}_{\mathrm{AR(3)}} &= 3.2\ [mm] \text{ and} \\ \mathrm{RMSE}_{\mathrm{AR(10)}} &= 3.2\ [mm]. \end{aligned}$$

This way, the higher orders of the AR processes do not generate a more suitable AR process to detect the trend, but the AR processes start to model the white noise. This can be seen in Figure 6.24, where, in case of high order AR processes like order ten, the complex value roots form a circle around the origin. They approximate a constant value in the spectrum, which equals the white noise's spectrum (see Appendix E.3). In other words: the AR estimation is over-fitting the time series while the TVAR estimate cannot do this. The reason for this is the fact, that the white noise consists of countless roots on a circle around the origin, which do not possess a trend in their motion. Since the linear roots can not move in circles, and so can not form constant circles, the TVAR estimation seems to be more robust to over-fitting.

6.2.1.3 Successive TVAR Process Estimate

Using the direct estimates of the TVAR(1) and TVAR(2) processes from the previous applications, section 4.3.3 also allows the estimation of higher order TVAR processes by the means of successive estimation of TVAR(1) and TVAR(2) processes. Therefore the residuals of one iteration is used as new observations in the following iteration. The AIC for TVAR processes of section 4.3.3 is used to find the most suitable TVAR process. The right side of Figure 6.16c depicts the AIC values of the TVAR process estimation for the time series of Figure 6.15c. The TVAR process minimizing the AIC is the TVAR(3) process. Its computation demands first the estimation of a TVAR(1) process, and then the estimation of a TVAR(2) process from the former residuals. Estimating this TVAR(3) process provides three time variable roots, including a complex conjugated pair and a real-valued root:

$$P_1 = 0.6955 - 0.0201t \qquad P_{2,3} = -0.0085 \pm 0.4090i + (0.0173 \pm 0.7379i)t \quad t \in [0.1].$$

The validation of the estimation is again done by the means of a moving window, which this time contains 700 observations. Under the assumption of stationarity, AR(3) processes are estimated for each window and the resulting roots are shown as a time track in Figure 6.25. Comparing this

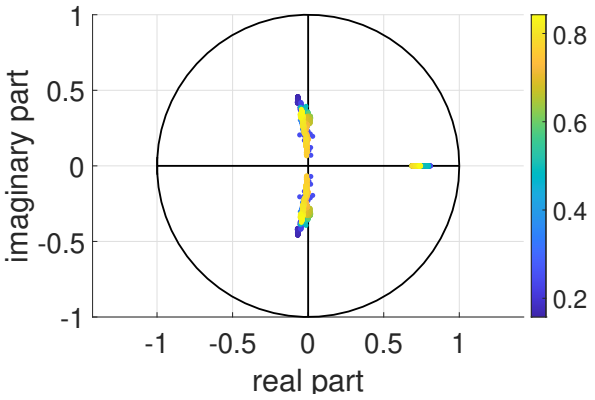

Figure 6.25: Roots of an AR(3) processes estimated for moving windows of 700 observations gliding over the GNSS series of Figure 6.15c.

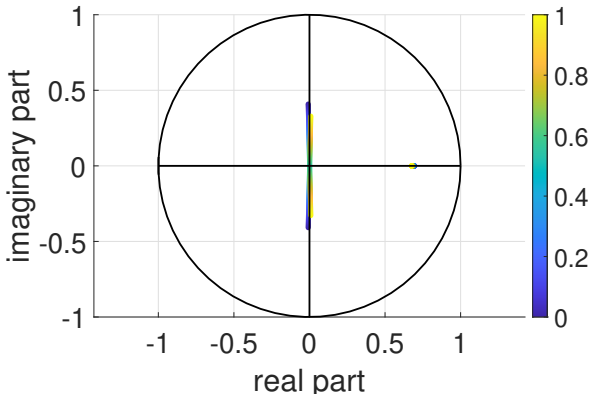

Figure 6.26: Time variable roots of the successive TVAR(3) processes with linear root motion estimated for the GNSS series of Figure 6.15c.

track of roots to the linear root of the successive TVAR(3) estimate depicted in Figure 6.26, shows

that the oscillation around the center of the discrete roots in Figure 6.25 was realized by the TVAR roots crossing the x-axis. This way, the linear root motion of the time variable estimate follows the movement of the point cloud created by the root of the individual windows.
For further comparisons, an AR estimation (again under the assumption of stationarity) is computed. Figure 6.16c depicts the AIC for the AR processes up to order ten. The most promising AR processes with local minima in the track of the AIC is an AR(3) (Figure 6.27), an AR(5) process (Figure 6.28) and an AR(10) process (Figure 6.29).

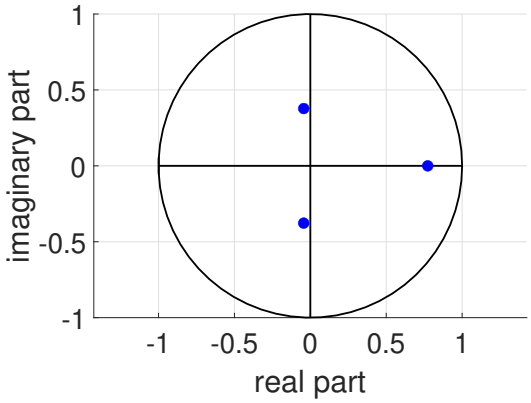

Figure 6.27: Roots of the AR(3) processes estimated for the time series of GNSS heights in Figure 6.15c.

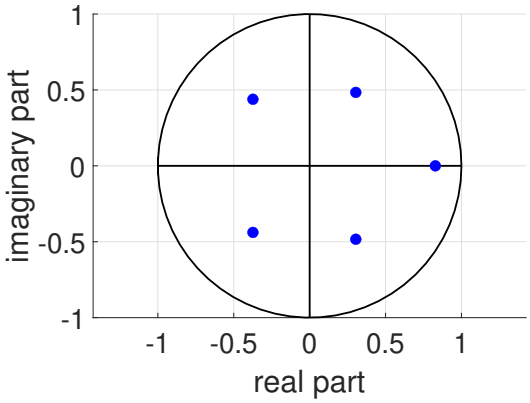

Figure 6.28: Roots of the AR(5) processes estimated for the time series of GNSS heights of Figure 6.15c.

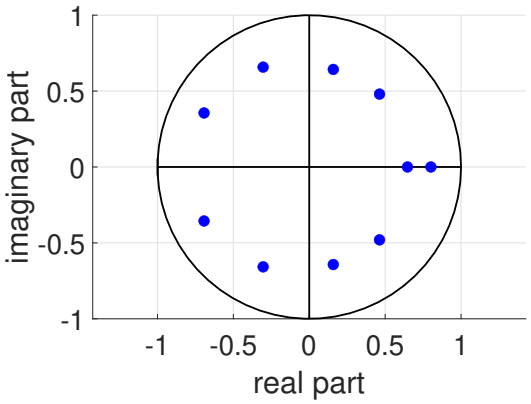

Figure 6.29: Roots of the AR(10) processes estimated for the time series of GNSS heights of Figure 6.15c

The RMSE values can be computed for each of these AR processes as well as for the TVAR process by the means of (6.1.9), which provides similar solutions:

$$\begin{aligned} \mathrm{RMSE}_{\mathrm{TVAR(3)}} &= 4.4\ [mm], \\ \mathrm{RMSE}_{\mathrm{AR(3)}} &= 4.4\ [mm], \\ \mathrm{RMSE}_{\mathrm{AR(5)}} &= 4.4\ [mm] \text{ and} \\ \mathrm{RMSE}_{\mathrm{AR(10)}} &= 4.3\ [mm]. \end{aligned}$$

These values in combination with the roots of the TVAR(10) process depicting a circle around the centre (see Figure 6.29), proves that the AR estimation is over-fitting (see E.3). Since the order three gives the minimum AIC value for the TVAR estimation, Figure 6.16c proves, that the TVAR process estimation with linear root motions, is more robust to over-fitting than the AR estimation.

6.2.1.4 TVAR(3) Process Estimates

Section 4.5.2 presented a last method to estimate TVAR processes with linear root movements, i.e., how to directly estimate TVAR(3) processes without using a successive method. In the previous three examples, the Gauss-Markov model (see (C.4.10)) does not give a solution when estimating the parameters by the non-linear conditions (4.5.11), (4.5.12), and (4.5.13). So these examples do not provide a solution of the direct estimation of TVAR(3) processes with linear roots. This differs from the example of Figure 6.16d. For this example AR processes, successive TVAR processes with linear root motion, as well as the direct TVAR(3) process with linear root motion should be estimated and compared with each other.
First we repeat the procedure of application 6.2.1.3. This means ten AR and eighteen TVAR process estimations. The resulting AIC values are depicted in Figure 6.16d. In case of the AR estimate there are three minima depicted: the AR processes of order three (see Figure 6.30), five (see Figure 6.31) and ten (see Figure 6.32). These roots look similar to the roots in Figure 6.27,

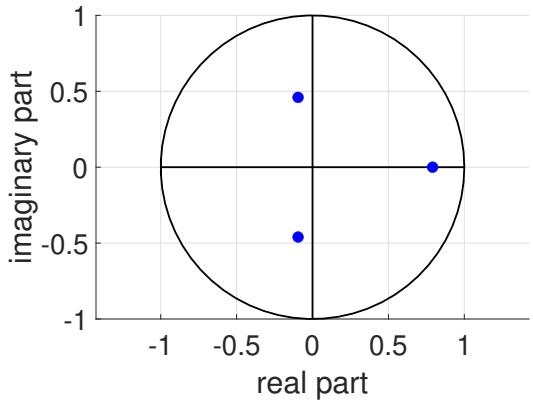

Figure 6.30: Roots of the AR(3) process of the GNSS heights of Figure 6.15d.

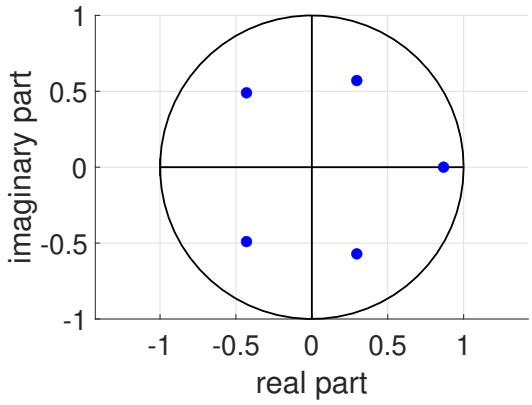

Figure 6.31: Roots of the AR(5) process of the GNSS heights of Figure 6.15d.

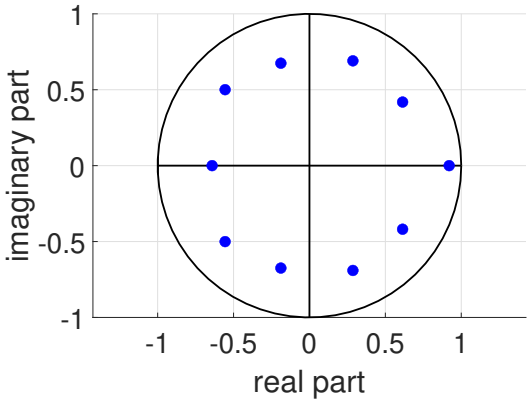

Figure 6.32: Roots of the AR(10) process of the GNSS heights in Figure 6.15d.

Figure 6.28 and Figure 6.29. Therefore the discussion of these roots is similar to the one in section 6.2.1.3. This is why further discussions of these roots should be taken from the previous example. However, in the case of the TVAR estimate there are two processes nearly equal with respect to the AIC: first the TVAR(1) process (see Figure 6.33) and second the TVAR(3) process estimated(see Figure 6.34). These root motions also show that this TVAR(1) process root movement corresponds to the real root's motion of the TVAR(3) process. This is the consequence of the fact, that the TVAR(3) process is the result of the process of first estimating the TVAR(1) process with the root of Figure 6.33, and then, estimating a TVAR(2) process whose root motion is described by the motion of the complex conjugated pair of roots of Figure 6.34. These roots are also similar to those

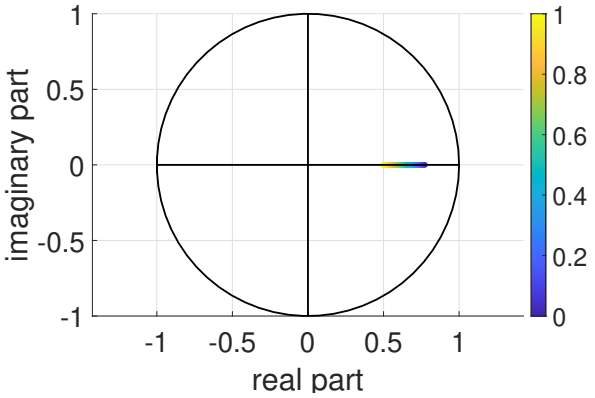

Figure 6.33: Roots of the TVAR(1) process of the GNSS heights of Figure 6.15d.

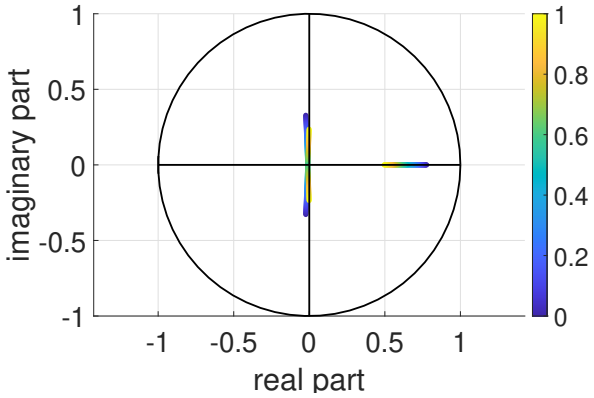

Figure 6.34: Roots of the TVAR(3) process of the GNSS heights of Figure 6.15d.

of the earlier application (see Figure 6.15c).
Much more interesting, however, is the comparison with the roots of a moving window. This window has a width of 450 observations and is applied as described in the previous sections. The AR(3) process roots shown in Figure 6.30 fit approximate these root motions, while linear root motions in Figure 6.33 and Figure 6.34 do not follow the movement of the window's roots.

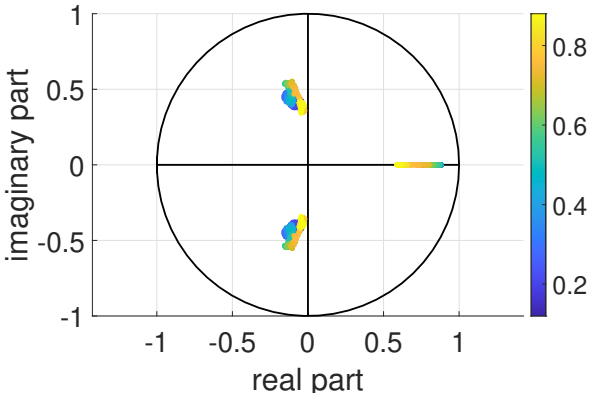

Figure 6.35: Roots of the AR(3) processes estimated for moving windows of 450 observations gliding over the GNSS series in Figure 6.15d.

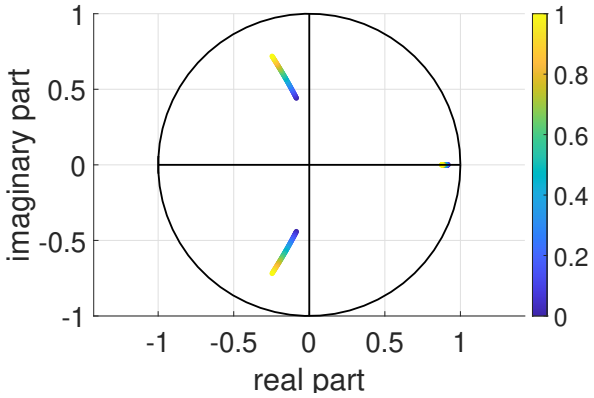

Figure 6.36: Linear roots of a direct estimate TVAR(3) process with linear root motion for the GNSS time series in Figure 6.15d.

The direct estimation of the TVAR(3) process poses the opposite. The roots of the direct estimation are shown in Figure 6.36. They, as well as their motions, fit the root approximation of the moving window of Figure 6.35. Furthermore, the complex conjugated pair of the direct estimated roots of Figure 6.36 posses approximately the same angle as the pair of complex conjugated roots of the moving window over time depicted in Figure 6.36. In particular, this means that for each fixed point in time, the spectra of the direct estimation and the ones of the moving are similar.
To prove, that, in this case, the direct TVAR(3) process estimate is the one to choose, the RMSE

is computed for all six estimations:

$$\begin{aligned}
\mathrm{RMSE}_{\mathrm{AR(3)}} &= 3.6\ [mm],\\
\mathrm{RMSE}_{\mathrm{AR(5)}} &= 3.6\ [mm],\\
\mathrm{RMSE}_{\mathrm{AR(10)}} &= 3.5\ [mm],\\
\mathrm{RMSE}_{\mathrm{TVAR(1)}} &= 3.6\ [mm],\\
\mathrm{RMSE}_{\mathrm{TVAR(3)}} &= 3.6\ [mm],\ \text{and}\\
\mathrm{RMSE}_{\mathrm{TVAR(3)direct}} &= 2.3\ [mm].
\end{aligned}$$

6.2.2 TVAR Process Estimates with Non-linear Root Motions

Sometimes it is not sufficient to describe the root motion by the means of a linear function. Therefore, this section shows how to estimate TVAR processes, in cases when the roots follow a quadratic function or when their root movements are composed of linear pieces, which ultimately serves to approximate complicated root motions. For this, two GNSS time series are used as examples. These are shown in Figure 6.37. Here, the GNSS heights of Figure 6.37a are used to estimate a TVAR process with quadratic root motions, while the TVAR process with piecewise linear root motion is estimated for the time series of GNSS heights shown in Figure 6.37b.

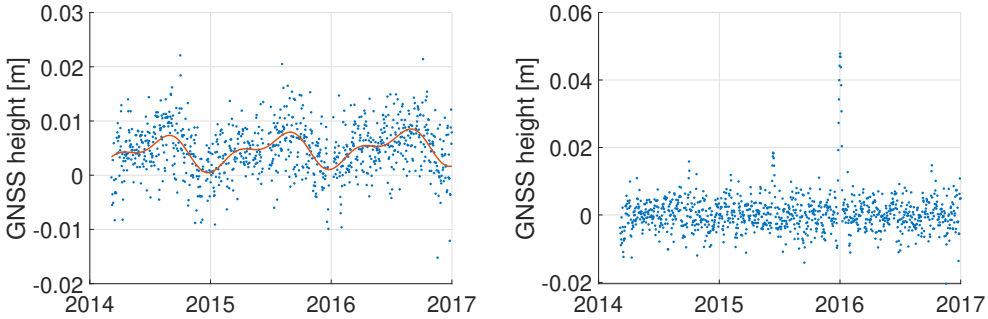

(a) ULLo00GBR in Ulapool (UK) from an early 2014 to the end of 2016.
Analysis center: Nevada Geodetic Laboratory (NGL14).

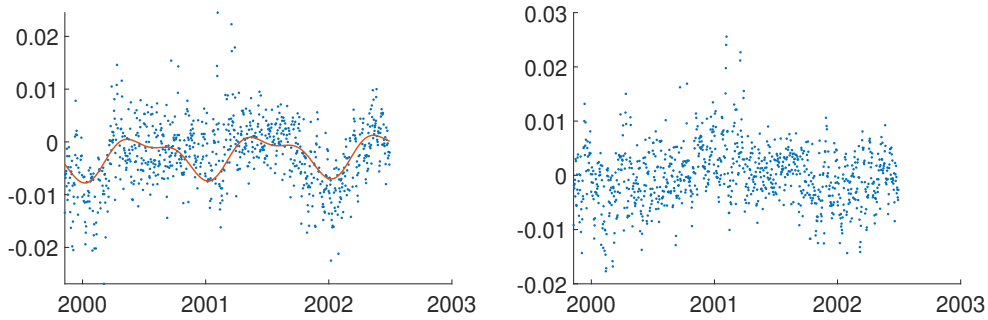

(b) HELG on Helgoland (Germany) from the end of 1999 to the end of 2002.
Analysis center: University of La Rochelle (URL6B).

Figure 6.37: Heights from GNSS stations for TVAR estimates with non-linear root motions, with the estimated trend (red), and on the right side the reduced and interpolated time series.

6.2.2.1 TVAR Process Estimates with Quadratic Root Motions

Normally, the evaluation of the application starts with a TVAR estimation and then checks if the estimated root motion fits the root motion of the moving window. However, the analysis of the time series of Figure 6.37a is structured the other way around: we first have a look of the roots of AR processes estimated for a moving window with the width of 500 observations, and then we estimate the TVAR processes.
Figure 6.38 shows, that the track of discrete roots pass first from a pair of complex conjugated roots to two real valued roots and then back again to a pair of complex conjugated roots.
The method of section 4.5.1 can be used, to estimate such complex root motion changes, as it allows to derive coefficients of the TVAR process and the necessary restrictions to estimate TVAR processes with quadratic root motion. The motion of the roots of the TVAR(2) estimation is depicted in Figure 6.39, which shows that the challenge of transferring a pair of complex conjugated roots first to two real valued roots and then back to a pair of complex conjugated roots has succeeded. So, this motion of roots can be constructed by TVAR processes with quadratic root motion.

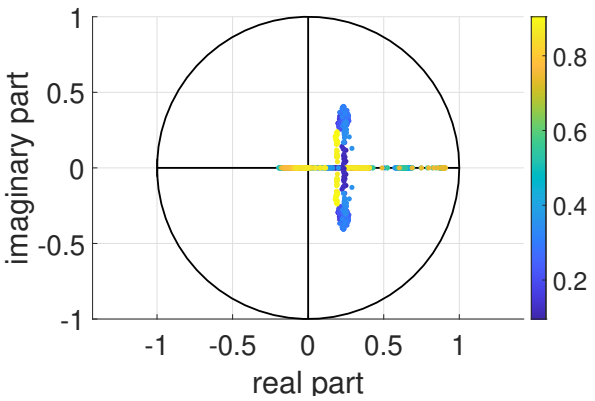

Figure 6.38: Roots of an AR(2) process estimated for moving windows of 500 observations gliding over the GNSS series of Figure 6.37a.

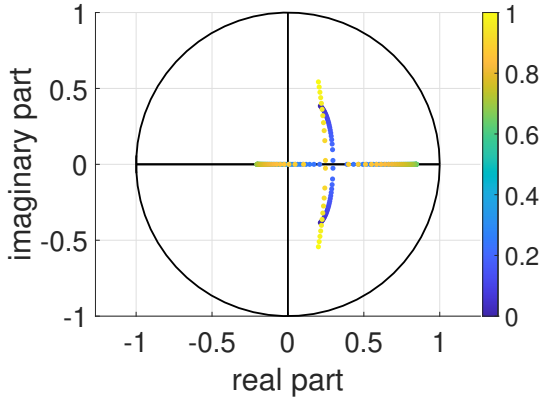

Figure 6.39: Root motion of a TVAR(2) process with quadratic roots, estimated for the GNSS time series of Figure 6.37a.

Note, that a switch from two real valued roots to a pair of complex conjugated roots is impossible for the case of TVAR estimations with linear roots. As such, it is not surprising that the TVAR(2) estimate provides two real valued roots as solution. These are shown in Figure 6.40.

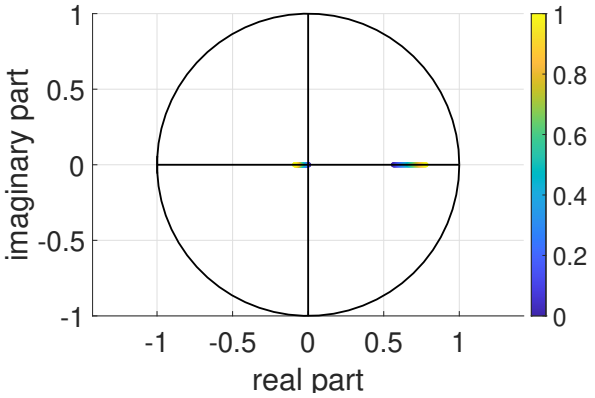

Figure 6.40: Roots of the successive TVAR(2) estimate with linear root motion for the time series from Figure 6.37a.

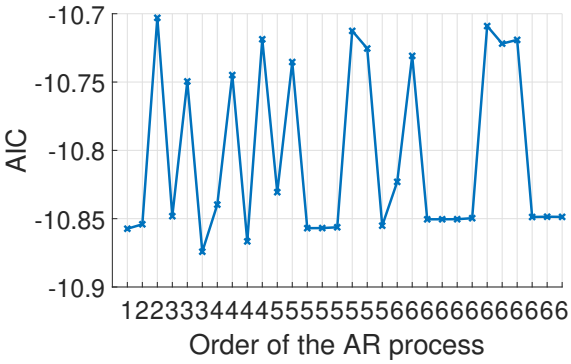

Figure 6.41: The AIC values for the TVAR process estimation wit linear root motion of the time series of GNSS heights in Figure 6.37a.

Additionally, Figure 6.41 provides a depiction of the AIC values for estimating TVAR processes. Here, it is visualized, that the AIC value is minimized by an estimation of a TVAR(3) process. This TVAR(3) process is constructed by first estimating a TVAR(1) process and then estimating a TVAR(2) process using the residuals from the first estimation as observations. The linear roots of the estimated TVAR(3) process are shown in Figure 6.43, while the corresponding roots of the moving window are shown in Figure 6.42. Comparing these two root tracks, it seems that, in this case, the TVAR(3) process with linear roots follows the roots of the moving window. This leads to the conclusion, that the choice of the root motion has a strong influence on the estimation TVAR process: it not only impacts the order, but also the movement of the roots and thus the change of the shape of the spectrum.
To compare these estimates, the RMSE is used:

$$\text{RMSE}_{\text{TVAR(3) linear roots}} = 4.31\ [mm] \text{ and}$$
$$\text{RMSE}_{\text{TVAR(2) quadratic roots}} = 4.25\ [mm].$$

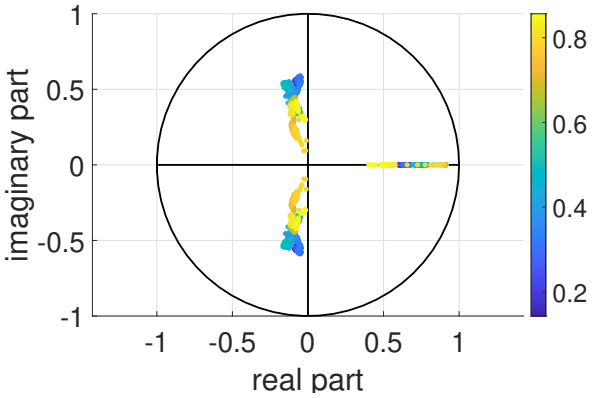

Figure 6.42: Roots of an AR(3) process estimated for moving windows of 200 observations gliding over the GNSS series in Figure 6.37a.

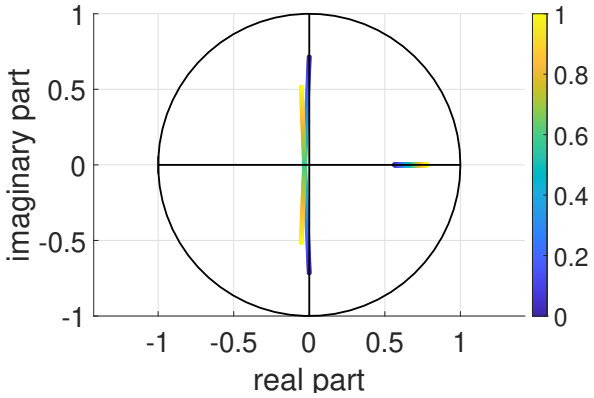

Figure 6.43: Root motions of the TVAR(3) estimate with linear root motion of the GNSS time series in Figure 6.37a.

This proves, that in this case, the TVAR process with quadratic root motion does not only approximate the roots from the moving window, but also has a smaller RMSE than the best TVAR process with linear root motion (here best means lowest value for the AIC). This solution suggests, that the restriction of TVAR processes with linear roots might not be flexible enough to compute TVAR processes in cases when a pair of complex conjugated roots transforms into two real valued roots, (or vice versa). Instead, a TVAR process is capable to achieve this.

6.2.2.2 TVAR Process Estimation with Piecewise Linear Root Motions

As soon as it is no longer enough to represent the root motion as a quadratic function, one should switch to piecewise linear root motions. To demonstrate this method, a TVAR process with linear root motion, as well as a TVAR process with piece wise linear root motions are estimated for the time series in Figure 6.37b, and the results are compared with the roots of a moving window.
We start by estimating the TVAR process with linear root motion, looking for the process that minimizes the AIC value (as it is done in application 6.2.1.1). Figure 6.44 shows, that the minimum AIC value corresponds to the TVAR(1) process. The resulting root of this process is depicted in Figure 6.45.
Then a moving window with a width of 20 observations is shifted over the time series and an AR(1) process is estimated for each window. The resulting roots are shown in Figure 6.46. Comparing the linear root movement of the TVAR(1) process (shown in Figure 6.45) with the track of the roots of the moving window (shown in Figure 6.46), one notices that there is a little movement shown in the linear approximation, while the moving windows' roots, cover the interval [-0.3,0.9]. The discrepancy between the results is due to the fact, that the track of the roots in Figure 6.46 do not change linearly. Figure 6.47 depicted this root motion according to the time. This way, the non-linear root motion is depicted.
Our goal is to remodel this track as accurately as possible, by estimating TVAR processes with piecewise linear root movements. For this piecewise estimation the intervals should all be the same width of 20 observations, which is the same size as the one of the moving window. Figure 6.47 shows how the approximation with piecewise linear roots follows the significant peaks, while strong fluctuations (as seen midway between 2001 and 2002) is filtered. This is also evident in the RMSE. When calculating these values for the estimations, using (6.1.9), the values

$$\begin{aligned} \text{RMSE}_{\text{TVAR(1) linear roots}} &= 4.27\ [mm], \\ \text{RMSE}_{\text{AR(1) moving window}} &= 4.09\ [mm] \text{ and} \\ \text{RMSE}_{\text{TVAR(1) piecewise linear root}} &= 4.11\ [mm] \end{aligned}$$

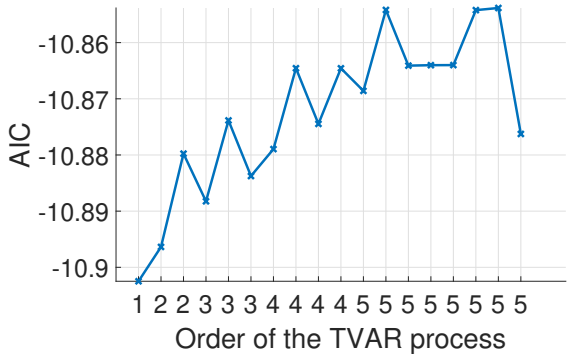

Figure 6.44: The AIC values for the TVAR process estimation wit linear root motion of the time series of GNSS heights in Figure 6.37b.

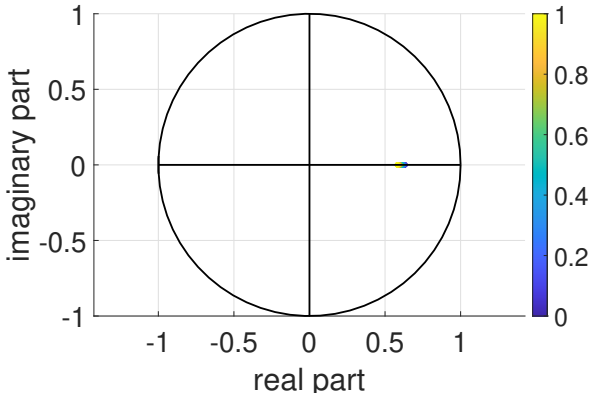

Figure 6.45: Root of a TVAR(1) process estimated of the GNSS series in Figure 6.37b.

are obtained. This concludes that complex root motions as in this example can be approximated by a piecewise linear approach.

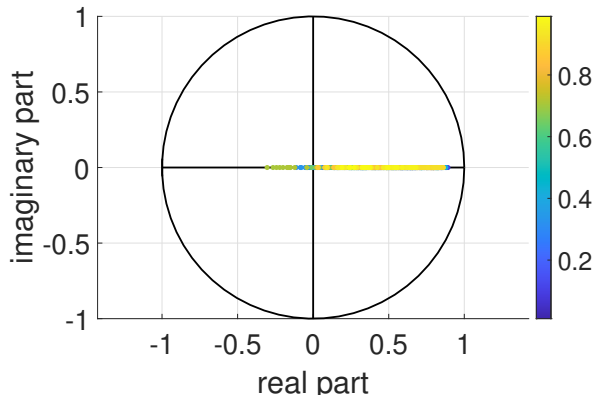

Figure 6.46: Roots of AR(1) processes estimated for moving windows of 20 observations gliding over the GNSS series in Figure 6.37b.

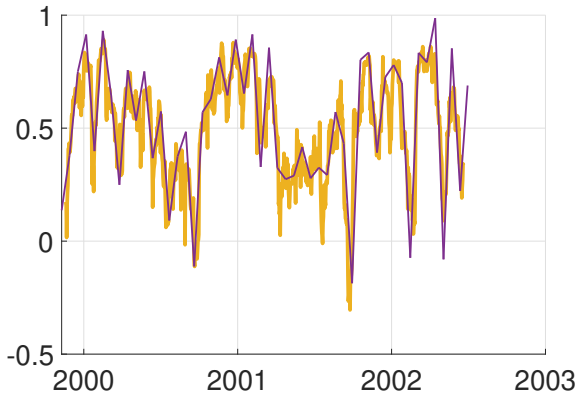

Figure 6.47: Comparison between the TVAR(1) process estimate with piecewise linear root motion (in violet) and the discrete roots of AR(1) estimates of a moving window (in orange). Both are estimated for the time series in Figure 6.37b.

6.3 Covariance Functions Derived from a Time Variable AR(1) Estimate

This section provide an investigation of global annual temperature anomalies. These time series show global annual temperature anomalies in which the man-made climate change has been eliminated.[5] Before estimating the AR(1) or TVAR(1) process, a linear trend is estimated and deducted from the data. This procedure as described in Appendix E.1.1. It will be shown, that the LSC using a CF from an AR process do not provide an adequate solution. Instead the CF must be provided by a TVAR process.

6.3.1 AR(1) Process with a Root near the Origin

If a AR(1) processes' root is near the origin, the recursive part is approximately zero. In this case, a large part of the signal is interpreted as noise, which in turn makes the result of the LSC nearly useless. To avoid this problem, TVAR(1) processes can be used for covariance modelling in LSC.

6.3.1.1 Data

A time series of global annual temperature anomalies from 1904 to 2014 is used to illustrate LSC using a TVAR(1) process. Before the AR estimation is calculated, this data is reduced by a linear trend as shown in Appendix E.1. This way, the mean value of the time series is reduced to $M\{E\{\boldsymbol{\mathcal{S}}\}\} = -1.2 \cdot 10^{-17} \approx 0$. The trend reduced time series shown in Figure 6.48.

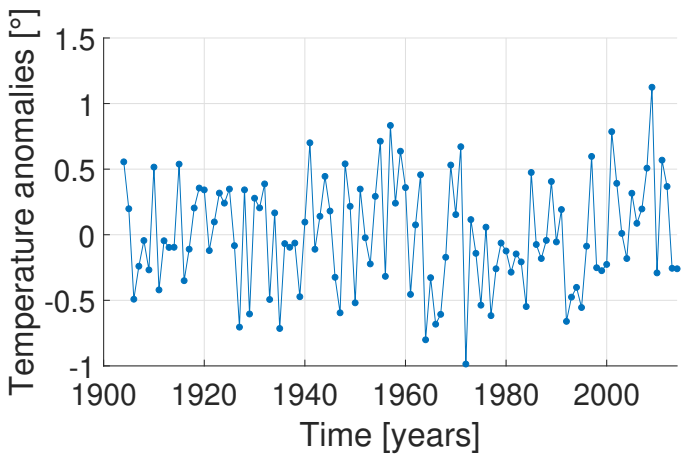

Figure 6.48: Annual temperature anomalies for the years 1904 to 2014 reduced by a linear trend.

6.3.1.2 Least-Squares Collocation using AR Estimation

The method of applying LSC using an AR process for covariance estimation is identical to the application of section 6.1. Due to this fact, the procedure will not be described in detail here again. The AR coefficients and the noise's variance are estimated by the Y.-W. equations. The AICs shown in Figure 6.49 provides the lowest value for an AR(1) process with the variance $\tilde{\sigma}^2_{\mathcal{E}} = 0.1690[^{\circ 2}]$ and the coefficient $\tilde{\alpha}_1 = 0.0028$. Since the AR(1) process' root corresponds to the coefficient, $P_1 = 0.0028$ can be determined directly. It is visualized in the unit circle in Figure 6.50. As discussed in section 6.1.3.2, the estimated variance $\sigma^2_{\mathcal{E}}$ is again divided into the variance of the AR process $\sigma^2_{\mathcal{S}}$ and the variance of the noise $\sigma^2_{\mathcal{N}}$:

$$\sigma^2_{\mathcal{S}} = 0.0640[^{\circ 2}] \qquad \sigma^2_{\mathcal{N}} = 0.1050[^{\circ 2}] \tag{6.3.1}$$

5. The data is available as an open source and can be downloaded from the website: https://esgf-data.dkrz.de/projects/esgf-dkrz/. The data itself was processed by different teams, how exactly this processing took place is described in the paper Eyring et al. 2016.

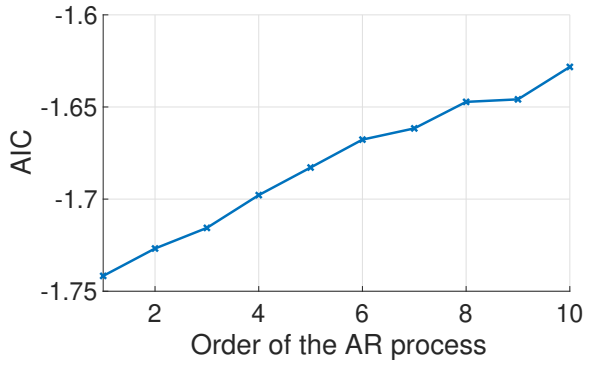

Figure 6.49: The AIC values for the AR estimate of the annual temperature anomalies of Figure 6.48 for order one to ten (with a minimum at one).

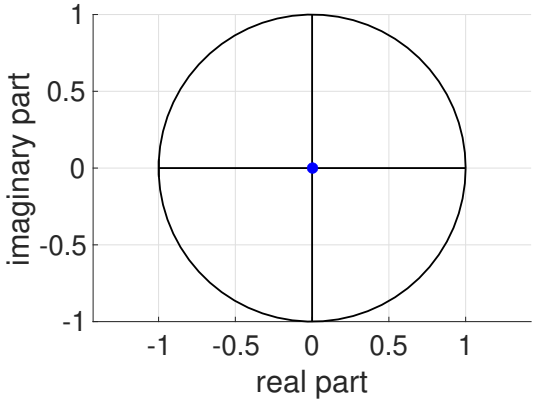

Figure 6.50: Roots of the AR(1) process estimated for the temperature anomalies of Figure 6.48.

Separating the variances, allows to determine the CF of the AR process. In the case of the AR(1) process, the only weight A_1 equals the variance (see Buttkus 2000, p. 247 eq. 11.30), i.e.

$$A_1 = \Sigma_0 = \frac{\sigma_{\mathcal{S}}^2}{1-\alpha_1^2} = 0.0640.$$

The CF can be determined by the means of

$$\gamma(h) = A_1 P_1^{|h|} = 0.0640 \cdot 0.0028^{|h|}. \tag{6.3.2}$$

Furthermore, the CF can be used to compute the entries of the covariance matrices for LSC (see section 2.2). The noise's covariance matrix (6.1.8) results directly from the noise's variance itself:

$$\Sigma\{\boldsymbol{\mathcal{N}}\} = \sigma_{\mathcal{N}}^2 \mathbb{1}_{n\times n} = 0.0640 \cdot \mathbb{1}_{n\times n}.$$

The covariance matrix of the signal is calculated in accordance to the CF of (6.3.2) and evaluated using integer distances ($h \in \{0, 1, 2, ..., n-1\}$):

$$\Sigma\{\boldsymbol{\mathcal{S}}\} = \begin{bmatrix} \gamma(0) & \gamma(1) & \gamma(2) & ... & \gamma(n-1) \\ \gamma(1) & \gamma(0) & \gamma(2) & ... & \gamma(n-2) \\ \gamma(2) & \gamma(1) & \gamma(0) & ... & \gamma(n-3) \\ ... & & & & \\ \gamma(n-1) & \gamma(n-2) & \gamma(n-3) & ... & \gamma(0) \end{bmatrix}_{n\times n}. \tag{6.3.3}$$

In addition the common covariance matrix is created. This includes 18 additional predicted values between the observations, computed by the means of the CF evaluated for the distances $h\{0, 1/19, 2/19, ..., n-1\}$:

$$\Sigma\{\widetilde{\boldsymbol{\mathcal{S}}}, \boldsymbol{\mathcal{S}}\} = \begin{bmatrix} \gamma(0) & \gamma(1) & \gamma(2) & ... & \gamma(n-1) \\ \gamma\left(\frac{1}{19}\right) & \gamma\left(1\frac{1}{19}\right) & \gamma\left(2\frac{1}{19}\right) & ... & \gamma\left(n-1-\frac{1}{19}\right) \\ \gamma\left(\frac{2}{19}\right) & \gamma\left(1\frac{2}{19}\right) & \gamma\left(2\frac{2}{19}\right) & ... & \gamma\left(n-1-\frac{2}{19}\right) \\ & & & & \\ ... & & & & \\ & & & & \\ \gamma(n-1) & \gamma(n-2) & \gamma(n-3) & ... & \gamma(0) \end{bmatrix}_{20n-19\times n}. \tag{6.3.4}$$

The result of LSC is depicted in Figure 6.51, which shows that the approximated signal does not significantly differ from zero. The reason for that is, there is only one coefficient that is close to zero. For this reason, most of the variance of the Y.-W. equations ($\sigma_{\mathcal{E}}^2$) is described by the variance of noise ($\sigma_{\mathcal{N}}^2$) rather than by the variance of the AR(1) process ($\sigma_{\mathcal{S}}^2$).

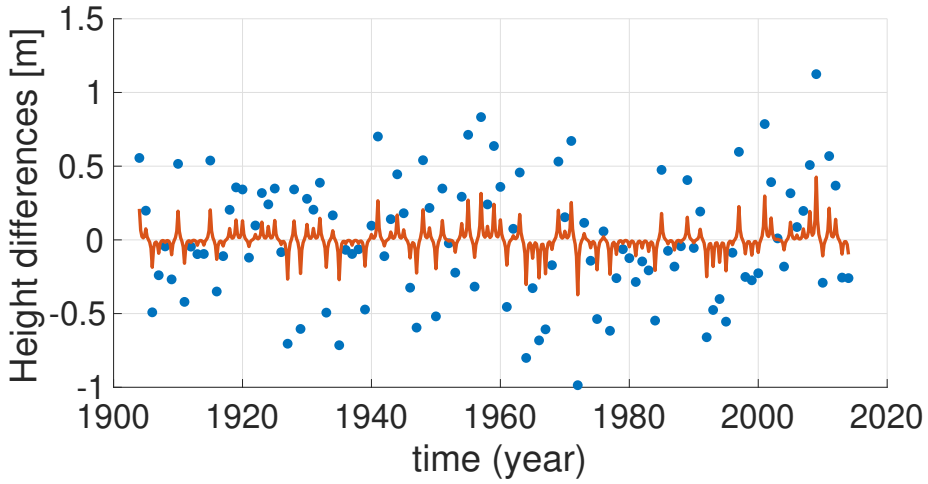

Figure 6.51: Annual temperature anomalies between the years 1904 and 2014 and the approximation by least-squares collocation using a CF of a AR(1) process.

6.3.1.3 Approximation of the Root Motion by a Moving Window

To check whether the process of Figure 6.48 is stationary, an AR(1) process is estimated for a moving window with a width of 22 observations, then the AR roots are plotted, whereby the time of the root is equal to the time in the moving window's centre. These roots are depicted in Figure 6.52. It seems that the roots move linearly, which is suspicious in such a way, that the moving window roots of a stationary process should be constantly the AR(1) coefficient. So the assumption, that the observations generate a stationary process, is not correct. The evaluation of this time series by the method of LSC demands an estimation by using a TVAR(1) processes.

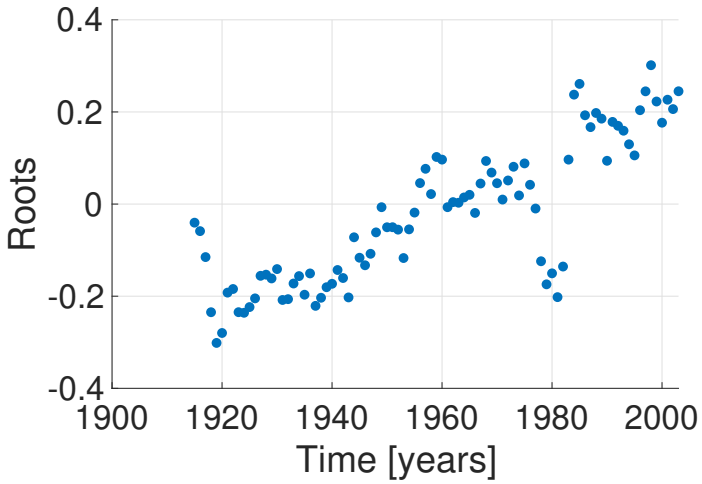

Figure 6.52: Roots of the AR(1) estimate using a moving window of 22 observations. Figure 6.48 provides the time series of temperature anomalies used for the estimation.

6.3.1.4 Least-Squares Collocation using a TVAR(1) Estimate

For the time series of Figure 6.48, a TVAR(1) process with linear root motion is estimated directly from the signal $\mathcal{S}$ (as described in Appendix C.2), while the matrices corresponding to the TVAR(1)

process as discussed in Appendix C.4. This leads to the parameter estimates

$$\overline{\beta_0^{(1)}} = -0.2394 \qquad \text{and} \qquad \overline{\beta_1^{(1)}} = 0.4434,$$

which describe the TVAR(1) coefficient. And, as for the AR(1) process, this coefficient corresponds to the time variable root of the CP shown in Figure 6.53:

$$P_1(t) = \alpha_1(t) = \overline{\beta_0^{(1)}} + \overline{\beta_0^{(1)}} \frac{t - t_0}{t_{\text{end}} - t_0} = -0.2394 + 0.4434 \frac{t - 1904}{110} \text{ with } t \in [1904, 2014].$$

Here, $t_0 = 1904$ is the start of the time series, and $t_{\text{end}} = 2014$ is the last year of the observed signal. For this example, the time variable coefficient $\alpha_1(t)$ can be used to estimate the variance of

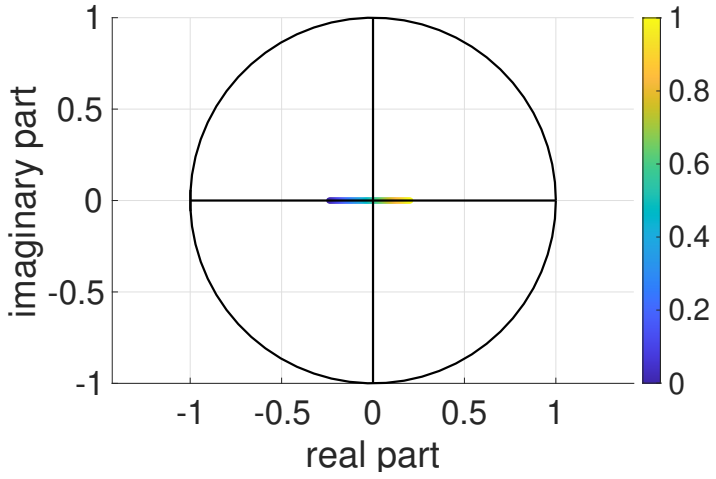

Figure 6.53: The roots for the TVAR(1) estimate of the annual temperature anomalies from Figure 6.48 for the continuous time $t_c \in [0, 1]$.

the process $\sigma_{\mathcal{E}}^2$ (as already show in section 4.1.3.2), providing

$$\sigma_{\mathcal{E}}^2 = 0.1682[^{\circ 2}]$$

In order to separate $\sigma_{\mathcal{E}}^2$ by variance component estimation into the variance of the TVAR(1) process $\sigma_{\mathcal{S}}^2$ and the variance of the noise $\sigma_{\mathcal{N}}^2$, decorrelation as shown in Förstner 1985 is used. Unfortunately, this method is only defined for time constant AR processes. However, it can be adapted to TVAR processes. Since this method uses the AR coefficients to decorrelate the observations, this can be done by the TVAR coefficient as well, results in the variances of the TVAR(1) process $\sigma_{\mathcal{S}}^2$ and the variance of the noise $\sigma_{\mathcal{N}}^2$, which in turn are the last parameters needed to calculate the CF:

$$\sigma_{\mathcal{S}}^2 = 0.1394[^{\circ 2}] \qquad \sigma_{\mathcal{N}}^2 = 0.0288[^{\circ 2}]. \tag{6.3.5}$$

Since $\overline{\beta_0^{(1)}} = -0.2394 < 0$, $\overline{\beta_1^{(1)}} = 0.4434 > 0$ and $\overline{\beta_0^{(1)}} + \overline{\beta_1^{(1)}} = 0.2039 > 0$, case three of section 5.3.2 applies, resulting in the CF

$$\begin{aligned}\gamma^{(3)}(h,t_c) =& \gamma(0,t_c)\left(\frac{|\overline{\beta_1^{(1)}}|}{(n-1)}\right)^{h(n-1)} \quad ... \\ & \begin{cases} \mathbb{P}\left(\left|f(\overline{\beta_0^{(1)}},\overline{\beta_1^{(1)}},t_c,h)\right|, h(n-1)\right) & \text{if } f(\overline{\beta_0^{(1)}},\overline{\beta_1^{(1)}},t_c,h) < 0 \\ \mathbb{P}\left(f(\overline{\beta_0^{(1)}},\overline{\beta_1^{(1)}},t_c,h), h(n-1)\right)\cos(h(n-1)\pi) & \text{else.} \end{cases} \\ =& \gamma(0,t_c)\left(\frac{0.4434}{110}\right)^{110h} \quad ... \\ & \begin{cases} \mathbb{P}\left(|f(-0.2394,0.4434,t_c,h)|, 110h\right) & \text{if } f(-0.2394,0.4434,t_c,h) < 0 \\ \mathbb{P}\left(f(-0.2394,0.4434,t_c,h), 110h\right)\cos(110h\pi) & \text{else.} \end{cases}\end{aligned} \tag{6.3.6}$$

Here, $n = 111$ is the length of the signal, and $\gamma(0,t_c)$ comprises the time variable variances which are computed by (5.3.1) for the times of the observed signal ($t_c \in [0,1]$)

$$\gamma(0,t_c) = \frac{\sigma_{\mathcal{S}}^2}{1-\alpha_1^2(t_c)} = \frac{0.1394}{1-(-0.2394+0.4434t_c)^2}.$$

Figure 6.54 illustrates how the variance decreases as long as the absolute value of the time variable

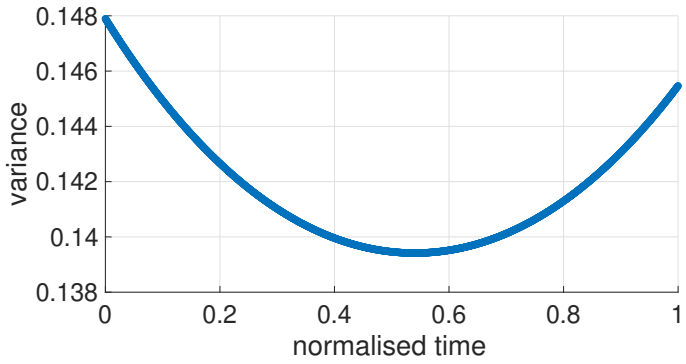

Figure 6.54: Variability in time of the variance for the TVAR(1) process with linear root motion, estimated for to the time series of Figure 6.48. The variance is evaluated by using the normalized time $[0,1]$.

coefficient $\alpha_1(t)$ decreases. Since the variances increases if the absolute value of the coefficient $\alpha_1(t)$ increases, leading to the minimum of $0.1394[^{\circ 2}]$ occurs exactly at the point in time when the TVAR(1) coefficient equals zero. Notice, the variance of the TVAR(1) process in this moment is equal to $\sigma_{\mathcal{S}}^2$. The time variable variance and the time CF allow to set up the LSC matrices. It results in the covariance matrix of the signal for the observed epoch

$$\Sigma\{\boldsymbol{\mathcal{S}}\} = \begin{bmatrix} \gamma(0,0) & \gamma(1,0) & \gamma(2,0) & ... & \gamma(n-1,0) \\ \gamma\left(1,\frac{1}{n-1}\right) & \gamma\left(0,\frac{1}{n-1}\right) & \gamma\left(1,\frac{1}{n-1}\right) & ... & \gamma\left(n-2,\frac{1}{n-1}\right) \\ \gamma\left(2,\frac{2}{n-1}\right) & \gamma\left(1,\frac{2}{n-1}\right) & \gamma\left(0,\frac{2}{n-1}\right) & ... & \gamma\left(n-3,\frac{2}{n-1}\right) \\ ... & & & & \\ \gamma(n-1,1) & \gamma(n-2,1) & \gamma(n-3,1) & ... & \gamma(0,1) \end{bmatrix}_{n\times n}, \tag{6.3.7}$$

and the covariance matrix of the noise

$$\Sigma\{\boldsymbol{\mathcal{N}}\} = \sigma_{\mathcal{N}}^2 \mathbb{1}_{n\times n} = 0.0288 \cdot \mathbb{1}_{n\times n}.$$

The joint covariance matrix of the time series and the predicted values is

$$\Sigma\{\tilde{\boldsymbol{\mathcal{S}}}, \boldsymbol{\mathcal{S}}\} = \begin{bmatrix} \gamma(0,0) & \gamma(1,0) & \gamma(2,0) & \dots & \gamma(n-1,0) \\ \gamma\left(\frac{1}{19}, \frac{1}{19(n-1)}\right) & \gamma\left(1\frac{1}{19}, \frac{1}{19(n-1)}\right) & \gamma\left(2\frac{1}{19}, \frac{1}{19(n-1)}\right) & \dots & \gamma\left(n-1-\frac{1}{19}, \frac{1}{19(n-1)}\right) \\ \gamma\left(\frac{2}{19}, \frac{2}{19(n-1)}\right) & \gamma\left(1\frac{2}{19}, \frac{2}{19(n-1)}\right) & \gamma\left(2\frac{2}{19}, \frac{2}{19(n-1)}\right) & \dots & \gamma\left(n-1-\frac{2}{19}, \frac{2}{19(n-1)}\right) \\ & \dots & & & \\ \gamma(n-1,1) & \gamma(n-2,1) & \gamma(n-3,1) & \dots & \gamma(0,1) \end{bmatrix}_{20n-19\times n} . \tag{6.3.8}$$

Since it has not yet been proven that the covariance function of (6.3.6) is positive definite, it must still be checked whether all eigenvalues of $\Sigma\{\boldsymbol{\mathcal{S}}\}$ are positive or not. The eigenvalues are determined by the means of the eigenvalue decomposition; since the smallest eigenvalue is $\lambda_{\min} = 0.0947 > 0$, it follows, that the matrix is positive definite. This ultimately allows the LSC. The resulting approximated time series is shown in Figure 6.55.

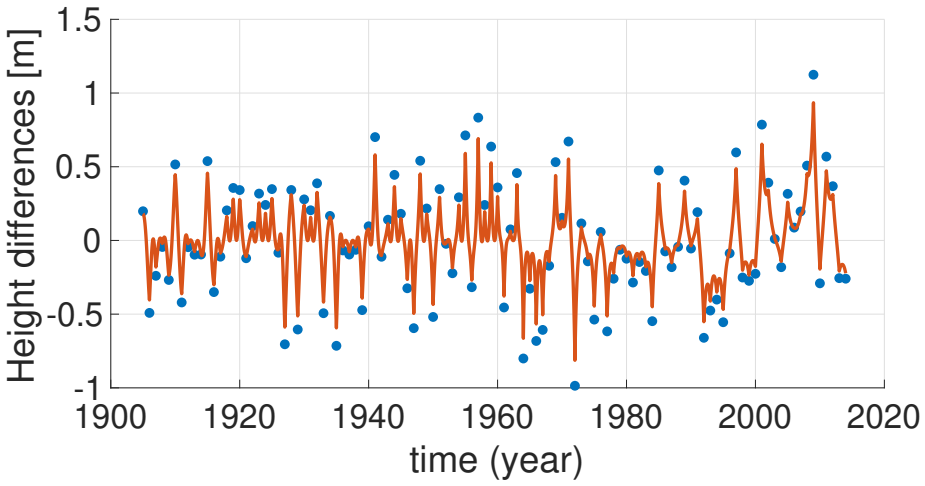

Figure 6.55: Annual temperature anomalies between the years 1904 and 2014 and the approximation by LSC using a CF of a TVAR(1) process.

6.3.1.5 Comparing both Least-Squares Collocation Solutions

When comparing the two solutions, it becomes apparent that the estimated variances $\sigma^2_{\hat{\varepsilon}}$ are of similar values. The same can be observed when the RMSE is calculated by (6.1.9). Hereby either the residuals are computed by

$$\mathcal{S}_j - \tilde{\mathcal{S}}_j = \mathcal{S}_j - \sum_{k=1}^{p} \alpha_k \mathcal{S}_{j-k}$$

in the case of the time stable AR process is used, or

$$\mathcal{S}_j - \tilde{\mathcal{S}}_j = \mathcal{S}_j - \sum_{k=1}^{p} \alpha_k(j) \mathcal{S}_{j-k}$$

in the case of TVAR processes. In both cases the RMSE values

$$\text{RMSE}_{\text{AR}} = 0.4096\ [^\circ] \qquad \text{RMSE}_{\text{TVAR}} = 0.4064\ [^\circ].$$

are nearly equal, but since the variance $\sigma_{\mathcal{E}}^2$ is composed of the variance of the AR or TVAR process and the variance of the white noise:

$$\sigma_{\mathcal{E}}^2 = \sigma_{\mathcal{S}}^2 + \sigma_{\mathcal{N}}^2,$$

the variance component estimation shows, that in case of the AR estimation

$$\sigma_{\mathcal{S}}^2 = 0.0640[^{\circ 2}] \qquad \text{and} \qquad \sigma_{\mathcal{N}}^2 = 0.1050[^{\circ 2}],$$

meaning that the variance of the signal accounts for only one-third of the total variance. In case of the TVAR estimation the variance components are estimated to

$$\sigma_{\mathcal{S}}^2 = 0.1394[^{\circ 2}] \qquad \text{and} \qquad \sigma_{\mathcal{N}}^2 = 0.0288[^{\circ 2}].$$

Since the LSC only reduce the part of the white noise, this means, that in case of the AR process the large part of the variance $\sigma_{\mathcal{E}}^2$ is eliminated by the LSC, while in case of the TVAR process the large part of the variance $\sigma_{\mathcal{E}}^2$ is modelled by the TVAR(1) process. This is also depicted in Figure 6.51, where the predicted values do not reproduce the observations. The solution of the LSC using TVAR processes is depicted in Figure 6.55, showing a function following the observations.

6.3.2 Modelling of Significant Characteristic Changes

Another problem that can occur when estimating an AR process is a change in the processes characteristics. This means, that the CF changes from a decreasing pure positive valued function to an oscillating function (or vice versa) (compare Figure 5.5).
While the coefficient of an AR process can only assume negative or positive values, the coefficient of a TVAR(1) process can change its sign. This sign change also changes the processes characteristic: an AR(1) process with negative coefficients mostly changes its sign from one observation to the other, while an AR(1) process with positive coefficients mostly retains the signs from one observation to the other. Figure 6.56 shows a time series changing this characteristic over time. The following examination determines how this can be modelled and adjusted by LSC with TVAR(1) processes.

6.3.2.1 Data

To illustrate how LSC performs with a signal with changing characteristics, a time series of annual temperature anomalies is used again, but this time the observations are taken from the interval 1899 to 2014. This data is reduced by a linear trend exactly as described in Appendix E.1, which reduced the mean value of the time series to $M\{E\{\boldsymbol{\mathcal{S}}\}\} = -1.7 \cdot 10^{-17} \approx 0$. The reduced time series is shown in Figure 6.56. This seems to be the same data as the one in the last example in section 6.3.1, but this time series of temperature anomalies was computed by another model and with different starting conditions.

6.3.2.2 Least-Squares Collocation using an AR Estimate

The estimation of the AR coefficients and the corresponding variance of the process $\sigma_{\mathcal{E}}^2$ is determined by the Y.-W. equations of orders one to ten and then compared with each other according to the AIC. Figure 6.58 visualizes these AIC values and shows, that the AR(1) with

$$\alpha_1 = 0.0443 \qquad \text{and} \qquad \sigma_{\mathcal{E}}^2 = 0.1974[^{\circ 2}]$$

is the minimum. The root of the AR(1) process

$$P_1 = \alpha_1 = 0.0443,$$

is very close to zero again, but this time, the variance component estimation states that

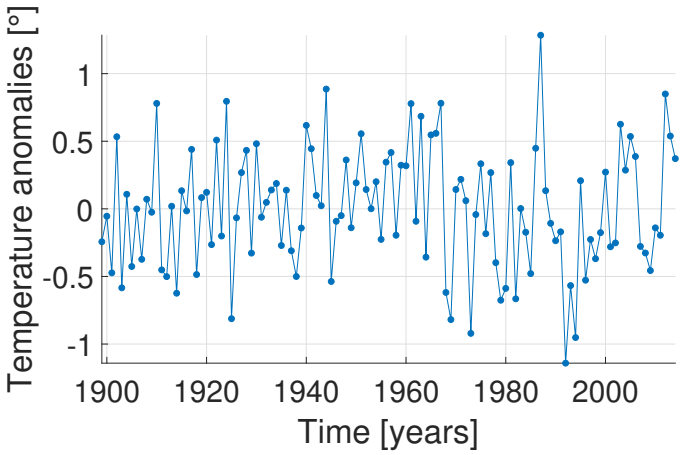

Figure 6.56: Annual temperature anomalies between the years 1899 and 2014, reduced by a linear trend.

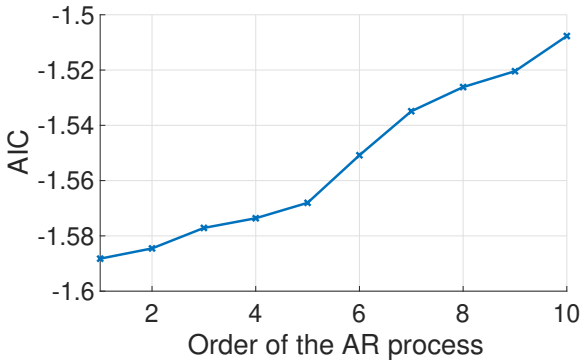

Figure 6.57: The AIC values for the AR estimate of the annual temperature anomalies of Figure 6.56 for order one to order ten (with a minimum at one).

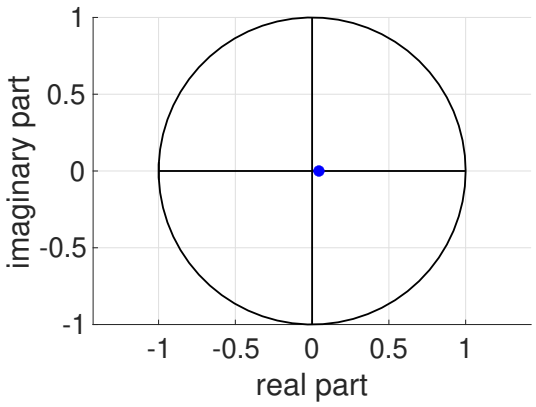

Figure 6.58: Roots of the AR(1) process estimated for the temperature anomalies of Figure 6.56.

$$\sigma_{\mathcal{S}}^2 = 0.1654[^{\circ 2}] \qquad \text{and} \qquad \sigma_{\mathcal{N}}^2 = 0.0320[^{\circ 2}],$$

meaning that, in this case, the variance of the AR process $\sigma_{\mathcal{S}}^2$ embodies the main contribution to the variance of the signal $\sigma_{\mathcal{E}}^2$.
This was the reason behind the discussion of changing to TVAR(1) processes in the previous example of 6.3.1. The weight follows from (B.1.3) in Appendix B.1:

$$A_1 = \sigma_{\mathcal{S}}^2/(1-\alpha^2) = 0.1657.$$

The CF is then

$$\gamma(h) = A_1 P_1^{|h|} = 0.1657 \cdot 0.0443^{|h|}. \tag{6.3.9}$$

The required covariance matrices are calculated the same way as in example 6.3.1. Thus, $\Sigma\{\boldsymbol{\mathcal{S}}\}$ equals (6.3.3), and $\Sigma\{\widetilde{\boldsymbol{\mathcal{S}}}, \boldsymbol{\mathcal{S}}\}$ equals (6.3.4), the only difference being that in this case, the CF of (6.3.9) is used. Further more the white noise covariance matrix change to

$$\Sigma\{\boldsymbol{\mathcal{N}}\} = \sigma_{\mathcal{N}}^2 \mathbb{1}_{n\times n} = 0.0320 \cdot \mathbb{1}_{n\times n}.$$

The approximation is again computed by the LSC of (6.1.1) again – Figure 6.59 show the results. As mentioned before, in this case, $\sigma_{\mathcal{S}}^2 = 0.1653[^{\circ 2}]$ is much higher than the variance of the noise $\sigma_{\mathcal{N}}^2 = 0.0640[^{\circ 2}]$ in application 6.3.1. As such, the predicted values of Figure 6.59 are much closer to the observations than the prediction of Figure 6.51.

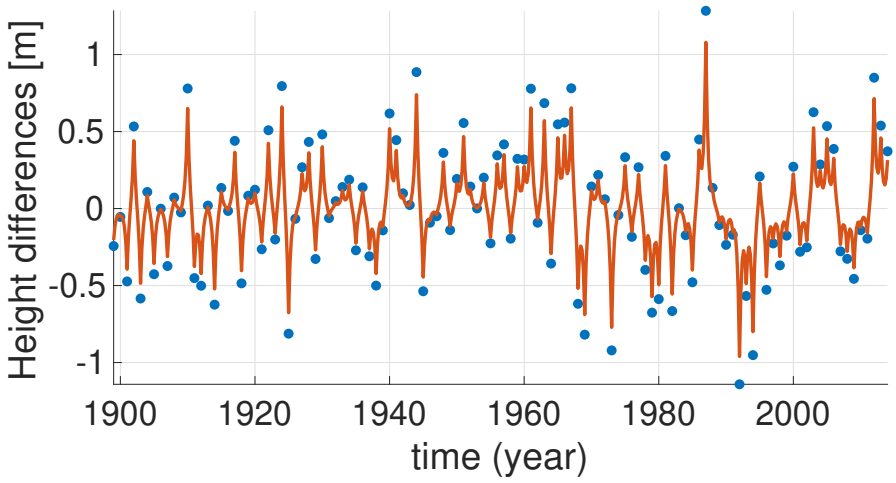

Figure 6.59: Annual temperature anomalies between the years 1899 and 2014 and the approximation by LSC using a CF of a AR(1) process.

6.3.2.3 Approximation of the Root Motion by a Moving Window

In this section, it is illustrated that the TVAR(1) process describes the process shown in Figure 6.56 better than the AR process. Following the concept introduced in section 2.5, this means that the time series is not stationary. For validation of the non-stationarity AR processes are estimated using 23 observations in a moving window. The resulting roots are shown in Figure 6.60. revealing a linear root motion.

6.3.2.4 Least-Squares Collocation using TVAR(1) Estimation

A time variable approach is chosen in which the root of the TVAR(1) process moves linearly, to approximate the roots of Figure 6.60. The procedure is the same as shown in section 6.3.1.4, providing the estimated coefficients

$$\overline{\beta_0^{(1)}} = -0.5423 \qquad \text{and} \qquad \overline{\beta_1^{(1)}} = 1.0486,$$

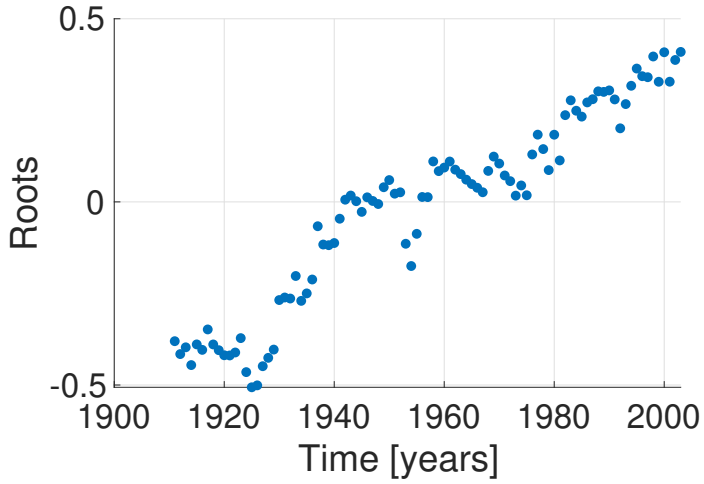

Figure 6.60: Roots for the AR(1) estimate of a moving window of 23 observed temperature anomalies of Figure 6.56.

which are equal to the root motion shown in Figure 6.61. The estimated noise $\sigma^2_{\mathcal{E}}$ is separated into the variance of TVAR process $\sigma^2_{\mathcal{S}}$ and the part of the noise $\sigma^2_{\mathcal{N}}$:

$$\sigma^2_{\mathcal{E}} = 0.1843[^{\circ 2}], \quad \sigma^2_{\mathcal{S}} = 0.1843[^{\circ 2}] \quad \text{and} \quad \sigma^2_{\mathcal{N}} = 5 \cdot 10^{-5}[^{\circ 2}],$$

revealing, that the variance of the noise is nearly zero. However, since

$$\overline{\beta_0^{(1)}} = -0.5423 < 0, \quad \overline{\beta_1^{(1)}} = 1.0486 > 0 \quad \text{and} \quad \overline{\beta_0^{(1)}} + \overline{\beta_1^{(1)}} = 0.5063 > 0.$$

the CF is calculated using the third case from section 5.3.2 again.The CF of the time series of $n = 116$ observations is given as

$$\gamma^{(3)}(h, t_c) = \gamma(0, t_c) \left(\frac{1.0486}{115} \right)^{115h} \cdots \begin{cases} \mathbb{P}\left(\left| f(-0.5423, 1.0486, t_c, h) \right|, 115h \right) & \text{if } f(-0.5423, 1.0486, t_c, h) < 0 \\ \mathbb{P}\left(f(-0.5423, 1.0486, t_c, h), 115h \right) \cos(115h\pi) & \text{else,} \end{cases} . \tag{6.3.10}$$

including the time variable variances of (5.3.1):

$$\gamma(0, t_c) = \frac{\sigma^2_{\mathcal{E}}}{1 - \alpha_1^2(t_c)} = \frac{0.1843}{1 - (-0.5423 + 1.0486 t_c)}$$

with $t_c \in [0, 1]$. These are also depicted in Figure 6.62.
To perform a LSC based on (6.1.1), the covariance matrices are determined. $\Sigma\{\boldsymbol{\mathcal{S}}\}$ is determined exactly as in (6.3.7), providing the smallest eigenvalue by $\lambda_{\min} = 0.0832$. Thus, $\Sigma\{\boldsymbol{\mathcal{S}}\}$ is positive definite. While $\Sigma\{\widetilde{\boldsymbol{\mathcal{S}}}, \boldsymbol{\mathcal{S}}\}$ is set up using (6.3.8), by evaluating the CF of (6.3.10). The noise's covariance matrix is provided by:

$$\Sigma\{\boldsymbol{\mathcal{N}}\} = \sigma^2_{\mathcal{N}} \mathbb{1}_{n \times n} = 5 \cdot 10^{-5} \cdot \mathbb{1}_{n \times n}.$$

The predicted values of the LSC are visualized as a function in Figure 6.63.

6.3.2.5 Comparison

In contrast to application 6.3.1, the reason for the successful application of LSC with a TVAR(1) process in this example lies in the ability to switch from negative valued roots to positive valued

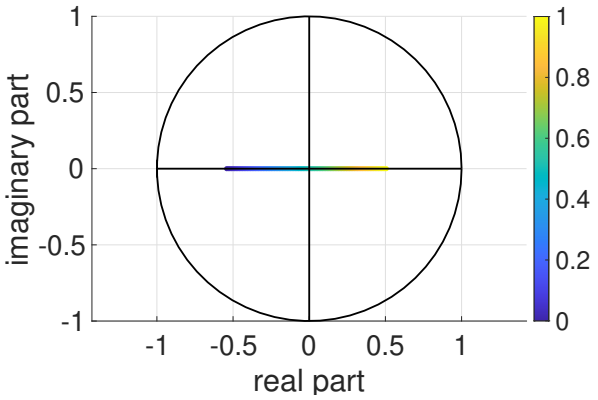

Figure 6.61: Roots for the TVAR(1) estimate of the temperature anomalies of Figure 6.48.

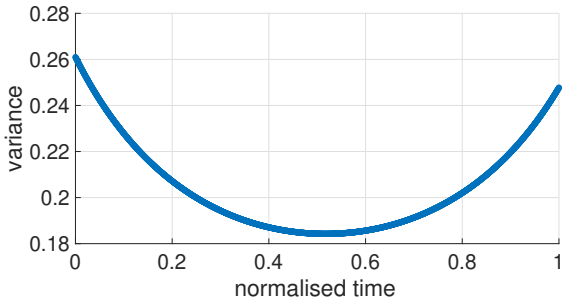

Figure 6.62: Variability in time of the variance for the TVAR(1) process with linear root motion, estimated for to the time series of Figure 6.56. The variance is evaluated by using the normalized time $[0, 1]$.

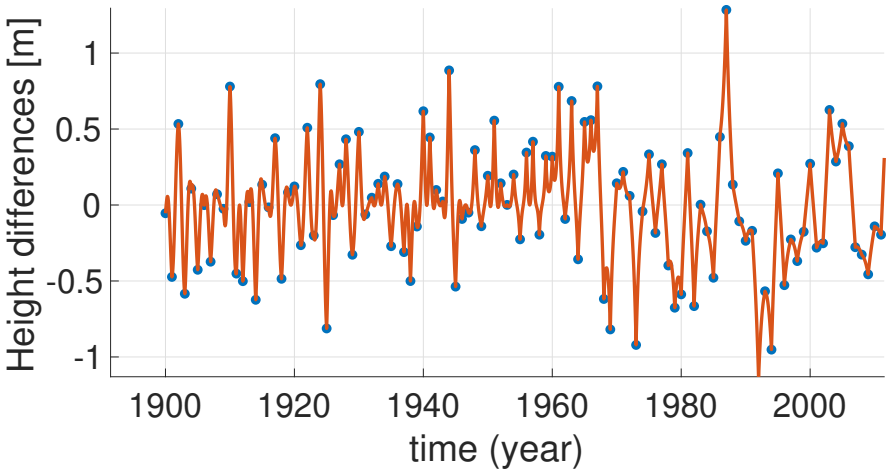

Figure 6.63: Annual temperature anomalies between the years of 1904 and 2014 and the approximation by LSC using a CF of a TVAR(1) process.

ones and the resulting change of the CF. While negative roots result in strongly oscillating signals, a positive root result in a slowly oscillating signal. In our case, slowly oscillating means that consecutive observations more likely have the same sign, wile strong oscillations means sign change in nearly every consecutive observation. This advantage of the LSC using TVAR processes becomes clear when comparing the solutions for the LSC with an AR process depicted in Figure 6.59 with the solutions for the LSC with a TVAR process depicted in Figure 6.63: while the predicted values from the AR approach in Figure 6.59 rapidly approaching zero in between the observations, the TVAR approach shown in Figure 6.63 shows that the predicted values does not only fit better to the given time series but also gives a smooth function in between the observations.

Chapter 7

Concluding Remarks

This chapter is divided into three sections: the first part provides a summary of the results of the previous chapters; the second part describes how far this work's objectives have been achieved; and the third part consists of the conclusions as well as further research.

7.1 Summary

Chapter 3: Continuous Covariance Functions for Time Constant AR Processes
In LSC, CFs are required to weights among observations. Since not every function fulfil the conditions of a CF, much of the work of LSC consists of finding suitable CFs. This chapter presented a method to automate the construction of CFs. It is called 'automatic', because -apart from the parameters of an AR process- no other estimated values are used. After the AR process with the lowest AIC is estimated, the sequence of covariances is adapted according to a continuous function by the use of the Y.-W. equations and the roots of the CP.

Chapter 4: Time Variable AR Processes
The problem solved in this chapter is to find a representation of a time variable process by a time variable AR (TVAR) process. In this auto regressive process the coefficients change over time. However, chapter 3 has also shown, that the CF does not directly dependent on the coefficients of the AR process, but on the roots of the CP. Therefore, in this chapter a method is developed that estimates TVAR processes with predetermined root motion. For the purpose of this study, the discussed movement of the roots is restricted to linear, quadratic and piecewise linear movements.

Chapter 5: Covariance Function of the Time Variable AR(1) Process
The use of nonstationary LSC requires the discrete covariances as well as the continuous CF of a TVAR process. In this chapter, both the discrete covariance sequence as well as the continuous CF of the TVAR(1) process with linear root motions are derived. In the time stable case, both the covariance sequence and the CF, only depend on the lag. But in the time variable case, these two functions first depend on the lag, second the epoch used to determine the covariance, and third, the condition of whether the second epoch finds itself earlier or later than the first one.

Chapter 6: Applications
Having derived these theories, there only remains their functional verification via practical applications. That is done in this chapter. In the first example, a time series of SLA data shows how a CF for a stationary process is determined using an AR estimation. With the help of this CF, it is possible to estimate an approximated function based on the observation using LSC. In addition, the representation of a CF from AR processes can be used to determine functionals of the observations. In this thesis, a case study of the derivative of the SLA data with respect to time was approximated.

The second application investigates nonstationary time series of GNSS heights. These time series were used to estimate TVAR processes with different yet predefined root motions. Subsequently, the estimated TVAR processes were validated by comparing the resulting time variable root with a sequence of discrete roots derived from AR processes, which were estimated for the observations in a moving window.

The third application concerns the calculation of the LSC for annual temperature anomalies. First, it was assumed that the time series was stationary. Thus, an AR process was estimated and the LSC is used to predict the values between the observations. Next, it was assumed that the same time series was nonstationary. Under this assumption, TVAR(1) processes were estimated and the time variable LSC computed. Since the prediction on the estimation times fits bedder to the observations, as well as the interpolated values does not become zero so fast shows that the nonstationary approach yields better results.

7.2 Contribution to the Contemporary Field

The derivation of **continuous CFs from AR processes** poses the first contribution of this work to current research. This method was used to construct CFs for LSC to predict values between the observed stationary time series. Especially the fact that a unique CF can be derived from each AR process, which does not demand further estimations, automates the modelling of CFs for covariance sequences. The estimate of time variable (TVAR) processes is another important contribution of this thesis. In this context, a **method to estimate TVAR processes with polynomial root motions** was developed. This method can be used to estimate TVAR processes whose roots of the CP move linearly, quadratically, or piecewise linearly over time. The most important contribution of this thesis, however is the **method of nonstationary least-squares collocation**. Deriving a discrete covariance sequence and a **continuous CF from a TVAR(1) process** allow the computation of covariance matrices for nonstationary time series. Finally, **an algorithm was implemented for each method**. This enables the application of these methods to real data and the subsequent comparison with other estimation methods.

7.3 Outlook and Conclusions

Although this thesis provides a possibility for nonstationary LSC, there is still a lot of room for further research. The estimation of the TVAR processes in this contribution, for example, is limited to quadratic and linear root movements. Modelling the roots motion with polynomials of higher order is an interesting topic for further investigations. However, other root movements (such as circulations around the origin) might be of interest. Especially with the CF of TVAR processes, a wide range of follow-up investigations still remains to be examined. Instead of calculating the eigenvalues of the covariance matrix to check whether the matrix is positive (semi-)definite or not, it would be interesting to investigate under which conditions the CF created by the TVAR(1) process is positive (semi-)definite. Additionally, the structure of this matrix has to be studied further. This applies to the inverse matrix and its structure as well. And finally, this remains also true for the question whether there are methods to determine CFs from TVAR processes with orders greater than one.

Appendix A

Introduction

A.1 Transformation from the Power Spectral Density Function to a Covariance Function

Given a time series $\{\mathcal{S}_k\}_{k\in\mathbb{Z}}$ and covariances $\{\Sigma_j\}_{j\in\mathbb{Z}}$ between two observations with lag j. For this time series, the PSD is computed by the formula

$$\text{PSD}(\{\mathcal{S}_k\}_{k\in\mathbb{Z}}) = |\mathcal{F}\{\{\mathcal{S}_k\}_{k\in\mathbb{Z}}\}(\nu)|^2.$$

It is necessary to show that the inverse FT of the PSD is equal to the discrete CF:

$$\begin{aligned}
\mathcal{F}^{-1}\{|\mathcal{F}\{\{\mathcal{S}_k\}_{k\in\mathbb{Z}}\}(\nu)|^2\}(t) &\overset{(1)}{=} \mathcal{F}^{-1}\{\mathcal{F}\{\{\mathcal{S}_k\}_{k\in\mathbb{Z}}\}(\nu)\mathcal{F}\{\{\mathcal{S}_k\}_{k\in\mathbb{Z}}\}(\nu)^*\}(t) \\
&\overset{(2)}{=} \mathcal{F}^{-1}\{\mathcal{F}\{\{\mathcal{S}_k\}_{k\in\mathbb{Z}}\}(\nu)\}(t) \circledast \mathcal{F}^{-1}\{\mathcal{F}\{\{\mathcal{S}_k\}_{k\in\mathbb{Z}}\}(\nu)^*\}(t) \\
&\overset{(3)}{=} \{\mathcal{S}_k\}_{k\in\mathbb{Z}} \circledast \{\mathcal{S}_k\}^*_{k\in\mathbb{Z}} \\
&\overset{(4)}{=} \{\mathcal{S}_k\}_{k\in\mathbb{Z}} \circledast \{\mathcal{S}_k\}_{k\in\mathbb{Z}} \\
&\overset{(5)}{=} \int_{-\infty}^{\infty} \{\mathcal{S}_k\}_{k\in\mathbb{Z}}\{\mathcal{S}_{k-j}\}_{j\in\mathbb{Z}}(dk) \\
&\overset{(6)}{=} \{\Sigma_j\}_{j\in\mathbb{Z}}.
\end{aligned}$$

First, the definition for the absolute value function of complex functions

$$|\mathcal{F}\{\{\mathcal{S}_k\}_{k\in\mathbb{Z}}\}(\nu)| = \sqrt{\mathcal{F}\{\{\mathcal{S}_k\}_{k\in\mathbb{Z}}\}(\nu)\mathcal{F}\{\{\mathcal{S}_k\}_{k\in\mathbb{Z}}\}(\nu)^*}$$

is used in (1). Here, $\mathcal{F}\{\{\mathcal{S}_k\}_{k\in\mathbb{Z}}\}(\nu)^*$ is the complex conjugate of $\mathcal{F}\{\{\mathcal{S}_k\}_{k\in\mathbb{Z}}\}(\nu)$. Next, the convolution theorem (see Buttkus 2000, p. 22, Table 2.1) is used in (2). The convolution theorem is provided by the equation

$$\mathcal{F}^{-1}\{X(\nu)Y(\nu)\}(t) = \mathcal{F}^{-1}\{X(\nu)\}(t) \circledast \mathcal{F}^{-1}\{Y(\nu)\}(t).$$

since the FT and the IFT cancel out each other, both transformations can be omitted, in step (3). And since $\mathcal{S}_t$ is real valued, it follows that $\{\mathcal{S}_k\}^*_{k\in\mathbb{Z}} = \{\mathcal{S}_k\}_{k\in\mathbb{Z}}$, as it was used in (4). In (5), the definition of convolution is used, i.e. $X(t) \circledast Y(t) = \int_{-\infty}^{\infty} X(t)Y(t-j)dt$. Finally, (6) is the definition of the discrete CF.

Appendix B

Continuous Covariance Function for Time Constant AR Processes

B.1 Determination of the Weights for Covariance Functions

Assuming that the parameters of an AR(p) process, as well as, p coefficients and the variance of noise $\sigma^2_{\mathcal{E}}$(see section 2.7) are given, the discrete covariances of this process are uniquely specified. The reorganized Y.-W. equations (see Schuh et al. 2014) are used to generate these from the parameters,

$$\begin{bmatrix} \Sigma_0 \\ \Sigma_1 \\ \Sigma_2 \\ \vdots \\ \Sigma_{p-1} \\ \Sigma_p \end{bmatrix} = \left(\begin{bmatrix} -1 & & & & & \\ \alpha_1 & -1 & & & & \\ \alpha_2 & \alpha_1 & -1 & & & \\ \vdots & \vdots & \vdots & \ddots & & \\ \alpha_{p-1} & \alpha_{p-2} & \alpha_{p-3} & \dots & -1 & \\ \alpha_p & \alpha_{p-1} & \alpha_{p-2} & \dots & \alpha_1 & -1 \end{bmatrix} + \begin{bmatrix} 0 & \alpha_1 & \dots & \alpha_{p-2} & \alpha_{p-1} & \alpha_p \\ 0 & \alpha_2 & \dots & \alpha_{p-1} & \alpha_p & \\ 0 & \alpha_3 & \dots & \alpha_p & & \\ \vdots & \vdots & \iddots & & & \\ 0 & \alpha_p & & & & \\ 0 & & & & & \end{bmatrix} \right)^{-1} \begin{bmatrix} -\sigma^2_{\mathcal{E}} \\ 0 \\ 0 \\ \vdots \\ 0 \\ 0 \end{bmatrix}. \tag{B.1.1}$$

Further entries of the discrete CF (i.e. Σ_j for $i > p$) can then be calculated using the Y.-W. equations for orders greater than p (see (2.8.3)).
As described in section 2.9, the determination of the required weights A_i of (3.1.2), demands the calculation of the unique roots P_k of the CP. With the help of these roots, (3.1.2) can be set up for p different yet arbitrary values ($j = j_1,\ j_2,\ j_3, ...,\ j_p$) and converted into the matrix vector notation:

$$\begin{bmatrix} \Sigma_{j_1} \\ \Sigma_{j_2} \\ \vdots \\ \Sigma_{j_p} \end{bmatrix} = \begin{bmatrix} P_1^{|j_1|} & P_2^{|j_1|} & \dots & P_p{}^{|j_1|} \\ P_1^{|j_2|} & P_2^{|j_2|} & \dots & P_p{}^{|j_2|} \\ \vdots & \vdots & & \vdots \\ P_1^{|j_p|} & P_2^{|j_p|} & \dots & P_p{}^{|j_p|} \end{bmatrix} \begin{bmatrix} A_1 \\ A_2 \\ \vdots \\ A_p \end{bmatrix}.$$

The unique solution of

$$\begin{bmatrix} A_1 \\ A_2 \\ \vdots \\ A_p \end{bmatrix} = \begin{bmatrix} P_1^{|j_1|} & P_2^{|j_1|} & \dots & P_p{}^{|j_1|} \\ P_1^{|j_2|} & P_2^{|j_2|} & \dots & P_p{}^{|j_2|} \\ \vdots & \vdots & & \vdots \\ P_1^{|j_p|} & P_2^{|j_p|} & \dots & P_p{}^{|j_p|} \end{bmatrix}^{-1} \begin{bmatrix} \Sigma_{j_1} \\ \Sigma_{j_2} \\ \vdots \\ \Sigma_{j_p} \end{bmatrix}. \tag{B.1.2}$$

allows the calculation of the weights.

B.1.1 Analytical Solutions for the Weights of AR(1) Processes

In particular, the discrete covariances Σ_j and the weights A_i can be computed analytically for AR(1) processes.
In this case, the reorganized Y.-W. equations of (B.1.1) provide the covariances Σ_0 and Σ_1:

$$\begin{aligned}\begin{bmatrix}\Sigma_0\\ \Sigma_1\end{bmatrix} &= \left(\begin{bmatrix}-1 & 0\\ \alpha_1 & -1\end{bmatrix} + \begin{bmatrix}0 & \alpha_1\\ 0 & 0\end{bmatrix}\right)^{-1}\begin{bmatrix}-\sigma_\mathcal{E}^2\\ 0\end{bmatrix}\\ &= \begin{bmatrix}-1 & \alpha_1\\ \alpha_1 & -1\end{bmatrix}^{-1}\begin{bmatrix}-\sigma_\mathcal{E}^2\\ 0\end{bmatrix}\\ &= \frac{1}{1-\alpha_1^2}\begin{bmatrix}-1 & -\alpha_1\\ -\alpha_1 & -1\end{bmatrix}\begin{bmatrix}-\sigma_\mathcal{E}^2\\ 0\end{bmatrix}\\ &= \frac{\sigma_\mathcal{E}^2}{1-\alpha_1^2}\begin{bmatrix}1\\ \alpha_1\end{bmatrix}.\end{aligned}$$

The system of equations in (B.1.2) is even easier to solve and directly provides the weight A_1:

$$\begin{aligned}A_1 &= (P_1^0)^{-1}\Sigma_0\\ A_1 &= \Sigma_0\\ A_1 &\overset{(1)}{=} \frac{\sigma_\mathcal{E}^2}{1-a_1^2}\\ A_1 &\overset{(2)}{=} \frac{\sigma_\mathcal{E}^2}{1-P_1^2}.\end{aligned} \tag{B.1.3}$$

(1) holds $\Sigma_0 = \sigma_\mathcal{E}^2/(1-a_1)$ (see Hamilton 1994, p. 53, eq. 3.4.4), while $P_1 = \alpha_1$ has been used in (2) (comp. (3.2.2)).

B.1.2 Analytical Solutions for the Weights of AR(2) Processes with two Complex Conjugated Roots

The derivation of the weights A_1 and A_2 in this case refer to the AR process, whose CP's roots form a complex conjugated pair. First the reorganized Y.-W. equations for the AR(2) process are used to derive the formulas of the first three discrete covariances:

$$\begin{aligned}\begin{bmatrix}\Sigma_0\\ \Sigma_1\\ \Sigma_2\end{bmatrix} &= \left(\begin{bmatrix}-1 & 0 & 0\\ \alpha_1 & -1 & 0\\ \alpha_2 & \alpha_1 & -1\end{bmatrix} + \begin{bmatrix}0 & \alpha_1 & \alpha_2\\ 0 & \alpha_2 & 0\\ 0 & 0 & 0\end{bmatrix}\right)^{-1}\begin{bmatrix}-\sigma_\mathcal{E}^2\\ 0\\ 0\end{bmatrix}\\ &= \begin{bmatrix}-1 & \alpha_1 & \alpha_2\\ \alpha_1 & \alpha_2-1 & 0\\ \alpha_2 & \alpha_1 & -1\end{bmatrix}^{-1}\begin{bmatrix}-\sigma_\mathcal{E}^2\\ 0\\ 0\end{bmatrix}\\ &= \frac{1}{-{\alpha_2}^3+\alpha_2^2+\alpha_2(1+\alpha_1^2)+\alpha_1^2-1}\begin{bmatrix}1-\alpha_2 & \alpha_1\alpha_2+\alpha_1 & \alpha_2^2-\alpha_2\\ \alpha_1 & 1-\alpha_2^2 & \alpha_1\alpha_2\\ \alpha_1^2-\alpha_2^2+\alpha_2 & \alpha_1\alpha_2+\alpha_1 & 1-\alpha_1^2-\alpha_2\end{bmatrix}\begin{bmatrix}-\sigma_\mathcal{E}^2\\ 0\\ 0\end{bmatrix}\\ &= \frac{-\sigma_\mathcal{E}^2}{-{\alpha_2}^3+\alpha_2^2+\alpha_2(1+\alpha_1^2)+\alpha_1^2-1}\begin{bmatrix}1-\alpha_2\\ \alpha_1\\ \alpha_1^2-\alpha_2^2\end{bmatrix}.\end{aligned}$$

To determine the weights of the AR(2) process, the coefficients α_1 and α_2 are replaced with the roots P_1 and P_2. The transformation is calculated according to the relation given in (3.2.3) and (3.2.4). Since the transition to the roots results in strong simplifications, the denominator must be

specially considered here:

$$\begin{aligned}
&-\alpha_2{}^3+\alpha_2^2+\alpha_2(1+\alpha_1^2)+\alpha_1^2-1\\
=&(P_1P_2)^3+(P_1P_2)^2-(P_1P_2)(1+(P_1+P_2)^2)+(P_1+P_2)^2-1\\
=&P_1{}^3P_2{}^3+P_1^2P_2^2-P_1P_2-P_1{}^3P_2-\mathbf{2}P_1^2P_2^2-P_1P_2{}^3+P_1^2+\mathbf{2}P_1P_2+P_2^2-1\\
=&P_1{}^3P_2{}^3\qquad\qquad\qquad-P_1{}^3P_2-\ P_1^2P_2^2-P_1P_2{}^3+P_1^2+\ \ P_1P_2+P_2^2-1\\
=&(1-P_1^2)(-P_1P_2{}^3+P_1P_2+P_2^2-1)\\
=&(1-P_1^2)(1-P_2^2)(P_1P_2-1)\\
=&-(1-P_1^2)(1-P_2^2)(1-P_1P_2).
\end{aligned}$$

(3.2.3) and (3.2.4) renders the determination of the denominator rather simple, means that the discrete covariances can now be specified directly. Also, the calculation only need Σ_0 and Σ_1 to determine the weights:

$$\begin{aligned}
\begin{bmatrix}\Sigma_0\\ \Sigma_1\end{bmatrix}&=\frac{-\sigma_\mathcal{E}^2}{-(1-P_1^2)(1-P_2^2)(1-P_1P_2)}\begin{bmatrix}1+P_1P_2\\ P_1+P_2\end{bmatrix}\\
&=\frac{\sigma_\mathcal{E}^2}{(1-P_1^2)(1-P_2^2)(1-P_1P_2)}\begin{bmatrix}1+P_1P_2\\ P_1+P_2\end{bmatrix}.
\end{aligned}\tag{B.1.4}$$

Finally, the weights are calculated with regards to (B.1.2):

$$\begin{aligned}
\begin{bmatrix}A_1\\ A_2\end{bmatrix}&=\begin{bmatrix}1&1\\ P_1&P_2\end{bmatrix}^{-1}\begin{bmatrix}\Sigma_0\\ \Sigma_1\end{bmatrix}\\
&=\frac{1}{P_2-P_1}\begin{bmatrix}P_2&-1\\ -P_1&1\end{bmatrix}\begin{bmatrix}\Sigma_0\\ \Sigma_1\end{bmatrix}\\
\Rightarrow A_1&=\frac{P_2\Sigma_0-\Sigma_1}{P_2-P_1}.
\end{aligned}$$

Due to the fact that the variance of the AR(2) process with two complex roots is real valued, and the fact that the roots are a complex conjugated pair ($P_1=P_2^*$) it follows, that the weights must build a pair of complex conjugated values as well (i.e. $A_1=A_2^*$). So, in order to determine the two weights, it only requires the calculation of A_1. With the discrete covariances of (B.1.4), the weight A_1 can be determined directly from the roots and the variance of the white noise:

$$\begin{aligned}
A_1&=\frac{\sigma_\mathcal{E}^2(P_2(1+P_1P_2)-(P_1+P_2))}{(P_2-P_1)(1-P_1^2)(1-P_2^2)(1-P_1P_2)}\\
&=\frac{\sigma_\mathcal{E}^2(P_2+P_1P_2^2-P_1-P_2)}{(P_2-P_1)(1-P_1^2)(1-P_2^2)(1-P_1P_2)}\\
&=\frac{\sigma_\mathcal{E}^2(P_1P_2^2-P_1)}{(P_2-P_1)(1-P_1^2)(1-P_2^2)(1-P_1P_2)}\\
&=\frac{\sigma_\mathcal{E}^2(-P_1)(1-P_2^2)}{(P_2-P_1)(1-P_1^2)(1-P_2^2)(1-P_1P_2)}\\
&=-\frac{\sigma_\mathcal{E}^2P_1}{(P_2-P_1)(1-P_1^2)(1-P_1P_2)}.
\end{aligned}\tag{B.1.5}$$

And analogously, the second weight results in

$$A_2=-\frac{\sigma_\mathcal{E}^2P_2}{(P_1-P_2)(1-P_2^2)(1-P_1P_2)}=A_1^*.$$

In addition, we can now also determine the real and imaginary parts of A_1 and A_2, for the AR(2) process with two complex conjugated roots. First of all, consider the variance (Σ_0):

$$\Sigma_0 = A_1 + A_2 = A_1 + A_1^* \qquad = 2\mathcal{R}(A_1).$$

Applying the first argument of (B.1.4) results in weight A_1's real part, (and thus directly in weight's A_2's real part as well):

$$\mathcal{R}(A_1) = \frac{\Sigma_0}{2} \qquad = \frac{\sigma_\mathcal{E}^2(1+P_1P_2)}{2(1-P_1^2)(1-P_2^2)(1-P_1P_2)}. \tag{B.1.6}$$

And the imaginary part equals the difference between A_1 (see (B.1.5)) and $\mathcal{R}(A_1)$ (see (B.1.6)) divided by i:

$$\begin{aligned}
\mathcal{I}(A_1) &= \frac{1}{i}(A_1 - \mathcal{R}(A_1)) \\
&= \frac{1}{i}\left(-\frac{\sigma_\mathcal{E}^2 P_1}{(P_2-P_1)(1-P_1^2)(1-P_1P_2)} - \frac{\sigma_\mathcal{E}^2(1+P_1P_2)}{2(1-P_1^2)(1-P_2^2)(1-P_1P_2)}\right) \\
&= \frac{1}{i}\frac{-2\sigma_\mathcal{E}^2 P_1(1-P_2^2) - \sigma_\mathcal{E}^2(1+P_1P_2)(P_2-P_1)}{2(P_2-P_1)(1-P_1^2)(1-P_2^2)(1-P_1P_2)} \\
&= \frac{1}{i}\frac{-\sigma_\mathcal{E}^2\left(2P_1 - 2P_1P_2^2 + P_2 - P_1 + P_1P_2^2 - P_1^2P_2\right)}{2(P_2-P_1)(1-P_1^2)(1-P_2^2)(1-P_1P_2)} \\
&= \frac{1}{i}\frac{-\sigma_\mathcal{E}^2\left(P_1 - P_1P_2^2 + P_2 \qquad\qquad - P_1^2P_2\right)}{2(P_2-P_1)(1-P_1^2)(1-P_2^2)(1-P_1P_2)} \\
&= \frac{1}{i}\frac{-\sigma_\mathcal{E}^2\left((P_1+P_2)(1-P_1P_2)\right)}{2(P_2-P_1)(1-P_1^2)(1-P_2^2)(1-P_1P_2)} \\
&= \frac{1}{i}\left(-\frac{\sigma_\mathcal{E}^2(P_1+P_2)}{2(P_2-P_1)(1-P_1^2)(1-P_2^2)}\right).
\end{aligned} \tag{B.1.7}$$

Since the real part of A_1 (see (B.1.7)) and the imaginary part of A_1 (see (B.1.7)) are rather similar, the can be transformed into each other by the formula

$$\mathcal{I}(A_1) = \frac{1}{i}\left(-\frac{(P_1+P_2)(1-P_1P_2)}{(P_2-P_1)(1+P_1P_2)}\mathcal{R}(A)\right) \tag{B.1.8}$$

and vice versa.

B.2 Real Part and Absolute Values for the Continuous Covariance Function

Section 3.1 introduced the continuous CF $\gamma(h)$, which becomes complex valued if at least one real root is negative. To understand this phenomenon, the negative real root P_l is rewritten in the representation

$$P_l = |P_l|e^{i\pi} \Rightarrow P_l^{|h|} = |P_l|^{|h|}e^{i\pi|h|}.$$

Unfortunately, the imaginary part of the exponential function $e^{i\pi|h|} = \cos(\pi h) + i\sin(\pi|h|)$ for $h \in \mathbb{R}$ does not necessarily disappear, since $\sin(\pi h)$ only equals zero for $h \in \mathbb{Z}_0$. The method of using the root as a suitable basis for the CF, demands its adaption in such a way that $\gamma(j) = \Sigma_j$ for all $j \in \mathbb{Z}_0$, while never becoming complex-valued.
However, the result of an exponentiation of a negative real root with $h \in (0,1)$ is complex valued. In Figure B.1 the real part, the imaginary part and the sum of both parts are shown for $P_1 = -0.8$. Since the imaginary part (**green**) never intersects with the discrete covariances (**blue** quadrates with **red** filling), this option is omitted. Since the global maximum should be localized at lag $h = 0$

(as required by the conditions from section 2.6), the sum of the complex and real part (**red**) is not a suitable CF as well. Concerning these three functions, only the real part perfectly reproduces the discrete covariances while having its global maximum at $h = 0$. Therefore the real part is used as a CF.

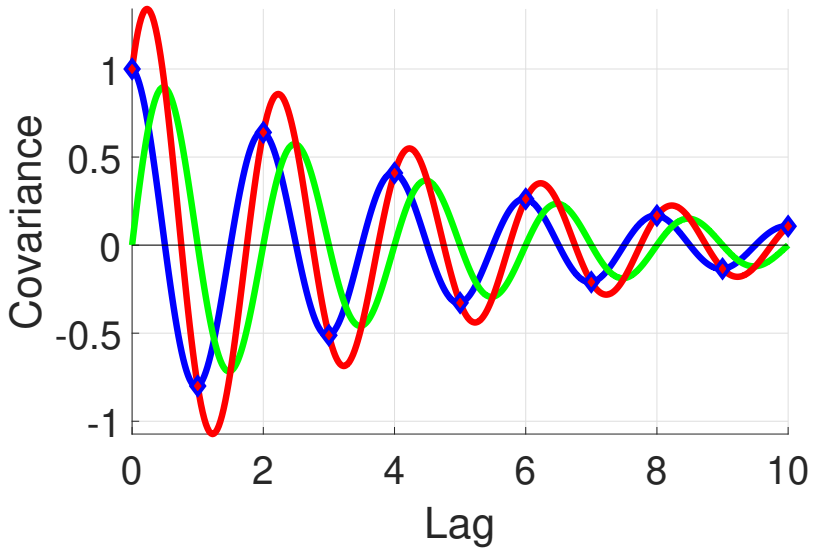

Figure B.1: Different ways to deal with the complex covariance function: only using the real part (**blue**), only using the imaginary part (**green**) or forming the sum of both (**red**). The **blue** quadrates with **red** filling represent the discrete covariances.

B.3 Power Spectral Density for the AR(1) and AR(2) Process

This work makes repeated use of the PSD of the AR(1) and AR(2) processes. Therefore, these are here both explicitly derived, which is done by evaluating (3.2.1). For the AR(1), process we obtain

$$\begin{aligned}
\mathcal{H}^2(\nu) &= \frac{\sigma_\mathcal{E}^2}{|1-\alpha_1 e^{-i2\pi\nu}|^2} \\
&= \frac{\sigma_\mathcal{E}^2}{(1-\alpha_1 e^{-i2\pi\nu})(1-\alpha_1 e^{i2\pi\nu})} \\
&= \frac{\sigma_\mathcal{E}^2}{1-\alpha_1(\underbrace{e^{-i2\pi\nu}+e^{i2\pi\nu}}_{2\cos(2\pi\nu)})+\alpha_1^2(\underbrace{e^{-i2\pi\nu}e^{i2\pi\nu}}_{1})} \\
&= \frac{\sigma_\mathcal{E}^2}{1-2\alpha_1\cos(2\pi\nu)+\alpha_1^2} \\
&\overset{(1)}{=} \frac{\sigma_\mathcal{E}^2}{1-2P_1\cos(2\pi\nu)+P_1^2}.
\end{aligned} \tag{B.3.1}$$

Since (3.2.2) provides that for the TVAR(1) process $\alpha_1 = P_1$ is valid, this can be used in (1) to change from the coefficient α_1 to the root P_1.
For the AR(2) process, the calculation of the PSD is considerably more challenging. However, regardless of whether the roots are real-valued or they build a complex conjugated pair, the here

derived PSD is valid. Using the coefficients α_1 and α_2, the spectrum can then be calculated as

$$\begin{aligned}
\mathcal{H}^2(\nu) &= \frac{\sigma_\mathcal{E}^2}{|1-\alpha_1 e^{-i2\pi\nu} - \alpha_2 e^{-i4\pi\nu}|^2} \\
&= \frac{\sigma_\mathcal{E}^2}{(1-\alpha_1 e^{-i2\pi\nu} - \alpha_2 e^{-i4\pi\nu})(1-\alpha_1 e^{i2\pi\nu} - \alpha_2 e^{i4\pi\nu})} \\
&\overset{(1)}{=} \sigma_\mathcal{E}^2\{1 - \alpha_1(\underbrace{e^{-i2\pi\nu} + e^{i2\pi\nu}}_{2\cos(2\pi\nu)}) - \alpha_2(\underbrace{e^{-i4\pi\nu} + e^{i4\pi\nu}}_{2\cos(4\pi\nu)})... \\
&\qquad + \alpha_1^2(\underbrace{e^{-i2\pi\nu}e^{i2\pi\nu}}_{1}) + \alpha_2^2(\underbrace{e^{-i4\pi\nu}e^{i4\pi\nu}}_{1})... \\
&\qquad + \alpha_1\alpha_2(\underbrace{\underbrace{e^{-i2\pi\nu}e^{i4\pi\nu}}_{e^{i2\pi\nu}} + \underbrace{e^{i2\pi\nu}e^{-i4\pi\nu}}_{e^{-i2\pi\nu}}}_{2\cos(2\pi\nu)})\}^{-1} \\
&= \frac{\sigma_\mathcal{E}^2}{1 - 2\alpha_1\cos(2\pi\nu) - 2\alpha_2\cos(4\pi\nu) + \alpha_1^2 + \alpha_2^2 + 2\alpha_1\alpha_2\cos(2\pi\nu)}.
\end{aligned} \tag{B.3.2}$$

In step (1), the brackets are multiplied and rearranged with according to the coefficients. This representation facilitates the transition from the coefficients (α_1 and α_2) to the roots (P_1 and P_2) (as shown in (3.2.3) and (3.2.4)):

$$\begin{aligned}
\mathcal{H}^2(\nu) &= \sigma_\mathcal{E}^2\{1 - 2(P_1+P_2)\cos(2\pi\nu)... \\
&\qquad + 2P_1P_2\cos(4\pi\nu) + \underbrace{(P_1+P_2)^2}_{P_1^2+2P_1P_2+P_2^2} + P_1^2P_2^2... \\
&\qquad - 2(P_1+P_2)P_1P_2\cos(2\pi\nu)\}^{-1} \\
&= \sigma_\mathcal{E}^2\{1 - 2(P_1+P_2)\cos(2\pi\nu) + P_1^2 + P_2^2... \\
&\qquad + P_1P_2(2 + 2\cos(4\pi\nu) - 2(P_1+P_2)\cos(2\pi\nu) + P_1P_2)\}^{-1}.
\end{aligned}$$

Thus the AR(2) process' spectrum can be calculated as the fraction

$$\begin{aligned}
&\mathcal{H}^2(\nu) \\
&= \frac{\sigma_\mathcal{E}^2}{1 - 2(P_1+P_2)\cos(2\pi\nu) + P_1^2 + P_2^2 + P_1P_2(2 + 2\cos(4\pi\nu) - 2(P_1+P_2)\cos(2\pi\nu) + P_1P_2)}.
\end{aligned} \tag{B.3.3}$$

B.4 Fourier Transformation of the Continuous Covariance Function

In order to compute the FT of the continuous CF $\gamma : \mathbb{R} \to \mathbb{R}$ provided by

$$\gamma(h) = \sum_{k=1}^{p} A_k P_k^{|h|},$$

the linearity of this transformation is first exploited in order to simplify the integral:

$$\begin{aligned}
\Gamma(\nu) :&= \mathcal{F}\{\gamma(h)\}(\nu) \\
&= \int_{-\infty}^{\infty} \sum_{k=1}^{p} A_k {P_k}^{|h|} e^{-i2\pi\nu h} dh \\
&\overset{(1)}{=} \sum_{k=1}^{p} \int_{-\infty}^{\infty} A_k {P_k}^{|h|} e^{-i2\pi\nu h} dh \\
&\overset{(2)}{=} \sum_{k=1}^{p} A_k \int_{-\infty}^{\infty} {P_k}^{|h|} e^{-i2\pi\nu h} dh.
\end{aligned} \tag{B.4.1}$$

sum and integral are exchanged, during the transformation (1). This is only possible if the sum converges absolutely, which is the case (due to having a finite sum, also converging absolutely). In (2), the linearity of the integration is used to extract the scalar A_k. For further analysis, the (potentially complex-valued) root P_k is replaced by

$$P_k = r_k e^{i\phi_k}, \tag{B.4.2}$$

which describes the complex number P_k by a radius r_k and an angle ϕ_k. If the radius is represented by an exponential function ($r_k = e^{\ln(r_k)}$), the exponential functions can be combined: $P_k = e^{\ln(r_k)+i\phi_k}$. This way, the integral in the FT simplifies to:

$$\begin{aligned}
\int_{-\infty}^{\infty} {P_k}^{|h|} e^{-i2\pi\nu h} dh &= \int_{-\infty}^{\infty} e^{(\ln(r_k)+i\phi_k)|h|} e^{-i2\pi\nu h} dh \\
&\overset{(1)}{=} \int_{-\infty}^{0} e^{(\ln(r_k)+i\phi_k)(-h)} e^{-i2\pi\nu h} dh + \int_{0}^{\infty} e^{(\ln(r_k)+i\phi_k)h} e^{-i2\pi\nu h} dh \\
&= \int_{-\infty}^{0} e^{(-\ln(r_k)+i(-\phi_k-2\pi\nu))h} dh + \int_{0}^{\infty} e^{(\ln(r_k)+i(\phi_k-2\pi\nu))h} dh \\
&= \left[\frac{1}{-\ln(r_k)+i(-\phi_k-2\pi\nu)} e^{(-\ln(r_k)+i(-\phi_k-2\pi\nu))h} \right]_{-\infty}^{0} \dots \\
&+ \left[\frac{1}{\ln(r_k)+i(\phi_k-2\pi\nu)} e^{(\ln(r_k)+i(\phi_k-2\pi\nu))h} \right]_{0}^{\infty}.
\end{aligned}$$

For step (1), the integral is divided into two parts at $h = 0$. The absolute value function can be eliminated by replacing $|h| = -h$ for the integral covering the negative area, and $|h| = h$ for the integral covering the positive area.
Solving the integral, requires the identification of the limits of the antiderivatives. Note that the fractions are not dependent on h, meaning that it is sufficient to determine the limits for the exponential functions.
For $h = 0$, one easily sees that the exponential function in both antiderivatives becomes 1. Regrettably, it is not as easy for the boundaries $\pm\infty$. By rewriting the exponential function as

$$e^{(\ln(r_k)+i(\phi_k-2\pi\nu))h} = r_k^h e^{i(\phi_k-2\pi\nu)h},$$

it is possible to dissect this exponential function into the radius of the root P_k with $r_k < 1$ and a value ($e^{i(\phi_k-2\pi\nu)}$) laying on the unit circle in the complex plane. If h is increased, the value of r_i^h shrinks, while the expression $e^{i(\phi_k-2\pi\nu)h}$ always remains a value on the unit circle in the complex plane. That means that the function $e^{(\ln(r_k)+i(\phi_k-2\pi\nu))h}$ for $h \in [0, \infty]$ describes a spiral starting at one and running towards zero at infinity. This is depicted in Figure (B.2). It should not go

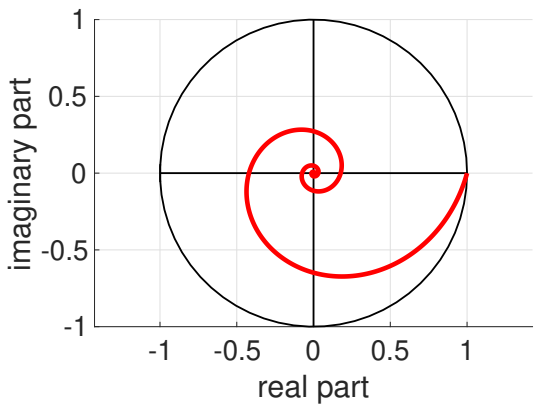

Figure B.2: Spiral motion of ${P_k}^{|h|}$ in the complex plane (if P_k is complex valued).

unmentioned that the case of the real root embodies a special case of the spiral, with an angle

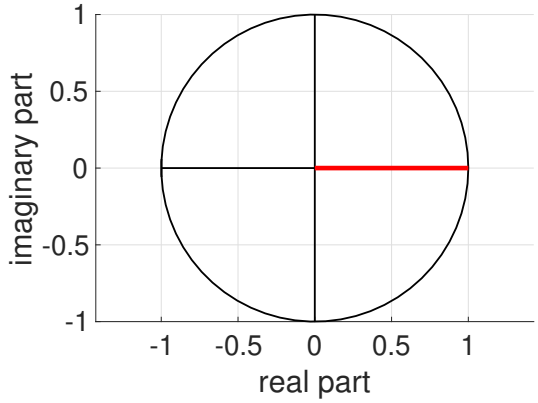

Figure B.3: Linear motion of ${P_k}^{|h|}$ in the complex plane (if P_k is positive and real valued).

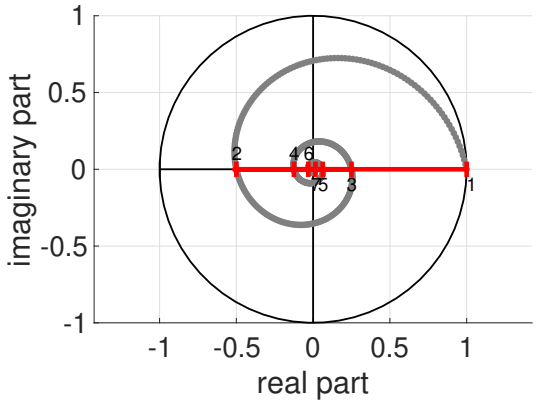

Figure B.4: Back and forth motion of ${P_k}^{|h|}$ in the complex plane (if P_k is negative and real valued).

of zero. The same applies to the real negative root. But even when only using the real part, it still runs against zero. These special cases are illustrated in Figure B.3 and Figure B.4. Since the convergence behaviour is equal for all three cases, these insights help to solve the integral, which results in

$$\begin{aligned}
\int_{-\infty}^{\infty} {P_k}^{|h|} e^{-i2\pi\nu h} dh &= \left(\frac{1}{-\ln(r_k) + i(-\phi_k - 2\pi\nu)} - 0 \right) + \left(0 - \frac{1}{\ln(r_k) + i(\phi_k - 2\pi\nu)} \right) \\
&= \frac{1}{-\ln(r_k) + i(-\phi_k - 2\pi\nu)} - \frac{1}{\ln(r_k) + i(\phi_k - 2\pi\nu)} \\
&= \frac{1}{(-\ln(r_k) - i\phi_k) - i2\pi\nu} - \frac{1}{(\ln(r_k) + i\phi_k) - i2\pi\nu} \\
&\overset{(1)}{=} \frac{1}{(-\ln(r_k) - i\phi_k) - i2\pi\nu} + \frac{1}{(-\ln(r_k) - i\phi_k) + i2\pi\nu} \\
&= \frac{(-\ln(r_k) - i\phi_k + i2\pi\nu) + (-\ln(r_k) - i\phi_k - i2\pi\nu)}{(-\ln(r_k) - i\phi_k)^2 - (i2\pi\nu)^2} \\
&= \frac{-2(\ln(r_k) + i\phi_k)}{(\ln(r_k) + i\phi_k)^2 + (2\pi\nu)^2} \\
&\overset{(2)}{=} \frac{-2\ln(P_k)}{(\ln(P_k))^2 + (2\pi\nu)^2}.
\end{aligned} \tag{B.4.3}$$

Note that the minus sign between the fractions has moved, in step (1), into the denominator of the second fraction. Step (2) is caused by replacing $\ln(r_k) + i\phi_k$ with $\ln(P_k)$. This corresponds to (B.4.2) (if the logarithm is applied on both sides). Combined with (B.4.1), this result yields the FT of the continuous CF:

$$\Gamma(\nu) = \sum_{k=1}^{p} A_k \frac{-2\ln(P_k)}{(\ln(P_k))^2 + (2\pi\nu)^2}. \tag{B.4.4}$$

B.5 Convolution of the Continuous Covariance Function with a Dirac Comb

The magic square in Figure 3.1 shows that the FT of the continuous CF $\Gamma(\nu)$ (see (B.4.4)) can be transferred to the FT of the discrete CF $\mathcal{H}^2(\nu)$ (see (3.2.1)) by convolution with the DC. This process is developed in five steps. The first step is shown in section B.5.1, and solves the convolution including the DDF and results in an infinite sum. In B.5.2, the individual summands are explicitly specified by a finite sum of integrals, which are in turn solved in section B.5.3. With the help of these integrals, the sum of the results from the convolution is solved in section B.5.4. **It should be noted that section B.5.3, and B.5.4 refer only to real roots.** Finally, section B.5.5 summarizes these steps and provides an outlook for the case of complex roots.

B.5.1 Elimination of the Dirac Delta Function

Since the DC or DDF is only implicitly represented as a distribution and has not been introduced as an explicit function, the first goal should be to remove it from the calculation:

$$\begin{aligned}
\Gamma(\nu) \circledast \sum_{l=-\infty}^{\infty} \delta(\nu - l) &\overset{(1)}{=} \int_{-\infty}^{\infty} \Gamma(u) \sum_{l=-\infty}^{\infty} \delta(u - (\nu - l))du \\
&\overset{(2)}{=} \int_{-\infty}^{\infty} \Gamma(u) \sum_{l=-\infty}^{\infty} \delta(u - \nu + l)du \\
&\overset{(3)}{=} \int_{-\infty}^{\infty} \Gamma(u) \sum_{m=-\infty}^{\infty} \delta(u - \nu - m)du \\
&\overset{(4)}{=} \int_{-\infty}^{\infty} \Gamma(u) \sum_{m=-\infty}^{\infty} \delta(u - (\nu + m))du \\
&\overset{(5)}{=} \int_{-\infty}^{\infty} \sum_{m=-\infty}^{\infty} \Gamma(u)\delta(u - (\nu + m))du \\
&\overset{(6)}{=} \sum_{m=-\infty}^{\infty} \underbrace{\int_{-\infty}^{\infty} \Gamma(u)\delta(u - (\nu + m))du}_{} \\
&\overset{(7)}{=} \sum_{m=-\infty}^{\infty} \qquad \Gamma(\nu + m). \qquad \text{(B.5.1)}
\end{aligned}$$

Not all of the transformations (1)–(7) used here are self-explanatory and therefore call for further elaboration. The transformation (1) is the definition of the convolution. However, the argument of DDF is given as $\nu - l$ and therefore this argument must be assembled in brackets. The transformations (2)-(4) deal only with the argument of the DDF. Thus, the extra bracket mentioned above is resolved in (2), which changes the sign of the parameter l. This change of sign is a hindrance and is undone in (3). For this, l is substituted by $-m$, which actually causes the limits of the sum to exchange places. However, this can be compensated by reversing the order of the summands in such a way, that the same sum limits remains the same. In step (4), ν and l are combined in brackets, so that they build one parameter, just as in step (1). In (5) and (6), the sequences in the calculation are swapped. Specifically, this means that in (5), $\Gamma(u)$ is integrated into the sum. This is possible because $\Gamma(u)$ is independent from the sum and can therefore be multiplied directly by the individual summands. And in step (6), the sum and the integral are exchanged, which is only possible if all the functions involved absolutely converge. Since both $\Gamma(\nu)$ and the DC are Fourier transformed functions, and IFT requires absolutely convergent functions, this condition is fulfilled. The purpose of all previous steps is to remove the DDF from the equation of (7). Here, it is possible to use the property of the DDF of (2.15.1), but one has still to make sure to use $(\nu + m)$ as one variable.

B.5.2 Rewriting $\Gamma(\nu + m)$ as a Sum

In this section, the PSD of discrete CF $\Gamma(\nu + m)$ is rewritten in a way, that it can be replaced by a sum of p summands. For this, we use the IFT:

$$\begin{aligned}\Gamma(\nu+m) &\overset{(1)}{=} \int_{-\infty}^{\infty} \overbrace{\qquad\gamma(h)\qquad}\, e^{-i2\pi mh}e^{-i2\pi\nu h}dh \\ &= \int_{-\infty}^{\infty} \overbrace{\sum_{k=1}^{p} A_k P_k^{|h|}}\, e^{-i2\pi mh}e^{-i2\pi\nu h}dh \qquad \text{(B.5.2)} \\ &\overset{(2)}{=} \sum_{k=1}^{p}\int_{-\infty}^{\infty} A_k P_k^{|h|}e^{-i2\pi mh}e^{-i2\pi\nu h}dh \\ &\overset{(3)}{=} \sum_{k=1}^{p} A_k \int_{-\infty}^{\infty} P_k^{|h|}e^{-i2\pi mh}e^{-i2\pi\nu h}dh. \qquad \text{(B.5.3)}\end{aligned}$$

The transformation (1) corresponds to the frequency shift of the IFT (see Buttkus 2000, p. 26 Table 2.2). For step (2), sum and integral are exchanged. This is possible, due to the circumstances mentioned above, i.e. if all summands absolutely converge. Finally, since the weights A_k do not depend on the integration variable h, it is possible to extract the weights A_k from the integral in (3).

B.5.3 Solving the Integral (for Real Roots)

When solving the integral of (B.5.3), the integral

$$\int_{-\infty}^{0} P_k^{-h}e^{-i2\pi\boldsymbol{\nu}h}e^{-i2\pi mh}dh + \int_{0}^{\infty} P_k^{h}e^{2\pi\nu h}e^{-i2\pi mh}dh = \int_{-\infty}^{\infty}(P_k e^{2\pi\nu})^{|h|}e^{-i2\pi mh}dh \qquad \text{(B.5.4)}$$

will frequently appear. Its solution is known from (B.4.3), except that P_k has to be replaced by $P_k e^{-i2\pi\nu}$:

$$\begin{aligned}\mathcal{F}\{\underbrace{P_k e^{-2\pi\nu}}_{\bar{P}_k})^{|h|}\}(m) &= \int_{-\infty}^{\infty}\bar{P}_k^{|h|}e^{i2\pi mh}dh \\ &= \frac{-2\ln(\bar{P}_k)}{\bar{P}_k^2+(2\pi m)^2} \\ &= \frac{-2(\ln(P_k)+i2\pi\nu)}{(\ln(P_k)+i2\pi\nu)^2+(2\pi m)^2}. \qquad \text{(B.5.5)}\end{aligned}$$

One has to be careful to see that, in this case, ν is no variable but a set value. The variable of the FT has been replaced by m.
Return to the integral in (B.5.3). In order to solve this integral, the absolute value function has to be removed, which is easily achieved by a case distinction:

$$\int_{-\infty}^{\infty} P_k^{|h|}e^{-i2\pi mh}e^{-i2\pi\nu h}dh = \underbrace{\int_{-\infty}^{0} P_k^{-h}e^{-i2\pi mh}e^{-i2\pi\nu h}dh}_{:=I} + \underbrace{\int_{0}^{\infty} P_k^{h}e^{-i2\pi mh}e^{-i2\pi\nu h}dh}_{:=II}. \qquad \text{(B.5.6)}$$

Furthermore, it is necessary to separate the integral II into its real and its imaginary part:

$$\begin{aligned}
&\int_0^\infty \quad P_k^h \quad e^{-i2\pi\nu h} \quad e^{-i2\pi mh} dh \\
&= \int_0^\infty P_k^h (\overbrace{\cos(2\pi\nu h) - i\sin(2\pi\nu h)}) e^{-i2\pi mh} dh \\
&\overset{(1)}{=} \int_0^\infty P_k^h (\cos(2\pi\nu h) - i\sin(2\pi\nu h) + \underbrace{i\sin(2\pi\nu h) - i\sin(2\pi\nu h)}_{=0}) e^{-i2\pi mh} dh \\
&= \int_0^\infty P_k^h (\underbrace{\cos(2\pi\nu h) + i\sin(2\pi\nu h)}) - 2i\sin(2\pi\nu h)) e^{-i2\pi mh} dh \\
&= \int_0^\infty P_k^h (\quad e^{(i2\pi\nu h)} \quad - 2i\sin(2\pi\nu h)) e^{-i2\pi mh} dh \\
&\overset{(2)}{=} \int_0^\infty P_k^h e^{(i2\pi\nu h)} e^{-i2\pi mh} dh - 2i \int_0^\infty P_k^h \sin(2\pi\nu h) e^{-i2\pi mh} dh.
\end{aligned} \tag{B.5.7}$$

Zero is added, in (1), with $0 = i\sin(2\pi\nu h) - i\sin(2\pi\nu h)$, while in (2), the linearity of the integral is exploited to split the integral into two parts. If the solution of integral II as given in (B.5.7) is used in (B.5.6), the real-valued integrals can be combined with the integral in (B.5.5):

$$\begin{aligned}
&\int_{-\infty}^\infty P_k^{|h|} e^{-i2\pi mh} e^{-i2\pi\nu h} dh \\
&= \int_{-\infty}^0 P_k^{-h} e^{-i2\pi mh} e^{-i2\pi\nu h} dh + \int_0^\infty P_k^h e^{-i2\pi mh} e^{-i2\pi\nu h} dh \\
&= \underbrace{\int_{-\infty}^0 P_k^{-h} e^{-i2\pi mh} e^{-i2\pi\nu h} dh + \int_0^\infty P_k^h e^{(i2\pi\nu h)} e^{-i2\pi mh} dh} \quad -2i \int_0^\infty P_k^h \sin(2\pi\nu h) e^{-i2\pi mh} dh \\
&= \int_{-\infty}^\infty (P_k e^{i2\pi\nu})^{|h|} e^{-i2\pi mh} dh \quad -2i \int_0^\infty P_k^h \sin(2\pi\nu h) e^{-i2\pi mh} dh \\
&= \frac{-2(\ln(P_k) + i2\pi\nu)}{(\ln(P_k) + i2\pi\nu)^2 + (2\pi m)^2} \quad -2i \underbrace{\int_0^\infty P_k^h \sin(2\pi\nu h) e^{-i2\pi mh} dh}_{:=III}.
\end{aligned} \tag{B.5.8}$$

Thus, solving the integral III in (B.5.8) served to calculate the integral in (B.5.3). The solution of integral III demands the trigonometric representation $e^{-i2\pi mh} = \cos(2\pi mh) - i\sin(2\pi mh)$ and the further separation of the integral:

$$\begin{aligned}
\int_0^\infty P_k^h \sin(2\pi\nu h) e^{-i2\pi mh} dh &= \int_0^\infty P_k^h \sin(2\pi\nu h)(\cos(2\pi mh) - i\sin(2\pi mh)) dh \\
&= \underbrace{\int_0^\infty P_k^h \sin(2\pi\nu h)\cos(2\pi mh) dh}_{:=IV} - i \underbrace{\int_0^\infty P_k^h \sin(2\pi\nu h)\sin(2\pi mh) dh}_{:=V}.
\end{aligned} \tag{B.5.9}$$

The integral V can be easily solved by adding the infinite sum with index m (see (B.5.1)), albeit $\sum_{m=-\infty}^{\infty}$ should only be considered in section B.5.4:

$$\begin{aligned}
&\sum_{m=-\infty}^{\infty}\int_0^{\infty} P_k^h \sin(2\pi\nu h)\sin(2\pi m h)dh \\
&\overset{(1)}{=} \sum_{m=-\infty}^{-1}\int_0^{\infty} P_k^h \sin(2\pi\nu h)\sin(2\pi m h)dh + 0 + \sum_{m=1}^{\infty}\int_0^{\infty} P_k^h \sin(2\pi\nu h)\sin(2\pi m h)dh \\
&\overset{(2)}{=} \sum_{m=1}^{\infty}\int_0^{\infty} P_k^h \sin(2\pi\nu h)\sin(2\pi(-m) h)dh + \sum_{m=1}^{\infty}\int_0^{\infty} P_k^h \sin(2\pi\nu h)\sin(2\pi m h)dh \\
&\overset{(3)}{=} -\sum_{m=1}^{\infty}\int_0^{\infty} P_k^h \sin(2\pi\nu h)\sin(2\pi m h)dh + \sum_{m=1}^{\infty}\int_0^{\infty} P_k^h \sin(2\pi\nu h)\sin(2\pi m h)dh \\
&= 0. \qquad \text{(B.5.10)}
\end{aligned}$$

In this calculation, (1) makes use of the fact that a sum can be divided. In particular, the sum is divided into negative values ($m \in (-\infty, -1]$), positive values ($m \in [1, \infty)$) and $m = 0$. Since $\sin(2\pi 0h) = 0$, the summand with $m = 0$ is equal to 0. The performance of a substitution in (2), with replacing m by $-m$, demands the subsequence inversion of the sum's summands. For the transformation (3), the linearity with respect to the sign of the sine function and the integral is used. At the end, there remains only the calculation of the integral IV. This is done by representing sine and cosine again as exponential functions:

$$\begin{aligned}
&\int_0^{\infty} P_k^h \qquad \sin(2\pi\nu h) \qquad \cos(2\pi m h) \quad dh \\
&= \int_0^{\infty} P_k^h \; \overbrace{\frac{e^{i2\pi\nu h} - e^{-i2\pi\nu h}}{2i}} \; \overbrace{\frac{e^{i2\pi m h} + e^{-i2\pi m h}}{2}} dh \\
&= \frac{1}{4i}\int_0^{\infty} P_k^h (e^{i2\pi\nu h} - e^{-i2\pi\nu h})(e^{i2\pi m h} + e^{-i2\pi m h})dh \\
&\overset{(1)}{=} \frac{1}{4i}\left[\int_0^{\infty} P_k^h e^{i2\pi\nu h} e^{i2\pi m h}dh + \int_0^{\infty} P_k^h e^{i2\pi\nu h} e^{-i2\pi m h}dh \;...\right. \\
&\qquad \left. - \left(\int_0^{\infty} P_k^h e^{-i2\pi\nu h} e^{i2\pi m h}dh + \int_0^{\infty} P_k^h e^{-i2\pi\nu h} e^{-i2\pi m h}dh\right)\right] \\
&\overset{(2)}{=} \frac{1}{4i}\left[\int_0^{\infty} P_k^h e^{i2\pi\nu h} e^{i2\pi m h}dh + \int_{-\infty}^{0} P_k^{-h} e^{-i2\pi\nu h} e^{i2\pi m h}dh \;... \qquad \text{(B.5.11)}\right. \\
&\qquad \left. - \left(\int_0^{\infty} P_k^h e^{-i2\pi\nu h} e^{i2\pi m h}dh + \int_{-\infty}^{0} P_k^{-h} e^{i2\pi\nu h} e^{i2\pi m h}dh\right)\right]. \qquad \text{(B.5.12)}
\end{aligned}$$

The penultimate step (1) not only the brackets are multiplied, but also the linearity of the integral function is used to divide the individual integral into four smaller integrals. Subsequently, a substitution is performed in (2) in which h is exchanged by $-h$, and the boundaries of integration have been reversed. Both, the substitution and the reversal of the integration boundaries, change the sign of the integral. Since this sign has been changed twice, it remains the same. (B.5.11) and (B.5.12) now contain the sum of (B.5.4). Now we find $P_k e^{i2\pi\nu}$ in the top line, and $P_k e^{-i2\pi\nu}$ in the bottom line. And now, due to (B.5.5), the integrals can be exchanged by the fractions:

$$\begin{aligned}
\int_0^{\infty} P_k^h \sin(2\pi\nu h)\cos(2\pi m h)dh &= \frac{1}{4i}\left[\int_{-\infty}^{\infty}(P_k^h e^{i2\pi\nu h})e^{i2\pi m h}dh - \int_{\infty}^{\infty}(P_k^h e^{-i2\pi\nu h})e^{i2\pi m h}dh\right] \\
&= \frac{1}{4i}\left[\frac{-2(\ln(P_k) + i2\pi\nu)}{(\ln(P_k) + i2\pi\nu)^2 + (2\pi m)^2} - \frac{-2(\ln(P_k) - i2\pi\nu)}{(\ln(P_k) - i2\pi\nu)^2 + (2\pi m)^2}\right].
\end{aligned}$$

Since the difference between a complex number and its complex conjugated counterpart yields the imaginary part ($\mathcal{I}(.)$) two times, the equation is equal to

$$\begin{aligned}&\frac{1}{4i}(2i)\mathcal{I}\left(\frac{-2(\ln(P_k)+i2\pi\nu)}{(\ln(P_k)+i2\pi\nu)^2+(2\pi m)^2}\right)\\&=\frac{1}{2}\mathcal{I}\left(\frac{-2(\ln(P_k)+i2\pi\nu)}{(\ln(P_k)+i2\pi\nu)^2+(2\pi m)^2}\right).\end{aligned}\tag{B.5.13}$$

To conclude these chapters, the solution (B.5.10) of the integral IV and the solution (B.5.13) of the integral V are inserted into the integral III (B.5.9):

$$\begin{aligned}&\int_{-\infty}^{\infty}P_k^{|h|}e^{-i2\pi mh}e^{-i2\pi\nu h}dh\\&=\frac{-2(\ln(P_k)+i2\pi\nu)}{(\ln(P_k)+i2\pi\nu)^2+(2\pi m)^2}-2i\frac{1}{2}\mathcal{I}\left(\frac{-2(\ln(P_k)+i2\pi\nu)}{(\ln(P_k)+i2\pi\nu)^2+(2\pi m)^2}\right)\\&=\frac{-2(\ln(P_k)+i2\pi\nu)}{(\ln(P_k)+i2\pi\nu)^2+(2\pi m)^2}-i\mathcal{I}\left(\frac{-2(\ln(P_k)+i2\pi\nu)}{(\ln(P_k)+i2\pi\nu)^2+(2\pi m)^2}\right).\end{aligned}$$

Thus, this formula represents the difference between a complex value and its imaginary part, therefore only leaving the real part of the complex value:

$$\int_{-\infty}^{\infty}P_k^{|h|}e^{-i2\pi mh}e^{-i2\pi\nu h}dh=\mathcal{R}\left(\frac{-2(\ln(P_k)+i2\pi\nu)}{(\ln(P_k)+i2\pi\nu)^2+(2\pi m)^2}\right).$$

For the FT of the continuous CF (see (B.5.3)), the result is:

$$\Gamma(\nu+m)=\sum_{k=1}^{p}A_k\mathcal{R}\left(\frac{-2(\ln(P_k)+i2\pi\nu)}{(\ln(P_k)+i2\pi\nu)^2+(2\pi m)^2}\right).\tag{B.5.14}$$

B.5.4 Dissolving the Sum (for Real Roots)

Solving the integral and inserting $\Gamma(\nu+m)$ from (B.5.14) in (B.5.1) results in

$$\Gamma(\nu)\circledast\sum_{l=-\infty}^{\infty}\delta(\nu-l)=\sum_{m=-\infty}^{\infty}\sum_{k=1}^{p}A_k\mathcal{R}\left(\frac{-2(\ln(P_k)+i2\pi\nu)}{(\ln(P_k)+i2\pi\nu)^2+(2\pi m)^2}\right).$$

Now, the infinite sum has to be solved. The first objective is to exchange the orders of the two sums and the real part:

$$\begin{aligned}\sum_{m=-\infty}^{\infty}\sum_{k=1}^{p}A_k\mathcal{R}\left(\frac{-2(\ln(P_k)+i2\pi\nu)}{(\ln(P_k)+i2\pi\nu)^2+(2\pi m)^2}\right)&\overset{(1)}{=}\sum_{k=1}^{p}\sum_{m=-\infty}^{\infty}A_k\mathcal{R}\left(\frac{-2(\ln(P_k)+i2\pi\nu)}{(\ln(P_k)+i2\pi\nu)^2+(2\pi m)^2}\right)\\&\overset{(2)}{=}\sum_{k=1}^{p}A_k\sum_{m=-\infty}^{\infty}\mathcal{R}\left(\frac{-2(\ln(P_k)+i2\pi\nu)}{(\ln(P_k)+i2\pi\nu)^2+(2\pi m)^2}\right)\\&\overset{(3)}{=}\sum_{k=1}^{p}A_k\mathcal{R}\left(\sum_{m=-\infty}^{\infty}\frac{-2(\ln(P_k)+i2\pi\nu)}{(\ln(P_k)+i2\pi\nu)^2+(2\pi m)^2}\right).\end{aligned}\tag{B.5.15}$$

For step (1), the order of the sums is exchanged. This allows to extract the weights A_p as constants from the inner sum in (2), and finally include the sum into $\mathcal{R}(.)$ in (3) (which is valid as $\mathcal{R}(a+b)=\mathcal{R}(a)+\mathcal{R}(b)\ \ \forall a,b\in\mathbb{C}$). Now, the sum can be solved individually without taking the real part or

the sum with index k into account. This way, the sum can be solved:

$$
\begin{aligned}
&\sum_{m=-\infty}^{\infty} \frac{-2(\ln(P_k)+i2\pi\nu)}{(\ln(P_k)+i2\pi\nu)^2+(2\pi m)^2} \\
&\overset{(1)}{=} \sum_{m=-\infty}^{-1} \frac{-2(\ln(P_k)+i2\pi\nu)}{(\ln(P_k)+i2\pi\nu)^2+(2\pi m)^2} + \frac{-2(\ln(P_k)+i2\pi\nu)}{(\ln(P_k)+i2\pi\nu)^2} + \sum_{m=1}^{\infty} \frac{-2(\ln(P_k)+i2\pi\nu)}{(\ln(P_k)+i2\pi\nu)^2+(2\pi m)^2} \\
&\overset{(2)}{=} \sum_{m=1}^{\infty} \frac{-2(\ln(P_k)+i2\pi\nu)}{(\ln(P_k)+i2\pi\nu)^2+(2\pi m)^2} + \frac{-2(\ln(P_k)+i2\pi\nu)}{(\ln(P_k)+i2\pi\nu)^2} + \sum_{m=1}^{\infty} \frac{-2(\ln(P_k)+i2\pi\nu)}{(\ln(P_k)+i2\pi\nu)^2+(2\pi m)^2} \\
&\overset{(3)}{=} \frac{-2(\ln(P_k)+i2\pi\nu)}{(\ln(P_k)+i2\pi\nu)^2} + 2\sum_{m=1}^{\infty} \frac{-2(\ln(P_k)+i2\pi\nu)}{(\ln(P_k)+i2\pi\nu)^2+(2\pi m)^2} \\
&\overset{(4)}{=} \frac{1}{(-\ln(P_k)-i2\pi\nu)/2} + 2\sum_{m=1}^{\infty} \frac{-2(\ln(P_k)+i2\pi\nu)}{(\ln(P_k)+i2\pi\nu)^2+(2\pi m)^2} \\
&\overset{(5)}{=} \frac{1}{(-\ln(P_k)-i2\pi\nu)/2} + 2\sum_{m=1}^{\infty} \frac{2^2(-\ln(P_k)-i2\pi\nu)/2}{((\ln(P_k)+i2\pi\nu)/2)^2 2^2+2^2(\pi m)^2} \\
&\overset{(6)}{=} \frac{1}{(-\ln(P_k)-i2\pi\nu)/2} + 2\sum_{m=1}^{\infty} \frac{(-\ln(P_k)-i2\pi\nu)/2}{((\ln(P_k)+i2\pi\nu)/2)^2+(\pi m)^2} \\
&\overset{(7)}{=} \frac{1}{(-\ln(P_k)-i2\pi\nu)/2} + 2\frac{(-\ln(P_k)-i2\pi\nu)}{2}\sum_{m=1}^{\infty} \frac{1}{((\ln(P_k)+i2\pi\nu)/2)^2+(\pi m)^2} \qquad \text{(B.5.16)} \\
&\overset{(8)}{=} \frac{1+P_k e^{i2\pi\nu}}{1-P_k e^{i2\pi\nu}}. \qquad \text{(B.5.17)}
\end{aligned}
$$

(1) divides the sum into three parts: the negative values ($m \in [-1,-\infty)$), the positive values ($m \in [1,\infty)$), and $m = 0$. Since m is squared, the sumands for $-m$ and m are the same and will therefore get replaced for each other in (2). As a result, the sums are equal and can be summarised in (3). After that, the first summand has to be put into the form $\frac{1}{x}$ by dividing the fraction by the numerator (step (4)). In (5), for each summand the sum, $[-\ln(P_k) \pm i2\pi\nu]$ is replaced by $2[-\ln(P_k) - i2\pi\nu]/2$. This is done for the denominators as well as for the counters. This representation allows the simplification of the fraction in (6), whereby 2^2 was reduced in the nominator and in the denominator. Finally, in (7), the numerator is extracted from the sum.
Step (8) is quite technical and is shown here separately: In Abramowitz et al. 1964, p. 83, eq. (4.5.12), the transformation between the $\coth(x)$ and $\cot(x)$ is represented by

$$\coth(x) = i\cot(ix).$$

In addition, the sum representation of the $\cot(x)$ (see Abramowitz et al. (1964, p. 75, eq. (4.3.91))) is given as:

$$\cot(x) = \frac{1}{x} + 2x\sum_{k=1}^{\infty} \frac{1}{x^2-(k\pi)^2}.$$

The combination of both sums results in the following sum representatin of $\coth(x)$:

$$\begin{aligned}\coth(x) &= i\left(\frac{1}{ix} + 2ix\sum_{k=1}^{\infty}\frac{1}{(ix)^2-(k\pi)^2}\right)\\ &= \frac{1}{x} + 2(-1)x\sum_{k=1}^{\infty}\frac{1}{(ix)^2-(k\pi)^2}\\ &= \frac{1}{x} + 2(-1)x\sum_{k=1}^{\infty}\frac{1}{-x^2-(k\pi)^2}\\ &= \frac{1}{x} + 2x\sum_{k=1}^{\infty}\frac{1}{x^2+(k\pi)^2}.\end{aligned}$$

Using $x = (-\ln(P_k) - i2\pi\nu)/2$ gives that (B.5.16) is equal to $\coth((-\ln(P_k) - i2\pi\nu)/2)$. If $\coth(x)$ is replaced by $\cosh(x)/\sinh(x)$, with

$$\cosh(x) = \frac{e^x + e^{-x}}{2} \qquad \text{and} \qquad \sinh(x) = \frac{e^x - e^{-x}}{2}$$

(see: Abramowitz et al. (1964, p.83, eq. (4.5.1), (4.5.2) and (4.5.6))), it becomes visible that

$$\coth(x) = \frac{e^x + e^{-x}}{e^x - e^{-x}} = \frac{e^x(1+e^{-2x})}{e^x(1-e^{-2x})} = \frac{1+e^{-2x}}{1-e^{-2x}}.$$

Since $x = (-\ln(P_k) - i2\pi\nu)/2$ is still valid, it follows:

$$\coth((-\ln(P_k) - i2\pi\nu)/2) = \frac{1+P_k e^{i2\pi\nu}}{1-P_k e^{i2\pi\nu}},$$

which proves that the transformation (8) in (B.5.16) is valid.

B.5.5 Conclusion

Thus, the convolution of the continuous CF and the DC can be described by inserting (B.5.17) in (B.5.15), yielding the function

$$\Gamma(\nu) \circledast \sum_{l=-\infty}^{\infty}\delta(\nu - l) = \sum_{k=1}^{p} A_k \mathcal{R}\left(\frac{1+P_k e^{i2\pi\nu}}{1-P_k e^{i2\pi\nu}}\right)$$

for real-valued roots. Facilitating the division into the real and the imaginary part, requiring the multiplication of the fraction with the complex conjugated value of the denominator divided by itself:

$$\begin{aligned}\frac{1+P_k e^{i2\pi\nu}}{1-P_k e^{i2\pi\nu}} &= \frac{1+P_k e^{i2\pi\nu}}{1-P_k e^{i2\pi\nu}}\frac{1-P_k e^{-i2\pi\nu}}{1-P_k e^{-i2\pi\nu}}\\ &= \frac{1+P_k e^{i2\pi\nu} - P_k e^{-i2\pi\nu} - P_k^2(e^{i2\pi\nu}e^{-i2\pi\nu})}{1-P_k e^{i2\pi\nu} - P_k e^{-i2\pi\nu} + {P_k}^2(e^{i2\pi\nu}e^{-i2\pi\nu})}\\ &= \frac{1+2i\mathcal{I}\left(P_k e^{i2\pi\nu}\right) - P_k^2}{1-2\mathcal{R}(P_k e^{i2\pi\nu}) + {P_k}^2}.\end{aligned} \tag{B.5.18}$$

Now the fraction's real part can be separated by removing the imaginary part from the numerator. This result, combined with (B.5.15), provides the general solution of the convolution in cases where all roots are real valued:

$$\begin{aligned}\Gamma(\nu) \circledast \sum_{l=-\infty}^{\infty}\delta(\nu - l) &= \sum_{k=1}^{p} A_k \mathcal{R}\left(\frac{1+2i\mathcal{I}\left(P_k e^{i2\pi\nu}\right) - P_k^2}{1-2\mathcal{R}(P_k e^{i2\pi\nu}) + {P_k}^2}\right)\\ &= \sum_{k=1}^{p} A_k \frac{1-P_k^2}{1-2\mathcal{R}(P_k e^{i2\pi\nu}) + {P_k}^2}.\end{aligned} \tag{B.5.19}$$

The first three subsections of this section are valid, even if the roots are complex valued. Starting in (B.5.2), it is possible to divide the sum into complex conjugated pairs of roots and real-valued roots:

$$\begin{aligned}\Gamma(\nu+m) &= \sum_{k=1}^{p} A_k \int_{-\infty}^{\infty} P_k^{|h|} e^{-i2\pi mh} e^{-i2\pi\nu h} dh \\ &= \underbrace{\sum_{k=1}^{2p_1} A_k \int_{-\infty}^{\infty} P_k^{|h|} e^{-i2\pi mh} e^{-i2\pi\nu h} dh}_{\text{sum of the complex-valued roots}} + \underbrace{\sum_{k=2p_1+1}^{p} A_k \int_{-\infty}^{\infty} P_k^{|h|} e^{-i2\pi mh} e^{-i2\pi\nu h} dh}_{\text{sum of the real-valued roots}}.\end{aligned}$$

The derivative from the section B.5.1 and B.5.2 apply for the sum of the real roots, while the formula for the complex conjugated pairs is found in section B.6.2.

B.6 Comparison between the Sampled Continuous CF and the Discrete CF for AR Processes of Order 1 and 2

This section demonstrates, that the FT of the CF $\Gamma(\nu)$ (see (B.4.4)) can be transferred to the FT of the discrete CF $\mathcal{H}^2(\nu)$ (see (3.2.1)) by a convolution with the DC (see (B.5.19)). This happens is done for two cases: first, in case of the AR(1) process, it provides the proof that the formulas (B.5.19) and (B.3.1) are identical. And secondly, it also proves that this equality holds also for the AR(2) process with two complex roots. Since, as mentioned before, each AR(p) process is a composition of AR(1) processes and AR(2) processes with two complex conjugate roots, it is sufficient to only consider these two cases.

B.6.1 Comparison of the Spectra for the AR(1) Process

It is now intended to prove that the PSD of the AR(1) process (which is shown in (B.3.1)):

$$\mathcal{H}^2(\nu) = \frac{\sigma_\varepsilon^2}{1 - 2P_1\cos(2\pi\nu) + P_1^2}. \tag{B.6.1}$$

and (B.5.19) for order $p = 1$:

$$\begin{aligned}\Gamma(\nu) \circledast \sum_{l=-\infty}^{\infty} \delta(\nu - l) &= A_1 \frac{1 - P_1^2}{1 - 2\mathcal{R}(P_1 e^{i2\pi\nu}) + P_1^2} \\ &\overset{(1)}{=} A_1 \frac{1 - P_1^2}{1 - 2P_1\cos(2\pi\nu) + P_1^2} \\ &\overset{(2)}{=} \frac{\sigma_\varepsilon^2}{1 - P_1^2} \frac{1 - P_1^2}{1 - 2P_1\cos(2\pi\nu) + P_1^2} \\ &= \frac{\sigma_\varepsilon^2}{1 - 2P_1\cos(2\pi\nu) + P_1^2}.\end{aligned} \tag{B.6.2}$$

are the same formula. Here, due to the fact that P_1 is real-valued for the AR(1) process, (1) derives from the equations $\mathcal{R}(P_1 e^{i2\pi\nu}) = P_1\cos(2\pi\nu)$. For A_1, equation (2) uses the weight calculated in (B.1.3). Since (B.6.1) and (B.6.2) are the same, the equality for the AR(1) process is proven.

B.6.2 Comparison of the Spectra for the AR(2) Process

The same can be shown for the AR(2) process with two complex conjugated roots ($P_1 = P_2^*$). Here, the PSD of the AR(2) process is obtained by the means of (B.3.3):

$$\begin{aligned}&\mathcal{H}^2(\nu)\\ &=\frac{\sigma_\mathcal{E}^2}{1-2(P_1+P_2)\cos(2\pi\nu)+P_1^2+P_2^2+P_1P_2(2+2\cos(4\pi\nu)-2(P_1+P_2)\cos(2\pi\nu)+P_1P_2)}.\end{aligned} \tag{B.6.3}$$

In order to compare this function with the result of the convolution ($\Gamma(\nu) \circledast \sum_{l=-\infty}^{\infty}\delta(\nu-l)$), and since (B.5.19) only applies to real roots, the convolution has to be derived again for a pair of complex conjugated roots starting from (B.5.2). The derivative is then divided into several steps. As such, section B.6.2.1 shows how the integral can be transformed from integrals including complex values to integrals including the distance r. Here r is the absolute value of the complex value. This results in two integrals, which are respectively solved in the sections B.6.2.2 and B.6.2.3. Section B.6.2.4 brings these integrals together. In the end the result is summarized in section B.6.2.5 and compared with the PSD in (B.6.3).

B.6.2.1 Conversion into Integrals via Real Values

The roots P_1 and P_2 of a TVAR(2) process are replaced by

$$P_1^{|h|} = r^{|h|}e^{i\phi|h|} \qquad\qquad P_2^{|h|} = r^{|h|}e^{i-\phi|h|}. \tag{B.6.4}$$

These are used in (B.5.2) with the intent to transform the integral. For all following integrals, the complex values are replaced by the radius r, for which the integral can be solved the same way as it was in the case of the real roots:

$$\sum_{m=-\infty}^{\infty}\int_{-\infty}^{\infty}\underbrace{\left(\underbrace{A_1P_1^{|h|}}_{\in\mathbb{C}}+\underbrace{A_2P_2^{|h|}}_{\in\mathbb{C}}\right)}_{\in\mathbb{R}}e^{-i2\pi mh}e^{-i2\pi\nu h}dh.$$

This leads us to in the first step of the transformation, which consists of the conversion of the sum of a complex conjugate pair into a real number

$$\begin{aligned}A_1P_1^{|h|}+A_2P_2^{|h|} &\overset{(1)}{=} A_1P_1^{|h|}+A_1^*(P_1^{|h|})^*\\ &= 2\mathcal{R}\left(A_1P_1^{|h|}\right)\\ &\overset{(2)}{=} 2\left(\mathcal{R}\left(A_1\right)\mathcal{R}\left(P_1^{|h|}\right)-\mathcal{I}\left(A_1\right)\mathcal{I}\left(P_1^{|h|}\right)\right).\end{aligned}$$

This transformation is achieved by using $A_2 = A_1^*$ if $P_2 = P_1^*$ for (1), while taking advantage of the fact that for two complex values c_1, c_2 $\mathcal{R}\left(c_1c_2\right) = \mathcal{R}\left(c_1\right)\mathcal{R}\left(c_2\right) - \mathcal{I}\left(c_1\right)\mathcal{I}\left(c_2\right)$ applies (see (2)). The real and imaginary part of A_1 have already been derived in (B.1.6) and (B.1.7). For the root, on the other hand, P_1 must be exchanged by (B.6.4):

$$\mathcal{R}\left(r^{|h|}e^{i\phi|h|}\right) = r^{|h|}\cos(\phi|h|) \qquad \text{and} \qquad \mathcal{I}\left(r^{|h|}e^{i\phi|h|}\right) = r^{|h|}\sin(\phi|h|).$$

The next step removes the sine and cosine by replacing them with the exponential function.

$$
\begin{aligned}
&\sum_{m=-\infty}^{\infty}\int_{-\infty}^{\infty} 2\left(\mathcal{R}\left(A_1\right) r^{|h|} \quad \cos(\phi|h|) - \mathcal{I}\left(A_1\right) r^{|h|} \quad \sin(\phi|h|)\right) e^{-i2\pi mh} e^{-i2\pi\nu h} dh \\
&= \sum_{m=-\infty}^{\infty}\int_{-\infty}^{\infty} 2\left(\mathcal{R}\left(A_1\right) r^{|h|} \overbrace{\frac{e^{i\phi|h|}+e^{-i\phi|h|}}{2}} - \mathcal{I}\left(A_1\right) r^{|h|} \overbrace{\frac{e^{i\phi|h|}-e^{-i\phi|h|}}{2}}\right) e^{-i2\pi mh} e^{-i2\pi\nu h} dh \\
&\overset{(1)}{=} \sum_{m=-\infty}^{\infty}\int_{-\infty}^{\infty} \mathcal{R}\left(A_1\right) r^{|h|}(e^{i\phi|h|}+e^{-i\phi|h|}) e^{-i2\pi mh} e^{-i2\pi\nu h} dh ... \\
&\quad - \sum_{m=-\infty}^{\infty}\int_{-\infty}^{\infty} \mathcal{I}\left(A_1\right) r^{|h|}(e^{i\phi|h|}-e^{-i\phi|h|}) e^{-i2\pi mh} e^{-i2\pi\nu h} dh \\
&= \mathcal{R}\left(A_1\right) \sum_{m=-\infty}^{\infty}\int_{-\infty}^{\infty} r^{|h|}(e^{i\phi|h|}+e^{-i\phi|h|}) e^{-i2\pi mh} e^{-i2\pi\nu h} dh ... \\
&\quad - \mathcal{I}\left(A_1\right) \sum_{m=-\infty}^{\infty}\int_{-\infty}^{\infty} r^{|h|}(e^{i\phi|h|}-e^{-i\phi|h|}) e^{-i2\pi mh} e^{-i2\pi\nu h} dh \\
&\overset{(2)}{=} \mathcal{R}\left(A_1\right) \underbrace{\sum_{m=-\infty}^{\infty}\left(\int_{-\infty}^{\infty} r^{|h|} e^{i\phi|h|} e^{-i2\pi mh} e^{-i2\pi\nu h} dh + \int_{-\infty}^{\infty} r^{|h|} e^{-i\phi|h|} e^{-i2\pi mh} e^{-i2\pi\nu h} dh\right)}_{:=I} ... \\
&\quad - \mathcal{I}\left(A_1\right) \underbrace{\sum_{m=-\infty}^{\infty}\left(\int_{-\infty}^{\infty} r^{|h|} e^{i\phi|h|} e^{-i2\pi mh} e^{-i2\pi\nu h} dh - \int_{-\infty}^{\infty} r^{|h|} e^{-i\phi|h|} e^{-i2\pi mh} e^{-i2\pi\nu h} dh\right)}_{:=II} . \qquad \text{(B.6.5)}
\end{aligned}
$$

In step (1) the linearity of the sum and the integral are used to separate the part with $\mathcal{R}(A_1)$ from the part with $\mathcal{I}(A_1)$. In order to arrive at the solution (2), the integral is split at the minus sign, allowing the application of the transformations from above in the resulting integrals. The advantage of this procedure is that the $\mathcal{R}(A_1)$ and $\mathcal{I}(A_1)$ are now outside the integral, while this formula, due to r, also states a FT of a real-valued number, like in the case of the AR(1) process.

B.6.2.2 Solving Integral I

To solve integral I, the first exponential function ($e^{i\phi|h|}$) has to be removed. This allows to get the same representation as in the AR(1) process, for which the integral has already been solved in section B.5. This is done simultaneously for the pair of integrals in I:

$$
\begin{aligned}
&\int_{-\infty}^{\infty} r^{|h|} e^{i\phi|h|} e^{-i2\pi mh} e^{-i2\pi\nu h} dh + \int_{-\infty}^{\infty} r^{|h|} e^{-i\phi|h|} e^{-i2\pi mh} e^{-i2\pi\nu h} dh \\
&= \int_{-\infty}^{0} r^{|h|} e^{i\phi|h|} e^{-i2\pi mh} e^{-i2\pi\nu h} dh + \int_{0}^{\infty} r^{|h|} e^{i\phi|h|} e^{-i2\pi mh} e^{-i2\pi\nu h} dh ... \\
&\quad + \int_{-\infty}^{0} r^{|h|} e^{-i\phi|h|} e^{-i2\pi mh} e^{-i2\pi\nu h} dh + \int_{0}^{\infty} r^{|h|} e^{-i\phi|h|} e^{-i2\pi mh} e^{-i2\pi\nu h} dh \\
&\overset{(1)}{=} \int_{-\infty}^{0} r^{|h|} e^{-i\phi h} e^{-i2\pi mh} e^{-i2\pi\nu h} dh + \int_{0}^{\infty} r^{|h|} e^{i\phi h} e^{-i2\pi mh} e^{-i2\pi\nu h} dh ... \\
&\quad + \int_{-\infty}^{0} r^{|h|} e^{i\phi h} e^{-i2\pi mh} e^{-i2\pi\nu h} dh + \int_{0}^{\infty} r^{|h|} e^{-i\phi h} e^{-i2\pi mh} e^{-i2\pi\nu h} dh \\
&\overset{(2)}{=} \int_{-\infty}^{0} r^{|h|} e^{-i2\pi mh} e^{-i2\pi(\nu+\phi/(2\pi))h} dh + \int_{0}^{\infty} r^{|h|} e^{-i2\pi mh} e^{-i2\pi(\nu-\phi/(2\pi))h} dh ... \\
&\quad + \int_{-\infty}^{0} r^{|h|} e^{-i2\pi mh} e^{-i2\pi(\nu-\phi/(2\pi))h} dh + \int_{0}^{\infty} r^{|h|} e^{-i2\pi mh} e^{-i2\pi(\nu+\phi/(2\pi))h} dh .
\end{aligned}
$$

(1), makes use of $e^{i\phi|h|} = e^{i\phi h}$ if the integration boundaries are positive, and of $e^{i\phi|h|} = e^{-i\phi h}$ if the integration boundaries are negative. Since the first exponential function no longer contains the absolute value of h, it can be combined with $e^{-i2\pi\nu h}$ in (2).
Submerging the green or yellow-backed integrals together in pairs results in two integrals, which have already been solved for the AR(1) process in section B.5. $\nu^+ := \nu + \phi/(2\pi)$ and $\nu^- := \nu - \phi/(2\pi)$ are defined for further editing. Using this notation, the sums can be transformed by (B.5.19):

$$\begin{aligned}
&\underbrace{\sum_{m=-\infty}^{\infty}\int_{-\infty}^{\infty} r^{|h|}e^{-i2\pi mh}e^{-i2\pi\nu^+ h}dh}_{} && + \underbrace{\sum_{m=-\infty}^{\infty}\int_{-\infty}^{\infty} r^{|h|}e^{-i2\pi mh}e^{-i2\pi\nu^- h}dh}_{}\\
&= \frac{1-r^2}{1-2\mathcal{R}(re^{i2\pi\nu^+})+r^2} && + \frac{1-r^2}{1-2\mathcal{R}(re^{i2\pi\nu^-})+r^2}\\
&= \frac{1-r^2}{1-2r\cos(2\pi\nu^+)+r^2} && + \frac{1-r^2}{1-2r\cos(2\pi\nu^-)+r^2}\\
&= \frac{1-r^2}{1-2r\cos(2\pi\nu+\phi)+r^2} && + \frac{1-r^2}{1-2r\cos(2\pi\nu-\phi)+r^2}\\
&\overset{(1)}{=} \frac{1-r^2}{(1-re^{i(2\pi\nu+\phi)})(1-re^{-i(2\pi\nu+\phi)})} && + \frac{1-r^2}{(1-re^{i(2\pi\nu-\phi)})(1-re^{-i(2\pi\nu-\phi)})},
\end{aligned}$$

where the last transformation (1) follows from (B.5.18). Now $(1-r^2)$ is excluded and the two fractions are expanded to the same denominator:

$$(1-r^2)\frac{(1-re^{i(2\pi\nu-\phi)})(1-re^{-i(2\pi\nu-\phi)})+(1-re^{i(2\pi\nu+\phi)})(1-re^{-i(2\pi\nu+\phi)})}{(1-re^{i(2\pi\nu+\phi)})(1-re^{-i(2\pi\nu+\phi)})(1-re^{i(2\pi\nu-\phi)})(1-re^{-i(2\pi\nu-\phi)})}.$$

Multiplying the two brackets allows to simplify the numerator. This result is already known from the derivative of (B.3.1):

$$\begin{aligned}
&(1-r^2)\frac{(1-2r\cos(2\pi\nu-\phi)+r^2)+(1-2r\cos(2\pi\nu+\phi)+r^2)}{(1-re^{i(2\pi\nu+\phi)})(1-re^{-i(2\pi\nu+\phi)})(1-re^{i(2\pi\nu-\phi)})(1-re^{-i(2\pi\nu-\phi)})}\\
&= (1-r^2)\frac{2-2r\cos(2\pi\nu-\phi)-2r\cos(2\pi\nu+\phi)+2r^2}{(1-re^{i(2\pi\nu+\phi)})(1-re^{-i(2\pi\nu+\phi)})(1-re^{i(2\pi\nu-\phi)})(1-re^{-i(2\pi\nu-\phi)})}.
\end{aligned}$$

And the cosine terms can be put together with the help of the addition theorems:

$$\begin{aligned}
&\sum_{m=-\infty}^{\infty}\left(\int_{-\infty}^{\infty} r^{|h|}e^{i\phi|h|}e^{-i2\pi mh}e^{-i2\pi\nu h}dh + \int_{-\infty}^{\infty} r^{|h|}e^{-i\phi|h|}e^{-i2\pi mh}e^{-i2\pi\nu h}dh\right)\\
&= (1-r^2)\frac{2-4r\cos(2\pi\nu)\cos(\phi)+2r^2}{(1-re^{i(2\pi\nu+\phi)})(1-re^{-i(2\pi\nu+\phi)})(1-re^{i(2\pi\nu-\phi)})(1-re^{-i(2\pi\nu-\phi)})}.
\end{aligned} \tag{B.6.6}$$

B.6.2.3 Solving Integral II

Continue with integral II. Here, the first part, equals the steps undertaken for integral I, only that the addition turns into a subtraction:

$$\begin{aligned}
&\int_{-\infty}^{\infty} r^{|h|}e^{i\phi|h|}e^{-i2\pi mh}e^{-i2\pi\nu h}dh - \int_{-\infty}^{\infty} r^{|h|}e^{-i\phi|h|}e^{-i2\pi mh}e^{-i2\pi\nu h}dh\\
&= \int_{-\infty}^{0} r^{|h|}e^{-i2\pi mh}e^{-i2\pi\nu^+ h}dh + \int_{0}^{\infty} r^{|h|}e^{-i2\pi mh}e^{-i2\pi\nu^- h}dh \ldots\\
&\quad - \int_{-\infty}^{0} r^{|h|}e^{-i2\pi mh}e^{-i2\pi\nu^- h}dh - \int_{0}^{\infty} r^{|h|}e^{-i2\pi mh}e^{-i2\pi\nu^+ h}dh.
\end{aligned}$$

While we again join the integrals of the same colour, we solve them separately. First, the borders of the first yellow integral are swapped:

$$\begin{aligned}\int_{-\infty}^{0} r^{|h|}e^{-i2\pi mh}e^{-i2\pi\nu^{+}h}dh &\overset{(1)}{=} \int_{-\infty}^{0} r^{-h}e^{-i2\pi mh}e^{-i2\pi\nu^{+}h}dh \\ &\overset{(2)}{=} -\int_{\infty}^{0} r^{\bar{h}}e^{i2\pi m\bar{h}}e^{i2\pi\nu^{+}\bar{h}}d\bar{h} \\ &\overset{(3)}{=} \int_{0}^{\infty} r^{\bar{h}}e^{-i2\pi m\bar{h}}e^{i2\pi\nu^{+}\bar{h}}d\bar{h}. \end{aligned} \tag{B.6.7}$$

Thus, the integral boundaries are reversed by three steps: first, I replacing the absolute function in (1), then substitute $-h$ with $\bar{h}$ (which involves a sign change for step (2)) and finally (3) exchange the integration boundaries, which reverses the sign changes. Since both yellow-coloured integrals now have the same boundaries, they can be solved together:

$$\begin{aligned}&\left(\int_{0}^{\infty} r^{\bar{h}}e^{-i2\pi m\bar{h}}e^{i2\pi\nu^{+}\bar{h}}d\bar{h} - \int_{0}^{\infty} r^{|h|}e^{-i2\pi mh}e^{-i2\pi\nu^{+}h}dh\right) \\ &\overset{(1)}{=} \int_{0}^{\infty} r^{h}\left(\underbrace{e^{i2\pi mh} - e^{-i2\pi mh}}\right)e^{-i2\pi\nu^{+}h}dh \\ &= \int_{0}^{\infty} r^{h} \quad 2i\sin(2\pi\nu h)e^{-i2\pi\nu^{+}h}dh \\ &= 2i\int_{0}^{\infty} r^{h}\sin(2\pi\nu h)e^{-i2\pi\nu^{+}h}dh.\end{aligned}$$

In (1) integrals not only have been contracted, but the same factors also have been isolated, leaving only the difference in brackets. This integral is equal to the integral III of (B.5.8), which has been calculated using (B.5.13). Thus,

$$\begin{aligned}2i\int_{0}^{\infty} r^{h}\sin(2\pi\nu h)e^{-i2\pi\nu^{+}h}dh &= 2i\frac{1}{2}\mathcal{I}\left(\frac{-2(\ln(P_k)+i2\pi\nu)}{(\ln(P_k)+i2\pi\nu)^2+(2\pi m)^2}\right) \\ &= i\mathcal{I}\left(\frac{-2(\ln(P_k)+i2\pi\nu)}{(\ln(P_k)+i2\pi\nu)^2+(2\pi m)^2}\right).\end{aligned}$$

Up to now, the infinite sum has been neglected for this integral. Since $\mathcal{I}(.)$ is a linear function with respect to addition, the infinite sum of the imaginary part is equal to the imaginary part of the sums. For this sum, the result has also already been calculated and can be found in (B.5.18). This time, we are interested in the imaginary part:

$$\begin{aligned}i\mathcal{I}\left(\sum_{m=-\infty}^{\infty}\frac{-2(\ln(P_k)+i2\pi\nu)}{(\ln(P_k)+i2\pi\nu)^2+(2\pi m)^2}\right) &= i\mathcal{I}\left(\frac{1+2i\mathcal{I}\left(P_k e^{i2\pi\nu}\right)-|P_k|^2}{1-2\mathcal{R}(P_k e^{i2\pi\nu})+|P_k|^2}\right) \\ &= i\frac{2\mathcal{I}\left(P_k e^{i2\pi\nu}\right)}{1-2\mathcal{R}(P_k e^{i2\pi\nu})+|P_k|^2} \\ &\overset{(1)}{=} i\frac{2r\sin(2\pi\nu+\phi)}{1-2\mathcal{R}(P_k e^{i2\pi\nu})+|P_k|^2} \\ &\overset{(2)}{=} i\frac{2r\sin(2\pi\nu+\phi)}{1-2r\cos(2\pi\nu+\phi)+r^2}.\end{aligned} \tag{B.6.8}$$

For the transformation (1), we use $P_1 = re^{i\phi}$ to merge the exponential functions $e^{i\phi}$ and $e^{i2\pi\nu}$ as above. The same happens in (2) with the denominator with the real part -here $|P_1| = r$ is additionally replaced. In the end, the only thing missing is the green-backed integral, which can be traced back to the yellow-backed one:

$$\begin{aligned}&\int_{0}^{\infty} r^{|h|}e^{-i2\pi mh}e^{-i2\pi\nu^{-}h}dh - \int_{-\infty}^{0} r^{|h|}e^{-i2\pi mh}e^{-i2\pi\nu^{-}h}dh \\ &= -\left(-\int_{0}^{\infty} r^{|h|}e^{-i2\pi mh}e^{-i2\pi\nu^{-}h}dh + \int_{-\infty}^{0} r^{|h|}e^{-i2\pi mh}e^{-i2\pi\nu^{-}h}dh\right).\end{aligned}$$

The Integrals in the brackets are the same as the first ones that are marked in yellow, except that v^+ has been replaced by v^-. This allows the sum and the integral to be solved directly by (B.6.8):

$$\int_0^\infty r^{|h|}e^{-i2\pi mh}e^{-i2\pi\nu^- h}dh - \int_0^\infty r^{|h|}e^{-i2\pi mh}e^{-i2\pi\nu^- h}dh = -i\frac{2r\sin(2\pi\nu-\phi)}{1-2r\cos(2\pi\nu-\phi)+r^2}. \quad \text{(B.6.9)}$$

In order to solve the integral II, the partial results of (B.6.8) and (B.6.9) are added and expanded to the same denominator:

$$\begin{aligned}
&i\frac{2r\sin(2\pi\nu+\phi)}{1-2r\cos(2\pi\nu+\phi)+r^2} - i\frac{2r\sin(2\pi\nu-\phi)}{1-2r\cos(2\pi\nu-\phi)+r^2}\\
&= \frac{2ir\sin(2\pi\nu+\phi)}{1-2r\cos(2\pi\nu+\phi)+r^2} - \frac{2ir\sin(2\pi\nu-\phi)}{1-2r\cos(2\pi\nu-\phi)+r^2}\\
&= \frac{2ir\sin(2\pi\nu+\phi)(1-2r\cos(2\pi\nu+\phi)+r^2) - 2ir\sin(2\pi\nu-\phi)(1-2r\cos(2\pi\nu-\phi)+r^2)}{(1-2r\cos(2\pi\nu+\phi)+r^2)(1-2r\cos(2\pi\nu-\phi)+r^2)}\\
&= \frac{2ir\sin(2\pi\nu+\phi)(1-2r\cos(2\pi\nu+\phi)+r^2) - 2ir\sin(2\pi\nu-\phi)(1-2r\cos(2\pi\nu-\phi)+r^2)}{(1-re^{i(2\pi\nu+\phi)})(1-re^{-i(2\pi\nu+\phi)})(1-re^{i(2\pi\nu-\phi)})(1-re^{-i(2\pi\nu-\phi)})}.
\end{aligned}$$

The nominator is the only part that is relevant in the following transformations. So, for reasons of simplicity, the denominator is omitted. In the first step, we dissolve the brackets:

$$\begin{aligned}
&2r\sin(2\pi\nu+\phi)(1-2r\cos(2\pi\nu-\phi)+r^2) && -2r\sin(2\pi\nu-\phi)(1-2r\cos(2\pi\nu+\phi)+r^2)\\
&= -2r\sin(2\pi\nu+\phi)2r\cos(2\pi\nu-\phi) && +2r\sin(2\pi\nu+\phi)(1+r^2)...\\
&+2r\sin(2\pi\nu-\phi)2r\cos(2\pi\nu+\phi) && -2r\sin(2\pi\nu-\phi)(1+r^2).
\end{aligned}$$

Summing up the left and right columns individually, allows to use the addition theorem for the sine in the first column:

$$\begin{aligned}
&-2r\sin(2\pi\nu+\phi)2r\cos(2\pi\nu-\phi) + 2r\sin(2\pi\nu-\phi)2r\cos(2\pi\nu+\phi)\\
&= -4r^2(\sin(2\pi\nu+\phi)\cos(2\pi\nu-\phi) - \sin(2\pi\nu-\phi)\cos(2\pi\nu+\phi))\\
&= -4r^2\sin((2\pi\nu+\phi)-(2\pi\nu-\phi))\\
&= -4r^2\sin(2\phi)\\
&= -8r^2\sin(\phi)\cos(\phi). \qquad \text{(B.6.10)}
\end{aligned}$$

We now also apply the addition theorem of the sine in the right column, but the other way around:

$$\begin{aligned}
&2r\sin(2\pi\nu+\phi)(1+r^2) - 2r\sin(2\pi\nu-\phi)(1+r^2)\\
&= 2r(1+r^2) \qquad (\sin(2\pi\nu+\phi) \qquad - \qquad \sin(2\pi\nu-\phi))\\
&= 2r(1+r^2)(\overbrace{\sin(2\pi\nu)\cos(\phi)+\cos(2\pi\nu)\sin(\phi)} - (\overbrace{\sin(2\pi\nu)\cos(\phi)-\cos(2\pi\nu)\sin(\phi)}))\\
&= 4r(1+r^2)\cos(2\pi\nu)\sin(\phi) \qquad \text{(B.6.11)}
\end{aligned}$$

Finally, the two parts (B.6.10) and (B.6.11) are combined into the numerator, which is inserted back into the fraction, thus solving the integral II:

$$\begin{aligned}
&\sum_{m=-\infty}^{\infty}\left(\int_{-\infty}^{\infty} r^{|h|}e^{i\phi|h|}e^{-i2\pi mh}e^{-i2\pi\nu h}dh - \int_{-\infty}^{\infty} r^{|h|}e^{-i\phi|h|}e^{-i2\pi mh}e^{-i2\pi\nu h}dh\right)\\
&= \frac{\sin(\phi)[-8r\cos(\phi)+(1+r^2)4r\cos(2\pi\nu)]}{(1-re^{i(2\pi\nu+\phi)})(1-re^{-i(2\pi\nu+\phi)})(1-re^{i(2\pi\nu-\phi)})(1-re^{-i(2\pi\nu-\phi)})}. \qquad \text{(B.6.12)}
\end{aligned}$$

B.6.2.4 Merging of the Integrals

Since integral I with solution (B.6.6) and integral II with solution (B.6.12) have the same denominator

$$\frac{1}{(1-re^{i(2\pi\nu+\phi)})(1-re^{-i(2\pi\nu+\phi)})(1-re^{i(2\pi\nu-\phi)})(1-re^{-i(2\pi\nu-\phi)})}, \qquad \text{(B.6.13)}$$

the two integrals in (B.6.5) are subtracted from each other by subtracting the numerators. So, for reasons of simplicity, the denominator is omitted once more. Rephrasing (B.6.5) should show that the numerator

$$\begin{aligned}&\mathcal{R}\left(A_1\right)(1-r^2)(2-4r\cos(2\pi\nu)\cos(\phi)+2r^2)\\&-\mathcal{I}\left(A_1\right)\sin(\phi)(1+r^2)\left[-\frac{8r\cos(\phi)}{1+r^2}+4r\cos(2\pi\nu)\right]\end{aligned}\tag{B.6.14}$$

is equal to $\sigma_{\mathcal{E}}^2$. Unfortunately, the numerator's terms still contain the real and the imaginary part of weight A_1, and must therefore be rewritten by the functions of r and ϕ. For this purpose, $\mathcal{I}(A_1)$ is converted by (B.1.8) into $\mathcal{R}(A_1)$:

$$\begin{aligned}\mathcal{I}(A_1)&=\frac{1}{i}\left(-\frac{(P_1+P_2)(1-P_1P_2)}{(P_2-P_1)(1+P_1P_2)}\mathcal{R}\left(A\right)\right)\\&=\frac{1}{i}\left(-\frac{2r\cos(\phi)(1-r^2)}{-2ir\sin(\phi)(1+r^2)}\mathcal{R}\left(A\right)\right)\\&=-\frac{2r\cos(\phi)(1-r^2)}{2r\sin(\phi)(1+r^2)}\mathcal{R}\left(A\right)\\&=-\frac{\cos(\phi)(1-r^2)}{\sin(\phi)(1+r^2)}\mathcal{R}\left(A\right).\end{aligned}$$

If $\mathcal{I}(A_1)$ is now inserted in (B.6.14), the denominator of $\mathcal{I}(A_1)$ is eliminated and $\mathcal{R}(A_1)(1-r^2)$ can be excluded:

$$\begin{aligned}&\mathcal{R}\left(A_1\right)(1-r^2)\left[2-4r\cos(2\pi\nu)\cos(\phi)+2r^2+\cos(\phi)\left[-\frac{8r\cos(\phi)}{1+r^2}+4r\cos(2\pi\nu)\right]\right]\\=&\mathcal{R}\left(A_1\right)(1-r^2)\left[2-4r\cos(2\pi\nu)\cos(\phi)+2r^2-\frac{8r\cos^2(\phi)}{1+r^2}+4r\cos(2\pi\nu)\cos(\phi)\right]\\=&\mathcal{R}\left(A_1\right)(1-r^2)\left[2+2r^2-\frac{8r\cos^2(\phi)}{1+r^2}\right]\\=&2\mathcal{R}\left(A_1\right)(1-r^2)\left[1+r^2-\frac{4r\cos^2(\phi)}{1+r^2}\right].\end{aligned}\tag{B.6.15}$$

Now, $\mathcal{R}(A_1)$ is changed from (B.1.6) to

$$\begin{aligned}\mathcal{R}(A_1)&=\frac{\sigma_{\mathcal{E}}^2(1+P_1P_2)}{2(1-P_1^2)(1-P_2^2)(1-P_1P_2)}\\&=\frac{\sigma_{\mathcal{E}}^2(1+r^2)}{2(1-P_1^2)(1-P_2^2)(1-r^2)},\end{aligned}$$

and inserted into (B.6.15) to finally obtain the result

$$\begin{aligned}&\sigma_{\mathcal{E}}^2\frac{1}{(1-P_1^2)(1-P_2^2)}(1+r^2)\left(1+r^2-\frac{4r\cos^2(\phi)}{1+r^2}\right)\\=&\sigma_{\mathcal{E}}^2\frac{1}{(1-P_1^2)(1-P_2^2)}\left(1+r^2+r^2+r^4-4r\cos^2(\phi)\right)\\=&\sigma_{\mathcal{E}}^2\frac{1}{(1-P_1^2)(1-P_2^2)}\left(1+2r^2+r^4-4r\cos^2(\phi)\right)\end{aligned}$$

for the numerator. By calculating

$$
\begin{aligned}
&(1-P_1^2)(1-P_2^2)\\
&=1-P_1^2-P_2^2+P_1^2P_2^2\\
&=1-r^2[\cos(\phi)+i\sin(\phi)]^2-r^2[\cos(\phi)-i\sin(\phi)]^2+r^4\\
&=1-r^2[\cos^2(\phi)+2i\cos(\phi)\sin(\phi)-\sin^2(\phi)+\cos^2(\phi)-2i\cos(\phi)\sin(\phi)-\sin^2(\phi)]+r^4\\
&=1-r^2[2\cos^2(\phi)-2\sin^2(\phi)]+r^4\\
&=1-r^2[2\cos^2(\phi)\overbrace{-2+2cos^2(\phi)}]+r^4\\
&=1-r^2[4\cos^2(\phi)-2]+r^4\\
&=1+2r^2+r^4-4r^2\cos^2(\phi),
\end{aligned}
$$

everything except $\sigma_\mathcal{E}^2$ is eliminated from the numerator in (B.6.14). We are now only left to show that (B.6.13) is equal to the denominator for the PSD of the discrete AR(2) process in (B.3.3):

$$
\begin{aligned}
&(1-re^{i(2\pi\nu+\phi)})(1-re^{-i(2\pi\nu+\phi)})(1-re^{i(2\pi\nu-\phi)})(1-re^{-i(2\pi\nu-\phi)})\\
\overset{(1)}{=}&(1-P_1e^{i2\pi\nu})(1-P_2e^{-i2\pi\nu})(1-P_2e^{i2\pi\nu})(1-P_1e^{-i2\pi\nu})\\
=&1-(P_1+P_2)(e^{i2\pi\nu}+e^{-i2\pi\nu})...\\
&+P_1^2+P_2^2+P_1P_2(e^{i2\pi\nu}e^{-i2\pi\nu}+e^{-i2\pi\nu}+e^{i2\pi\nu}+e^{i2\pi\nu}e^{i2\pi\nu}+e^{-i2\pi\nu}e^{-i2\pi\nu})...\\
&-P_1^2P_2(e^{-i2\pi\nu}+e^{i2\pi\nu})-P_1P_2^2(e^{i2\pi\nu}+e^{-i2\pi\nu})...\\
&+P_1^2P_2^2\\
=&1-2(P_1+P_2)\cos(2\pi\nu)...\\
&+P_1^2+P_2^2+\underline{P_1P_2(2+2\cos(4\pi\nu))}...\\
&-\underline{P_1^2P_2\cos(2\pi\nu)}-\underline{P_1P_2^2\cos(2\pi\nu)}...\\
&+\underline{P_1^2P_2^2}\\
=&1-2(P_1+P_2)\cos(2\pi\nu)+P_1^2+P_2^2+\underline{P_1P_2(2+2\cos(4\pi\nu)-(P_1+P_2)\cos(2\pi\nu)+P_1P_2)}.
\end{aligned}
\tag{B.6.16}
$$

In (1), the definitions: $P_1=re^{i2\pi\phi}$ and $P_2=re^{-i2\pi\phi}$ are used. Showing that the numerator can be simplified to $\sigma_\mathcal{E}^2$ and that the denominator can be simplified to (B.6.16) provides the result of the convolution of the FT of the continuous CF $\Gamma(\nu)$ and the DC for a pair of complex conjugated roots as:

$$
\begin{aligned}
&\Gamma(\nu)\circledast\sum_{l=-\infty}^{\infty}\delta(\nu-l)\\
=&\frac{\sigma_\mathcal{E}^2}{1-2(P_1+P_2)\cos(2\pi\nu)+P_1^2+P_2^2+P_1P_2(2+2\cos(4\pi\nu)-(P_1+P_2)\cos(2\pi\nu)+P_1P_2)}.
\end{aligned}
\tag{B.6.17}
$$

B.6.2.5 Conclusion

The comparison of (B.6.17) and (B.6.3) verifies that both spectra are the same. This proves that the FT of the convolution of the continuous CF (3.1.4) and the DC is the same function as the PSD of the discrete AR(2) process.

B.7 Sign Changes of the Real Part of the Roots

This section shows how a pair of complex conjugated roots P_k $k\in\{1,2\}$ with a negative real part are converted into a representation of roots $\bar{P}_k$ with $k\in\{1,2\}$ and a positive real part. Furthermore, it provides a demonstration of how the conversion changes the weights A_k for the covariance function in (3.1.3) to new weights $\bar{A}_k$.

B.7.1 Alternative Representation of the Roots

Given $P_1 = -a + ib$ and $P_2 = -a - ib$, with $a, b \in \mathbb{R}^+$ as a complex conjugated pair of roots with negative real parts, they can be rewritten as

$$\begin{aligned} P_1 &= -a + ib \\ &= (-1)(a - ib) \\ &= e^{i\pi} \underbrace{(a - ib)}_{\bar{P}_2} \\ &= e^{i\pi} \bar{P}_2 \end{aligned} \qquad \text{and} \qquad \begin{aligned} P_2 &= -a - ib \\ &= (-1)(a + ib) \\ &= e^{i\pi} \underbrace{(a + ib)}_{\bar{P}_1} \\ &= e^{i\pi} \bar{P}_1. \end{aligned}$$

It follows that the roots $\bar{P}_1$ and $\bar{P}_2$ form a complex conjugated pair with positive real parts. In addition, the new roots are as far away from the origin as P_1 and P_2, and thus lie again in the unit circle. Moreover, the sign of the imaginary part also change. That means, if P_1 and $\bar{P}_1$ describe the roots with positive imaginary part, and P_2 and $\bar{P}_2$ describe the roots with negative imaginary part, then $\bar{P}_1$ arises from P_2 and $\bar{P}_2$ from P_1.

B.7.2 Consequences for the Coefficients of the Covariance Function

The transition from the roots P_1 and P_2 with negative real part to the roots $\bar{P}_1$ and $\bar{P}_2$ with positive real part also affects the coefficients A_1 and A_2 of the covariance function (see (3.1.3)). (B.1.5) is used to calculate the weights A_1 and A_2 from roots with negative real part. However, this time, the roots are exchanged by $P_1 = -\bar{P}_2$ and $P_2 = -\bar{P}_1$:

$$\begin{aligned} A_1 &= \frac{\sigma_\mathcal{E}^2 P_1}{(P_2 - P_1)(1 - P_1^2)(1 - P_1 P_2)} \\ &= \frac{\sigma_\mathcal{E}^2 (-\bar{P}_2)}{((-\bar{P}_1 - (-\bar{P}_2))(1 - (-\bar{P}_2)^2)(1 - (-\bar{P}_2)(-\bar{P}_1))} \\ &= \frac{\mathbf{(-1)}\sigma_\mathcal{E}^2 \bar{P}_2}{\mathbf{(-1)}(\bar{P}_1 - \bar{P}_2)(1 - \bar{P}_2^2)(1 - \bar{P}_2 \bar{P}_1)} \\ &= \frac{\sigma_\mathcal{E}^2 \bar{P}_2}{(\bar{P}_1 - \bar{P}_2)(1 - \bar{P}_2^2)(1 - \bar{P}_2 \bar{P}_1)} \\ &= \bar{A}_2. \end{aligned}$$

The same analogy applies to the derivation of $A_2 = \bar{A}_1$.

B.8 Fourier Transformation of a Positive Definite Function multiplied by Cosine

Let $f(h)$ be a positive definite function ($\mathcal{F}\{f(h)\}(\nu) > 0 \ \forall \nu \in \mathbb{R}$). If the function

$$g(h) := f(h) \cos(a 2\pi h)$$

is the product of $f(h)$ and a non-shifted cosine with $a \in \mathbb{R}$, then $g(h)$ is again positive definite. The proof for this is provided by the convolution theorem (see (2.12.3)). It leads to:

$$\begin{aligned} \mathcal{F}\{g(h)\}(\nu) &= \mathcal{F}\{f(h) \cos(a 2\pi h)\}(\nu) \\ &= \mathcal{F}\{f(h)\}(\nu) \circledast \mathcal{F}\{\cos(a 2\pi h)\}(\nu). \end{aligned}$$

By using

$$\mathcal{F}\{\cos(a 2\pi h)\}(\nu) = \frac{1}{2}(\delta(\nu - a) + \delta(\nu + a))$$

(see Buttkus 2000, p. 46, eq. (3.26)), the FT of $g(h)$ can be calculated as

$$\begin{aligned}\mathcal{F}\{g(h)\}(\nu) &= \mathcal{F}\{f(h)\}(\nu) \circledast \left[\frac{1}{2}(\delta(\nu-a)+\delta(\nu+a))\right] \\ &= \frac{1}{2}\left[\mathcal{F}\{f(h)\}(\nu) \circledast \delta(\nu-a) + \mathcal{F}\{f(h)\}(\nu) \circledast \delta(\nu+a)\right].\end{aligned}$$

With the help of the definition of the DDF (in (2.15.1)), the convolution can be replaced with

$$\begin{aligned}\mathcal{F}\{f(h)\}(\nu) \circledast \delta(\nu-a) &= \int_{-\infty}^{\infty} \mathcal{F}\{f(h)\}(x)\delta(x-(\nu-a))dx \\ &= \mathcal{F}\{f(h)\}(\nu-a),\end{aligned}$$

which results in a shifted FT of $f(h)$. Analogously, it follows that

$$\mathcal{F}\{f(h)\}(\nu) \circledast \delta(\nu+a) = \mathcal{F}\{f(h)\}(\nu+a).$$

Which means that $\mathcal{F}\{g(h)\}(\nu)$ is half of the sum of two shifted positive functions, and therefore is also positive.
Only for the sake of completeness, let us also look at the inverse transformation. By using a frequency shift of IFT (see (2.12.5)), it follows that

$$\mathcal{F}\{f(h)\}(a+\nu) = \mathcal{F}\{f(h)\}(\nu)e^{i2\pi ah} \qquad \text{and} \qquad \mathcal{F}\{f(h)\}(\nu-a) = \mathcal{F}\{f(h)\}(\nu)e^{i2\pi(-a)h}.$$

By inserting these equations, we can see that

$$\begin{aligned}&\mathcal{F}^{-1}\left\{\frac{1}{2}(\mathcal{F}\{f(h)\}(\nu-a)+\mathcal{F}\{f(h)\}(\nu+a))\right\}(h) \\ =&\frac{1}{2}\left[\mathcal{F}^{-1}\left\{\mathcal{F}\{f(h)\}(\nu-a)\right\}(h) + \mathcal{F}^{-1}\left\{\mathcal{F}\{f(h)\}(\nu+a)\right\}(h)\right] \\ =&\frac{1}{2}\left[\mathcal{F}^{-1}\left\{\mathcal{F}\{f(h)\}(\nu)e^{i2\pi ah}\right\}(h) + \mathcal{F}^{-1}\left\{\mathcal{F}\{f(h)\}(\nu)e^{-i2\pi ah}\right\}(h)\right] \\ =&\frac{1}{2}\left[f(h)e^{i2\pi ah} + f(h)e^{-i2\pi ah}\right] \\ =&f(h)\underbrace{\frac{e^{i2\pi ah}+e^{-i2\pi ah}}{2}} \\ =&f(h) \quad \cos(2\pi ah)\end{aligned}$$

is valid.

B.9 Determining the Real Part of Fractions with Complex Denominators

For (3.3.4), it is necessary to show that

$$\mathcal{R}\left(\frac{P_1}{(P_2-P_1)}\frac{1}{(1-P_1^2)}\frac{\ln(P_1)}{(\ln(P_1))^2+(2\pi\nu)^2}\right) = \frac{-\ln(r)\sin(\phi)(1+r^2)-\phi\cos(\phi)(1-r^2)}{2\sin(\phi)[(1-r^2\cos^2(\phi)+r^2\sin^2(\phi))^2+(2r^2\cos(\phi)\sin(\phi))^2][(\ln(r)^2-\phi^2+(2\pi\nu)^2)^2+(2\ln(r)\phi)^2]} \tag{B.9.1}$$

in cases of the roots from (3.3.2) and (3.3.3):

$$\begin{aligned}&P_1 = r(\cos(\phi)+i\sin(\phi)) \text{ and} \\ &P_2 = r(\cos(\phi)-i\sin(\phi)) \\ &\quad \text{with } r\in(0,1), \text{ and } \phi\in(0,\pi).\end{aligned} \tag{B.9.2}$$

To prove this, two steps are necessary: first, the imaginary part must be removed from the denominator in each fraction, which is done in section B.9.1. The imaginary part can simply be removed from a fraction of a numerator a and a real-valued denominator b:

$$\mathcal{R}\left(\frac{a}{b}\right) = \frac{\mathcal{R}(a)}{b}.$$

As such, secondly, we only need the real part of the product of the numerators, which is determined in section B.9.2. This will prove the construction statement (B.9.1).

B.9.1 Elimination of Imaginary Parts from the Denominators

To eliminate the imaginary part of a fraction's denominator, the fraction is expanded by the complex conjugate counterpart of the denominator. This was already done with the second and third fractions on the left side of (B.9.1). In the case of the first fraction, there is no real part in its denominator. Here it is suffices to multiply nominator and the denominator with i:

1. the first fraction $\frac{P_1}{P_2-P_1}$ gives

$$\begin{aligned}
\frac{P_1}{P_2 - P_1} &= \frac{r(\cos(\phi) + i\sin(\phi))}{r(\cos(\phi) - i\sin(\phi)) - r(\cos(\phi) + i\sin(\phi))} \\
&= \frac{r(\cos(\phi) + i\sin(\phi))}{r(\cos(\phi) - i\sin(\phi) - \cos(\phi) - i\sin(\phi))} \\
&= \frac{\cos(\phi) + i\sin(\phi)}{(\cos(\phi) - i\sin(\phi) - \cos(\phi) - i\sin(\phi))} \\
&= \frac{\cos(\phi) + i\sin(\phi)}{-i2\sin(\phi)} \\
&\overset{(1)}{=} \frac{-\sin(\phi) + i\cos(\phi)}{2\sin(\phi)},
\end{aligned} \tag{B.9.3}$$

   where (1) arises from an expansion with $1 = \frac{i}{i}$.

2. For the second fraction $\frac{1}{1-P_1^2}$, the real and the imaginary part must first be separated in the denominator, in order to convert them into

$$\begin{aligned}
\frac{1}{1 - P_1^2} &= \frac{1}{1 - r^2(\cos(\phi) + i\sin(\phi))^2} \\
&= \frac{1}{1 - r^2[\cos^2(\phi) + 2i\cos(\phi)\sin(\phi) - \sin^2(\phi)]} \\
&= \frac{1}{[1 - r^2\cos^2(\phi) + r^2\sin^2(\phi)] - i[2r^2\cos(\phi)\sin(\phi)]} \\
&\overset{(1)}{=} \frac{1 - r^2\cos^2(\phi) + r^2\sin^2(\phi) + i[2r^2\cos(\phi)\sin(\phi)]}{(1 - r^2\cos^2(\phi) + r^2\sin^2(\phi))^2 + (2r^2\cos(\phi)\sin(\phi))^2}.
\end{aligned} \tag{B.9.4}$$

   In (1), an expansion of the fraction is done, witch is provided by multiplication of the nominator and the denominator with the complex conjugated of the denominator: $1 - r^2\cos^2(\phi) + r^2\sin^2(\phi) + i[2\cos(\phi)\sin(\phi)]$. This way, the denominator becomes real valued.

3. Before the third fraction can be expanded, the imaginary and the real part must again be

separated from each other:

$$\begin{aligned}\frac{\ln(P_1)}{(\ln(P_1))^2+(2\pi\nu)^2} &\overset{(1)}{=} \frac{\ln(e^{\ln(r)+i\phi})}{[\ln(e^{\ln(r)+i\phi})]^2+(2\pi\nu)^2}\\ &= \frac{\ln(r)+i\phi}{[\ln(r)+i\phi]^2+(2\pi\nu)^2}\\ &= \frac{\ln(r)+i\phi}{\ln(r)^2+2i\ln(r)\phi-\phi^2+(2\pi\nu)^2}\\ &= \frac{\ln(r)+i\phi}{[\ln(r)^2-\phi^2+(2\pi\nu)^2]+i[2\ln(r)\phi]}\\ &= \frac{[\ln(r)+i\phi][\ln(r)^2-\phi^2+(2\pi\nu)^2-i2\ln(r)\phi]}{(\ln(r)^2-\phi^2+(2\pi\nu)^2)^2+(2\ln(r)\phi)^2}. \end{aligned} \tag{B.9.5}$$

In this case -contrast to the other two fractions- the numerator can be simplified, leading to

$$\begin{aligned}&[\ln(r)+i\phi][\ln(r)^2-\phi^2+(2\pi\nu)^2-i2\ln(r)\phi]\\ =&\ln(r)^3\underline{-\ln(r)\phi^2}+\ln(r)(2\pi\nu)^2\underline{+2\ln(r)\phi^2} && +i[\underline{\ln(r)^2\phi}-\phi^3+\phi(2\pi\nu)^2\underline{-2\ln(r)^2\phi}]\\ =&\ln(r)^3\mathbf{+\ln(r)\phi^2}+\ln(r)(2\pi\nu)^2 && +i[\mathbf{-\ln(r)^2\phi}-\phi^3+\phi(2\pi\nu)^2]\\ =&\ln(r)[\ln(r)^2+\phi^2+(2\pi\nu)^2] && +i(-\phi)[\ln(r)^2+\phi^2-(2\pi\nu)^2]\\ =&\ln(r)[\ln(r)^2+\phi^2+(2\pi\nu)^2] && -i\phi[\ln(r)^2+\phi^2-(2\pi\nu)^2]. \end{aligned} \tag{B.9.6}$$

B.9.2 Multiplication of the Numerators

This section calculates the product of the numerators from the previous section B.9.1. First, we multiply the numerators of (B.9.3) and (B.9.4):

$$\begin{aligned}&(-\sin(\phi)+i\cos(\phi))\left(1-r^2\cos^2(\phi)+r^2\sin^2(\phi)+i[2r^2\cos(\phi)\sin(\phi)]\right)\\ =&-\sin(\phi)\{1-r^2\cos^2(\phi)+r^2\sin^2(\phi)\}-2r^2\cos^2(\phi)\sin(\phi)...\\ &+i[\cos(\phi)\{1-r^2\cos^2(\phi)+r^2\sin^2(\phi)\}-2r^2\cos(\phi)\sin^2(\phi)]\\ \overset{(1)}{=}&-\sin(\phi)\{1\underline{-r^2\cos^2(\phi)}+r^2\sin^2(\phi)+\underline{2r^2\cos^2(\phi)}\}...\\ &+i[\cos(\phi)\{1-r^2\cos^2(\phi)+\underline{r^2\sin^2(\phi)-2r^2\sin^2(\phi)}\}]\\ =&-\sin(\phi)\{1+\mathbf{r^2\cos^2(\phi)}+r^2\sin^2(\phi)\}...\\ &+i[\cos(\phi)\{1-r^2\cos^2(\phi)\mathbf{-r^2\sin^2(\phi)}\}]\\ =&-\sin(\phi)\{1+r^2\left(\cos^2(\phi)+\sin^2(\phi)\right)\}...\\ &+i[\cos(\phi)\{1-r^2\left(\cos^2(\phi)+\sin^2(\phi)\right)\}]\\ =&-\sin(\phi)\{1+r^2\}+i\cos(\phi)\{1-r^2\}. \end{aligned}$$

In (1), $-2r^2\cos^2(\phi)\sin(\phi)$ is moved into the curly brackets of the real part by being divided by $-\sin(\phi)$. Furthermore, $-2r^2\cos(\phi)\sin^2(\phi)$ is shifted into the curly brackets of the imaginary part by being divided by $\cos(\phi)$.
The result must now be multiplied by the nominator of the third fraction (which is shown in (B.9.6)):

$$\begin{aligned}&\{-\sin(\phi)(1+r^2)+i\cos(\phi)(1-r^2)\}\{\ln(r)[\ln(r)^2+\phi^2+(2\pi\nu)^2]-i\phi[\ln(r)^2+\phi^2-(2\pi\nu)^2]\}\\ =&-\ln(r)\sin(\phi)(1+r^2)[\ln(r)^2+\phi^2+(2\pi\nu)^2]+\phi\cos(\phi)(1-r^2)[\ln(r)^2+\phi^2-(2\pi\nu)^2]\\ &+i\left[\ln(r)\cos(\phi)(1-r^2)[\ln(r)^2+\phi^2+(2\pi\nu)^2]-\phi\sin(\phi)(1+r^2)[\ln(r)^2+\phi^2-(2\pi\nu)^2]\right]. \end{aligned}$$

Only the real part is simplified as, for our case, the imaginary part is irrelevant:

$$
\begin{aligned}
& -\ln(r)\sin(\phi)(1+r^2)[\ln(r)^2+\phi^2+(2\pi\nu)^2]+\phi\cos(\phi)(1-r^2)[\ln(r)^2+\phi^2-(2\pi\nu)^2] \\
\overset{(1)}{=}\; & -\ln(r)\sin(\phi)(1+r^2)[\ln(r)^2+\phi^2]\; -\ln(r)\sin(\phi)(1+r^2)(2\pi\nu)^2 \ldots \\
& +\; \phi\cos(\phi)(1-r^2)[\ln(r)^2+\phi^2]\; -\phi\cos(\phi)(1-r^2)(2\pi\nu)^2 \\
\overset{(2)}{=}\; & \left[-\ln(r)\sin(\phi)(1+r^2)+\phi\cos(\phi)(1-r^2)\right][\ln(r)^2+\phi^2] \ldots \\
& +\left[-\ln(r)\sin(\phi)(1+r^2)-\phi\cos(\phi)(1-r^2)\right](2\pi\nu)^2. \qquad \text{(B.9.7)}
\end{aligned}
$$

In (1), the brackets $[\ln(r)^2+\phi^2+(2\pi\nu)^2]$ and $[\ln(r)^2+\phi^2-(2\pi\nu)^2]$ are dissolved, whereby $(\ln(r)^2+\phi^2)$ is used as one variable. This allows to combine the terms with $(\ln(r)^2+\phi^2)$ and $(2\pi\nu)^2$ in (2). Dividing this result by the product of the three real denominators given by $2\sin(\phi)$ from (B.9.3), $(1-r^2\cos^2(\phi)+r^2\sin^2(\phi))^2+(2r^2\cos(\phi)\sin(\phi))^2$ from (B.9.4) and $(\ln(r)^2-\phi^2+(2\pi\nu)^2)^2+(2\ln(r)\phi)^2$ from (B.9.5), shows that equation (B.9.1) is correct. In addition, as (B.9.2) only consists of quadratic terms and $\sin(\phi)$ with $\phi\in(0,\pi)$, the denominator is positive for all its permitted values.

Appendix C

Time Variable AR Processes

C.1 Using Yule-Walker Equations to Derive Time Variable AR Processes

In this chapter, the Y.-W. equations for TVAR processes are derived in the same way as in the case of time stable AR processes cf. section 2.8. Let $\mathcal{S}_t$ and $\mathcal{S}_{t-j}$ be two states of the time series of equation (4.1.1) with $t, j \in \mathbb{Z}$ and $j \geq 0$ (thus $t \geq t-j$). We need to obtain the covariance between a value and its predecessors. The product of these two states can be calculated as

$$\begin{aligned}\mathcal{S}_t\mathcal{S}_{t-j} &= (\alpha_1(t)\mathcal{S}_{t-1} + \alpha_2(t)\mathcal{S}_{t-2} + ... + \alpha_p(t)\mathcal{S}_{t-p} + \mathcal{E}_t)\mathcal{S}_{t-j} \\ &= \alpha_1(t)\mathcal{S}_{t-1}\mathcal{S}_{t-j} + \alpha_2(t)\mathcal{S}_{t-2}\mathcal{S}_{t-j} + ... + \alpha_p(t)\mathcal{S}_{t-p}\mathcal{S}_{t-j} + \mathcal{E}_t\mathcal{S}_{t-j}. \end{aligned} \tag{C.1.1}$$

In addition, the coefficients $\alpha_k(t) = \sum_{l=0}^{q_k} \beta_l^{(k)} b_l(t)$ are continuous functions represented as a linear combination of basis functions as introduced in (4.1.2). These basis functions are deterministic, even though they are variable in time. Since $\alpha_k(t)$ are all deterministic, it follows that $E\{\alpha_k(t)\} = \alpha_k(t)$. Applying the expectation operator to both sides of the equation (C.1.1) yields

$$\begin{aligned}\Sigma_{-j}(t) :&= E\{\mathcal{S}_t\mathcal{S}_{t-j}\} \\ &= \alpha_1(t)E\{\mathcal{S}_{t-1}\mathcal{S}_{t-j}\} + \alpha_2(t)E\{\mathcal{S}_{t-2}\mathcal{S}_{t-j}\} + ... + \alpha_p(t)E\{\mathcal{S}_{t-p}\mathcal{S}_{t-j}\} + E\{\mathcal{E}_t\mathcal{S}_{t-j}\} \\ &= \alpha_1(t)\overbrace{\Sigma_{-j+1}(t-1)} + \alpha_2(t)\overbrace{\Sigma_{-j+2}(t-2)} + ... + \alpha_p(t)\overbrace{\Sigma_{-j+p}(t-p)} + E\{\mathcal{E}_t\mathcal{S}_{t-j}\} \\ &= \begin{cases} \alpha_1(t)\Sigma_1(t-1) + \alpha_2(t)\Sigma_2(t-2) + ... + \alpha_p(t)\Sigma_p(t-p) + \sigma_{\mathcal{E}}^2 & \text{if } j = 0 \\ \alpha_1(t)\Sigma_{1-j}(t-1) + \alpha_2(t)\Sigma_{2-j}(t-2) + ... + \alpha_p(t)\Sigma_{p-j}(t-p) & \text{else.} \end{cases} \end{aligned} \tag{C.1.2}$$

The two resulting equations are very similar to the Y.-W. equations for time stable AR processes described in (2.8.2) and (2.8.3). To determine the covariance between an initial observation $\mathcal{S}_t$ and a subsequent observation $\mathcal{S}_{t+j}$, this time $\mathcal{S}_t$ is expanded by (4.1.1). So first the product is determined:

$$\begin{aligned}\mathcal{S}_{t+j}\mathcal{S}_t =&(\alpha_1(t+j)\mathcal{S}_{t+j-1} + \alpha_2(t+j)\mathcal{S}_{t+j-2} + ... + \alpha_p(t+j)\mathcal{S}_{t+j-p} + \mathcal{E}_{t+j})\mathcal{S}_t \\ =&\alpha_1(t+j)\mathcal{S}_{t+j-1}\mathcal{S}_t + \alpha_2(t+j)\mathcal{S}_{t+j-2}\mathcal{S}_t + ... + \alpha_p(t+j)\mathcal{S}_{t+j-p}\mathcal{S}_t + \mathcal{E}_{t+j}\mathcal{S}_t. \end{aligned}$$

And then, we use the expectation operator to calculate the covariance between an observation and some point in the future:

$$\begin{aligned}&\Sigma_j(t) := E\{\mathcal{S}_{t+j}\mathcal{S}_t\} \\ =&\alpha_1(t+j)E\{\mathcal{S}_{t+j-1}\mathcal{S}_t\} + \alpha_2(t+j)E\{\mathcal{S}_{t+j-2}\mathcal{S}_t\} + ... + \alpha_p(t+j)E\{\mathcal{S}_{t+j-p}\mathcal{S}_t\} + E\{\mathcal{E}_{t+j}\mathcal{S}_t\} \\ =&\alpha_1(t+j)\Sigma_{j-1}(t) + \alpha_2(t+j)\Sigma_{j-2}(t) + ... + \alpha_p(t+j)\Sigma_{j-p}(t) + E\{\mathcal{E}_{t+j}\mathcal{S}_t\} \\ =&\begin{cases} \alpha_1(t)\Sigma_{-1}(t) + \alpha_2(t)\Sigma_{-2}(t) + ... + \alpha_p(t)\Sigma_{-p}(t) + \sigma_{\mathcal{E}}^2 & \text{if } j = 0 \\ \alpha_1(t+j)\Sigma_{j-1}(t) + \alpha_2(t+j)\Sigma_{j-2}(t) + ... + \alpha_p(t+j)\Sigma_{j-p}(t) & \text{else.} \end{cases} \end{aligned} \tag{C.1.3}$$

While equation (C.1.2) shows that the coefficients $\alpha_l(t)$ of the time variable Y.-W. equations concerning previous observations are all evaluated at time t, the coefficients of the time variable Y.-W. equation for subsequent observations in (C.1.3) are all evaluated for different times depending on the lag j. In contrast, the covariances change in (C.1.2) according to the value of j, while remaining constant in (C.1.3). This means that the development of CF depends on whether the covariance concern a state in the future or the past.

C.2 General Estimate of Time Variable AR Processes Gained from Basis Functions

Given a sequence $\boldsymbol{\mathcal{S}} = [\mathcal{S}_1, \mathcal{S}_2, ..., \mathcal{S}_n]$ of n observations. Then, a TVAR process gained from basis functions and order p

$$\begin{array}{ccccc} \underbrace{\mathcal{S}_t} & + & \underbrace{(-\mathcal{E}_t)} & = & \underbrace{\begin{bmatrix}\mathcal{S}_{t-1} & \mathcal{S}_{t-2} & ... & \mathcal{S}_{t-p}\end{bmatrix}_{[1\times p]} \begin{bmatrix}\mathbb{1}b_0(t) & | & \mathbb{1}b_1(t) & | & ... & | & \mathbb{1}b_q(t)\end{bmatrix}_{[p\times pq]}} & \boldsymbol{\beta} \\ y_i & + & e_i & = & \boldsymbol{X}_i & & & & \boldsymbol{\beta} \end{array} \quad \text{(C.2.1)}$$

can be estimated by a least-squares adjustment. To find the unknown parameters in the vector $\boldsymbol{\beta}$, the matrices and vectors in (C.2.1) must be created. The following scheme shows how to create these matrices and vectors, as well as how to compute the adjustment's results:

1. Setting up the observation vector $\boldsymbol{y}$:

$$\boldsymbol{y} = \boldsymbol{\mathcal{S}}^T(p+1:n) = \begin{bmatrix}\mathcal{S}_{p+1} & \mathcal{S}_{p+2} & ... & \mathcal{S}_n\end{bmatrix}^T. \quad \text{(C.2.2)}$$

   Since (C.2.1) and (4.1.1) cannot be established for the first p observations, $\boldsymbol{y}$ does not contain them.

2. Constructing the design matrix $\boldsymbol{X}$ by the means of the observation equation (4.1.1):

   (a) *General Layout and calculation Simplification*
   In order to obtain the matrix $\boldsymbol{X}$, the observation equations cf. (4.1.1) are used and grouped according to the observations in $\boldsymbol{y}$:

$$\begin{aligned} \boldsymbol{X} &= \begin{bmatrix} \boldsymbol{X}_1 \\ \boldsymbol{X}_2 \\ \vdots \\ \boldsymbol{X}_{n-p} \end{bmatrix} \\ &= \begin{bmatrix} \begin{bmatrix}\mathcal{S}_p & \mathcal{S}_{p-1} & ... & \mathcal{S}_1\end{bmatrix} & \begin{bmatrix}\mathbb{1}b_0(p+1) & | & \mathbb{1}b_1(p+1) & | & ... & | & \mathbb{1}b_q(p+1)\end{bmatrix} \\ \begin{bmatrix}\mathcal{S}_{p+1} & \mathcal{S}_p & ... & \mathcal{S}_2\end{bmatrix} & \begin{bmatrix}\mathbb{1}b_0(p+2) & | & \mathbb{1}b_1(p+2) & | & ... & | & \mathbb{1}b_q(p+2)\end{bmatrix} \\ \vdots & \vdots \\ \begin{bmatrix}\mathcal{S}_{n-1} & \mathcal{S}_{n-2} & ... & \mathcal{S}_{n-p}\end{bmatrix} & \begin{bmatrix}\mathbb{1}b_0(n) & | & \mathbb{1}b_1(n) & | & ... & | & \mathbb{1}b_q(n)\end{bmatrix} \end{bmatrix}. \end{aligned}$$

   Notice, that the vectors containing the signal $\mathcal{S}_t$ with $t \in \{1, 2, ..., n-1\}$ are $n-p$ vectors of the same length p. These vectors combined to a matrix yields the Toeplitz form:

$$\boldsymbol{T} = \begin{bmatrix} \mathcal{S}_p & \mathcal{S}_{p-1} & ... & \mathcal{S}_1 \\ \mathcal{S}_{p+1} & \mathcal{S}_p & ... & \mathcal{S}_2 \\ \vdots \\ \mathcal{S}_{n-1} & \mathcal{S}_{n-2} & ... & \mathcal{S}_{n-p} \end{bmatrix}. \quad \text{(C.2.3)}$$

   Each multiplication of $\boldsymbol{T}$ with one column of the blocks of the right part of $\boldsymbol{X}$ yields a matrix vector product. By the means of using the vectors

$$\boldsymbol{b}_k := \begin{bmatrix}b_k(p+1) & b_k(p+2) & ... & b_k(n)\end{bmatrix}^T$$

with $k \in [0, q]$ and the definition of the matrix-vector-product

$$\boldsymbol{T} \odot \boldsymbol{b}_k := \begin{bmatrix} \mathcal{S}_{p+1} b_k(p+1) & \mathcal{S}_{p-1} b_k(p+1) & ... & \mathcal{S}_1 b_k(p+1) \\ \mathcal{S}_{p+1} b_k(p+2) & \mathcal{S}_p b_k(p+2) & ... & \mathcal{S}_2 b_k(p+2) \\ \vdots & & & \\ \mathcal{S}_{n-1} b_k(n) & \mathcal{S}_{n-2} b_k(n) & ... & \mathcal{S}_{n-p} b_k(n) \end{bmatrix}, \tag{C.2.4}$$

$\boldsymbol{X}$ can be calculated by the simplified formula

$$\boldsymbol{X} = \left[\; \boldsymbol{T} \odot \boldsymbol{b}_0 \;\middle|\; \boldsymbol{T} \odot \boldsymbol{b}_1 \;\middle|\; ... \;\middle|\; \boldsymbol{T} \odot \boldsymbol{b}_q \; \right]. \tag{C.2.5}$$

(b) *Adjustments for Cases of variations in Parameter Numbers*
As specified in (4.1.2), the number of parameters q_k of the coefficients $\alpha_k(t)$ may vary. In this case, follow step 2a) to gain

$$q = \max_{k=1,...,p} (q_k)$$

and then eliminate the unused $\beta_l^{(k)}$ by deleting the corresponding columns from $\boldsymbol{X}$. Note that the parameter vector $\boldsymbol{\beta}$ follows no specific order. So, it is up to the structure of the design matrix to ensure the correct assignment of the parameters to the values in $\boldsymbol{\beta}$ (see Appendix C.3).

3. Approximation of the estimated parameters $\tilde{\boldsymbol{\beta}}$: using the Gauss-Markov model (Koch 1999, chapter 3) now allows to estimate the parameter vector and the corresponding cofactor matrix can now be estimated:

$$\tilde{\boldsymbol{\beta}} = (\boldsymbol{X}^T \boldsymbol{X})^{-1} \boldsymbol{X}^T \boldsymbol{y} \tag{C.2.6}$$

$$Q\{\tilde{\boldsymbol{\beta}}\} = (\boldsymbol{X}^T \boldsymbol{X})^{-1}. \tag{C.2.7}$$

C.3 Design Matrices of Coefficients with Different Parameter Numbers

Suppose a TVAR(3) process is given, where the first coefficient is represented by two parameters ($q_1 = 1$), the second by three parameters ($q_2 = 2$), and the third by two parameters ($q_3 = 1$):

$$\begin{aligned} \alpha_1(t) &= \beta_0^{(1)} b_0(t) + \beta_1^{(1)} b_1(t) \\ \alpha_2(t) &= \beta_0^{(2)} b_0(t) + \beta_1^{(2)} b_1(t) + \beta_2^{(2)} b_2(t) \\ \alpha_3(t) &= \beta_0^{(3)} b_0(t) + \beta_1^{(3)} b_0(t). \end{aligned}$$

For a time series $\boldsymbol{\mathcal{S}} = [\mathcal{S}_1, \mathcal{S}_2, ..., \mathcal{S}_n]$ and a time vector $\boldsymbol{t} = [t_1, t_2, ..., t_n]$, this demands to find the best fitting parameters $\beta_{(l)}^{(k)}$. To do so, first of all, the Toeplitz matrix $\boldsymbol{T}$ is set up:

$$\boldsymbol{T} = \begin{bmatrix} \mathcal{S}_3 & \mathcal{S}_2 & \mathcal{S}_1 \\ \mathcal{S}_4 & \mathcal{S}_3 & \mathcal{S}_2 \\ \vdots & & \\ \mathcal{S}_{n-1} & \mathcal{S}_{n-2} & \mathcal{S}_{n-3} \end{bmatrix}. \tag{C.3.1}$$

Second the $q + 1 = \max\{1, 2, 1\} + 1 = 3$ vectors in which the basis functions are located are demanded. For this example, these are

$$\boldsymbol{b}_0 = \begin{bmatrix} b_0(t_4) \\ b_0(t_5) \\ \vdots \\ b_0(t_n) \end{bmatrix}, \boldsymbol{b}_1 = \begin{bmatrix} b_1(t_4) \\ b_1(t_5) \\ \vdots \\ b_1(t_n) \end{bmatrix}, \text{and } \boldsymbol{b}_2 = \begin{bmatrix} b_2(t_4) \\ b_2(t_5) \\ \vdots \\ b_2(t_n) \end{bmatrix}. \tag{C.3.2}$$

Now, we use the toeplitz matrix of (C.3.1), as well as the basis vectors of (C.3.2), to form the matrix vector product of (C.2.4). (C.2.5) then provides the initial design matrix

$$\boldsymbol{X}_{q=3} = \left[\ \boldsymbol{T}\odot\boldsymbol{b}_0 \ \middle|\ \boldsymbol{T}\odot\boldsymbol{b}_1 \ \middle|\ \boldsymbol{T}\odot\boldsymbol{b}_2\ \right] \qquad \text{with}$$

$$\boldsymbol{T}\odot\boldsymbol{b}_0 = \begin{bmatrix} \mathcal{S}_3 b_0(t_4) & \mathcal{S}_2 b_0(t_4) & \mathcal{S}_1 b_0(t_4) \\ \mathcal{S}_4 b_0(t_5) & \mathcal{S}_3 b_0(t_5) & \mathcal{S}_2 b_0(t_5) \\ \vdots & & \\ \mathcal{S}_{n-1} b_0(t_n) & \mathcal{S}_{n-2} b_0(t_n) & \mathcal{S}_{n-3} b_0(t_n) \end{bmatrix},$$

$$\boldsymbol{T}\odot\boldsymbol{b}_1 = \begin{bmatrix} \mathcal{S}_3 b_1(t_4) & \mathcal{S}_2 b_1(t_4) & \mathcal{S}_1 b_1(t_4) \\ \mathcal{S}_4 b_1(t_5) & \mathcal{S}_3 b_1(t_5) & \mathcal{S}_2 b_1(t_5) \\ \vdots & & \\ \mathcal{S}_{n-1} b_1(t_n) & \mathcal{S}_{n-2} b_1(t_n) & \mathcal{S}_{n-3} b_1(t_n) \end{bmatrix} \qquad \text{and}$$

$$\boldsymbol{T}\odot\boldsymbol{b}_2 = \begin{bmatrix} \mathcal{S}_3 b_2(t_4) & \mathcal{S}_2 b_2(t_4) & \mathcal{S}_1 b_2(t_4) \\ \mathcal{S}_4 b_2(t_5) & \mathcal{S}_3 b_2(t_5) & \mathcal{S}_2 b_2(t_5) \\ \vdots & & \\ \mathcal{S}_{n-1} b_2(t_n) & \mathcal{S}_{n-2} b_2(t_n) & \mathcal{S}_{n-3} b_2(t_n) \end{bmatrix}.$$

This results in the design matrix $\boldsymbol{X}_{q=3}$, which is needed to estimate the parameter vector

$$\boldsymbol{\beta}_{q=3} = \begin{bmatrix} \beta_0^{(1)} & \beta_0^{(2)} & \beta_0^{(3)} & \beta_1^{(1)} & \beta_1^{(2)} & \beta_1^{(3)} & \beta_2^{(1)} & \beta_2^{(2)} & \beta_2^{(3)} \end{bmatrix}^T.$$

However, since the task specifically demands to determine the parameter vector

$$\boldsymbol{\beta} = \begin{bmatrix} \beta_0^{(1)} & \beta_0^{(2)} & \beta_0^{(3)} & \beta_1^{(1)} & \beta_1^{(2)} & \beta_1^{(3)} & \beta_2^{(3)} \end{bmatrix}^T,$$

we also need to delete some columns from $X_{q=3}$. For example, this can be achieved by multiplying it with the matrix

$$\boldsymbol{G} = \begin{bmatrix} 1 & 0 & 0 & 0 & 0 & 0 & 0 & 0 & 0 \\ 0 & 1 & 0 & 0 & 0 & 0 & 0 & 0 & 0 \\ 0 & 0 & 1 & 0 & 0 & 0 & 0 & 0 & 0 \\ 0 & 0 & 0 & 1 & 0 & 0 & 0 & 0 & 0 \\ 0 & 0 & 0 & 0 & 1 & 0 & 0 & 0 & 0 \\ 0 & 0 & 0 & 0 & 0 & 1 & 0 & 0 & 0 \\ 0 & 0 & 0 & 0 & 0 & 0 & 0 & 1 & 0 \end{bmatrix}:$$

$$\boldsymbol{\beta}_{q=3} = \left[\begin{array}{ccc|ccc|ccc} \beta_0^{(1)} & \beta_0^{(2)} & \beta_0^{(3)} & \beta_1^{(1)} & \beta_1^{(2)} & \beta_1^{(3)} & \beta_2^{(1)} & \beta_2^{(2)} & \beta_2^{(3)} \end{array}\right]^T$$

$$\boldsymbol{X}_{q=3} = \left[\begin{array}{ccc|ccc|ccc} \mathcal{S}_3 b_0(t_4) & \mathcal{S}_2 b_0(t_4) & \mathcal{S}_1 b_0(t_4) & \mathcal{S}_3 b_1(t_4) & \mathcal{S}_2 b_1(t_4) & \mathcal{S}_1 b_1(t_4) & \mathcal{S}_3 b_2(t_4) & \mathcal{S}_2 b_2(t_4) & \mathcal{S}_1 b_2(t_4) \\ \mathcal{S}_4 b_0(t_5) & \mathcal{S}_3 b_0(t_5) & \mathcal{S}_2 b_0(t_5) & \mathcal{S}_4 b_1(t_5) & \mathcal{S}_3 b_1(t_5) & \mathcal{S}_2 b_1(t_5) & \mathcal{S}_4 b_2(t_5) & \mathcal{S}_3 b_2(t_5) & \mathcal{S}_2 b_2(t_5) \\ \vdots & & & \vdots & & & \vdots & & \\ \mathcal{S}_{n-1} b_0(t_n) & \mathcal{S}_{n-2} b_0(t_n) & \mathcal{S}_{n-3} b_0(t_n) & \mathcal{S}_{n-1} b_1(t_n) & \mathcal{S}_{n-2} b_1(t_n) & \mathcal{S}_{n-3} b_1(t_n) & \mathcal{S}_{n-1} b_2(t_n) & \mathcal{S}_{n-2} b_2(t_n) & \mathcal{S}_{n-3} b_2(t_n) \end{array}\right]$$

$$\boldsymbol{\beta} = \boldsymbol{\beta}_{q=3} \cdot \boldsymbol{G} \Big\downarrow \boldsymbol{X} = \boldsymbol{X}_{q=3} \cdot \boldsymbol{G}$$

$$\boldsymbol{\beta} = \left[\begin{array}{ccc|ccc|c} \beta_0^{(1)} & \beta_0^{(2)} & \beta_0^{(3)} & \beta_1^{(1)} & \beta_1^{(2)} & \beta_1^{(3)} & \beta_2^{(3)} \end{array}\right]^T$$

$$\boldsymbol{X} = \left[\begin{array}{ccc|ccc|c} \mathcal{S}_3 b_0(t_4) & \mathcal{S}_2 b_0(t_4) & \mathcal{S}_1 b_0(t_4) & \mathcal{S}_3 b_1(t_4) & \mathcal{S}_2 b_1(t_4) & \mathcal{S}_1 b_1(t_4) & \mathcal{S}_2 b_2(t_4) \\ \mathcal{S}_4 b_0(t_5) & \mathcal{S}_3 b_0(t_5) & \mathcal{S}_2 b_0(t_5) & \mathcal{S}_4 b_1(t_5) & \mathcal{S}_3 b_1(t_5) & \mathcal{S}_2 b_1(t_5) & \mathcal{S}_3 b_2(t_5) \\ \vdots & & & \vdots & & & \vdots \\ \mathcal{S}_{n-1} b_0(t_n) & \mathcal{S}_{n-2} b_0(t_n) & \mathcal{S}_{n-3} b_0(t_n) & \mathcal{S}_{n-1} b_1(t_n) & \mathcal{S}_{n-2} b_1(t_n) & \mathcal{S}_{n-3} b_1(t_n) & \mathcal{S}_{n-2} b_2(t_n) \end{array}\right].$$

C.4 Estimation of Time Variable AR(1) and AR(2) Processes with Linear Root Movements

Here, the Gauss-Markov model from Appendix C.2 is adapted to the restriction, that the roots movement is linear (discussed in section 4.3). From (4.3.3), it follows that the basis functions form a polynomial ring with degree p:

$$b_k(t) = t^k \text{ for } k = 1, 2, ..., p \text{ and } t = p+1,\ p+2,\ , ..., n.$$

Therefore, it is possible to describe the vectors of basis functions for monomials as

$$\boldsymbol{b}_k = \begin{bmatrix} t(p+1)^k & t(p+2)^k & ... & t(n)^k \end{bmatrix} =: \boldsymbol{t}^{\odot k}.$$

These vectors, in combination with the Toeplitz matrices $\boldsymbol{T}$ from (C.3.1), allows the creation of the design matrix $\boldsymbol{X}_{q=p}$ by using the approach as shown in Appendix C.3:

$$\boldsymbol{X}_{q=p} = \left[\ \boldsymbol{T} \ \middle|\ \boldsymbol{T} \odot \boldsymbol{t} \ \middle|\ \boldsymbol{T} \odot \boldsymbol{t}^{\odot 2} \ \middle|\ ... \ \middle|\ \boldsymbol{T} \odot \boldsymbol{t}.^{\odot p} \ \right]. \tag{C.4.1}$$

Now, the unused parameters must be deleted. Since the sum of (4.3.3) has the lover bound zero and the upper bound k, (the order of the coefficient,) all $\beta_l^{(k)}$ with $l > k$ must be deleted in the parameter vector:

$$\begin{bmatrix} \underbrace{\beta_0^{(1)} \quad \beta_0^{(2)} \quad ... \quad \beta_0^{(p)}}_{p \text{ elements}} \Big| \underbrace{\beta_1^{(1)} \quad \beta_1^{(2)} \quad ... \quad \beta_1^{(p)}}_{p \text{ elements}} \Big| \underbrace{\beta_2^{(1)} \quad \beta_2^{(2)} \quad ... \quad \beta_2^{(p)}}_{p \text{ elements}} \Big| ... \Big| \underbrace{\beta_1^{(p)} \quad \beta_2^{(p)} \quad ... \quad \beta_p^{(p)}}_{p \text{ elements}} \end{bmatrix}^T$$

$$\downarrow$$

$$\begin{bmatrix} \underbrace{\beta_0^{(1)} \quad \beta_0^{(2)} \quad ... \quad \beta_0^{(p)}}_{p \text{ elements}} \Big| \underbrace{\beta_1^{(1)} \quad \beta_1^{(2)} \quad ... \quad \beta_1^{(p)}}_{p \text{ elements}} \Big| \underbrace{\beta_2^{(2)} \quad \beta_2^{(3)} \quad ... \quad \beta_2^{(p)}}_{p-1 \text{ elements}} \Big| ... \Big| \underbrace{\beta_p^{(p)}}_{1 \text{ element}} \end{bmatrix}^T. \tag{C.4.2}$$

The same has to be done for the corresponding columns in the design matrix $\boldsymbol{X}_{q=p}$ in C.4.1. In order to easily represent $\boldsymbol{X}$ after the elimination of the parameters, the notation

$$\boldsymbol{T}_j := \boldsymbol{T}(:, j : end) = \underbrace{\left.\begin{bmatrix} \mathcal{S}_{p-j} & \mathcal{S}_{p-j-1} & ... & \mathcal{S}_1 \\ \mathcal{S}_{p-j-1} & \mathcal{S}_{p-j-2} & ... & \mathcal{S}_2 \\ & \vdots & & \\ \mathcal{S}_{n-j-1} & \mathcal{S}_{n-j-2} & ... & \mathcal{S}_{n-p} \end{bmatrix}\right\} n-p \text{ elements}}_{p-j \text{ elements}} \tag{C.4.3}$$

is introduced. Thus, the design matrix can be represented via

$$\boldsymbol{X} = \left[\ \boldsymbol{T} \ \middle|\ \boldsymbol{T} \odot \boldsymbol{t} \ \middle|\ \boldsymbol{T}_2 \odot \boldsymbol{t}^{\odot 2} \ \middle|\ \boldsymbol{T}_3 \odot \boldsymbol{t}^{\odot 3} \ \middle|\ ... \ \middle|\ \boldsymbol{T}_p \odot \boldsymbol{t}^{\odot p} \ \right]. \tag{C.4.4}$$

This design matrix and the observation vector from (C.2.2) now allow the performance of an adjustment. However, as discussed in section 4.3.2, additional restrictions still need to be applied to the parameters in cases where the orders of the TVAR process are higher than one.

C.4.1 Design matrix of the TVAR(1) Process

It now follows that the TVAR(1) process can be computed by using the design matrix

$$\boldsymbol{X} = \begin{bmatrix} \begin{bmatrix} \mathcal{S}_1 \\ \mathcal{S}_2 \\ \mathcal{S}_3 \\ \vdots \\ \mathcal{S}_{n-1} \end{bmatrix} \Bigg\| \begin{bmatrix} \mathcal{S}_1 \\ \mathcal{S}_2 \\ \mathcal{S}_3 \\ \vdots \\ \mathcal{S}_{n-1} \end{bmatrix} \odot \begin{bmatrix} 0 \\ \frac{1}{n} \\ \frac{2}{n} \\ \vdots \\ 1 \end{bmatrix} \end{bmatrix} \tag{C.4.5}$$

and the observation vector:

$$\boldsymbol{y} = \begin{bmatrix} \mathcal{S}_2 & \mathcal{S}_3 & \dots & \mathcal{S}_n \end{bmatrix}^T.$$

Since section 4.3.2 has also shown that no further restrictions are required for the TVAR(1) process with linear root motion, the parameter estimation is done after the estimation of $\boldsymbol{\beta}$ by the means of the Gauss-Markov model (see (C.2.6) and (C.2.7)).

Design and Condition Matrix of the TVAR(2) Process

In case of the TVAR(2) process, we append another block to $\boldsymbol{X}$, while $\boldsymbol{T}$ becomes a matrix,

$$\boldsymbol{T} = \begin{bmatrix} \mathcal{S}_2 & \mathcal{S}_1 \\ \mathcal{S}_3 & \mathcal{S}_2 \\ \mathcal{S}_4 & \mathcal{S}_3 \\ \vdots & \vdots \\ \mathcal{S}_{n-1} & \mathcal{S}_{n-2} \end{bmatrix}.$$

Then the design matrix changes into

$$\boldsymbol{X} = \begin{bmatrix} \begin{bmatrix} \mathcal{S}_2 & \mathcal{S}_1 \\ \mathcal{S}_3 & \mathcal{S}_2 \\ \mathcal{S}_4 & \mathcal{S}_3 \\ \vdots & \vdots \\ \mathcal{S}_{n-1} & \mathcal{S}_{n-2} \end{bmatrix} \Bigg\| \begin{bmatrix} \mathcal{S}_2 & \mathcal{S}_1 \\ \mathcal{S}_3 & \mathcal{S}_2 \\ \mathcal{S}_4 & \mathcal{S}_3 \\ \vdots & \vdots \\ \mathcal{S}_{n-1} & \mathcal{S}_{n-2} \end{bmatrix} \odot \begin{bmatrix} 0 \\ \frac{1}{n} \\ \frac{2}{n} \\ \vdots \\ 1 \end{bmatrix} \Bigg\| \begin{bmatrix} \mathcal{S}_1 \\ \mathcal{S}_2 \\ \mathcal{S}_3 \\ \vdots \\ \mathcal{S}_{n-2} \end{bmatrix} \odot \begin{bmatrix} 0 \\ \frac{1}{n^2} \\ \frac{2^2}{n^2} \\ \vdots \\ 1 \end{bmatrix} \end{bmatrix}, \tag{C.4.6}$$

while the observation vector

$$\boldsymbol{y} = \begin{bmatrix} \mathcal{S}_3 & \mathcal{S}_4 & \dots & \mathcal{S}_n \end{bmatrix}^T$$

is shortened by an additional observation. To include the restriction of (4.3.9),

$$\mathcal{C}^{\text{lin}}(\boldsymbol{\beta}) = (\beta_0^{(1)})^2\beta_2^{(2)} + \beta_0^{(2)}(\beta_1^{(1)})^2 - \beta_0^{(1)}\beta_1^{(1)}\beta_1^{(2)} + 4\beta_0^{(2)}\beta_2^{(2)} - (\beta_1^{(2)})^2 \stackrel{!}{=} 0, \tag{C.4.7}$$

a adjustment depending on the restriction is used (see Koch 1999, chapter 3.5.5). The linearized condition matrix derives from the partial derivatives:

$$\begin{aligned} \boldsymbol{H}^T &= \begin{bmatrix} \frac{\delta\mathcal{C}^{\text{lin}}(\boldsymbol{\beta})}{\delta\beta_0^{(1)}} & \frac{\delta\mathcal{C}^{\text{lin}}(\boldsymbol{\beta})}{\delta\beta_0^{(2)}} & \frac{\delta\mathcal{C}^{\text{lin}}(\boldsymbol{\beta})}{\delta\beta_1^{(1)}} & \frac{\delta\mathcal{C}^{\text{lin}}(\boldsymbol{\beta})}{\delta\beta_1^{(2)}} & \frac{\delta\mathcal{C}^{\text{lin}}(\boldsymbol{\beta})}{\delta\beta_2^{(2)}} \end{bmatrix} \\ &= \begin{bmatrix} 2\beta_0^{(1)}\beta_2^{(2)} - \beta_1^{(1)}\beta_1^{(2)} & (\beta_1^{(1)})^2 + 4\beta_2^{(2)} & 2\beta_0^{(2)}\beta_1^{(1)} & -\beta_0^{(1)}\beta_1^{(1)} - 2\beta_1^{(2)} & (\beta_0^{(1)})^2 + 4\beta_0^{(2)} \end{bmatrix}. \end{aligned} \tag{C.4.8}$$

The estimation also requires the cofactor matrix of the parameters, which can be calculated by referring to

$$Q\{\tilde{\boldsymbol{\beta}}\} = (\boldsymbol{X}^T\boldsymbol{X})^{-1} \tag{C.4.9}$$

(see KOCH 1999, p. 158, eq. 3.23). These matrices, allows the calculation of the new parameters -which now also fulfils the (linearized) conditions,

$$\hat{\boldsymbol{\beta}} = \tilde{\boldsymbol{\beta}} - \Sigma\{\tilde{\boldsymbol{\beta}}\}\boldsymbol{H}\left(\boldsymbol{H}^T\Sigma\{\boldsymbol{\beta}\}\boldsymbol{H}\right)^{-1}\boldsymbol{H}^T\tilde{\boldsymbol{\beta}} \quad - \tag{C.4.10}$$

in the following step. These parameters fulfil the non-linear condition of $\mathcal{C}(\boldsymbol{\beta})$, as well as they minimize the sum of the residuals $\boldsymbol{v} = \boldsymbol{y} - \boldsymbol{X}\boldsymbol{\beta}$. The cofactor matrix of the parameters is then

$$Q\{\hat{\boldsymbol{\beta}}\} = Q\{\tilde{\boldsymbol{\beta}}\} - \Sigma\{\tilde{\boldsymbol{\beta}}\}\boldsymbol{H}(\boldsymbol{H}^T\Sigma\{\tilde{\boldsymbol{\beta}}\}\boldsymbol{H})^{-1}\boldsymbol{H}^T\Sigma\{\tilde{\boldsymbol{\beta}}\}. \tag{C.4.11}$$

(C.4.7) is a non-linear equation. In order to apply the restrictions to the parameters, this equation must be linearized and computed iteratively until the non-linearized conditions of (C.4.7) are met. To keep the linear equations of the Gauss-Markov model outside of the iterative part, the application of the restrictions following a separate, second step. This way, only the restriction (i.e. the non-linear equation,) is used within the iterations, while the solution of the linear part is computed in the first step.

C.5 Extending the Time Variable AR(p) Process to a Time Variable AR(p+1) or Time Variable AR(p+2) Process

The extension of a TVAR(p) estimate to a TVAR(p+1) or TVAR(p+2) estimate, requires a process S_t with the TVAR(p) coefficients $\alpha_k(t)$:

$$\mathcal{S}_t = \sum_{k=1}^{p} \alpha_k(t)\mathcal{S}_{t-k} + \mathcal{E}_t.$$

Next we need to expand the TVAR(p) estimate by the means of a TVAR(1) or TVAR(2) process. This requires to first separate the residuals (represented as the white noise part of the TVAR estimate,) and then to declare them as new observations:

$$\begin{aligned}\bar{\mathcal{S}}_t &:= \mathcal{E}_t \\ &= \mathcal{S}_t - \sum_{k=1}^{p} \alpha_k(t)\mathcal{S}_{t-k}.\end{aligned} \tag{C.5.1}$$

With the TVAR(1) estimate for the process $\bar{\mathcal{S}}_t$, which is described by

$$\bar{\mathcal{S}}_t = \bar{\alpha}_1(t)\bar{\mathcal{S}}_{t-1} + \bar{\mathcal{E}}_t,$$

the entire process can also be rewritten as:

$$\begin{aligned}\mathcal{S}_t - \sum_{k=1}^{p} \alpha_k(t)\mathcal{S}_{t-k} &= \bar{\alpha}_1(t)\left(\mathcal{S}_{t-1} - \sum_{k=1}^{p} \alpha_k(t-1)\mathcal{S}_{t-1-k}\right) + \bar{\mathcal{E}}_t \\ \Leftrightarrow \mathcal{S}_t &= \sum_{k=1}^{p} \alpha_k(t)\mathcal{S}_{t-k} + \bar{\alpha}_1(t)\mathcal{S}_{t-1} - \sum_{k=1}^{p} \bar{\alpha}_1(t)\alpha_k(t-1)\mathcal{S}_{t-1-k} + \bar{\mathcal{E}}_t \\ &\overset{(1)}{=} \sum_{k=1}^{p} \alpha_k(t)\mathcal{S}_{t-k} + \bar{\alpha}_1(t)\mathcal{S}_{t-1} - \sum_{m=2}^{p+1} \bar{\alpha}_1(t)\alpha_{m-1}(t-1)\mathcal{S}_{t-m} + \bar{\mathcal{E}}_t \\ &= \left(\alpha_1(t) + \bar{\alpha}_1(t)\right)\mathcal{S}_{t-1}... \\ &\quad + \sum_{k=2}^{p} \left(\alpha_k(t) - \bar{\alpha}_1(t)\alpha_{k-1}(t-1)\right)\mathcal{S}_{t-k}... \\ &\quad - \bar{\alpha}_1(t)\alpha_p(t-1)\mathcal{S}_{t-(p+1)} + \bar{\mathcal{E}}_t.\end{aligned} \tag{C.5.2}$$

When transforming, note that in step (1), $m = k + 1$ has been substituted. Furthermore, the evaluation of $\alpha_k(t-1)$ demands specific care as its '−1' refers to the continuous index of the time vector. For example, when transforming the time vector into the interval $[0, 1]$, t must not be transformed individually, but must be considered together with $t-1$. Nevertheless, this result shows that by the means of TVAR(1) estimation for $\mathcal{E}_t$, a TVAR(p+1) process for $\mathcal{S}_t$ can be established. In case a TVAR(2) process is more suitable for $\bar{\mathcal{S}}_t$, then

$$\bar{\mathcal{S}}_t = \bar{\alpha}_1(t)\bar{\mathcal{S}}_{t-1} + \bar{\alpha}_2(t)\bar{\mathcal{S}}_{t-2} + \bar{\mathcal{E}}_t.$$

If $\bar{\mathcal{S}}_t$ is here replaced by (C.5.1), then

$$\begin{aligned}
&\mathcal{S}_t - \sum_{k=1}^{p} \alpha_k(t)\mathcal{S}_{t-k} \\
&\quad = \bar{\alpha}_1(t)\left(\mathcal{S}_{t-1} - \sum_{k=1}^{p} \alpha_k(t-1)\mathcal{S}_{t-1-k}\right) + \bar{\alpha}_2(t)\left(\mathcal{S}_{t-2} - \sum_{k=1}^{p} \alpha_k(t-2)\mathcal{S}_{t-2-k}\right) + \bar{\mathcal{E}}_t.
\end{aligned}$$

A TVAR(p+2) process is obtained by separating $\mathcal{S}_t$ and by spifflicating the term:

$$\begin{aligned}
\mathcal{S}_t =& \sum_{k=1}^{p} \alpha_k(t)\mathcal{S}_{t-k} + \bar{\alpha}_1(t)\left(\mathcal{S}_{t-1} - \sum_{k=1}^{p} \alpha_k(t-1)\mathcal{S}_{t-1-k}\right)... \\
&+ \bar{\alpha}_2(t)\left(\mathcal{S}_{t-2} - \sum_{k=1}^{p} \alpha_k(t-2)\mathcal{S}_{t-2-k}\right) + \bar{\mathcal{E}}_t \\
=& \sum_{k=1}^{p} \alpha_k(t)\mathcal{S}_{t-k} + \bar{\alpha}_1(t)\mathcal{S}_{t-1} - \sum_{k=1}^{p} \bar{\alpha}_1(t)\alpha_k(t-1)\mathcal{S}_{t-1-k}... \\
&+ \bar{\alpha}_2(t)\mathcal{S}_{t-2} - \sum_{k=1}^{p} \bar{\alpha}_2(t)\alpha_k(t-2)\mathcal{S}_{t-2-k} + \bar{\mathcal{E}}_t \\
=& \sum_{k=1}^{p} \alpha_k(t)\mathcal{S}_{t-k} + \bar{\alpha}_1(t)\mathcal{S}_{t-1} - \sum_{m=2}^{p+1} \bar{\alpha}_1(t)\alpha_{m-1}(t-1)\mathcal{S}_{t-m}... \\
&+ \bar{\alpha}_2(t)\mathcal{S}_{t-2} - \sum_{m=3}^{p+2} \bar{\alpha}_2(t)\alpha_{m-2}(t-2)\mathcal{S}_{t-m} + \bar{\mathcal{E}}_t \\
=&(\alpha_1(t) + \bar{\alpha}_1(t))\mathcal{S}_{t-1}... \\
&+ (\alpha_2(t) - \bar{\alpha}_1(t)\alpha_1(t-1) + \bar{\alpha}_2(t))\mathcal{S}_{t-2}... \\
&+ \sum_{k=3}^{p} \left(\alpha_k(t) - \bar{\alpha}_1(t)\alpha_{k-1}(t-1) - \bar{\alpha}_2(t)\alpha_{k-2}(t-2)\right)\mathcal{S}_{t-k}... \\
&+ \left(-\bar{\alpha}_1(t)\alpha_p(t-1) - \bar{\alpha}_2(t)\alpha_{p-1}(t-2)\right)\mathcal{S}_{t-(p+1)}... \\
&- \bar{\alpha}_2(t)\alpha_p(t-2)\mathcal{S}_{t-(p+2)} + \bar{\mathcal{E}}_t.
\end{aligned} \tag{C.5.3}$$

The transformations are done in the same way as described for the case of the TVAR(1) process.

C.6 Composition Options of the TVAR Process Estimate

In the case of computing a TVAR(p) process by the successive estimating TVAR(1) and TVAR(2) processes, the order of these processes is essential. This is shown by the two examples in this chapter. Therefore, we use the time series

$$\boldsymbol{\mathcal{S}} = \begin{bmatrix} \mathcal{S}_1 & \mathcal{S}_2 & \mathcal{S}_3 & ... & \mathcal{S}_n \end{bmatrix}^T.$$

to estimate TVAR(p) processes successive by using different combinations of TVAR(1) and TVAR(2) processes, and compare the results.

In addition, to distinguish between the estimate of a TVAR(1) and a TVAR(2) process. Thus, the coefficients of a TVAR(1) estimate are represented by $\theta_k(t)$, and the coefficients of a TVAR(2) estimate by $\vartheta_k(t)$.

C.6.1 Iterative Estimation of a TVAR(2) Process with two Real Valued Roots

There are two ways to realize a TVAR(2) process consisting of two real roots when using successive estimation: directly via a TVAR(2) process with two real-valued roots, and on the other hand via two consecutive TVAR(1) estimates. In the first case, the model

$$\mathcal{S}_t = \vartheta_1(t)\mathcal{S}_{t-1} + \vartheta_2(t)\mathcal{S}_{t-2} + \mathcal{E}_t \qquad \forall t > 2 \tag{C.6.1}$$

is set up and solved. To replace the coefficients $\vartheta_k(t)$ by the roots of the CP $P_k(t)$, (4.3.1) can be used to obtain

$$\vartheta_1(t) = P_1(t) + P_2(t) \qquad \text{and} \qquad \vartheta_2(t) = -P_1(t)P_2(t).$$

Inserting this result in (C.6.1) gives

$$\mathcal{S}_t = (P_1(t) + P_2(t))\mathcal{S}_{t-1} - P_1(t)P_2(t)\mathcal{S}_{t-2} + \mathcal{E}_t \qquad \forall t > 2. \tag{C.6.2}$$

The case of the TVAR(1) estimation demands a two-step approach; i.e. first estimate the TVAR(1) process

$$\mathcal{S}_t = \theta_1(t)\mathcal{S}_{t-1} + \mathcal{E}_t \qquad \forall t > 1,$$

and then constructing the time series

$$\bar{\mathcal{S}}_t := \mathcal{E}_t = \mathcal{S}_t - \theta_1(t)\mathcal{S}_{t-1} \tag{C.6.3}$$

by the means of (C.5.1). For this time series, a TVAR(1) process with coefficient $\bar{\theta}_1(t)$ is estimated:

$$\bar{\mathcal{S}}_t = \bar{\theta}_1(t)\bar{\mathcal{S}}_{t-1} + \bar{\mathcal{E}}_t \qquad \forall t > 2.$$

Exchanging $\bar{\mathcal{S}}_t$ back to $\mathcal{S}_t - \theta_1(t)\mathcal{S}_{t-1}$ (see C.6.3) provides the representation

$$\mathcal{S}_t - \theta_1(t)\mathcal{S}_{t-1} = \bar{\theta}_1(t)\left(\mathcal{S}_{t-1} - \theta_1(t-1)\mathcal{S}_{t-2}\right) + \bar{\mathcal{E}}_t.$$

To change this equation into the shape of a TVAR(2) process, $\mathcal{S}_t$ is separated and the factors of $\mathcal{S}_{t-1}$ and $\mathcal{S}_{t-2}$ are separately combined:

$$\begin{aligned}\mathcal{S}_t =& \theta_1(t)\mathcal{S}_{t-1} + \bar{\theta}_1(t)\left(\mathcal{S}_{t-1} - \theta_1(t-1)\mathcal{S}_{t-2}\right) + \bar{\mathcal{E}}_t \\ =& \left(\theta_1(t) + \bar{\theta}_1(t)\right)\mathcal{S}_{t-1} - \bar{\theta}_1(t)\theta_1(t-1)\mathcal{S}_{t-2} + \bar{\mathcal{E}}_t \qquad \forall t > 2.\end{aligned} \tag{C.6.4}$$

Since the root motions are retained in the iterative procedure for each iteration it applies that

$$P_1(t) = \theta_1(t) \qquad \text{and} \qquad P_2(t) = \bar{\theta}_1(t),$$

meaning that it follows from (C.6.4) that

$$\mathcal{S}_t = \left(P_1(t) + P_2(t)\right)\mathcal{S}_{t-1} - P_1(t-1)P_2(t)\mathcal{S}_{t-2} + \bar{\mathcal{E}}_t \qquad \forall t > 2. \tag{C.6.5}$$

The result of (C.6.5) can also be found in Kamen 1988, p. 267, eq.(11)–(12). Since the first coefficient is only $P_1(t)$ and not $P_1(t-1)$, the direct comparison with (C.6.2) shows that these results are not only different, but, since $P_1(t)$ and $P_1(t-1)$ appear together, that they can also not be translated into each other by a time shift in the root $P_1(t)$.

C.6.2 The Successive Estimation of a TVAR(3) Process

There are three cases to represent a TVAR(3) process by TVAR(1) and TVAR(2) processes:

1. by successive estimation of three TVAR(1) processes,
2. by a TVAR(1) process followed by a TVAR(2) process estimation or
3. vice versa, first the TVAR(2) and then the TVAR(1) estimation.

That the first case differs from the following two is illustrated in section C.6.1. We now turn our attention to the second and third case, which, as we will show, also differ. For this purpose, the resulting TVAR(3) processes are explicitly set up and then compared to both estimation strategies. When looking at the second possibility, it is apparent that, as in section C.6.1, a TVAR(1) process is estimated. Since these steps are identical, the same time series ($\bar{\mathcal{S}}_t$) of (C.6.3) is obtained. This time series is now used to estimate a TVAR(2) process:

$$\bar{\mathcal{S}}_t = \bar{\vartheta}_1(t)\bar{\mathcal{S}}_{t-1} + \bar{\vartheta}_2(t)\bar{\mathcal{S}}_{t-2} + \bar{\mathcal{E}}_t \qquad \forall t > 3.$$

In this TVAR(2) process, $\bar{\mathcal{S}}_t$ is again replaced by (C.6.3) to get

$$\mathcal{S}_t - \theta_1(t)\mathcal{S}_{t-1} = \bar{\vartheta}_1(t)\left(\mathcal{S}_{t-1} - \theta_1(t-1)\mathcal{S}_{t-2}\right) + \bar{\vartheta}_2(t)\left(\mathcal{S}_{t-2} - \theta_1(t-2)\mathcal{S}_{t-3}\right) + \bar{\mathcal{E}}_t,$$

which is then converted into the TVAR(3) process

$$\begin{aligned}\mathcal{S}_t =& \theta_1(t)\mathcal{S}_{t-1} + \bar{\vartheta}_1(t)\left(\mathcal{S}_{t-1} - \theta_1(t-1)\mathcal{S}_{t-2}\right) + \bar{\vartheta}_2(t)\left(\mathcal{S}_{t-2} - \theta_1(t-2)\mathcal{S}_{t-3}\right) + \bar{\mathcal{E}}_t \\ =& \left(\theta_1(t) + \bar{\vartheta}_1(t)\right)\mathcal{S}_{t-1} + \left(\bar{\vartheta}_2(t) - \bar{\vartheta}_1(t)\theta_1(t-1)\right)\mathcal{S}_{t-2} - \bar{\vartheta}_2(t)\theta_1(t-2)\mathcal{S}_{t-3} + \bar{\mathcal{E}}_t \qquad \forall t > 3.\end{aligned} \tag{C.6.6}$$

Since the roots of the successively estimated TVAR(3) process coincide with the roots of the estimated TVAR(1) and TVAR(2) process –we still needs to determine the roots of the CP of the TVAR(3).
The third possibility requires the same transformations, only the other way around. Fortunately, the method to estimate the TVAR(2) process by the means of observations is exactly the same as the one used for the second case in section C.6.1. The correlating time series can thus be computed via:

$$\bar{\mathcal{S}}_t := \mathcal{S}_t - \vartheta_1(t)\mathcal{S}_{t-1} - \vartheta_2(t)\mathcal{S}_{t-2} \qquad \forall t > 2. \tag{C.6.7}$$

For this time series, we estimate a TVAR(1) process

$$\bar{\mathcal{S}}_t = \bar{\theta}_1(t)\bar{\mathcal{S}}_t + \bar{\mathcal{E}}_t \qquad \forall t > 3.$$

As in the second case, $\bar{\mathcal{S}}_t$ is replaced by (C.6.7):

$$\mathcal{S}_t - \vartheta_1(t)\mathcal{S}_{t-1} - \vartheta_2(t)\mathcal{S}_{t-2} = \bar{\theta}_1(t)\left(\mathcal{S}_{t-1} - \vartheta_1(t-1)\mathcal{S}_{t-2} - \vartheta_2(t-1)\mathcal{S}_{t-3}\right) + \bar{\mathcal{E}}_t.$$

To get the representation of the TVAR(3) process, we move $-(\vartheta_1(t)\mathcal{S}_{t-1} + \vartheta_2(t)\mathcal{S}_{t-2})$ to the other side and the simplify the expression, which results in

$$\begin{aligned}\mathcal{S}_t =& \vartheta_1(t)\mathcal{S}_{t-1} + \vartheta_2(t)\mathcal{S}_{t-2} + \bar{\theta}_1(t)\left(\mathcal{S}_{t-1} - \vartheta_1(t-1)\mathcal{S}_{t-2} - \vartheta_2(t-1)\mathcal{S}_{t-3}\right) + \bar{\mathcal{E}}_t \\ =& \left(\vartheta_1(t) + \bar{\theta}_1(t)\right)\mathcal{S}_{t-1} + \left(\vartheta_2(t) - \bar{\theta}_1(t)\vartheta_1(t-1)\right)\mathcal{S}_{t-2} - \bar{\theta}_1(t)\vartheta_2(t-1)\mathcal{S}_{t-3} + \bar{\mathcal{E}}_t \qquad \forall t > 3.\end{aligned} \tag{C.6.8}$$

The comparison between the coefficients of (C.6.6) and (C.6.8) shows that a shift in time does not work to convert them into each, which means that they are also two completely different TVAR(3) processes.

C.7 The AIC for Time Variable AR Processes

Section 2.18 shows that the AIC consists of several components that need to be adapted according to the application in question. By inserting (2.18.1) in (2.18.2), we gain

$$AIC = \ln\left(\frac{\boldsymbol{e}^T\boldsymbol{e}}{\#\text{obs}}\right) + \frac{2(\#\text{param}+1)}{\#\text{obs}} \tag{C.7.1}$$

with $\boldsymbol{e}^T\boldsymbol{e} = (\boldsymbol{y} - \tilde{\boldsymbol{y}}(\boldsymbol{\phi}))^T(\boldsymbol{y} - \tilde{\boldsymbol{y}}(\boldsymbol{\phi}))$ as the square sum of the residuals.

C.7.1 AIC for TVAR Processes with Polynomial Coefficients

In this section, we develop the AIC for the TVAR estimate with the design matrix of (C.4.4), the parameter vector (C.4.2) and the observation vector (C.2.2). Note that, due to the lack of restrictions, –like the one for the TVAR(2) process with linear root motion (see (C.4.7))– this estimate does not necessarily result in linear root movements. To accommodate the AIC of (C.7.1) for TVAR processes, it is sufficient to adjust the number of observations (#obs) and number of parameters (#param).
Note that the term 'number of observations' is here somewhat misleading. Since this number is not about the number of observations (n) itself, but about the length of the observation vector $\boldsymbol{y}$. In section C.2, it is shown that this vector does not contain the first p elements, so:

$$\#\text{obs} = n - p.$$

#param is the length of the parameter vector of (4.1.6). In Contrast to the time stable case, where the number of parameters is equal to the order of the AR process, the number of parameters in case of a TVAR estimation, is two ($\beta_0^{(1)}$ and $\beta_1^{(1)}$) if the coefficient is $\alpha_1(t)$, and increases by one with each order, meaning that $\alpha_k(t)$ consists of $k+1$ parameters (cf. (4.3.3)). Thus, a TVAR(p) process includes

$$\#\text{param} = 2 + 3 + 4 + ... + (p+1) = \sum_{k=2}^{p+1} k$$

parameters. It is further possible to simplify this sum by creating the Gaussian sum formula ($\sum_{k=1}^{p+1} k = \frac{(p+1)(p+2)}{2}$, see Bronstein et al. 2006, p. 19, eq. (1.55)). Therefore it is necessary to expanding the equation with $0 = 1 - 1$:

$$\begin{aligned}
\#\text{param} &= -1 + \underbrace{1 + \sum_{k=2}^{p+1} k}_{\sum_{k=1}^{p+1} k} \\
&= -1 + \sum_{k=1}^{p+1} k \\
&= -1 + \frac{(p+1)(p+2)}{2} \qquad \text{(C.7.2)} \\
&= -\frac{2}{2} + \frac{p^2+3p+2}{2} \\
&= \frac{p^2+3p}{2}. \qquad \text{(C.7.3)}
\end{aligned}$$

Now that the number of observations and the number of parameters are known, (C.7.1) can be expressed using (C.7.2) for the estimation of the parameters according to section 4.3.1:

$$AIC = \ln\left(\frac{\boldsymbol{e}^T\boldsymbol{e}}{n-p}\right) + \frac{(p+1)(p+2)}{n-p}.$$

The computation of the AIC was undertaken under the assumption that

$$2\left(\frac{p^2+3p}{2}+1\right)=2\frac{p^2+3p+2}{2}=(p+1)(p+2)$$

is valid.

C.7.2 AIC for Successively Estimated TVAR Processes with Linear Root Motions

As described in Section 4.3.3, TVAR(p) processes can be estimated by the successive estimation of TVAR(1) and TVAR(2) processes. However, in this case, we are confronted with a different number of parameters. Using a TVAR(1) process, results in two additional parameters for every estimation. Using a TVAR(2) process results in five parameters and one additional restriction. This restriction, however allows to express one parameter by a linear combination of the others. In this case:

$$\beta_1^{(2)}=\sqrt{(\beta_0^{(1)})^2\beta_2^{(2)}+\beta_0^{(2)}(\beta_1^{(1)})^2-\beta_0^{(1)}\beta_1^{(1)}\beta_1^{(2)}+4\beta_0^{(2)}\beta_2^{(2)}}.$$

This results in $5-1=4$ additional parameters for the two complex conjugated roots, which corresponds to two parameters per order (just like in the TVAR(1) process). Thus, regardless of the choice of order, $\#\text{param}=2p$ applies, whereby the AIC can be represented in a simplified way as

$$AIC=\ln\left(\frac{\boldsymbol{e}^T\boldsymbol{e}}{n-p}\right)+\frac{2(2p+1)}{n-p}.$$

C.8 Conditions for Quadratic Root Movements for the TVAR(2) Process Estimation

To ensure that the root motion of a TVAR(2) process follows a quadratic polynomial, the restriction

$$\sqrt{\left(\frac{\alpha_1(t)}{2}\right)^2+\alpha_2(t)}\overset{!}{=}f_1+f_2t+f_3t^2 \tag{C.8.1}$$

must be fulfilled. Because of (4.5.1), the TVAR coefficients

$$\alpha_1(t)=\beta_0^{(1)}+\beta_1^{(1)}t+\beta_2^{(1)}t^2 \text{ and } \alpha_2(t)=\beta_0^{(2)}+\beta_1^{(2)}t+\beta_2^{(2)}t^2+\beta_3^{(2)}t^3+\beta_4^{(2)}t^4 \tag{C.8.2}$$

apply. Inserting the coefficients into the restriction (C.8.1) and squaring both sides, provides aa polynomial of degree four. This way, the root in (C.8.2) vanishes. In addition, $\alpha_1(t)$ and $\alpha_2(t)$ are replaced by (C.8.2), simplifying the term:

$$\begin{aligned}
&\left(\frac{\beta_0^{(1)}+\beta_1^{(1)}t+\beta_2^{(1)}t^2}{2}\right)^2+\beta_0^{(2)}+\beta_1^{(2)}t+\beta_2^{(2)}t^2+\beta_3^{(2)}t^3+\beta_4^{(2)}t^4\\
=&\frac{(\beta_0^{(1)})^2}{4}+\frac{\beta_0^{(1)}\beta_1^{(1)}}{2}t+\frac{\beta_0^{(1)}\beta_2^{(1)}}{2}t^2+\frac{(\beta_1^{(1)})^2}{4}t^2+\frac{\beta_1^{(1)}\beta_2^{(1)}}{2}t^3+\frac{(\beta_2^{(1)})^2}{4}t^4...\\
&+\beta_0^{(2)}+\beta_1^{(2)}t+\beta_2^{(2)}t^2+\beta_3^{(2)}t^3+\beta_4^{(2)}t^4\\
=&\left(\frac{(\beta_0^{(1)})^2}{4}+\beta_0^{(2)}\right)+\left(\frac{\beta_0^{(1)}\beta_1^{(1)}}{2}+\beta_1^{(2)}\right)t+\left(\frac{\beta_0^{(1)}\beta_2^{(1)}}{2}+\frac{(\beta_1^{(1)})^2}{4}+\beta_2^{(2)}\right)t^2...\\
&+\left(\frac{\beta_1^{(1)}\beta_2^{(1)}}{2}+\beta_3^{(2)}\right)t^3+\left(\frac{(\beta_2^{(1)})^2}{4}+\beta_4^{(2)}\right)t^4.
\end{aligned} \tag{C.8.3}$$

The right side in (C.8.2) is simply squared:

$$(f_1 + f_2 t + f_3 t^2)^2 = f_1^2 + 2f_1 f_2 t + (2f_1 f_3 + f_2^2)t^2 + 2f_2 f_3 t^3 + f_3^2 t^4. \tag{C.8.4}$$

The variables f_1 and f_3 can be determined directly by comparing the coefficients of the monomials t^0 and t^4 provided by (C.8.3) and (C.8.4):

$$f_1^2 = \frac{(\beta_0^{(1)})^2}{4} + \beta_0^{(2)} \qquad \text{and} \qquad f_3^2 = \frac{(\beta_2^{(1)})^2}{4} + \beta_4^{(2)}. \tag{C.8.5}$$

Now, there are three terms, and one of them has to be selected to determine f_2. Here, we use the monomials of (C.8.3) and (C.8.4) with the basis t are to determine f_2. Since only f_1^2 can be determined by C.8.5, the sign of f_1 is undetermined. To circumvent this problem, we compute f_2^2 instead of f_2:

$$\begin{aligned} 2f_1 f_2 &= \frac{\beta_0^{(1)}\beta_1^{(1)}}{2} + \beta_1^{(2)} \\ &= \frac{\beta_0^{(1)}\beta_1^{(1)} + 2\beta_1^{(2)}}{2} \\ \Rightarrow f_2 &= \frac{\beta_0^{(1)}\beta_1^{(1)} + 2\beta_1^{(2)}}{4f_1} \\ \Rightarrow f_2^2 &= \frac{(\beta_0^{(1)}\beta_1^{(1)} + 2\beta_1^{(2)})^2}{16f_1^2}. \end{aligned}$$

By inserting (C.8.5) for f_1^2, it follows that

$$\begin{aligned} f_2^2 &= \frac{(\beta_0^{(1)}\beta_1^{(1)} + 2\beta_1^{(2)})^2}{16\left(\frac{(\beta_0^{(1)})^2}{4} + \beta_0^{(2)}\right)} \\ &= \frac{(\beta_0^{(1)}\beta_1^{(1)} + 2\beta_1^{(2)})^2}{4((\beta_0^{(1)})^2 + 4\beta_0^{(2)})}. \end{aligned} \tag{C.8.6}$$

The analogous transformation of the fourth term (the one including a monomial with the basis t^3) in (C.8.3) and (C.8.4) yields

$$\begin{aligned} f_2^2 &= \frac{(\beta_1^{(1)}\beta_2^{(1)} + 2\beta_3^{(2)})^2}{16\left(\frac{(\beta_2^{(1)})^2}{4} + \beta_4^{(2)}\right)} \\ &= \frac{(\beta_1^{(1)}\beta_2^{(1)} + 2\beta_3^{(2)})^2}{4((\beta_2^{(1)})^2 + 4\beta_4^{(2)})}. \end{aligned} \tag{C.8.7}$$

By equating the formulas for f_2^2 of (C.8.6) and (C.8.7), the restriction

$$\begin{aligned} &\frac{(\beta_0^{(1)}\beta_1^{(1)} + 2\beta_1^{(2)})^2}{4((\beta_0^{(1)})^2 + 4\beta_0^{(2)})} && \stackrel{!}{=} \frac{(\beta_1^{(1)}\beta_2^{(1)} + 2\beta_3^{(2)})^2}{4((\beta_2^{(1)})^2 + 4\beta_4^{(2)})} \\ \stackrel{(1)}{\Leftrightarrow} &(\beta_0^{(1)}\beta_1^{(1)} + 2\beta_1^{(2)})^2((\beta_2^{(1)})^2 + 4\beta_4^{(2)}) && \stackrel{!}{=} (\beta_1^{(1)}\beta_2^{(1)} + 2\beta_3^{(2)})^2((\beta_0^{(1)})^2 + 4\beta_0^{(2)}) \\ \Leftrightarrow &(\beta_0^{(1)}\beta_1^{(1)} + 2\beta_1^{(2)})^2((\beta_2^{(1)})^2 + 4\beta_4^{(2)}) && -(\beta_1^{(1)}\beta_2^{(1)} + 2\beta_3^{(2)})^2((\beta_0^{(1)})^2 + 4\beta_0^{(2)}) \stackrel{!}{=} 0 \end{aligned} \tag{C.8.8}$$

is obtained, which provides the first of two restrictions for the parameters for quadratic root motion of the TVAR(2) process. In the transformation to (1), both sides of the equation are multiplied

by $4((\beta_0^{(1)})^2 + 4\beta_0^{(2)})((\beta_2^{(1)})^2 + 4\beta_4^{(2)})$. The second restriction results again from a comparison of (C.8.3) with (C.8.4), especially from the coefficient comparison of the monomials with the basis t^2:

$$\begin{aligned} & 2f_1f_3 + f_2^2 && \stackrel{!}{=} \frac{\beta_0^{(1)}\beta_2^{(1)}}{2} + \frac{(\beta_1^{(1)})^2}{4} + \beta_2^{(2)} \\ \Leftrightarrow\ & 2f_1f_3 && \stackrel{!}{=} \frac{\beta_0^{(1)}\beta_2^{(1)}}{2} + \frac{(\beta_1^{(1)})^2}{4} + \beta_2^{(2)} - f_2^2. \end{aligned}$$

Again, we are forced with the problem of the unknown sign of f_1 and f_3, and again both sides of the equation are squared to obtain a unique solution:

$$\begin{aligned} & 4f_1^2f_3^2 && \stackrel{!}{=} \left(\frac{\beta_0^{(1)}\beta_2^{(1)}}{2} + \frac{(\beta_1^{(1)})^2}{4} + \beta_2^{(2)} - f_2^2\right)^2 \\ \Leftrightarrow\ & 4f_1^2f_3^2 - \left(\frac{\beta_0^{(1)}\beta_2^{(1)}}{2} + \frac{(\beta_1^{(1)})^2}{4} + \beta_2^{(2)} - f_2^2\right)^2 && \stackrel{!}{=} 0. \end{aligned}$$

Using f_1^2, and f_3^2 from (C.8.5) and f_2^2 from (C.8.6) results in the restriction:

$$4\left(\frac{(\beta_0^{(1)})^2}{4} + \beta_0^{(2)}\right)\left(\frac{(\beta_2^{(1)})^2}{4} + \beta_4^{(2)}\right) - \left(\frac{\beta_0^{(1)}\beta_2^{(1)}}{2} + \frac{(\beta_1^{(1)})^2}{4} + \beta_2^{(2)} - \frac{(\beta_0^{(1)}\beta_1^{(1)} + 2\beta_1^{(2)})^2}{4((\beta_0^{(1)})^2 + 4\beta_0^{(2)})}\right)^2 \stackrel{!}{=} 0. \tag{C.8.9}$$

Altogether, this means that this section provides the development of the conditions (C.8.8) and (C.8.9), which represent the sufficient conditions for the roots of a TVAR(2) process possessing a quadratic track over time.

C.9 Transforming *q(t)* and *r(t)* from the TVAR(3) Estimation into Polynomials

In this section, the auxiliary functions $q(t)$ and $r(t)$ (that arise in the TVAR(3) estimation in section 4.5.2) are rewritten as polynomials. In order to do so, the auxiliary values (2.17.3) and (2.17.4) are converted into functions, by replacing c_i by $-\alpha_i(t)$:

$$\begin{aligned} r(t) &= \frac{1}{6}(\alpha_1(t)\alpha_2(t) + 3\alpha_3(t)) - \left(\frac{-\alpha_1(t)}{3}\right)^3 \\ &= \frac{1}{6}\alpha_1(t)\alpha_2(t) + \frac{1}{2}\alpha_3(t) + \left(\frac{\alpha_1(t)}{3}\right)^3 \qquad \text{and} \\ q(t) &= \frac{-\alpha_2(t)}{3} - \left(\frac{-\alpha_1(t)}{3}\right)^2 \\ &= -\frac{\alpha_2(t)}{3} - \left(\frac{\alpha_1(t)}{3}\right)^2. \end{aligned}$$

Using the time variable coefficients of (4.5.4), (4.5.5) and (4.5.6), this can be rewritten as polynomials. Thus $r(t)$ provides a polynomial degree three:

$$\begin{aligned}
r(t) =& \frac{1}{6}(\beta_0^{(1)} + \beta_1^{(1)}t)(\beta_0^{(2)} + \beta_1^{(2)}t + \beta_2^{(2)}t^2) + \frac{1}{2}(\beta_0^{(3)} + \beta_1^{(3)}t + \beta_2^{(3)}t^2 + \beta_3^{(3)}t^3) + \frac{1}{3^3}(\beta_0^{(1)} + \beta_1^{(1)}t)^3 \\
=& \frac{\beta_0^{(1)}\beta_0^{(2)}}{6} + \frac{\beta_0^{(1)}\beta_1^{(2)} + \beta_1^{(1)}\beta_0^{(2)}}{6}t + \frac{\beta_0^{(1)}\beta_2^{(2)} + \beta_1^{(1)}\beta_1^{(2)}}{6}t^2 + \frac{\beta_1^{(1)}\beta_2^{(2)}}{6}t^3 \ldots \\
&+ \frac{\beta_0^{(3)}}{2} + \frac{\beta_1^{(3)}}{2}t + \frac{\beta_2^{(3)}}{2}t^2 + \frac{\beta_3^{(3)}}{2}t^3 \ldots \\
&+ \frac{(\beta_0^{(1)})^3}{3^3} + \frac{(\beta_0^{(1)})^2\beta_1^{(1)}}{3^2}t + \frac{\beta_0^{(1)}(\beta_1^{(1)})^2}{3^2}t^2 + \frac{(\beta_1^{(1)})^3}{3^3}t^3 \\
=& \frac{(\beta_0^{(1)})^3}{3^3} + \frac{\beta_0^{(1)}\beta_0^{(2)}}{6} + \frac{\beta_0^{(3)}}{2} \ldots \\
&+ \left(\frac{(\beta_0^{(1)})^2\beta_1^{(1)}}{3^2} + \frac{\beta_0^{(1)}\beta_1^{(2)} + \beta_1^{(1)}\beta_0^{(2)}}{6} + \frac{\beta_1^{(3)}}{2}\right)t \ldots \\
&+ \left(\frac{\beta_0^{(1)}(\beta_1^{(1)})^2}{3^2} + \frac{\beta_0^{(1)}\beta_2^{(2)} + \beta_1^{(1)}\beta_1^{(2)}}{6} + \frac{\beta_2^{(3)}}{2}\right)t^2 \ldots \\
&+ \left(\frac{(\beta_1^{(1)})^3}{3^3} + \frac{\beta_1^{(1)}\beta_2^{(2)}}{6} + \frac{\beta_3^{(3)}}{2}\right)t^3;
\end{aligned}$$

and $q(t)$ results in a polynomial of degree two:

$$\begin{aligned}
q(t) =& -\frac{\beta_0^{(2)} + \beta_1^{(2)}t + \beta_2^{(2)}t^2}{3} - \frac{(\beta_0^{(1)} + \beta_1^{(1)}t)^2}{3^2} \\
=& -\frac{\beta_0^{(2)} + \beta_1^{(2)}t + \beta_2^{(2)}t^2}{3} - \frac{(\beta_0^{(1)})^2 + 2\beta_0^{(1)}\beta_1^{(1)}t + (\beta_1^{(1)})^2t^2}{3^2} \\
=& -\left(\frac{(\beta_0^{(1)})^2}{3^2} + \frac{\beta_0^{(2)}}{3}\right) - \left(\frac{2\beta_0^{(1)}\beta_1^{(1)}}{3^2} + \frac{\beta_1^{(2)}}{3}\right)t - \left(\frac{(\beta_1^{(1)})^2}{3^2} + \frac{\beta_2^{(2)}}{3}\right)t^2.
\end{aligned}$$

C.10 Conditions for Linear Root Movement when using Direct TVAR(3) Estimation

In order to fulfil the two restrictions (4.5.7) and (4.5.8) for the direct estimation of a TVAR(3) processes with linear roots (see section 4.5.2), the conditions first demands rephrasing. Because of (2.17.5) and (2.17.6),

$$s_1(t)s_2(t) = -q(t) \qquad \text{and} \tag{C.10.1}$$

$$s_1^3(t) + s_2^3(t) = 2r(t). \tag{C.10.2}$$

applies. Here, $q(t)$ and $r(t)$ are the time variable versions of (2.17.3) and (2.17.4), as derived in Appendix C.9. This gives

$$\begin{aligned}
2r(t) =& \left(\frac{2(\beta_0^{(1)})^3}{3^3} + \frac{\beta_0^{(1)}\beta_0^{(2)}}{3} + \beta_0^{(3)}\right) + \left(\frac{2(\beta_0^{(1)})^2\beta_1^{(1)}}{3^2} + \frac{\beta_0^{(1)}\beta_1^{(2)} + \beta_1^{(1)}\beta_0^{(2)}}{3} + \beta_1^{(3)}\right)t \ldots \\
&+ \left(\frac{2\beta_0^{(1)}(\beta_1^{(1)})^2}{3^2} + \frac{\beta_0^{(1)}\beta_2^{(2)} + \beta_1^{(1)}\beta_1^{(2)}}{3} + \beta_2^{(3)}\right)t^2 + \left(\frac{2(\beta_1^{(1)})^3}{3^3} + \frac{\beta_1^{(1)}\beta_2^{(2)}}{3} + \beta_3^{(3)}\right)t^3
\end{aligned} \tag{C.10.3}$$

and

$$-q(t) = \left(\frac{(\beta_0^{(1)})^2}{3^2} + \frac{\beta_0^{(2)}}{3}\right) + \left(\frac{2\beta_0^{(1)}\beta_1^{(1)}}{3^2} + \frac{\beta_1^{(2)}}{3}\right)t + \left(\frac{(\beta_1^{(1)})^2}{3^2} + \frac{\beta_2^{(2)}}{3}\right)t^2, \tag{C.10.4}$$

which, because of the conditions in (C.10.1) and (C.10.2), must simultaneously fulfil the equations

$$\begin{aligned} 2r(t) &\stackrel{!}{=} (f_1 + f_2 t)^3 + (g_1 + g_2 t)^3 \\ &= (f_1^3 + g_1^3) + 3(f_1^2 f_2 + g_1^2 g_2)t + 3(f_1 f_2^2 + g_1 g_2^2)t^2 + (f_2^3 + g_2^3)t^3 \end{aligned} \tag{C.10.5}$$

and

$$\begin{aligned} -q(t) &\stackrel{!}{=} (f_1 + f_2 t)(g_1 + g_2 t) \\ &= f_1 g_1 + (f_1 g_2 + f_2 g_1)t + (f_2 g_2)t^2. \end{aligned} \tag{C.10.6}$$

If the polynomials in (C.10.3) and (C.10.5) are equal, each monomial must also be equal, which results in four restrictions. The same happens if (C.10.4) and (C.10.6) are equal, which adds another three restrictions. The resulting restrictions are shown in table (C.1). The next step is to

	Monomial	Restriction
$2r(t)$	1	$\frac{2(\beta_0^{(1)})^3}{3^3} + \frac{\beta_0^{(1)}\beta_0^{(2)}}{3} + \beta_0^{(3)} \stackrel{!}{=} f_1^3 + g_1^3$ (C.10.7)
	t	$\frac{2(\beta_0^{(1)})^2\beta_1^{(1)}}{3^2} + \frac{\beta_0^{(1)}\beta_1^{(2)} + \beta_1^{(1)}\beta_0^{(2)}}{3} + \beta_1^{(3)} \stackrel{!}{=} 3(f_1^2 f_2 + g_1^2 g_2)$ (C.10.8)
	t^2	$\frac{2\beta_0^{(1)}(\beta_1^{(1)})^2}{3^2} + \frac{\beta_0^{(1)}\beta_2^{(2)} + \beta_1^{(1)}\beta_1^{(2)}}{3} + \beta_2^{(3)} \stackrel{!}{=} 3(f_1 f_2^2 + g_1 g_2^2)$ (C.10.9)
	t^3	$\frac{2(\beta_1^{(1)})^3}{3^3} + \frac{\beta_1^{(1)}\beta_2^{(2)}}{3} + \beta_3^{(3)} \stackrel{!}{=} f_2^3 + g_2^3$ (C.10.10)
$-q(t)$	1	$\frac{(\beta_0^{(1)})^2}{3^2} + \frac{\beta_0^{(2)}}{3} \stackrel{!}{=} f_1 g_1$ (C.10.11)
	t	$\frac{2\beta_0^{(1)}\beta_1^{(1)}}{3^2} + \frac{\beta_1^{(2)}}{3} \stackrel{!}{=} f_1 g_2 + f_2 g_1$ (C.10.12)
	t^2	$\frac{(\beta_1^{(1)})^2}{3^2} + \frac{\beta_2^{(2)}}{3} \stackrel{!}{=} f_2 g_2.$ (C.10.13)

Table C.1: Coefficient comparison for the restrictions of TVAR(3) estimates with linear root motions

determine the variables f_1 and g_1. For this, both sides of restriction (C.10.11) are potentiated by 3:

$$\left(\frac{(\beta_0^{(1)})^2}{3^2} + \frac{\beta_0^{(2)}}{3}\right)^3 = f_1^3 g_1^3. \tag{C.10.14}$$

If f_1^3 and g_1^3 are now considered as roots of a polynomial of order two, just as the polynomial given by Bronstein et al. (2006, p. 44):

$$x^2 + c_1 x + c_2 = (x - f_1^3)(x - g_1^3) = x^2 - (f_1^3 + g_1^3)x + f_1^3 g_1^3, \tag{C.10.15}$$

then the coefficients in fact are already known. This is so, because (C.10.7) provides $c_1 = -f_1^3 - g_1^3$, while (C.10.14) provides $c_2 = f_1^3 g_1^3$, and so the first root f_1^3 can be calculated directly by the means

of the pq-formula (see 2.17.2):

$$f_1^3 = \frac{f_1^3+g_1^3}{2} + \sqrt{\left(\frac{f_1^3+g_1^3}{2}\right)^2 - f_1^3 g_1^3}$$
$$= \frac{(\beta_0^{(1)})^3}{3^3} + \frac{\beta_0^{(1)}\beta_0^{(2)}}{6} + \frac{\beta_0^{(3)}}{2} + \sqrt{\left(\frac{(\beta_0^{(1)})^3}{3^3} + \frac{\beta_0^{(1)}\beta_0^{(2)}}{6} + \frac{\beta_0^{(3)}}{2}\right)^2 - \left(\frac{(\beta_0^{(1)})^2}{3^2} + \frac{\beta_0^{(2)}}{3}\right)^3}. \tag{C.10.16}$$

The root in (C.10.16) can be simplified to

$$\left(\frac{(\beta_0^{(1)})^3}{3^3} + \frac{\beta_0^{(1)}\beta_0^{(2)}}{6} + \frac{\beta_0^{(3)}}{2}\right)^2 - \left(\frac{(\beta_0^{(1)})^2}{3^2} + \frac{\beta_0^{(2)}}{3}\right)^3$$
$$= \boxed{\frac{(\beta_0^{(1)})^6}{3^6}} + 2\frac{(\beta_0^{(1)})^4\beta_0^{(2)}}{2\cdot 3^4} + 2\frac{(\beta_0^{(1)})^3\beta_0^{(3)}}{2\cdot 3^3} + \frac{(\beta_0^{(1)})^2(\beta_0^{(2)})^2}{2^2\cdot 3^2} + 2\frac{\beta_0^{(1)}\beta_0^{(2)}\beta_0^{(3)}}{2^2\cdot 3} + \frac{(\beta_0^{(3)})^2}{2^2}\ldots$$
$$\boxed{-\frac{(\beta_0^{(1)})^6}{3^6}} - 3\frac{(\beta_0^{(1)})^4\beta_0^{(2)}}{3^5} - 3\frac{(\beta_0^{(1)})^2(\beta_0^{(2)})^2}{3^4} - \frac{(\beta_0^{(2)})^3}{3^3}$$
$$= \boxed{\frac{(\beta_0^{(1)})^4\beta_0^{(2)}}{3^4}} + \frac{(\beta_0^{(1)})^3\beta_0^{(3)}}{3^3} + \frac{(\beta_0^{(1)})^2(\beta_0^{(2)})^2}{2^2\cdot 3^2} + \frac{\beta_0^{(1)}\beta_0^{(2)}\beta_0^{(3)}}{2\cdot 3} + \frac{(\beta_0^{(3)})^2}{2^2}\ldots$$
$$\boxed{-\frac{(\beta_0^{(1)})^4\beta_0^{(2)}}{3^4}} - \frac{(\beta_0^{(1)})^2(\beta_0^{(2)})^2}{3^3} - \frac{(\beta_0^{(2)})^3}{3^3}$$
$$= \frac{(\beta_0^{(1)})^3\beta_0^{(3)}}{3^3} + \boxed{\frac{3(\beta_0^{(1)})^2(\beta_0^{(2)})^2}{2^2\cdot 3^3}} + \frac{\beta_0^{(1)}\beta_0^{(2)}\beta_0^{(3)}}{2\cdot 3} + \frac{(\beta_0^{(3)})^2}{2^2}\boxed{-\frac{2^2(\beta_0^{(1)})^2(\beta_0^{(2)})^2}{2^2\cdot 3^3}} - \frac{(\beta_0^{(2)})^3}{3^3}$$
$$= \frac{(\beta_0^{(1)})^3\beta_0^{(3)}}{3^3} + \frac{\beta_0^{(1)}\beta_0^{(2)}\beta_0^{(3)}}{2\cdot 3} + \frac{(\beta_0^{(3)})^2}{2^2}\boxed{-\frac{(\beta_0^{(1)})^2(\beta_0^{(2)})^2}{2^2\cdot 3^3}} - \frac{(\beta_0^{(2)})^3}{3^3}.$$

Here, the red boxes in the first and second rows indicate identical terms with different signs that cancel each other out, while the two blue boxes of the penultimate row are merged into the blue box of the last row. Inserting the results in (C.10.16) yields:

$$f_1^3 = \frac{(\beta_0^{(1)})^3}{3^3} + \frac{\beta_0^{(1)}\beta_0^{(2)}}{6} + \frac{\beta_0^{(3)}}{2} + \sqrt{\frac{(\beta_0^{(1)})^3\beta_0^{(3)}}{3^3} + \frac{\beta_0^{(1)}\beta_0^{(2)}\beta_0^{(3)}}{2\cdot 3} + \frac{(\beta_0^{(3)})^2}{2^2} - \frac{(\beta_0^{(1)})^2(\beta_0^{(2)})^2}{2^2\cdot 3^3} - \frac{(\beta_0^{(2)})^3}{3^3}}. \tag{C.10.17}$$

The same simplification can also be done for the second root g_1 of (C.10.15):

$$g_1^3 = \frac{f_1^3+g_1^3}{2} - \sqrt{\left(\frac{f_1^3+g_1^3}{2}\right)^2 - f_1^3 g_1^3}$$
$$= \frac{(\beta_0^{(1)})^3}{3^3} + \frac{\beta_0^{(1)}\beta_0^{(2)}}{6} + \frac{\beta_0^{(3)}}{2} - \sqrt{\frac{(\beta_0^{(1)})^3\beta_0^{(3)}}{3^3} + \frac{\beta_0^{(1)}\beta_0^{(2)}\beta_0^{(3)}}{2\cdot 3} + \frac{(\beta_0^{(3)})^2}{2^2} - \frac{(\beta_0^{(1)})^2(\beta_0^{(2)})^2}{2^2\cdot 3^3} - \frac{(\beta_0^{(2)})^3}{3^3}}. \tag{C.10.18}$$

Notice the change of the sign (extra visualized by the red minus '$-$'). For the variables f_2 and g_2, we use the restrictions in (C.10.10) and (C.10.13) to reveal that

$$\frac{2(\beta_1^{(1)})^3}{3^3} + \frac{\beta_1^{(1)}\beta_2^{(2)}}{3} + \beta_3^{(3)} = f_2^3 + g_2^3$$
$$\frac{(\beta_1^{(1)})^2}{3^2} + \frac{\beta_2^{(2)}}{3} = f_2 g_2$$

is valid. These are the same equations as used in the case of f_1 in (C.10.17) and of g_1 in (C.10.18), except that $\beta_0^{(1)}$ is exchanged for $\beta_1^{(1)}$, $\beta_0^{(2)}$ by $\beta_2^{(2)}$, and $\beta_0^{(3)}$ by $\beta_3^{(3)}$. Thus, the result can be represented directly by exchanging these variables in (C.10.17) and in (C.10.18):

$$f_2^3 = \frac{(\beta_1^{(1)})^3}{3^3} + \frac{\beta_1^{(1)}\beta_2^{(2)}}{6} + \frac{\beta_3^{(3)}}{2} + \sqrt{\frac{(\beta_1^{(1)})^3\beta_3^{(3)}}{3^3} + \frac{\beta_1^{(1)}\beta_2^{(2)}\beta_3^{(3)}}{2\cdot 3} + \frac{(\beta_3^{(3)})^2}{2^2} - \frac{(\beta_1^{(1)})^2(\beta_2^{(2)})^2}{2^2\cdot 3^3} - \frac{(\beta_2^{(2)})^3}{3^3}} \tag{C.10.19}$$

and

$$g_2^3 = \frac{(\beta_1^{(1)})^3}{3^3} + \frac{\beta_1^{(1)}\beta_2^{(2)}}{6} + \frac{\beta_3^{(3)}}{2} - \sqrt{\frac{(\beta_1^{(1)})^3\beta_3^{(3)}}{3^3} + \frac{\beta_1^{(1)}\beta_2^{(2)}\beta_3^{(3)}}{2\cdot 3} + \frac{(\beta_3^{(3)})^2}{2^2} - \frac{(\beta_1^{(1)})^2(\beta_2^{(2)})^2}{2^2\cdot 3^3} - \frac{(\beta_2^{(2)})^3}{3^3}}. \tag{C.10.20}$$

Now that the third potency of the variables f_1, f_2, g_1 and g_2 are determined by (C.10.17), (C.10.18), (C.10.19) and (C.10.20), we can use them in the restrictions with the mixed terms in (C.10.8), (C.10.9) and (C.10.12):

$$\mathcal{C}_1^{\mathrm{TVAR}(3)}(\boldsymbol{\beta}) = \frac{2(\beta_0^{(1)})^2\beta_1^{(1)}}{3^2} + \frac{\beta_0^{(1)}\beta_1^{(2)} + \beta_1^{(1)}\beta_0^{(2)}}{3} + \beta_1^{(3)} - 3\left[\left(\sqrt[3]{f_1^3}\right)^2\sqrt[3]{f_2^3} + \left(\sqrt[3]{g_1^3}\right)^2\sqrt[3]{g_2^3}\right] \stackrel{!}{=} 0 \tag{C.10.21}$$

$$\mathcal{C}_2^{\mathrm{TVAR}(3)}(\boldsymbol{\beta}) = \frac{2\beta_0^{(1)}(\beta_1^{(1)})^2}{3^2} + \frac{\beta_0^{(1)}\beta_2^{(2)} + \beta_1^{(1)}\beta_1^{(2)}}{3} + \beta_2^{(3)} - 3\left[\sqrt[3]{f_1^3}\left(\sqrt[3]{f_2^3}\right)^2 + \sqrt[3]{g_1^3}\left(\sqrt[3]{g_2^3}\right)^2\right] \stackrel{!}{=} 0 \tag{C.10.22}$$

$$\mathcal{C}_3^{\mathrm{TVAR}(3)}(\boldsymbol{\beta}) = \frac{2\beta_0^{(1)}\beta_0^{(2)}}{3^2} + \frac{\beta_1^{(2)}}{3} - \sqrt[3]{f_1^3}\sqrt[3]{g_2^3} + \sqrt[3]{f_2^3}\sqrt[3]{g_1^3} \stackrel{!}{=} 0 \tag{C.10.23}$$

Ultimately (C.10.21), (C.10.22) and (C.10.23) provide the non-linear constraints of the parameters $\beta_l^{(k)}$ of the TVAR(3) process estimation. With that all roots move linear in time.

C.11 Derivation of the Conditional Matrices according to the Parameters

Section C.4 described the process of how to estimate a TVAR(2) process by the means of two steps: in the first step, in order to fit the observations as closely as possible, the parameters $\tilde{\boldsymbol{\beta}}$ of the TVAR process and its cofactor matrix $Q\{\tilde{\boldsymbol{\beta}}\}$ are estimated. In a second step, further restrictions are placed on the parameters, in such a way, that the root moves linearly in time. A conditional matrix $\boldsymbol{H}^T$ is derived, to apply the restrictions. This matrix allows the determination of the parameters $\hat{\boldsymbol{\beta}}$ that best fit the observations and additionally fulfil the restrictions, while its cofactor matrix ($Q\{\hat{\boldsymbol{\beta}}\}$) is derived in (C.4.11).
In order to add the restrictions for approaches with different TVAR estimation methods, the formulas themselves remain the same, while the matrix $\boldsymbol{H}^T$ has to be updated according to the alternative restrictions.
In this section, we establish the condition matrices $\boldsymbol{H}^T$ for the for the TVAR(2) estimation with piecewise linear root motions (see section 4.4.5), for the TVAR(2) process with quadratic root motions (see section 4.5.1), and for the TVAR(3) process with linear root motion (see section 4.5.2). For this purpose, the following sections specify the conditional functions $\mathcal{C}(\boldsymbol{\beta})$ and their linearizations.

C.11.1 Condition Matrix for the TVAR(2) Process with Piecewise Linear Root Motions

In the case of piecewise estimation discussed in section 4.4, a distinction is made between two intervals (see section 4.4.4) and any interval η of N intervals (see section 4.4.5). Since the case of two intervals stats a special case of the general form (with $\eta = 2$), the section only discusses the derivative of the general condition of (4.4.11):

$$\begin{aligned}\mathcal{C}_\eta^{\mathrm{PW}}(\boldsymbol{\beta}) = &\left(\beta_0^{(1,I)} + \sum_{\mu=1}^{\eta-1}\beta_1^{(1,\mu)}\right)^2 \beta_2^{(2,\eta)} + \left(\beta_0^{(2,I)} + \sum_{\mu=1}^{\eta-1}(\beta_1^{(2,\mu)} + \beta_2^{(2,\mu)})\right)(\beta_1^{(1,\eta)})^2 \ldots \\ &- \left(\beta_0^{(1,I)} + \sum_{\mu=1}^{\eta-1}\beta_1^{(1,\mu)}\right)\beta_1^{(1,\eta)}\beta_1^{(2,\eta)} + 4\left(\beta_0^{(2,I)} + \sum_{\mu=1}^{\eta-1}(\beta_1^{(2,\mu)} + \beta_2^{(2,\mu)})\right)\beta_2^{(2,\eta)} - (\beta_1^{(2,\eta)})^2.\end{aligned}$$

$\mathcal{C}_\eta^{\mathrm{PW}}(\boldsymbol{\beta})$ provides a restrictions for each interval. The derivative of the condition of the η's interval with respect to the vector $\boldsymbol{\beta}$ is symbolized by

$$\boldsymbol{H}_\eta := \left[\begin{array}{cc|ccc|c|ccc} \frac{\delta\mathcal{C}_\eta^{\mathrm{PW}}(\boldsymbol{\beta})}{\delta\beta_0^{(1,I)}} & \frac{\delta\mathcal{C}_\eta^{\mathrm{PW}}(\boldsymbol{\beta})}{\delta\beta_0^{(2,I)}} & \frac{\delta\mathcal{C}_\eta^{\mathrm{PW}}(\boldsymbol{\beta})}{\delta\beta_1^{(1,I)}} & \frac{\delta\mathcal{C}_\eta^{\mathrm{PW}}(\boldsymbol{\beta})}{\delta\beta_1^{(2,I)}} & \frac{\delta\mathcal{C}_\eta^{\mathrm{PW}}(\boldsymbol{\beta})}{\delta\beta_2^{(2,I)}} & \ldots & \frac{\delta\mathcal{C}_\eta^{\mathrm{PW}}(\boldsymbol{\beta})}{\delta\beta_1^{(1,N)}} & \frac{\delta\mathcal{C}_\eta^{\mathrm{PW}}(\boldsymbol{\beta})}{\delta\beta_1^{(2,N)}} & \frac{\delta\mathcal{C}_\eta^{\mathrm{PW}}(\boldsymbol{\beta})}{\delta\beta_2^{(2,N)}} \end{array}\right].$$

The vector $\boldsymbol{H}_\eta$ for $\eta \in [1, N]$ is the ηs column of $\boldsymbol{H}^T$. The sum representation of $\mathcal{C}_\eta^{\mathrm{PW}}(\boldsymbol{\beta})$ allows the division of the derivatives into five groups (see Table C.2). The choice of the groups depends on the parameters used for the derivative. The representation of the parameter as

$$\beta_0^{(1,I)} + \sum_{\mu=1}^{\eta-1}\beta_1^{(1,\mu)} \qquad \text{and} \qquad \beta_0^{(2,I)} + \sum_{\mu=1}^{\eta-1}(\beta_1^{(2,\mu)} + \beta_2^{(2,\mu)})$$

helps by this choice of the right group. Furthermore, in each group, the derivative of $\mathcal{C}_\eta^{\mathrm{PW}}(\boldsymbol{\beta})$, always gives the same result (see table C.2).

C.11.2 Condition Matrix for the TVAR(2) Process for Quadratic Root Motion

The TVAR(2) process with quadratic roots motions from section 4.5.1 must fulfil two condition functions. In order to guarantee that these are fulfilled after the estimation, a matrix $\boldsymbol{H}^T$ of two columns is created, to symbolize the derivatives of a conditions $\mathcal{C}_1^{\mathrm{quad}}(\boldsymbol{\beta})$ and $\mathcal{C}_2^{\mathrm{quad}}(\boldsymbol{\beta})$ with respect to the parameter vector $\boldsymbol{\beta}$:

$$\boldsymbol{H}^T = \left[\begin{array}{cccccccc} \frac{\delta\mathcal{C}_1^{\mathrm{quad}}(\boldsymbol{\beta})}{\delta\beta_0^{(1)}} & \frac{\delta\mathcal{C}_1^{\mathrm{quad}}(\boldsymbol{\beta})}{\delta\beta_0^{(2)}} & \frac{\delta\mathcal{C}_1^{\mathrm{quad}}(\boldsymbol{\beta})}{\delta\beta_1^{(1)}} & \frac{\delta\mathcal{C}_1^{\mathrm{quad}}(\boldsymbol{\beta})}{\delta\beta_1^{(2)}} & \frac{\delta\mathcal{C}_1^{\mathrm{quad}}(\boldsymbol{\beta})}{\delta\beta_2^{(1)}} & \frac{\delta\mathcal{C}_1^{\mathrm{quad}}(\boldsymbol{\beta})}{\delta\beta_2^{(2)}} & \frac{\delta\mathcal{C}_1^{\mathrm{quad}}(\boldsymbol{\beta})}{\delta\beta_3^{(2)}} & \frac{\delta\mathcal{C}_1^{\mathrm{quad}}(\boldsymbol{\beta})}{\delta\beta_4^{(2)}} \\ \frac{\delta\mathcal{C}_2^{\mathrm{quad}}(\boldsymbol{\beta})}{\delta\beta_0^{(1)}} & \frac{\delta\mathcal{C}_2^{\mathrm{quad}}(\boldsymbol{\beta})}{\delta\beta_0^{(2)}} & \frac{\delta\mathcal{C}_2^{\mathrm{quad}}(\boldsymbol{\beta})}{\delta\beta_1^{(1)}} & \frac{\delta\mathcal{C}_2^{\mathrm{quad}}(\boldsymbol{\beta})}{\delta\beta_1^{(2)}} & \frac{\delta\mathcal{C}_2^{\mathrm{quad}}(\boldsymbol{\beta})}{\delta\beta_2^{(1)}} & \frac{\delta\mathcal{C}_2^{\mathrm{quad}}(\boldsymbol{\beta})}{\delta\beta_2^{(2)}} & \frac{\delta\mathcal{C}_2^{\mathrm{quad}}(\boldsymbol{\beta})}{\delta\beta_3^{(2)}} & \frac{\delta\mathcal{C}_2^{\mathrm{quad}}(\boldsymbol{\beta})}{\delta\beta_4^{(2)}} \end{array}\right].$$

Table C.3 provides the derivatives of the first condition of (4.5.2)

$$\mathcal{C}_1^{\mathrm{quad}}(\boldsymbol{\beta}) = \left(\beta_0^{(1)}\beta_1^{(1)} + 2\beta_1^{(2)}\right)^2\left((\beta_2^{(1)})^2 + 4\beta_4^{(2)}\right) - \left(\beta_1^{(1)}\beta_2^{(1)} + 2\beta_3^{(2)}\right)^2\left((\beta_0^{(1)})^2 + 4\beta_0^{(2)}\right) \stackrel{!}{=} 0,$$

and Table C.4 provides the derivatives of the second condition of (4.5.3)

$$\begin{aligned}&\mathcal{C}_2^{\mathrm{quad}}(\boldsymbol{\beta}) \\ &= 4\left(\frac{(\beta_0^{(1)})^2}{4} + \beta_0^{(2)}\right)\left(\frac{(\beta_2^{(1)})^2}{4} + \beta_4^{(2)}\right) - \left(\frac{\beta_0^{(1)}\beta_2^{(1)}}{2} + \frac{(\beta_1^{(1)})^2}{4} + \beta_2^{(2)} - \frac{(\beta_0^{(1)}\beta_1^{(1)} + 2\beta_1^{(2)})^2}{4((\beta_0^{(1)})^2 + 4\beta_0^{(2)})}\right)^2 \stackrel{!}{=} 0.\end{aligned}$$

The derivatives are computed with respect to the parameters $\boldsymbol{\beta}$.

Parameter in Group	Derivative of $\mathcal{C}_\eta^{\mathrm{PW}}(\boldsymbol{\beta})$
$\beta_0^{(1,I)}$ $\beta_1^{(1,\mu)}$ with $\mu < \eta$	$2\left(\beta_0^{(1,I)} + \sum_{\mu=1}^{\eta-1} \beta_1^{(1,\mu)}\right)\beta_2^{(2,\eta)} - \beta_1^{(1,\eta)}\beta_1^{(2,\eta)}$
$\beta_0^{(2,I)}$ $\beta_1^{(2,\mu)}$ with $\mu < \eta$ $\beta_2^{(2,\mu)}$ with $\mu < \eta$	$(\beta_1^{(1,\eta)})^2 + 4\beta_2^{(2,\eta)}$
$\beta_1^{(1,\eta)}$	$2\left(\beta_0^{(2,I)} + \sum_{\mu=1}^{\eta-1}(\beta_1^{(2,\mu)} + \beta_2^{(2,\mu)})\right)\beta_1^{(1,\eta)} - \left(\beta_0^{(1,I)} + \sum_{\mu=1}^{\eta-1}\beta_1^{(1,\mu)}\right)\beta_1^{(2,\eta)}$
$\beta_1^{(2,\eta)}$	$-\left(\beta_0^{(1,I)} + \sum_{\mu=1}^{\eta-1}\beta_1^{(1,\mu)}\right)\beta_1^{(1,\eta)} - 2\beta_1^{(2,\eta)}$
$\beta_2^{(2,\eta)}$	$\left(\beta_0^{(1,I)} + \sum_{\mu=1}^{\eta-1}\beta_1^{(1,\mu)}\right)^2 + 4\left(\beta_0^{(2,I)} + \sum_{\mu=1}^{\eta-1}(\beta_1^{(2,\mu)} + \beta_2^{(2,\mu)})\right)$
$\beta_k^{(l,\mu)}$ with $k \leq 2, l \leq k, \mu > \eta$,	0

Table C.2: Partial derivative of the condition for linear root motions of TVAR processes with piecewise linear root motion for the η-th interval (with respect to the parameters).

Parameter	Derivative of $\mathcal{C}_1^{\mathrm{quad}}$
$\beta_0^{(1)}$	$2\left(\beta_0^{(1)}\beta_1^{(1)} + 2\beta_1^{(2)}\right)\left((\beta_2^{(1)})^2 + 4\beta_4^{(2)}\right)\beta_1^{(1)} - 2\beta_0^{(1)}\left(\beta_1^{(1)}\beta_2^{(1)} + 2\beta_3^{(2)}\right)^2$
$\beta_1^{(1)}$	$2\left(\beta_0^{(1)}\beta_1^{(1)} + 2\beta_1^{(2)}\right)\left((\beta_2^{(1)})^2 + 4\beta_4^{(2)}\right)\beta_0^{(1)} - 2\left(\beta_1^{(1)}\beta_2^{(1)} + 2\beta_3^{(2)}\right)\left((\beta_0^{(1)})^2 + 4\beta_0^{(2)}\right)\beta_2^{(1)}$
$\beta_2^{(1)}$	$2\left(\beta_0^{(1)}\beta_1^{(1)} + 2\beta_1^{(2)}\right)^2\beta_2^{(1)} - 2\left(\beta_1^{(1)}\beta_2^{(1)} + 2\beta_3^{(2)}\right)\left((\beta_0^{(1)})^2 + 4\beta_0^{(2)}\right)\beta_1^{(1)}$
$\beta_0^{(2)}$	$-4\left(\beta_1^{(1)}\beta_2^{(1)} + 2\beta_3^{(2)}\right)^2$
$\beta_1^{(2)}$	$4\left(\beta_0^{(1)}\beta_1^{(1)} + 2\beta_1^{(2)}\right)\left((\beta_2^{(1)})^2 + 4\beta_4^{(2)}\right)$
$\beta_2^{(2)}$	0
$\beta_3^{(2)}$	$-4\left(\beta_1^{(1)}\beta_2^{(1)} + 2\beta_3^{(2)}\right)\left((\beta_0^{(1)})^2 + 4\beta_0^{(2)}\right)$
$\beta_4^{(2)}$	$4\left(\beta_0^{(1)}\beta_1^{(1)} + 2\beta_1^{(2)}\right)^2$

Table C.3: Partial derivative of the first equations of condition $\mathcal{C}_1^{\mathrm{quad}}(\boldsymbol{\beta})$ for the quadratic root motion (with respect to the parameters).

Parameter	Derivative of $\mathcal{C}_2^{\text{quad}}$
$\beta_0^{(1)}$	$2\beta_0^{(1)}\left(\frac{(\beta_2^{(1)})^2}{4}+\beta_4^{(2)}\right)$ $-2\left(\frac{\beta_0^{(1)}\beta_2^{(1)}}{2}+\frac{(\beta_1^{(1)})^2}{4}+\beta_2^{(2)}-\frac{(\beta_0^{(1)}\beta_1^{(1)}+2\beta_1^{(2)})^2}{4((\beta_0^{(1)})^2+4\beta_0^{(2)})}\right)\left(\frac{\beta_2^{(1)}}{2}-\frac{\beta_1^{(1)}(\beta_0^{(1)}\beta_1^{(1)}+2\beta_1^{(2)})((\beta_0^{(1)})^2+4\beta_0^{(2)})-\beta_0^{(1)}(\beta_0^{(1)}\beta_1^{(1)}+2\beta_1^{(2)})^2}{2((\beta_0^{(1)})^2+4\beta_0^{(2)})}\right)$
$\beta_1^{(1)}$	$-2\left(\frac{\beta_0^{(1)}\beta_2^{(1)}}{2}+\frac{(\beta_1^{(1)})^2}{4}+\beta_2^{(2)}-\frac{(\beta_0^{(1)}\beta_1^{(1)}+2\beta_1^{(2)})^2}{4((\beta_0^{(1)})^2+4\beta_0^{(2)})}\right)\left(\frac{\beta_1^{(1)}}{2}-\frac{\beta_0^{(1)}(\beta_0^{(1)}\beta_1^{(1)}+2\beta_1^{(2)})}{2((\beta_0^{(1)})^2+4\beta_0^{(2)})}\right)$
$\beta_2^{(1)}$	$2\beta_2^{(1)}\left(\frac{(\beta_0^{(1)})^2}{4}+\beta_0^{(2)}\right)-\beta_0^{(1)}\left(\frac{\beta_0^{(1)}\beta_2^{(1)}}{2}+\frac{(\beta_1^{(1)})^2}{4}+\beta_2^{(2)}-\frac{(\beta_0^{(1)}\beta_1^{(1)}+2\beta_1^{(2)})^2}{4((\beta_0^{(1)})^2+4\beta_0^{(2)})}\right)$
$\beta_0^{(2)}$	$4\left(\frac{(\beta_2^{(1)})^2}{4}+\beta_4^{(2)}\right)-2\left(\frac{\beta_0^{(1)}\beta_2^{(1)}}{2}+\frac{(\beta_1^{(1)})^2}{4}+\beta_2^{(2)}-\frac{(\beta_0^{(1)}\beta_1^{(1)}+2\beta_1^{(2)})^2}{4((\beta_0^{(1)})^2+4\beta_0^{(2)})}\right)\left(\frac{\beta_0^{(1)}\beta_1^{(1)}+2\beta_1^{(2)}}{(\beta_0^{(1)})^2+4\beta_0^{(2)}}\right)^2$
$\beta_1^{(2)}$	$2\left(\frac{\beta_0^{(1)}\beta_2^{(1)}}{2}+\frac{(\beta_1^{(1)})^2}{4}+\beta_2^{(2)}-\frac{(\beta_0^{(1)}\beta_1^{(1)}+2\beta_1^{(2)})^2}{4((\beta_0^{(1)})^2+4\beta_0^{(2)})}\right)\left(\frac{\beta_0^{(1)}\beta_1^{(1)}+2\beta_1^{(2)}}{(\beta_0^{(1)})^2+4\beta_0^{(2)}}\right)$
$\delta\beta_2^{(2)}$	$-2\left(\frac{\beta_0^{(1)}\beta_2^{(1)}}{2}+\frac{(\beta_1^{(1)})^2}{4}+\beta_2^{(2)}-\frac{(\beta_0^{(1)}\beta_1^{(1)}+2\beta_1^{(2)})^2}{4((\beta_0^{(1)})^2+4\beta_0^{(2)})}\right)$
$\beta_3^{(2)}$	0
$\beta_4^{(2)}$	$4\left(\frac{(\beta_0^{(1)})^2}{4}+\beta_0^{(2)}\right)$

Table C.4: Partial derivatives of the first equations of condition $\mathcal{C}_2^{\text{quad}}(\boldsymbol{\beta})$ for the quadratic root motion (with respect to the parameters).

C.11.3 Condition Matrix for the TVAR(3) Process with Linear Root Motions

Section 4.5.2 presents the conditions of the linear root motions of a TVAR(3) process, described by

$$\begin{aligned}
\mathcal{C}_1^{\mathrm{TVAR(3)}}(\boldsymbol{\beta}) &= \frac{2(\beta_0^{(1)})^2\beta_1^{(1)}}{3^2} + \frac{\beta_0^{(1)}\beta_1^{(2)} + \beta_1^{(1)}\beta_0^{(2)}}{3} + \beta_1^{(3)} - 3\left[f_1^2 f_2 + g_1^2 g_2\right] &&\stackrel{!}{=} 0\\
\mathcal{C}_2^{\mathrm{TVAR(3)}}(\boldsymbol{\beta}) &= \frac{2\beta_0^{(1)}(\beta_1^{(1)})^2}{3^2} + \frac{\beta_0^{(1)}\beta_2^{(2)} + \beta_1^{(1)}\beta_1^{(2)}}{3} + \beta_2^{(3)} - 3\left[f_1 f_2^2 + g_1 g_2^2\right] &&\stackrel{!}{=} 0\\
\mathcal{C}_3^{\mathrm{TVAR(3)}}(\boldsymbol{\beta}) &= \frac{2\beta_0^{(1)}\beta_1^{(1)}}{3^2} + \frac{\beta_1^{(2)}}{3} - f_1 g_2 + f_2 g_1 &&\stackrel{!}{=} 0
\end{aligned}$$

with

$$\begin{aligned}
f_1 &= \sqrt[3]{u_1 + w_1}, & f_2 &= \sqrt[3]{u_2 + w_2},\\
g_1 &= \sqrt[3]{u_1 - w_1} \quad \text{and} & g_2 &= \sqrt[3]{u_2 - w_2}.
\end{aligned}$$

The formulae have been simplified and the definitions

$$\begin{aligned}
u_1 &= \frac{(\beta_0^{(1)})^3}{3^3} + \frac{\beta_0^{(1)}\beta_0^{(2)}}{6} + \frac{\beta_0^{(3)}}{2},\\
u_2 &= \frac{(\beta_1^{(1)})^3}{3^3} + \frac{\beta_1^{(1)}\beta_2^{(2)}}{6} + \frac{\beta_3^{(3)}}{2},\\
w_1 &= \sqrt{\frac{(\beta_0^{(1)})^3\beta_0^{(3)}}{3^3} + \frac{\beta_0^{(1)}\beta_0^{(2)}\beta_0^{(3)}}{2\cdot 3} + \frac{(\beta_0^{(3)})^2}{2^2} - \frac{(\beta_0^{(1)})^2(\beta_0^{(2)})^2}{2^2\cdot 3^3} - \frac{(\beta_0^{(2)})^3}{3^3}} \quad \text{and}\\
w_2 &= \sqrt{\frac{(\beta_1^{(1)})^3\beta_3^{(3)}}{3^3} + \frac{\beta_1^{(1)}\beta_2^{(2)}\beta_3^{(3)}}{2\cdot 3} + \frac{(\beta_3^{(3)})^2}{2^2} - \frac{(\beta_1^{(1)})^2(\beta_2^{(2)})^2}{2^2\cdot 3^3} - \frac{(\beta_2^{(2)})^3}{3^3}}
\end{aligned}$$

are introduced here. The division of each condition into three formulas helps in determining the derivatives. These derivatives are again used to fill a condition matrix $\boldsymbol{H}^T$ from the use in the constrained adjustment. Note that the derivatives of f_1, g_1, f_2 and g_2 are very similar. Thus, for f_1 we can see that

$$\begin{aligned}
\frac{\delta f_1}{\delta\beta_0^{(1)}} &= \frac{\delta f_1}{\delta(u_1+w_1)}\left(\frac{\delta u_1}{\delta\beta_0^{(1)}} + \frac{\delta w_1}{\delta\beta_0^{(1)}}\right)\\
&= \frac{1}{3f_1^2}\left[\frac{(\beta_0^{(1)})^2}{3^2} + \frac{\beta_0^{(2)}}{6} + \frac{1}{2w_1}\left(\frac{(\beta_0^{(1)})^2\beta_0^{(3)}}{3^2} + \frac{\beta_0^{(2)}\beta_0^{(3)}}{2\cdot 3} - \frac{\beta_0^{(1)}(\beta_0^{(2)})^2}{2\cdot 3^3}\right)\right], \qquad \text{(C.11.1)}\\
\frac{\delta f_1}{\delta\beta_0^{(2)}} &= \frac{\delta f_1}{\delta(u_1+w_1)}\left(\frac{\delta u_1}{\delta\beta_0^{(2)}} + \frac{\delta w_1}{\delta\beta_0^{(2)}}\right)\\
&= \frac{1}{3f_1^2}\left[\frac{\beta_0^{(1)}}{6} + \frac{1}{2w_1}\left(\frac{\beta_0^{(1)}\beta_0^{(3)}}{2\cdot 3} - \frac{(\beta_0^{(1)})^2\beta_0^{(2)}}{2\cdot 3^3} - \frac{(\beta_0^{(2)})^2}{3^2}\right)\right] \qquad \text{and} \qquad \text{(C.11.2)}\\
\frac{\delta f_1}{\delta\beta_0^{(3)}} &= \frac{\delta f_1}{\delta(u_1+w_1)}\left(\frac{\delta u_1}{\delta\beta_0^{(3)}} + \frac{\delta w_1}{\delta\beta_0^{(3)}}\right)\\
&= \frac{1}{3f_1^2}\left[\frac{1}{2} + \frac{1}{2w_1}\left(\frac{(\beta_0^{(1)})^3}{3^3} + \frac{\beta_0^{(1)}\beta_0^{(2)}}{2\cdot 3} + \frac{(\beta_0^{(3)})}{2}\right)\right] \qquad \text{(C.11.3)}
\end{aligned}$$

apply. All other partial derivatives of f_1 (with respect to the parameters) are equal to zero. Since the difference between f_1 and g_1 is only the sign, while the difference between u_1 and u_2 are the indices of the $\beta_l^{(k)}$:

$$\beta_0^{(1)} = \beta_1^{(1)}, \beta_0^{(2)} = \beta_2^{(2)} \text{ and } \beta_0^{(3)} = \beta_3^{(3)},$$

the other functions do not require manual derivatives. Same is valid for the derivative of g_2. The derivatives of the three conditions can then be easily taken from Table C.5.

Parameter	Derivative of $\mathcal{C}_1^{\text{TVAR(3)}}(\boldsymbol{\beta})$	Derivative of $\mathcal{C}_2^{\text{TVAR(3)}}(\boldsymbol{\beta})$	Derivative of $\mathcal{C}_3^{\text{TVAR(3)}}(\boldsymbol{\beta})$
$\beta_0^{(1)}$	$\frac{4}{3^2}\beta_0^{(1)}\beta_1^{(1)} + \frac{\beta_1^{(2)}}{3} - 6\left[f_1 f_2 \frac{\delta f_1}{\delta \beta_0^{(1)}} + g_1 g_2 \frac{\delta g_1}{\delta \beta_0^{(1)}}\right]$	$\frac{2}{3^2}(\beta_1^{(1)})^2 + \frac{\beta_2^{(2)}}{3} - 3\left[f_2^2 \frac{\delta f_1}{\delta \beta_0^{(1)}} + g_2^2 \frac{\delta g_1}{\delta \beta_0^{(1)}}\right]$	$\frac{2}{3^2}\beta_1^{(1)} - \left[g_2 \frac{\delta f_1}{\delta \beta_0^{(1)}} + f_2 \frac{\delta g_1}{\delta \beta_0^{(1)}}\right]$
$\beta_1^{(1)}$	$\frac{2}{3^2}(\beta_0^{(1)})^2 + \frac{\beta_0^{(2)}}{3} - 3\left[f_1^2 \frac{\delta f_2}{\delta \beta_1^{(1)}} + g_1^2 \frac{\delta g_2}{\delta \beta_1^{(1)}}\right]$	$\frac{4}{3^2}\beta_0^{(1)}\beta_1^{(1)} + \frac{\beta_1^{(2)}}{3} - 6\left[f_1 f_2 \frac{\delta f_2}{\delta \beta_1^{(1)}} + g_1 g_2 \frac{\delta g_2}{\delta \beta_1^{(1)}}\right]$	$\frac{2}{3^2}\beta_0^{(1)} - \left[f_1 \frac{g_2}{\delta \beta_1^{(1)}} + g_1 \frac{f_2}{\delta \beta_1^{(1)}}\right]$
$\beta_0^{(2)}$	$\frac{\beta_1^{(1)}}{3} - 6\left[f_1 f_2 \frac{\delta f_1}{\delta \beta_0^{(2)}} + g_1 g_2 \frac{\delta g_1}{\delta \beta_0^{(2)}}\right]$	$-3\left[f_2^2 \frac{\delta f_1}{\delta \beta_0^{(2)}} + g_2^2 \frac{\delta g_1}{\delta \beta_0^{(2)}}\right]$	$-\left[g_2 \frac{\delta f_1}{\delta \beta_0^{(2)}} + f_2 \frac{\delta g_1}{\delta \beta_0^{(2)}}\right]$
$\beta_1^{(2)}$	$\frac{\beta_0^{(1)}}{3}$	$\frac{\beta_1^{(1)}}{3}$	$\frac{1}{3}$
$\beta_2^{(2)}$	$-3\left[f_1^2 \frac{\delta f_2}{\delta \beta_2^{(2)}} + g_1^2 \frac{\delta g_2}{\delta \beta_2^{(2)}}\right]$	$\frac{\beta_0^{(1)}}{3} - 6\left[f_1 f_2 \frac{\delta f_2}{\delta \beta_2^{(2)}} + g_1 g_2 \frac{\delta g_2}{\delta \beta_2^{(2)}}\right]$	$-\left[f_1 \frac{\delta g_2}{\delta \beta_2^{(2)}} + g_1 \frac{\delta f_2}{\delta \beta_2^{(2)}}\right]$
$\beta_0^{(3)}$	$-6\left[f_1 f_2 \frac{\delta f_1}{\delta \beta_0^{(3)}} + g_1 g_2 \frac{\delta g_1}{\delta \beta_0^{(3)}}\right]$	$-3\left[f_2^2 \frac{\delta f_1}{\delta \beta_0^{(3)}} + g_2^2 \frac{\delta g_1}{\delta \beta_0^{(3)}}\right]$	$-\left[g_2 \frac{\delta f_1}{\delta \beta_0^{(3)}} + f_2 \frac{\delta g_1}{\delta \beta_0^{(3)}}\right]$
$\beta_1^{(3)}$	1	0	0
$\beta_2^{(3)}$	0	1	0
$\beta_3^{(3)}$	$-3\left[f_1^2 \frac{\delta f_2}{\delta \beta_3^{(3)}} + g_1^2 \frac{\delta g_2}{\delta \beta_3^{(3)}}\right]$	$-6\left[f_1 f_2 \frac{\delta f_2}{\delta \beta_3^{(3)}} + g_1 g_2 \frac{\delta g_2}{\delta \beta_3^{(3)}}\right]$	$-\left[f_1 \frac{\delta g_2}{\delta \beta_3^{(3)}} + g_1 \frac{\delta f_2}{\delta \beta_3^{(3)}}\right]$

Table C.5: Partial derivative of the first condition $\mathcal{C}_1^{\text{TVAR(3)}}(\boldsymbol{\beta})$ for linear root movements of a TVAR(3) process (with respect to the parameters).

Appendix D

Covariance Function of Time Variable AR Processes with Linear Root Motion

D.1 Conversion of TVAR(1) parameters between non-normalized and normalized time intervals

In this section, we will first show how the transformation of the discrete epochs $t \in \{1, 2, ..., n\}$ into $\bar{t} = \{0, 1/(n-1), 2/(n-1), ..., 1\}$ (or the normalization) affects the estimation of the TVAR(1) process. And then, we will further show, how the coefficients $\beta_0^{(1)}$ and $\beta_1^{(1)}$ (estimated using t) can be converted to the parameters $\overline{\beta}_0^{(1)}$ and $\overline{\beta}_1^{(1)}$ by the means of an estimate using $\bar{t}$.
We need the transformation of t into $\bar{t}$. Fortunately, this transformation is given by

$$\bar{t} = \frac{t-1}{n-1},$$

with the inverse transformation

$$t = \bar{t}(n-1) + 1. \tag{D.1.1}$$

The transformation for the required parameters follows from

$$\begin{aligned}
\alpha_1(t) &= \beta_0^{(1)} + \beta_1^{(1)} t \\
&= \beta_0^{(1)} + \beta_1^{(1)} (\bar{t}(n-1) + 1) \\
&= \underbrace{\beta_0^{(1)} + \beta_1^{(1)}}_{\overline{\beta_0^{(1)}}} + \underbrace{\beta_1^{(1)}(n-1)\bar{t}}_{\overline{\beta_1^{(1)}}\bar{t}.}
\end{aligned}$$

If both, the coefficients representation and the time vector change, it influences the lag of the covariance of two signals j. These must then be replaced by

$$\begin{aligned}
\bar{j} &= \overline{t+j} - \bar{t} \\
&= \frac{(t+j)-1}{n-1} - \frac{t-1}{n-1} \\
&= \frac{t-t-1+1+j}{n-1} \\
&= \frac{j}{n-1}.
\end{aligned}$$

Accordingly, the inverse transformation is given as:

$$j = \bar{j}(n-1).$$

D.2 Proof of the Continuous Representation of the Variances of a TVAR(1) Process with Linear Root Motion

In (5.3.1), it was shown that the continuous function

$$\gamma(0,t_c) = \frac{\sigma_\mathcal{E}^2}{1-\alpha_1^2(t_c)},$$

serves to compute the variances of a TVAR(1) process. Section 5.3.1 had shown how the time variable variance is converging to this function if the sampling rate becomes higher. In order to verify this, we are demonstrating that –under the assumption that the variance at a discrete time $t-\Delta t$ follows from $\gamma(0,t-\Delta t) = \frac{\sigma_\mathcal{E}^2}{1-\alpha_1^2(t-\Delta t)}$– the equation is evaluated at the limes $\Delta t \to 0$, i.e.

$$\begin{aligned}
\gamma(0,t) &= \lim_{\Delta t\to 0} \alpha_1^2(t)\gamma(0,t-\Delta t) + \sigma_\mathcal{E}^2 \\
&= \lim_{\Delta t\to 0} \alpha_1^2(t)\frac{\sigma_\mathcal{E}^2}{1-\alpha_1^2(t-\Delta t)} + \sigma_\mathcal{E}^2 \\
&= \lim_{\Delta t\to 0} \frac{\alpha_1^2(t)\sigma_\mathcal{E}^2}{1-\alpha_1^2(t-\Delta t)} + \frac{\sigma_\mathcal{E}^2 - \alpha_1^2(t-\Delta t)\sigma_\mathcal{E}^2}{1-\alpha_1^2(t-\Delta t)} \\
&= \lim_{\Delta t\to 0} \frac{\sigma_\mathcal{E}^2[\alpha_1^2(t) - \alpha_1^2(t-\Delta t) + 1]}{1-\alpha_1^2(t-\Delta t)} \\
&= \frac{\sigma_\mathcal{E}^2[\alpha_1^2(t) - \alpha_1^2(t) + 1]}{1-\alpha_1^2(t)} \\
&= \frac{\sigma_\mathcal{E}^2}{1-\alpha_1^2(t)}.
\end{aligned}$$

This proof is based on the induction principle and, gains its applicability from the fact that the initialization with

$$\gamma(0,0) = \Sigma_0(1) = \frac{1}{1-\alpha_1^2(0)}$$

is predefined.

D.3 Covariance Function between Discrete Values

When calculating covariances, individual observations with individual epochs τ_1 and τ_2 are rather given than an epoch and a lag with $h = \tau_2 - \tau_1 > 0$. For this reason, we rewrite the covariance of (5.3.7) into:

$$\begin{aligned}
&\gamma(h)(\tau_1) \\
&= \gamma_{\tau_2-\tau_1}(\tau_1) \\
&= \Sigma_0(\tau_1)\left(\frac{\overline{\beta_1^{(1)}}}{n-1}\right)^{\frac{\tau_2-\tau_1}{n-1}} \mathbb{P}\left(\frac{\overline{\beta_0^{(1)}}(n-1)}{\overline{\beta_1^{(1)}}} + \tau_1(n-1) + 1, (\tau_2-\tau_1)(n-1)\right).
\end{aligned}$$

D.4 Rewriting a Product of Decreasing Entries into a Product of Increasing Entries

When looking at

$$\prod_{\ell=1}^{j} \frac{|\overline{\beta_0^{(1)}}|(n-1)}{|\overline{\beta_1^{(1)}}|} - t - \ell + 1,$$

it is apparent that the factors in each step, become smaller by one. This is caused by the negative sign of l. To rewrite the product into one with increasing factors thus demands to dissolve the product sign:

$$\begin{aligned}
&\prod_{\ell=1}^{j} \frac{\overline{|\beta_0^{(1)}|}(n-1)}{\overline{|\beta_1^{(1)}|}} - t - \ell + 1 \\
&= \left(\frac{\overline{|\beta_0^{(1)}|}(n-1)}{\overline{|\beta_1^{(1)}|}} - t\textbf{-1+1} \right) \left(\frac{\overline{|\beta_0^{(1)}|}(n-1)}{\overline{|\beta_1^{(1)}|}} - t\textbf{-2+1} \right) ... \\
&\left(\frac{\overline{|\beta_0^{(1)}|}(n-1)}{\overline{|\beta_1^{(1)}|}} - t\textbf{-(}j\textbf{-1)+1} \right) \left(\frac{\overline{|\beta_0^{(1)}|}(n-1)}{\overline{|\beta_1^{(1)}|}} - t - \boldsymbol{j}\textbf{+1} \right).
\end{aligned}$$

In this representation, the bold part of the form $-a+1$ with $a \in [1, 2, ..., j]$ can now be replaced by $j - (j + a) + 1$:

$$\begin{aligned}
&\left(\frac{\overline{|\beta_0^{(1)}|}(n-1)}{\overline{|\beta_1^{(1)}|}} - t\textbf{+}\boldsymbol{j} - (\boldsymbol{j}\textbf{+1})\textbf{+1} \right) \left(\frac{\overline{|\beta_0^{(1)}|}(n-1)}{\overline{|\beta_1^{(1)}|}} - t\textbf{+}\boldsymbol{j} - (\boldsymbol{j}\textbf{+2})\textbf{+1} \right) ... \\
&\left(\frac{\overline{|\beta_0^{(1)}|}(n-1)}{\overline{|\beta_1^{(1)}|}} - t\textbf{+}\boldsymbol{j} - (\boldsymbol{j}\textbf{+(}\boldsymbol{j}\textbf{-1))+1} \right) \left(\frac{\overline{|\beta_0^{(1)}|}(n-1)}{\overline{|\beta_1^{(1)}|}} - t\textbf{+}\boldsymbol{j} - (\boldsymbol{j}\textbf{+}\boldsymbol{j}\textbf{)+1} \right) \\
&= \left(\frac{\overline{|\beta_0^{(1)}|}(n-1)}{\overline{|\beta_1^{(1)}|}} - t - \boldsymbol{j}\textbf{+}\boldsymbol{j} \right) \left(\frac{\overline{|\beta_0^{(1)}|}(n-1)}{\overline{|\beta_1^{(1)}|}} - t - \boldsymbol{j}\textbf{+(}\boldsymbol{j} - \textbf{1)} \right) ... \\
&\left(\frac{\overline{|\beta_0^{(1)}|}(n-1)}{\overline{|\beta_1^{(1)}|}} - t - \boldsymbol{j}\textbf{+ 2} \right) \left(\frac{\overline{|\beta_0^{(1)}|}(n-1)}{\overline{|\beta_1^{(1)}|}} - t - \boldsymbol{j}\textbf{+ 1} \right).
\end{aligned}$$

In the last step, the order of the factors is reversed in such a way that –with the help of

$$\begin{aligned}
&\left(\frac{\overline{|\beta_0^{(1)}|}(n-1)}{\overline{|\beta_1^{(1)}|}} - t - \boldsymbol{j}\textbf{+ 1} \right) \left(\frac{\overline{|\beta_0^{(1)}|}(n-1)}{\overline{|\beta_1^{(1)}|}} - t - \boldsymbol{j}\textbf{+ 2} \right) ... \\
&\left(\frac{\overline{|\beta_0^{(1)}|}(n-1)}{\overline{|\beta_1^{(1)}|}} - t - \boldsymbol{j}\textbf{+(}\boldsymbol{j} - \textbf{1)} \right) \left(\frac{\overline{|\beta_0^{(1)}|}(n-1)}{\overline{|\beta_1^{(1)}|}} - t - \boldsymbol{j}\textbf{+}\boldsymbol{j} \right) \\
&= \prod_{\ell=1}^{j} \frac{\overline{|\beta_0^{(1)}|}(n-1)}{\overline{|\beta_1^{(1)}|}} - t - j + \ell \quad -
\end{aligned}$$

a product, whose factors are ascending again, results. So all in all, it is valid to replace

$$\prod_{\ell=1}^{j} \frac{\overline{|\beta_0^{(1)}|}(n-1)}{\overline{|\beta_1^{(1)}|}} - t - \ell + 1 = \prod_{\ell=1}^{j} \frac{\overline{|\beta_0^{(1)}|}(n-1)}{\overline{|\beta_1^{(1)}|}} - t - j + \ell. \tag{D.4.1}$$

Appendix E

Application

E.1 Trend Reduction

This section describes, the method of estimating a deterministic trend, approximating the observations $\boldsymbol{\mathcal{L}} = [\mathcal{L}_1, \mathcal{L}_2, ..., \mathcal{L}_n]$. The estimate is used to detrend the observations, in order to obtain the signal $\tilde{\boldsymbol{\mathcal{S}}} = \boldsymbol{\mathcal{L}} - \boldsymbol{A}_t\xi$. Due to the required prerequisite to use the LSC as shown in section 2.1, the expected value of the detrended data must be zero: $E\{\mathcal{S}_k\} = 0 \ \forall k \in \{1, 2, ..., n\}$. Here, the parameters $\boldsymbol{\xi}$ are estimated in order to fit the observations $\boldsymbol{\mathcal{L}}$. They still including the additional signal $\boldsymbol{\mathcal{S}}$, we want to filter later:

$$\boldsymbol{\mathcal{L}} - \boldsymbol{\mathcal{S}} = \boldsymbol{A}\boldsymbol{\xi}.$$

E.1.1 Trend reduction using a Linear Function

The observation equation for the linear approximation for the kth element in the vector $\boldsymbol{\mathcal{L}}$ is obtained by

$$\mathcal{L}_k - \mathcal{S}_k = \boldsymbol{A}_k\boldsymbol{\xi} = \xi(1) + \xi(2)t_k. \tag{E.1.1}$$

Here, $\xi(1)$ is equal to the observation of $t_k = 0$, while $\xi(2)$ is the slope of the linear function. They are joint together in the parameter vector

$$\boldsymbol{\xi} = \begin{bmatrix}\xi(1)\\ \xi(2)\end{bmatrix}. \tag{E.1.2}$$

The entries of the kth row of the design matrix are found by deriving the observation equation (E.1.1) with respect to the parameters from (E.1.2):

$$\boldsymbol{A} = \begin{bmatrix}1 & t_1\\ 1 & t_2\\ 1 & t_3\\ \vdots & \vdots\\ 1 & t_n\end{bmatrix}.$$

This way the parameters of the linear function in $\boldsymbol{\xi}$ can be estimated by a minimization of the least-squares adjustment with the solution

$$\tilde{\boldsymbol{\xi}} = (\boldsymbol{A}^T\boldsymbol{A})^{-1}\boldsymbol{A}^T(\boldsymbol{\mathcal{L}} - \boldsymbol{\mathcal{S}}). \tag{E.1.3}$$

(This corresponds to the solution of the Gauss-Markov model from Koch 1999, chapter 3). These parameters allow to reduce the observations $\boldsymbol{\mathcal{L}}$ by the trend and thus to get the signal:

$$\boldsymbol{\mathcal{S}} = \boldsymbol{\mathcal{L}} - \boldsymbol{A}\tilde{\boldsymbol{\xi}} \tag{E.1.4}$$

with

$$E\{\boldsymbol{\mathcal{S}}\} = \begin{bmatrix} 0 \\ 0 \\ \vdots \\ 0 \end{bmatrix}.$$

E.1.2 Trend Reduction Using Trigonometric Functions

In cases when an oscillating trend has to be reduced, the design matrix contains cosine and sine functions. For the purposes of this study, we estimate the oscillations whose periods of multiple years or parts of one year. Since the observation are given in years, the linear relationship between the observations and the parameters is easily obtained:

$$\begin{aligned} \mathcal{L}_k - \mathcal{S}_k = \boldsymbol{A}_k\boldsymbol{\xi} = &\sum_{m=1}^{o} \xi(2m-1)\cos\left(\frac{2\pi}{365.25m}t\right) + \xi(2m)\sin\left(\frac{2\pi}{365.25m}t\right) + ... \\ &\sum_{l=2}^{o} \xi(200+2l-1)\cos\left(\frac{2\pi}{365.25}lt\right) + \xi(200+2l)\sin\left(\frac{2\pi}{365.25}lt\right), \end{aligned} \tag{E.1.5}$$

where $\mathcal{L}_k$ is the observation at time t_k. This equation (E.1.5) shows that $\xi(2m-1)$, $\xi(2m)$, $\xi(2o+2l-1)$ and $\xi(2o+2l)$ for $j,l = 1,2,...,o$ are the $4o$ unknown coefficients in the vector

$$\boldsymbol{\xi} = \begin{bmatrix} \xi(1) \\ \xi(2) \\ \vdots \\ \xi(4o) \end{bmatrix},$$

The k-th row of the design matrix is provided by

$$\boldsymbol{A}_k = \begin{bmatrix} \boldsymbol{B}_1 & \boldsymbol{B}_2 \end{bmatrix}.$$

with $\boldsymbol{B}_1$ contains the entries derived by the derivative of (E.1.5) with respect to the parameters $\xi(1), \xi(2), ..., \xi(2o)$:

$$\boldsymbol{B}_1 = \begin{bmatrix} \cos\left(\frac{2\pi}{365.25}t\right) & \sin\left(\frac{2\pi}{365.25}t\right) & \cos\left(\frac{2\pi}{365.25\cdot 2}t\right) & \sin\left(\frac{2\pi}{365.25\cdot 2}t\right) & ... & \cos\left(\frac{2\pi}{365.25\cdot o}t\right) & \sin\left(\frac{2\pi}{365.25\cdot o}t\right) \end{bmatrix},$$

and with $\boldsymbol{B}_2$ contains the entries derived by the derivative of (E.1.5) with respect to the parameters $\xi(201), \xi(202), ..., \xi(400)$:

$$\boldsymbol{B}_2 = \begin{bmatrix} \cos\left(\frac{2\pi}{365.25}2t\right) & \sin\left(\frac{2\pi}{365.25}2t\right) & \cos\left(\frac{2\pi}{365.25}4t\right) & \sin\left(\frac{2\pi}{365.25}4t\right) & ... & \cos\left(\frac{2\pi}{365.25}ot\right) & \sin\left(\frac{2\pi}{365.25}ot\right) \end{bmatrix}.$$

The vectors $\boldsymbol{A}_k$ allows to compute the Gauss-Markov model, which means that the estimation of the unknown parameters is again given by (E.1.2). These parameters can finally be used to reduce the observations by the trend (see (E.1.4)).

E.1.3 Trend Reduction Using a Combined Model of Linear and Trigonometric Functions

To approximate the observations, the estimation of a linear trend and the estimation of a sum of trigonometric functions can be combined as

$$\mathcal{L}_k - \mathcal{S}_k = \boldsymbol{A}_k\boldsymbol{\xi} = \xi(1) + \xi(2)t_k + \sum_{j=1}^{o} \xi(2j+1)\cos(j\cdot t_k 2\pi) + \xi(2j+2)\sin(j\cdot t_k 2\pi).$$

In this model, first, the number of unknown parameters in the vector

$$\boldsymbol{\xi} = \begin{bmatrix} \xi(1) \\ \xi(2) \\ \xi(3) \\ \xi(4) \\ \vdots \\ \xi(2o+2) \end{bmatrix}$$

equals $o + 2$, whereby the two addition entries are the parameters of the linear part. This means that the design matrix also is increased by two columns, so that the k-th row is given by

$$\boldsymbol{A}_k = \begin{bmatrix} 1 & t_k & \cos(t_k 2\pi) & \sin(t_k 2\pi) & \cos(4t_k\pi) & \sin(4t_k\pi) & \dots & \cos(2ot_k\pi) & \sin(2ot_k\pi) \end{bmatrix}.$$

Once more, to compute the signal by reducing the trend like it is shown in (E.1.4), the parameters are estimated by the Gauss-Markov model given in (E.1.2).

E.2 Derivative of a Covariance Function from AR Processes

The CF and its derivative are required to fill the matrices needed to apply LSC. In the case of a CF from AR processes, we see that the CF shows some advantages due to its generally simple form

$$\gamma(h) = \sum_{k=1}^{p} A_k \hat{P}_k{}^{|h|}. \tag{E.2.1}$$

When deriving this function, we need to pay attention to the case distinction from Appendix B.2:

$$\hat{P}_k{}^{|h|} = \begin{cases} P_k{}^{|h|} & \text{if } \mathcal{R}(P_k) \geq 0 \\ \cos(\pi h)(-P_k)^{|h|} & \text{else.} \end{cases} \tag{E.2.2}$$

To obtain the derivative of the CF, the linearity of the derivative function is used to show, that it is sufficient to derive the roots $\hat{P}_k$ in (E.2.2) with respect to the lag h and use it again in the CF in (E.2.1):

$$\frac{d}{dh}\gamma(h) = \sum_{k=1}^{p} A_k \frac{d}{dh}\hat{P}_k \tag{E.2.3}$$

with

$$\frac{d}{dh}\hat{P}_k{}^{|h|} = \begin{cases} \ln(P_k) P_k{}^{|h|} & \text{if } \mathcal{R}(P_k) \geq 0 \\ \cos(\pi h)\ln(-P_k)(-P_k)^{|h|} - \pi \sin(\pi h)(-P_k)^{|h|} & \text{else.} \end{cases} \tag{E.2.4}$$

Because, $P_k{}^{|h|}$ as well as the trigonometric functions $\cos(\pi h)$ and $\sin(\pi h)$, they all are infinitely differentiable, the CF is infinitely smooth, or in other words: arbitrarily differentiable.

E.3 Approximation of White Noise using an AR Process

The white noise process of variance $\sigma^2_{\mathcal{N}}$ is defined as process with mean zero and discrete CF:

$$\Sigma_j = \begin{cases} \sigma^2_{\mathcal{N}} & \text{if } j = 0 \\ 0 & \text{else.} \end{cases}$$

The spectrum of this process is defined by a constant value, which further more, is equal to the white noise's variance $\sigma^2_{\mathcal{N}}$ (see Schuh 2016, eq. 190). This process' spectrum can be approximated

by an AR process. In this case the roots of the AR process build a circle around the origin. In order to prove this assumption the PSD of an AR process with equidistant root on a circle around the origin is computed and compared to the PSD of a white noise process. The parameter of the white noise's variance is constant ($\sigma^2_{\mathcal{N}} = 5$), while the number of roots (or AR coefficients) increases for each simulation. Since the visual proof can be seen for low order AR processes, the orders used here are one, five and ten. These roots lie equidistant on a circle of radius 0.5 around the origin, and they are further transformed into the AR process' coefficients α_p (as it is done in (4.3.1)). In order to compute the AR process' PDFs, these coefficients as well as (2.13.2) are used.
Figure E.2 shows that the PSD of an AR process with roots on a circle approximates a white noise process with the same variance as the white noise part of the AR process. As the order of the AR process increases, the PSDs of the white noise and the AR process becoming ever more similar.
In order to prove that this approximation does not require the circle of radius $r = 0.5$, the roots of an AR(10) process are used to approximate the PSD of a white noise process once more. But this time the roots form a circle of radius $r = 0.7$ and the white noise's variance is $\sigma^2_{\mathcal{N}} = 3$. This approximation is pictured in Figure E.1, and proves that, as long as enough roots are on a circle, the approximation is successful, regardless of the white noise's variance. Notice that with increasing radius r the number of roots needed to approximate the white noise also increases.

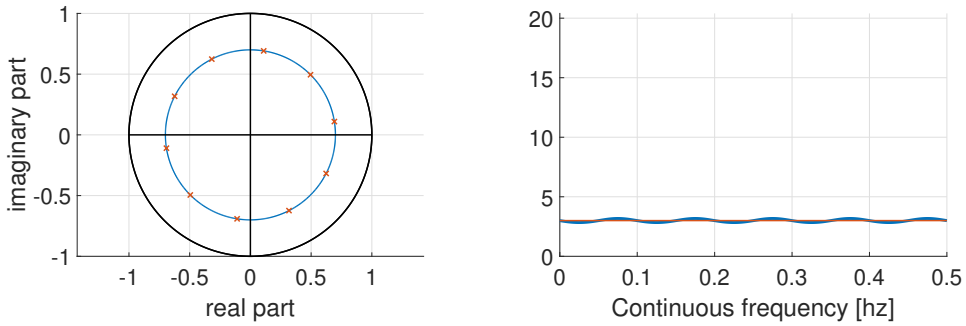

Figure E.1: The left coordinate system shows the AR(10) Process's roots (red cross) lying on the circle with radius $r = 0.7$ around the origin (in blue). And the right figure shows the corresponding PDF (in blue) and the PDF of the white noise with variance $\sigma^2_{\mathcal{N}} = 3$ (in red).

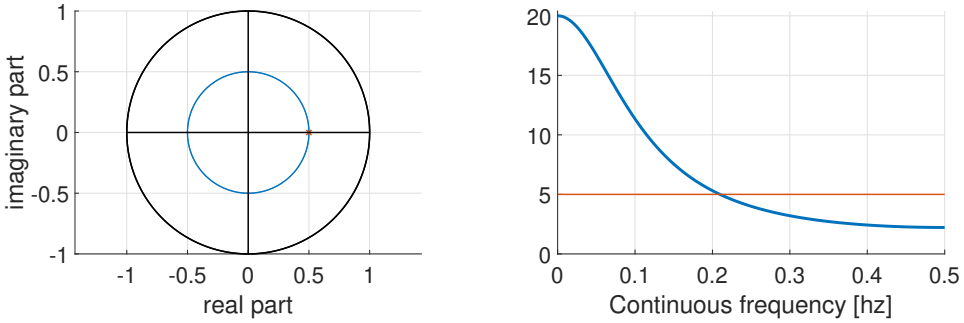

(a) The left coordinate system shows the AR(1) Process's root of 0.5 (red cross) lying on the circle with radius $r = 0.5$ around the origin (in blue). The right figure shows the corresponding PDF (in blue) compared to the PDF of the white noise with variance $\sigma^2_{\mathcal{N}} = 5$ (in red).

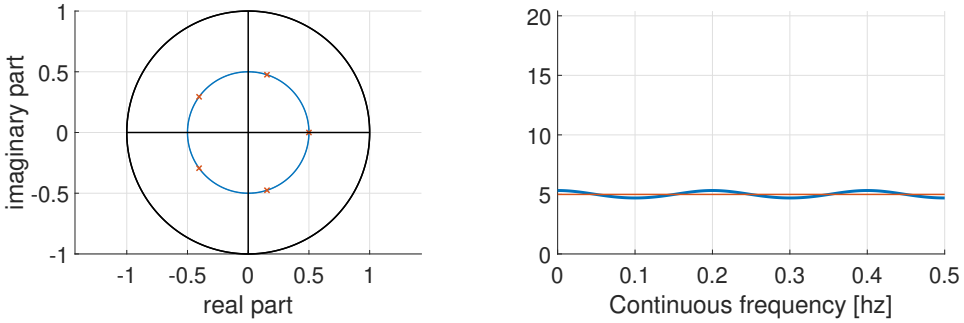

(b) The left coordinate system shows the AR(5) Process's roots (red cross) lying equidistant on the circle with radius $r = 0.5$ (in blue) around the origin. The right figure shows the corresponding PDF in blue compared to the PDF of the white noise with variance $\sigma^2_{\mathcal{N}} = 5$ in red.

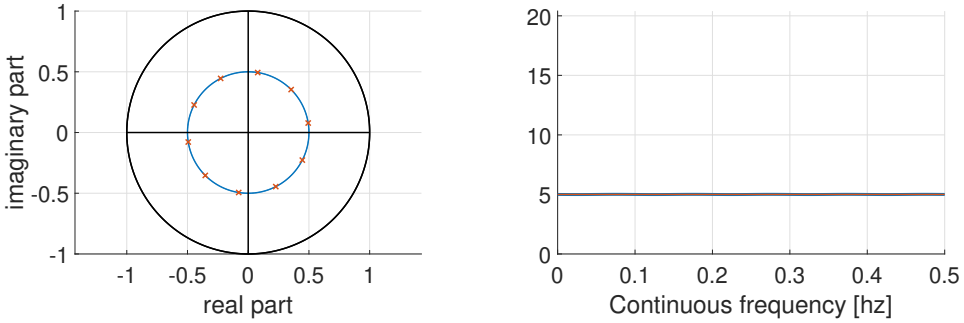

(c) The left coordinate system shows the AR(10) Process's roots (red cross) lying equidistant on the circle with radius $r = 0.5$ around the origin (in blue). The right figure shows the corresponding PDF (in blue) compared to the PDF of the white noise with variance $\sigma^2_{\mathcal{N}} = 5$ (in red).

Figure E.2: The left column shows the roots of three AR processes of order one, five and ten. These roots all lie on a circle with radius $r = 0.5$. The right column shows the corresponding PDFs. From top to bottom how the approximation of the white noise's PSD improves.

Appendix F

Acronyms

AIC Akaike information criterion.

AR autoregressive.

AR(p) autoregressive process of order p.

ARMA autoregressive moving average.

BLUP best linear unbiased prediction.

CDF cumulative distribution function.

CF covariance function.

CP characteristic polynomial.

DC Dirac delta comb.

DDF Dirac delta function.

DE difference equation.

ESD energy spectral density.

FT Fourier transformation.

GNSS Global Navigation Satellite Systems.

i.i.d independently and identically distributed.

IFT inverse Fourier transform.

LSC least-squares collocation.

MA moving average.

PDF probability density function.

PSD power spectral density.

RMSE root mean square error.

RSS residual sum of squares.

SLA sea level anomalies.

TVAR time variable autoregressive.

TVAR(p) time variable autoregressive process of order p.

Y.-W. Yule-Walker.

Appendix G

Notation

$\alpha_k / \alpha_k(t)$ k-th coefficient of an AR process/ k-th coefficient of a TVAR process.

c_k k-th coefficient of a polynomial $\mathcal{P}_p(x)$.

$\beta_l^{(k)}$ parameters for the representation of the coefficients of a TVAR process via basis functions; i.e. $\alpha_k(t) = \sum_{l=0}^{q_k} \beta_l^{(k)} b_l(t)$.

$\overline{\beta_0^{(1)}}, \overline{\beta_1^{(1)}}$ parameters for the representation of the coefficients of a TVAR(1) process with linear root motion and the temporal argument is normalized: $\alpha_1(j) = \overline{\beta_0^{(1)}} + \overline{\beta_1^{(1)}} \bar{j}$, with $\bar{j} = \frac{j-1}{n-1}$.

$\chi(x)$ the characteristic polynomial of an AR process with coefficients α_1, α_2, ..., α_p given by: $x^p - \alpha_1 x^{p-1} - \alpha_2 x^{p-2} - ... - \alpha_p$.

θ, ϑ replacement for the coefficients $\alpha_k(t)$ for the TVAR(3) processes to distinguish between the coefficients of the TVAR(1) process ($\theta_k(t)$) and the coefficients of the TVAR(2) process ($\vartheta_k(t)$).

$.^*$ given a complex value $x = a + bi$, then $x^* = a - bi$ is the complex conjugated value.

$\mathcal{C}(\boldsymbol{\beta})$ a condition that depends on the parameters $\boldsymbol{\beta}$ that must return zero to maintain a given root movement.

$g_1 \circledast g_2 = \int_{-\infty}^{\infty} g_1(x) g_2(t-x) dx$ convolution of two continuous functions.

$g_1 \star g_2 = \int_{-\infty}^{\infty} g_1(x) g_2(x+t) dx$ correlation between two continuous functions.

$\sum_{l=-\infty}^{\infty} \delta(h - l\Delta_j)$ Dirac delta comb.

$\{.\}_{j \in \mathbb{Z}}$ discrete sequence of observations with equidistant lag.

h argument of the continuous covariance function: $h \in \mathbb{R}^+$.

Δh lag between two signals. Also used to define the argument of the continuous covariance function: $\Delta h \in \mathbb{R}^+$.

j discrete integer value $j \in \mathbb{N}$.

Δj discrete distance of a signal with equidistant observations. $\Delta j \in \mathbb{N}$.

$\bar{j}$ representation of $j \in \{1, 2, ..., n\}$ in the normalized interval $[0, 1]$. $\bar{j} = \frac{j-1}{n-1}$.

$\overline{\Delta j}$ distance between the $\bar{j} \in [0, 1]$: $\overline{\Delta j} = \frac{\Delta j}{n-1}$.

$E\{.\}$ mean operator/ expectation operator.

$\mathbb{E}(.)$ energy of a sequence or function.

$\mathcal{E}_t$ independently and identically distributed random variable with variance $\sigma_{\mathcal{E}}^2$.

$F_{.}(.)$ cumulative distribution function.

$f_{.}(.)$ probability density function.

$\mathcal{F}\{.\}(\nu)$ Fourier transform with argument ν.

$\mathcal{F}^{-1}\{.\}(t)$ inverse Fourier transform with argument t.

$\gamma(h)/\gamma_{\Delta_h}(h)$ continuous covariance function evaluated at h/ continuous covariance function of a TVAR process at time h, evaluated for a time in the future $h + \Delta_h$.

$\mathbb{\Gamma}$ **(.)** the Gamma function is the faculty function extended for all values in $\mathbb{R}$.

$\Gamma(.)$ Fourier transform of the covariance function $\gamma(.)$.

$\boldsymbol{T} \odot \boldsymbol{b}$ matrix vector product of matrix $\boldsymbol{T}$ and vector $\boldsymbol{b}$: $\boldsymbol{X} = \boldsymbol{T} \odot \boldsymbol{b}$. The result $\boldsymbol{X}$ is a matrix with the same dimension as $\boldsymbol{T}$. Here, the i, j-th entry is calculated via $\boldsymbol{X}_{i,j} = \boldsymbol{T}_{i,j}\boldsymbol{b}_i$.

$\boldsymbol{t}^{\odot j}$ the exponent j is applied element-wise for every entry in $\boldsymbol{t}$. If $\boldsymbol{t} = [t_1, t_2, ...t_n]^T$, then $\boldsymbol{t}^{\odot j} = [t_1^j, t_2^j, ...t_n^j]^T$.

$\mathcal{I}(.)$ imaginary part of a complex value.

$\mathcal{L}_t$ observations/ random variable.

$M\{.\}$ mean value of a given vector.

n number of observations.

m number of parameters.

$\mathbb{P}(t, j)$ Pochhammer's symbol, which describes the product: $\prod_{k=0}^{j} t + k$.

$\mathcal{P}_p(x)$ polynomial of order p with variable x described by the product: $x^p + c_1 x^{p-1} + c_2 x^{p-2} + ... + c_p$.

$P_k/P_k(t)$ k-th root of the CP for an AR Process / k-th root of the CP for a TVAR Process.

$Q\{.\}$ cofactor matrix of the entries in a vector.

$\mathcal{R}(.)$ real part of a complex value.

$\zeta_l^{(k)}$ l-th parameter of the k-th time variable roots with basis functions: $P_k(t) = \sum_{l=0}^{q} \zeta_l^{(k)} \bar{b}_l(t)$.

$\mathcal{S}_t$ signal, corresponds to the trend reduced observations.

$\tilde{\mathcal{S}}$ predicted Signal.

$\sigma_{.}^2$ variance.

$\Sigma_{.}/\Sigma_{\Delta j}(j)$ covariance between two times with distance ./ time variable covariance between two times with distance Δj starting from time j.

$\Sigma\{.\}/\Sigma\{.,.\}$ covariance matrix of the entries in a vector/ common covariance matrix between two vectors.

A_k weight for the k-th root to calculate the covariance function: $\gamma(j) = \sum_{k=1}^{p} A_k P_k$.

List of Figures

List of Tables

Bibliography

Abel, N. H., and E. Galois. 1889. "Beweis der Unmöglichkeit der algebraischen Auflösung der allgemeinen Gleichungen, welche den vierten Grad übersteigen." In *Abhandlungen über die Algebraische Auflösung der Gleichungen,* edited by N. H. Abel and E. Galois, 8–28. Berlin, Heidelberg: Springer. isbn: 978-3-642-52006-8. https://doi.org/10.1007/978-3-642-52006-8_2.

Abramowitz, M., and I. A. Stegun. 1964. *Handbook of Mathematical Functions with Formulas, Graphs, and Mathematical Tables.* Ninth Dover printing, tenth GPO printing. New York City: Dover.

Akaike, H. 1974. "A new look at the statistical model identification." *IEEE transactions on automatic control* 19 (6): 716–723.

Albertella, A., F. Migliaccio, M. Reguzzoni, and F. Sansò. 2004. "Wiener filters and collocation in satellite gradiometry." In *V Hotine-Marussi Symposium on Mathematical Geodesy,* edited by Fernando Sansò, 32–38. Berlin, Heidelberg: Springer. isbn: 978-3-662-10735-5. https://doi.org/10.1007/978-3-662-10735-5_5.

Alkhatib, H., M. Omidalizarandi, and B. Kargoll. 2021. "A Bootstrap Approach to Testing for Time-Variability of AR Process Coefficients in Regression Time Series with t-Distributed White Noise Components." In *IX Hotine-Marussi Symposium on Mathematical Geodesy,* edited by Pavel Novák, Mattia Crespi, Nico Sneeuw, and Fernando Sansò, 191–197. Cham: Springer International Publishing. isbn: 978-3-030-54267-2. https://doi.org/10.1007/1345_2019_78.

Arabelos, D., and C. C. Tscherning. 1998. "The use of least suqares collocation method in global gravity field modeling." *Physics and Chemistry of the Earth* 23, no. 1 (January 1, 1998): 1–12. issn: 0079-1946. https://doi.org/10.1016/S0079-1946(97)00234-6.

Box, G. E. P., and G. M. Jenkins. 1970. *Time Series Analysis: Forecasting and Control.* Holden-Day. isbn: 978-0-8162-1094-7.

Brockmann, J. M., T. Schubert, and W.-D. Schuh. 2021. "An Improved Model of the Earth's Static Gravity Field Solely Derived from Reprocessed GOCE Data." *Surveys in Geophysics* (January 18, 2021). issn: 1573-0956. https://doi.org/10.1007/s10712-020-09626-0.

Brockwell, P. J., and R. A. Davis. 1991. *Time Series: Theory and Methods.* Springer Series in Statistics. New York, NY: Springer. isbn: 978-1-4419-0319-8. https://doi.org/10.1007/978-1-4419-0320-4.

Bronstein, I., K. Semendjajew, G. Musiol, and H. Mühlig. 2006. *Taschenbuch der Mathematik. 6. überarbeitete und ergänzte Auflage.*

Buttkus, B. 2000. *Spectral Analysis and Filter Theory in Applied Geophysics.* Berlin Heidelberg: Springer. isbn: 978-3-540-62674-9. https://doi.org/10.1007/978-3-642-57016-2.

Cubadda, G., S. Grassi, and B. Guardabascio. 2025. "The time-varying Multivariate Autoregressive Index model." *International Journal of Forecasting* 41 (1): 175–190. issn: 0169-2070. https://doi.org/https://doi.org/10.1016/j.ijforecast.2024.04.007.

Dahlhaus, R. 1997. "Fitting Time Series Models to Nonstationary Processes." *The Annals of Statistics* 25, no. 1 (February): 1–37. ISSN: 0090-5364, 2168-8966. https://doi.org/10.1214/aos/1034276620.

Dermanis, A. 1984. "Kriging and collocation: A comparison." *Manuscripta geodaetica* 9 (3): 159–167.

Doganalp, S., and H. Z. Selvi. 2015. "Local geoid determination in strip area projects by using polynomials, least-squares collocation and radial basis functions." *Measurement* 73 (September 1, 2015): 429–438. ISSN: 0263-2241. https://doi.org/10.1016/j.measurement.2015.05.030.

Eyring, V., S. Bony, G. A. Meehl, C. A. Senior, B. Stevens, R. J. Stouffer, and K. E. Taylor. 2016. "Overview of the Coupled Model Intercomparison Project Phase 6 (CMIP6) experimental design and organization." *Geoscientific Model Development* 9 (5): 1937–1958. https://doi.org/10.5194/gmd-9-1937-2016.

Förstner, W. 1985. "Determination of the additive noise variance in observed autoregressive processes using variance component estimation technique," 263–274. 2. München: R. Oldenbourg Verlag.

Galois, E. 1846. "Discussion on the process of pure analysis." *Journal de Mathématiques Pures et Appliqués* 11:381–444.

Gilardoni, M., M. Reguzzoni, and D. Sampietro. 2012. "A least-squares collocation procedure to merge local geoids with the aid of satellite-only global gravity models: the Italian-Swiss geoid case study" (April 1, 2012): 8061.

Goldberg, S. 1986. *Introduction to Difference Equations.* Reprint edition. New York: Dover Publications, January 1, 1986. ISBN: 978-0-486-65084-5.

Grenander, U. 1959. *Probability and statistics: the Harald Cramér volume.* Open Library ID: OL5790464M. Stockholm, New York: Almqvist & Wiksell.

Grenier, Y. 1983. "Time-dependent ARMA modeling of nonstationary signals." Conference Name: IEEE Transactions on Acoustics, Speech, and Signal Processing, *IEEE Transactions on Acoustics, Speech, and Signal Processing* 31, no. 4 (August): 899–911. ISSN: 0096-3518. https://doi.org/10.1109/TASSP.1983.1164152.

Hall, M., A. V. Oppenheim, and A. Willsky. 1977. "Time-varying parametric modeling of speech." In *1977 IEEE Conference on Decision and Control including the 16th Symposium on Adaptive Processes and A Special Symposium on Fuzzy Set Theory and Applications,* 1085–1091. 1977 IEEE Conference on Decision and Control including the 16th Symposium on Adaptive Processes and A Special Symposium on Fuzzy Set Theory and Applications. December. https://doi.org/10.1109/CDC.1977.271732.

Hamden, M. H., A. H. Md Din, D. D. Wijaya, M. Y. M. Yusoff, and M. F. Pa'suya. 2021. "Regional Mean Sea Surface and Mean Dynamic Topography Models Around Malaysian Seas Developed From 27 Years of Along-Track Multi-Mission Satellite Altimetry Data." Publisher: Frontiers, *Frontiers in Earth Science* 9 (September 9, 2021). ISSN: 2296-6463. https://doi.org/10.3389/feart.2021.665876.

Hamilton, J. D. 1994. *Time Series Analysis.* Princeton, New Jersey: Princeton University Press. ISBN: 978-0-691-04289-3.

Haslbeck, J. M. B., L. F. Bringmann, and L. J. Waldorp. 2021. "A Tutorial on Estimating Time-Varying Vector Autoregressive Models." Publisher: Routledge, *Multivariate Behavioral Research* 56 (1): 120–149. https://doi.org/10.1080/00273171.2020.1743630.

Jendges, L. 2022. "Can AR processes be used to locally improve the resolution of gravity fields represented by SH?" Talk, FROGS 2022, Essen.

Jin, T., J. Li, and W. Jiang. 2016. "The global mean sea surface model WHU2013." *Geodesy and Geodynamics,* Special Issue: Geodetic and Geophysical Observations and Applications and Implications, 7, no. 3 (May 1, 2016): 202–209. issn: 1674-9847. https://doi.org/10.1016/j.geog.2016.04.006.

Kamen, E. W. 1988. "The Poles and Zeros of a Linear Time-Varying System." *Linear Algebra and its Applications* 98 (January 1, 1988): 263–289. issn: 0024-3795. https://doi.org/10.1016/0024-3795(88)90168-1.

Kargoll, B., M. Omidalizarandi, H. Alkhatib, and W.-D. Schuh. 2018. "Further results on a modified EM algorithm for parameter estimation in linear models with time-dependent autoregressive and t-Distributed errors." In *Time series analysis and forecasting,* edited by Ignacio Rojas, Hector Pomares, and Olga Valenzuela, 323–337. Cham: Springer International Publishing. isbn: 978-3-319-96944-2.

Khintchine, A. 1934. "Korrelationstheorie der stationären stochastischen Prozesse." *Mathematische Annalen* 109, no. 1 (December 1, 1934): 604–615. issn: 1432-1807. https://doi.org/10.1007/BF01449156.

Koch, K.-R. 1999. *Parameter Estimation and Hypothesis Testing in Linear Models.* Berlin, Heidelberg: Springer. isbn: 978-3-642-08461-4. https://doi.org/10.1007/978-3-662-03976-2.

Korte, J., J. M. Brockmann, and W.-D. Schuh. 2018. *Least Squares Collocation with Finite and Recursive Defined Covariance Functions Using Function Values and Derivatives.* Talk at the IX Hotine Marussi Symposium. Rome, Italy.

Korte, J., J. M. Brockmann, and W.-D. Schuh. 2023a. "A Comparison between Successive Estimate of TVAR(1) and TVAR(2) and the Estimate of a TVAR(3) Process." *Engineering Proceedings* 39 (1): 90. issn: 2673-4591. https://doi.org/10.3390/engproc2023039090.

Korte, J., T. Schubert, J. M. Brockmann, and W.-D. Schuh. 2023b. "On the Estimation of Time Varying AR Processes," 1–6. International Association of Geodesy Symposia. Berlin, Heidelberg: Springer. https://doi.org/10.1007/1345_2023_188.

Korte, J., T. Schubert, J.M. Brockmann, and W.-D. Schuh. 2021. "A Mathematical Investigation of a Continuous Covariance Function Fitting with Discrete Covariances of an AR Process." *International Conference on Time Series and Forecasting (ITISE 2021), Engineering Proceedings* 5 (1): 18. https://doi.org/10.3390/engproc2021005018.

Krarup, T. 1969. "A Contribution to the Mathematical Foundation of Physical Geodesy." *Geod. Inst. Copenhagen* 44 (January 1, 1969).

Krasbutter, I., J. M. Brockmann, H. Goiginger, B. Kargoll, R. Pail, and W.-D. Schuh. 2011. "Refinement of the Stochastic Model of GOCE Scientific Data in along Time Series." In *Proceedings of the 4th International GOCE User Workshop,* edited by L. Ouwehand. ESA Publication SP-696, ESA/ESTEC, ISBN (Online) 978-92-9092-260-5, ISSN 1609-042X.

Krasbutter, I., B. Kargoll, and W.-D. Schuh. 2015. "Magic Square of Real Spectral and Time Series Analysis with an Application to Moving Average Processes." In *The 1st International Workshop on the Quality of Geodetic Observation and Monitoring Systems (QuGOMS'11), IAG Symposia,* edited by H. Kutterer, F. Seitz, H. Alkhatib, and M. Schmidt, 140:9–14. International Association of Geodesy Symposia. Springer. isbn: 978-3-319-10827-8.

Li, X., and J. Yuan. 2024. "DeepTVAR: Deep learning for a time-varying VAR model with extension to integrated VAR." *International Journal of Forecasting* 40 (3): 1123–1133. issn: 0169-2070. https://doi.org/https://doi.org/10.1016/j.ijforecast.2023.10.001.

Loth, I., B. Kargoll, and W.-D. Schuh. 2021. "Non-Recursive Representation of an Autoregressive Process within the Magic Square." In *IX Hotine-Marussi Symposium on Mathematical Geodesy,* edited by Pavel Novák, Mattia Crespi, Nico Sneeuw, and Fernando Sansò, 183–189. Cham: Springer International Publishing. isbn: 978-3-030-54267-2. https://doi.org/10.1007/1345_2019_60.

Moon, T. K., and J. H. Gunther. 2020. "Estimation of Autoregressive Parameters from Noisy Observations Using Iterated Covariance Updates." *Entropy* 22, no. 5 (May 19, 2020): 572. issn: 1099-4300. https://doi.org/10.3390/e22050572.

Moritz, H. 1972. *Advanced Least-Squares Methods.* Vol. 175. Ohio: Ohio State University Research Foundation Columbus.

Moritz, H. 1973. *Least-Squares Collocation.* Reihe A 75. München: Deutsche Geodätische Kommission.

Moritz, H. 1980. *Advanced Physical Geodesy.* Karlsruhe: Wichmann. isbn: 978-0-85626-195-4.

Priestley, M. B. 1983. *Spectral Analysis and Time Series, Two-Volume Set: Volumes I and II.* Amsterdam Heidelberg: Academic Press, February 11, 1983. isbn: 978-0-12-564922-3.

Priestley, M. B. 1988. "Non-linear and non-stationary time series analysis." *London: Academic Press.*

Ramouz, S., Y. Afrasteh, M. Reguzzoni, A. Safari, and A. Saadat. 2019. "IRG2018: A regional geoid model in Iran using Least Squares Collocation." *Studia Geophysica et Geodaetica* 63, no. 2 (April 1, 2019): 191–214. issn: 1573-1626. https://doi.org/10.1007/s11200-018-0116-4.

Reguzzoni, M., L. Rossi, C. I. De Gaetani, S. Caldera, and R. Barzaghi. 2022. "GNSS-Based Dam Monitoring: The Application of a Statistical Approach for Time Series Analysis to a Case Study." Number: 19 Publisher: Multidisciplinary Digital Publishing Institute, *Applied Sciences* 12, no. 19 (January): 9981. issn: 2076-3417. https://doi.org/10.3390/app12199981.

Reguzzoni, M., F. Sansó, and G. Venuti. 2005. "The Theory of General Kriging, with Applications to the Determination of a Local Geoid." *Geophysical Journal International* 162 (2): 303–314. issn: 0956-540X. https://doi.org/10.1111/j.1365-246X.2005.02662.x.

Rossi, L., M. Reguzzoni, Ö. Koç, G. Rosi, and F. Migliaccio. 2022. "Assessment of gravity field recovery from a quantum satellite mission with atomic clocks and cold atom gradiometers." *Quantum Science and Technology* 8, no. 1 (December): 014009. https://doi.org/10.1088/2058-9565/aca8cc.

Sansò, F. 1985. "The Analysis of Time Series with Applications to Geodetic Control Problems." In *Optimization and Design of Geodetic Networks,* edited by Erik W. Grafarend and Fernando Sansò, 436–525. Berlin, Heidelberg: Springer. isbn: 978-3-642-70659-2. https://doi.org/10.1007/978-3-642-70659-2_17.

Sansò, F., and W.-D. Schuh. 1987. "Finite covariance functions." *Bulletin Géodésique* 61 (4): 331–347. https://doi.org/10.1007/BF02520559.

Schlittgen, R., and B. H. Streitberg. 1991. *Zeitreihenanalyse.* 4., Aufl. edition. Berlin: Oldenbourg Wissenschaftsverlag, January 1, 1991. isbn: 978-3-486-21908-1.

Schubert, T., J. M. Brockmann, J. Korte, and W.-D. Schuh. 2021a. "On the Family of Covariance Functions Based on ARMA Models." Number: 1 Publisher: Multidisciplinary Digital Publishing Institute, *Engineering Proceedings* 5 (1): 37. issn: 2673-4591. https://doi.org/10.3390/engproc2021005037.

Schubert, T., J. M. Brockmann, and W.-D. Schuh. 2021b. "Identification of Suspicious Data for Robust Estimation of Stochastic Processes." In *IX Hotine-Marussi Symposium on Mathematical Geodesy,* edited by Pavel Novák, Mattia Crespi, Nico Sneeuw, and Fernando Sansò, 199–207. Cham: Springer International Publishing. isbn: 978-3-030-54267-2. https://doi.org/10.1007/1345_2019_80.

Schubert, T., J. M. Brockmann, and W.-D. Schuh. 2021c. "Identification of Suspicious Data for Robust Estimation of Stochastic Processes." In *IX Hotine-Marussi Symposium on Mathematical Geodesy,* edited by Pavel Novák, Mattia Crespi, Nico Sneeuw, and Fernando Sansò, 199–207. Cham: Springer International Publishing. isbn: 978-3-030-54267-2.

Schubert, T., J. Korte, J. M. Brockmann, and W.-D. Schuh. 2020. "A Generic Approach to Covariance Function Estimation Using ARMA-Models." Number: 4 Publisher: Multidisciplinary Digital Publishing Institute, *Mathematics* 8, no. 4 (April): 591. issn: 2227-7390. https://doi.org/10.3390/math8040591.

Schubert, T., and W.-D. Schuh. 2024. "A Flexible Family of Compactly Supported Covariance Functions Based on Cutoff Polynomials." In *X Hotine-Marussi Symposium on Mathematical Geodesy,* edited by Jeffrey T. Freymueller and Laura Sánchez, 139–147. Cham: Springer International Publishing. isbn: 978-3-031-55360-8. https://doi.org/10.1007/1345_2023_200.

Schuh, W.-D. 1996. *Tailored Numerical Solution Strategies for the Global Determination of the Earth's Gravity Field.* Graz: Mitteilungen der Geodätischen Institute der TU.

Schuh, W.-D. 2003a. *GOCE Gravity Field Determination - Simulation Studies.* Status Seminar Bavarian State Mapping Agency (BLVA), Munich, June 12-13, 2003. Observation of the System Earth from Space.

Schuh, W.-D. 2003b. "The Processing of Band-Limited Measurements; Filtering Techniques in the Least Squares Context and in the Presence of Data Gaps." In *Earth Gravity Field from Space - From Sensors to Earth Sciences,* edited by G. Beutler, M. R. Drinkwater, R. Rummel, and R. von Steiger, 108:67–78. Space Science Reviews.

Schuh, W.-D. 2016. In *Handbuch der Geodäsie,* edited by W. Freeden and R. Rummel, vol. Erdmessung und Satellitengeodäsie, 73–121. Springer Reference Naturwissenschaften. Springer Spektrum.

Schuh, W.-D. 2022. "Geostatistik." lecture notes, Theoretical Geodesy, University of Bonn.

Schuh, W.-D., and J. M. Brockmann. 2019. "Numerical Treatment of Covariance Stationary Processes in Least Squares Collocation." In *Handbuch der Geodäsie: 6 Bände,* edited by Willi Freeden and Reiner Rummel, 1–37. Berlin, Heidelberg: Springer. isbn: 978-3-662-46900-2. https://doi.org/10.1007/978-3-662-46900-2_95-1.

Schuh, W.-D., J. Korte, T. Schubert, and J. M. Brockmann. 2023. "Modeling of Inhomogeneous Spatio-Temporal Signals by Least Squares Collocation." Berlin, Heidelberg: Springer Berlin Heidelberg. https://doi.org/10.1007/1345_2023_202.

Schuh, W.-D., I. Krasbutter, and B. Kargoll. 2014. "Korrelierte Messung - Was Nun?" In *Zeitabhängige Messgrößen - Ihre Daten Haben (Mehr-)Wert,* edited by Hans Neuner, 74:85–101. DVW-Schriftenreihe. Schuh-etal$_1$4. Wißner, Augsburg.

Siemes, Ch., W.-D. Schuh, J. Cai, N. Sneeuw, and O. Baur. 2007. "GOCE Data Processing: The Numerical Challange of Data Gaps." In *Proceedings of the Status Seminar Geotechnologien, "'Observation of the System Earth from Space"', Munich, Nov. 22-23, 2007,* 11:99–105. Geotechnologien, Science Report.

Slepian, D. 1978. "Prolate Spheroidal Wave Functions, Fourier Analysis, and Uncertainty—V: The Discrete Case." *Bell System Technical Journal* 57 (5): 1371–1430. issn: 1538-7305. https://doi.org/10.1002/j.1538-7305.1978.tb02104.x.

Teunissen, P. J. G. 2007. "Best prediction in linear models with mixed integer/real unknowns: theory and application." *Journal of Geodesy* 81, no. 12 (December 1, 2007): 759–780. ISSN: 1432-1394. https://doi.org/10.1007/s00190-007-0140-6.

Watts, D. G., and G. Jenkins. 1968. *Spectral analysis and its applications.* San Francisco: Holden-Day. ISBN: 978-0-8162-4464-5.

Wold, H. 1938. "A study in the analysis of stationary time series." PhD diss., Almqvist & Wiksell Uppsala.

Yuan, J., J. Guo, X. Liu, C. Zhu, Y. Niu, Z. Li, B. Ji, and Y. Ouyang. 2020. "Mean sea surface model over China seas and its adjacent ocean established with the 19-year moving average method from multi-satellite altimeter data." *Continental Shelf Research* 192 (January 1, 2020): 104009. ISSN: 0278-4343. https://doi.org/10.1016/j.csr.2019.104009.